



ΕΘΝΙΚΟ ΜΕΤΣΟΒΙΟ ΠΟΛΥΤΕΧΝΕΙΟ
ΣΧΟΛΗ ΠΟΛΙΤΙΚΩΝ ΜΗΧΑΝΙΚΩΝ
ΤΟΜΕΑΣ ΥΔΑΤΙΚΩΝ ΠΟΡΩΝ ΚΑΙ
ΠΕΡΙΒΑΛΛΟΝΤΟΣ
ΕΡΓΑΣΤΗΡΙΟ ΛΙΜΕΝΙΚΩΝ ΕΡΓΩΝ

«ΠΙΘΑΝΟΤΙΚΟΣ ΣΧΕΔΙΑΣΜΟΣ ΠΑΡΑΚΤΙΩΝ ΕΡΓΩΝ»

“PROBABILISTIC DESIGN OF COASTAL STRUCTURES”

ΔΙΔΑΚΤΟΡΙΚΗ ΔΙΑΤΡΙΒΗ

για τον Επιστημονικό Τίτλο της Διδάκτορα Μηχανικού υποβληθείσα
στη Σχολή Πολιτικών Μηχανικών του Εθνικού Μετσόβιου Πολυτεχνείου

ΔΗΜΗΤΡΑ Ι. ΜΑΛΛΙΟΥΡΗ

Διπλωματούχος Πολιτικός Μηχανικός ΕΜΠ, ΜΔΕ ΕΜΠ

ΑΘΗΝΑ, Νοέμβριος 2020

NATIONAL TECHNICAL UNIVERSITY OF ATHENS
SCHOOL OF CIVIL ENGINEERING
DEPARTMENT OF WATER RESOURCES AND ENVIRONMENTAL
ENGINEERING
LABORATORY OF HARBOUR WORKS

“PROBABILISTIC DESIGN OF COASTAL STRUCTURES”

DISSERTATION
for the degree of Doctor of Philosophy
submitted to School of Civil Engineering of National Technical University of Athens

by
Dimitra I. Malliouri
Defended in public: 9.10.2020
in Athens, Greece

Members of the Examining Committee:

Assoc. Prof. Vasiliki K. Tsoukala	School of Civil Eng., NTUA	<i>Supervisor</i>
Prof. Emer. Constantine D. Memos	School of Civil Eng., NTUA	<i>Adv. Committee</i>
Dr. Takvor H. Soukissian	Institute of Ocean., HCMR	<i>Adv. Committee</i>
Prof. Theophanis V. Karambas	Dep. of Civil Eng., AUTH	
Prof. Georgios Galanis	Dep. of Math., HNA	
Assist. Prof. Vasiliki Katsardi	School of Civil Eng., UTH	
Prof. John Dalsgaard Sørensen	Dep. of the Built Env., Aalborg Un.	

Acknowledgements

Upon completion of the present study I would like to deeply thank my supervisor, Associate Professor Vasiliki Tsoukala for assigning this very interesting and challenging thesis, as well as for her continued support and guidance. I would also like to thank her for trusting me to play an important role in research programs, and for our meaningful discussions that enabled me to overcome various problems that arose throughout the course of this research.

I would like to sincerely thank Professor Emeritus Constantine Memos for serving on my Advisory Committee, his significant role in contributing valuable comments, and his continued support and guidance. I have enjoyed our fruitful discussions during the course of my research and his comments and recommendations were invaluable.

I would also like to express my sincere thanks to Research Director Takvor Soukissian for serving on my Advisory Committee and for contributing valuable comments and reviews to my thesis. Working with him was very helpful and instructive for me due to his experience and expertise in stochastic modeling of met-ocean characteristics.

Special thanks are also due to Professor Theofanis Karambas, Professor Georgios Galanis, Assistant Professor Vasiliki Katsardi, and Professor John Dalsgaard Sørensen for serving on the defence committee of my dissertation, and for contributing valuable comments and reviews to my thesis.

Most of all, I would like to thank my parents, Chrysavgi and Ioannis, and my sister, Georgia, for their continuous encouragement and support at all levels for accomplishing this work. It would not have been possible without them. I am very grateful for the support and patience from the special person in my life, Alexandros.

I would also like to acknowledge the support that I received from my close friends: Franka, Giouli, Sofia, Giota, Xenia, Aggelos, Antonis, and Dimos.

My sincere gratitude goes to the research group: Nikos, Andreas, Michalis, Tasos, Maria-Eirini, Vasilis, Vanesa, and Christina.

I would also like to acknowledge DHI for freely providing me with the software license of MIKE 21 for educational purposes as a part of my thesis, Hellenic Centre for Marine Research (POSEIDON system) and Puertos del Estado for kindly providing me with wave and sea level measurements.

Copyright © Dimitra I. Malliouri 2020

All rights reserved.

To my parents

Εκτενής Ελληνική Περίληψη

Πιθανοτικός Σχεδιασμός Παράκτιων Έργων

Δήμητρα Ι. Μαλλιούρη

Εθνικό Μετσόβιο Πολυτεχνείο
Σχολή Πολιτικών Μηχανικών
Τομέας Υδατικών Πόρων και Περιβάλλοντος
Εργαστήριο Λιμενικών Έργων

1. Εισαγωγή

Στη σημερινή εποχή, γίνεται ολοένα και πιο αντιληπτό ότι οι παράκτιες κατασκευές θα πρέπει να σχεδιάζονται με τέτοιο τρόπο ώστε να ικανοποιούν προκαθορισμένα επίπεδα ασφάλειας και απόδοσης, δηλ. προκαθορισμένα επίπεδα αξιοπιστίας, έχοντας λάβει υπόψη όλες τις αβεβαιότητες που σχετίζονται με τις παραμέτρους φόρτισης, αντίστασης ή αντοχής, και των εργαλείων σχεδιασμού. Αυτό μπορεί να επιτευχθεί με την εφαρμογή μίας κατάλληλης μεθοδολογίας ικανής να εκτιμήσει με ακρίβεια το επίπεδο αξιοπιστίας μίας παράκτιας κατασκευής, δηλ. την πιθανότητα αστοχίας της κατά τη διάρκεια της λειτουργία της, ή αλλιώς κατά τη διάρκεια της ζωής της. Η πιθανότητα αυτή αστοχίας της κατασκευής θα πρέπει να είναι μικρότερη ή ίση από μία επιτρεπόμενη πιθανότητα αστοχίας, η οποία εξαρτάται από το μέγεθος των επιπτώσεων της αστοχίας της κατασκευής. Ως εκ τούτου, μέθοδοι βασιζόμενες στην αξιοπιστία θα πρέπει να υιοθετηθούν για τον σχεδιασμό των παράκτιων κατασκευών.

Οι μέθοδοι σχεδιασμού των παράκτιων κατασκευών που βασίζονται στην αξιοπιστία διακρίνονται σε τέσσερις κατηγορίες, οι οποίες σχετίζονται με την ακρίβεια στην εκτίμηση της αξιοπιστίας των στοιχείων της κατασκευής και στη θεώρηση των εμπλεκόμενων αβεβαιοτήτων, που σχετίζονται με τις θαλάσσιες φορτίσεις, και αναφέρονται παρακάτω [1]:

- Ντετερμινιστικές μέθοδοι (Επίπεδο 0)
- Ημι-πιθανοτικές μέθοδοι (Επίπεδο I)

- Πιθανοτικές μέθοδοι με προσεγγίσεις (Επίπεδο II)
- Πλήρως πιθανοτικές μέθοδοι (Επίπεδο III)

Η παραδοσιακή πρακτική σχεδιασμού των παράκτιων κατασκευών είναι συνήθως ντετερμινιστικής φύσης (Επίπεδο 0), σύμφωνα με την οποία η αξιοπιστία των κατασκευών βασίζεται στην πιθανότητα υπέρβασης του φορτίου σχεδιασμού. Ειδικότερα, υιοθετείται η έννοια των κυματικών παραμέτρων σχεδιασμού, και ειδικότερα του σημαντικού ύψους κύματος, το οποίο συνδέεται με μία συγκεκριμένη περίοδο επαναφοράς [2].

Εκτός της ντετερμινιστικής μεθόδου, η μέθοδος των μερικών συντελεστών μπορεί, επίσης, να εφαρμοστεί, η οποία βασίζεται σε πρότυπα [3]. Η συγκεκριμένη προσέγγιση σχεδιασμού ταξινομείται στις ημι-πιθανοτικές μεθόδους (Επίπεδο I), αλλά η προσέγγιση αυτή δεν επιτρέπει μία ακριβή εκτίμηση της αξιοπιστίας του σχεδιασμού. Για το λόγο αυτό, θα μπορούσαν να χρησιμοποιηθούν πλήρως πιθανοτικές μέθοδοι που λαμβάνουν υπόψη τις αβεβαιότητες όλων των στοχαστικών μεταβλητών φόρτισης και αντοχής της κατασκευής.

Οι πλήρως πιθανοτικές μέθοδοι (Επίπεδο III) ανήκουν στην κατηγορία των προηγμένων πιθανοτικών μεθόδων, οι οποίες χρησιμοποιούν τη συνάρτηση της από κοινού πυκνότητας πιθανότητας όλων των εμπλεκόμενων στοχαστικών μεταβλητών. Υπάρχουν δύο κύριες μέθοδοι που ανήκουν στη συγκεκριμένη κατηγορία, οι οποίες είναι η μέθοδος Άμεσης Ολοκλήρωσης (DIM) και η μέθοδος Monte Carlo (MCM). Επιπρόσθετα, μία άλλη δυνατότητα εκτίμησης της αξιοπιστίας σχεδιασμού μία κατασκευής, η οποία θεωρείται ωστόσο λιγότερο ακριβής, παρέχεται μέσω των μεθόδων με προσεγγίσεις (Επίπεδο II).

Σημειώνεται ότι η πιθανοτική αναπαράσταση των περιβαλλοντικών παραμέτρων στη θέση των παράκτιων έργων είναι πολύ σημαντική για τον σχεδιασμό των έργων αυτών, που βασίζεται στην αξιοπιστία. Ωστόσο, υπάρχει έλλειψη μακροπρόθεσμων περιβαλλοντικών δεδομένων στη θέση των παράκτιων έργων, η οποία βρίσκεται συνήθως στα ενδιάμεσα (ως προς το βάθος) νερά, καθιστώντας ιδιαίτερα δύσκολη την εκτίμηση της συνάρτησης της από κοινού πυκνότητας πιθανότητας των περιβαλλοντικών στοχαστικών παραμέτρων.

Τέτοια δεδομένα θα μπορούσαν να είναι μετρήσεις κυματικών παραμέτρων, διακύμανσης της στάθμης της θάλασσας π.χ. λόγω αστρονομικής ή μετεωρολογικής παλίρροιας, ταχύτητα θαλάσσιων ρευμάτων κλπ., τα οποία θα πρέπει να συλλέγονται στην περιοχή του έργου. Αυτά θα μπορούσαν να βρεθούν από:

- (i) Μετρήσεις στη θέση του έργου που να καλύπτουν μία χρονική περίοδο αρκετών ετών. Προφανώς, τέτοιες μετρήσεις είναι δυσεύρετες.

(ii) Μετρήσεις ίδιου τύπου αλλά στα βαθιά νερά, εάν η θέση των έργων είναι σε πιο ρηχά νερά, που να καλύπτουν μία χρονική περίοδο αρκετών ετών. Τότε, είτε γραμμικά (π.χ. [4]) είτε μη γραμμικά ([5]; [6]; [7]) μοντέλα διάδοσης κυματισμών μπορούν να εφαρμοσθούν για να μεταφέρουν κάθε θαλάσσια κατάσταση από τα βαθιά σε πιο ρηχά νερά.

(iii) Εκτιμήσεις από μεθόδους ανάλυσης στο παρελθόν για αρκετά έτη ([8]; [1]). Ειδικότερα, όσον αφορά στο μακροπρόθεσμο κυματικό κλίμα στη θέση των παράκτιων έργων, ανεμολογικά δεδομένα στην περιοχή της κυματογένεσης μπορούν να χρησιμοποιηθούν (π.χ. [9]), σε συνδυασμό με το ενεργό ανάπτυγμα πελάγους, για να παραχθεί αυτή η πληροφορία υπό ένα πιθανοτικό πλαίσιο.

Είναι πλέον ξεκάθαρο ότι στόχος της προαναφερόμενης συλλογής δεδομένων αποτελεί η απόκτηση μίας πιθανοτικής αναπαράστασης του μακροπρόθεσμου κυματικού κλίματος, της στάθμης της θάλασσας και άλλων περιβαλλοντικών παραμέτρων στη θέση των παράκτιων έργων. Στην περίπτωση όπου υπάρχουν διαθέσιμες μετρήσεις στα βαθιά νερά, σημειώνεται ότι τα μη γραμμικά μοντέλα είναι πιο ακριβή από τα γραμμικά, καθώς λαμβάνουν υπόψη τις μη γραμμικότητες και τις γραμμικές αλληλεπιδράσεις των κυματισμών. Ωστόσο, τα μη γραμμικά μοντέλα μπορεί να γίνουν ιδιαίτερα απαιτητικά υπολογιστικά και χρονοβόρα, ειδικά όταν απαιτείται η μεταφορά του μακροπρόθεσμου κυματικού κλίματος από τα βαθιά σε πιο ρηχά νερά.

Στη συνέχεια, τονίζεται, ότι η πληροφορία σχετικά με τις συνθήκες της θάλασσας είναι ουσιαστική για τον σχεδιασμό των υπεράκτιων και παράκτιων έργων. Αυτό σημαίνει ότι η πληροφορία, σχετικά με τις πιο ακραίες θαλάσσιες συνθήκες που προβλέπονται να συμβούν κατά τη διάρκεια ζωής των έργων αυτών, δεν είναι η μόνη που είναι χρήσιμη για το σχεδιασμό. Εξίσου σημαντική πληροφορία είναι και αυτή, που σχετίζεται με τη συχνότητα εμφάνισης όλων των καταστάσεων της θάλασσας, η οποία μπορεί να χρησιμοποιηθεί για την εκτίμηση πιθανοτήτων ζημιάς και αστοχίας των κατασκευών ώστε να εξασφαλισθεί η ευστάθεια τους στη διάρκεια της ζωής τους.

Συνεχίζοντας, στο σημείο αυτό, η περιγραφή των θαλάσσιων καταστάσεων επιτυγχάνεται σε μεγάλο βαθμό με την πιθανοτική κατανομή του σημαντικού ύψους κύματος H_s , η οποία μπορεί να εκτιμηθεί από τη στατιστική ανάλυση δεδομένων που καλύπτουν δεκάδες χρόνια. Ισχύει, προφανώς, ότι όσο μεγαλύτερη είναι η χρονική περίοδος που καλύπτουν τα δεδομένα, τόσο πιο αξιόπιστη είναι και η περιγραφή του μακροπρόθεσμου κυματικού κλίματος, που εξάγεται από το εν λόγω σύνολο δεδομένων [10].

Ωστόσο, τις τελευταίες δεκαετίες έχει γίνει αποδεκτός και ο ρόλος άλλων κυματικών παραμέτρων, εκτός του H_s , στην ευστάθεια των παράκτιων και υπεράκτιων έργων (π.χ. [11],

[12]) και κατ' επέκταση στην εκτίμηση της αξιοπιστίας των κατασκευών αυτών. Συνεπώς, η πληροφορία σχετικά με τις μακροπρόθεσμες κυματικές στατιστικές έχει επεκταθεί σε σημαντικό βαθμό, συμπεριλαμβάνοντας τη μέση κυματική περίοδο T_m , και τη μέση ή κυρίαρχη κατεύθυνση θ_m , που αντιπροσωπεύουν μία θαλάσσια κατάσταση.

Επιπρόσθετα, όλες οι κρίσιμες περιβαλλοντικές παράμετροι, αλλά και η μεταξύ τους στατιστική συσχέτιση (εφόσον αυτή είναι σημαντική), θα πρέπει να λαμβάνονται υπόψη με δόκιμο τρόπο, κατά τον σχεδιασμό των παράκτιων κατασκευών. Ένα χαρακτηριστικό παράδειγμα στατιστικής συσχέτισης μεταξύ περιβαλλοντικών παραμέτρων είναι αυτή που παρατηρείται συνήθως μεταξύ της μέσης κυματικής περιόδου T_m , ή της περιόδου αιχμής T_p , με το σημαντικό ύψος κύματος H_s , και αυτή μεταξύ της περιόδου T και του ύψους κύματος H εντός μίας θαλάσσιας κατάστασης, όσον αφορά στις μακροπρόθεσμες και βραχυπρόθεσμες κυματικές στατιστικές, αντίστοιχα. Επίσης, έχει παρατηρηθεί και η επίδραση της κατεύθυνσης στις μακροπρόθεσμες κυματικές στατιστικές [13]. Επιπλέον, το σημαντικό ύψος κύματος και η διακύμανση της στάθμης της θάλασσας λόγω μετεωρολογικής παλίνρροιας, από την επίδραση βαρομετρικών συστημάτων και ισχυρών ανέμων, εμφανίζουν συχνά συσχέτιση σε μερικό βαθμό.

Προκειμένου να εκτιμηθεί η συνάρτηση της από κοινού πυκνότητας πιθανότητας των H_s και T_m , απαιτείται η εφαρμογή μοντέλων πιθανοτικών κατανομών δύο μεταβλητών, που λαμβάνουν υπόψη τη στατιστική συσχέτιση μεταξύ τους. Μία πρώτη προσέγγιση είχε προταθεί από τον Ochi [14], ο οποίος υιοθέτησε τη λογαριθμοκανονική πιθανοτική κατανομή για να αναπαραστήσει τα H_s και T_m , η οποία προέρχεται από μία εκθετική μετατροπή της κανονικής κατανομής δύο μεταβλητών. Αυτή η προσέγγιση, παρόλο που είναι εύκολη στην εφαρμογή, βασίζεται στην υπόθεση ότι οι λογάριθμοι των δεδομένων ακολουθούν κανονική κατανομή, και παρά το γεγονός ότι αυτό μπορεί να ισχύει για χαμηλές και μεσαίες τιμές του H_s , δεν ισχύει για υψηλές τιμές του H_s . Μία λογαριθμοκανονική καμπύλη δύο μεταβλητών με διόρθωση στην κύρτωση [15] ήταν μία προσπάθεια βελτίωσης του προαναφερόμενου μοντέλου. Επιπρόσθετα, ένα μοντέλο, που στηρίζεται στην περιθώρια κατανομή του H_s και τη δεσμευμένη κατανομή του T_p δεδομένου του H_s , θα μπορούσε να αυξήσει την ακρίβεια και την ευελιξία του, και υιοθετήθηκε από τον Haver [16], και τους Bitner-Gregersen and Haver [17]. Οι Guedes Soares et al. [18], Lucas and Guedes Soares [19], και Papanikolaou et al. [20] έχουν χρησιμοποιήσει ένα παρόμοιο μοντέλο στηριζόμενο στην περιθώρια κατανομή του H_s και τη δεσμευμένη κατανομή του T_m δεδομένου του H_s , το οποίο θα αναφέρεται στο εξής ως μοντέλο δεσμευμένης πιθανότητας. Άλλες προσεγγίσεις έχουν παράλληλα αναπτυχθεί για τον ίδιο σκοπό (π.χ. [21]). Ωστόσο, στις περιπτώσεις που εξετάστηκαν από τους Lucas and Guedes Soares [19] και Papanikolaou et al. [20], αποδείχθηκε ότι το μοντέλο

δεσμευμένης πιθανότητας ήταν ικανό να αναπαραστήσει με περισσότερη ακρίβεια τα δεδομένα των H_s και T_m από τα άλλα μοντέλα που εξέτασαν. Ως εκ τούτου, στην παρούσα διατριβή το εν λόγω μοντέλο χρησιμοποιείται για την εφαρμογή κατανομών των H_s και T_m στα διαθέσιμα δεδομένα.

Όσον αφορά στη βραχυπρόθεσμη πιθανοτική αναπαράσταση των θαλάσσιων κυματισμών, ο Longuet-Higgins [22] ήταν ο πρώτος που την εισήγαγε, επεκτείνοντας την εργασία του Rice [23] πάνω στον ηλεκτρονικό θόρυβο, και υπολόγισε τη συνάρτηση από κοινού πυκνότητας πιθανότητας του ύψους H και της περιόδου κύματος T για κυματισμούς στενού ενεργειακού φάσματος. Ωστόσο, ένα μειονέκτημα του συγκεκριμένου μοντέλου ήταν η συμμετρία της από κοινού κατανομής των H και T γύρω από μία αδιάστατη χαρακτηριστική περίοδο. Αργότερα, ο Longuet-Higgins [24] αναδιατύπωσε τη θεωρία του [22], λαμβάνοντας υπόψη την τάση των κυματισμών με μικρή περίοδο να συνδυάζονται με μικρά ύψη, ενώ των κυματισμών με μεγάλα ύψη να συνδέονται με μεγάλες περιόδους. Άλλοι ερευνητές που μελέτησαν τη συνάρτηση από κοινού πυκνότητας πιθανότητας των H και T για στενά φάσματα ήταν οι Cavanié et al. [25], Lindgren and Rychlik [26], και Shum and Melville [27].

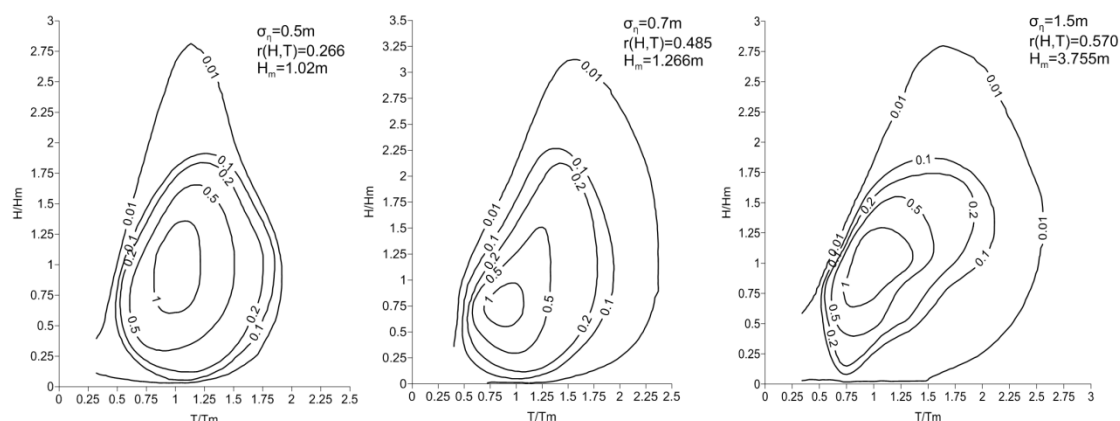
Αργότερα, ο Memos [28] αναθεώρησε τα υπάρχοντα αποτελέσματα και πρότεινε θεωρητικές προσεγγίσεις της συνάρτησης από κοινού πυκνότητας πιθανότητας των H και T , οι οποίες αφορούσαν σε στενά και ευρέα φάσματα κυματισμών και προσέφεραν μία πιο ρεαλιστική αναπαράσταση των θαλάσσιων κυματισμών από τις προσεγγίσεις που υπέθεταν μόνο στενά φάσματα. Επιπρόσθετα, οι Memos and Tzanis [29], στηριζόμενοι στη θεωρητική προσέγγιση του Memos [28], παρήγαγαν αριθμητικά αποτελέσματα της βραχυπρόθεσμης από κοινού κατανομής των H και T για τα βαθιά νερά οπουδήποτε εύρους φάσματος. Οι παράμετροι που απαιτούνται για να προσδιορίσουν τη συνάρτηση από κοινού πυκνότητας πιθανότητας των H και T στα βαθιά νερά είναι ο συντελεστής συσχέτισης $r(H,T)$, ή η τυπική απόκλιση της ανύψωσης της ελεύθερης επιφάνειας και μία χαρακτηριστική παράμετρος κλίσης των κυματισμών. Οι Memos and Tzanis [30] έκαναν ορισμένες τροποποιήσεις και επεκτάσεις στην εργασία τους αυτή, διαχωρίζοντας τους κυματισμούς από-θάλασσας από τους υπόλοιπους θαλάσσιους ανεμογενείς κυματισμούς και εφάρμοσαν ένα κριτήριο θραύσης των κυματισμών στα βαθιά νερά.

Ο Πίνακας 1 περιέχει ενδεικτικές τιμές του μέσου ύψους κύματος H_m , με αντίστοιχες τιμές τυπικής απόκλισης της ανύψωσης της ελεύθερης επιφάνειας της θάλασσας σ_η , και με αντίστοιχες τιμές γραμμικού συντελεστή συσχέτισης $r(H,T)$ [31]. Ενδεικτικά, τρία γραφήματα που προέκυψαν από τη μεθοδολογία των Memos and Tzanis [30] και του Tzanis [31] απεικονίζονται στην Εικόνα 1. Ο Πίνακας 1 περιέχει τις τιμές του H_m , οι οποίες

αντιστοιχίζονται με συγκεκριμένες τιμές της ανύψωσης της ελεύθερης επιφάνειας της θάλασσας σ_η , και τιμές γραμμικού συντελεστή συσχέτισης $r(H,T)$ [31].

Πίνακας 1 Καταστάσεις της θάλασσας με συγκεκριμένες τιμές των σ_η , $r(H,T)$ and H_m [31]

Τυπική απόκλιση σ_η	Συντελεστής συσχέτισης $r(H,T)$	Μέσο ύψος κύματος H_m
0.5m	0.266	1.020m
0.6m	0.383	1.103m
0.7m	0.485	1.266m
1.0m	0.495	2.187m
1.5m	0.570	3.755m



Εικόνα 1 Συνάρτηση από κοινού πυκνότητας πιθανότητας των H/H_m και T/T_m στα βαθιά νερά για συγκεκριμένες τιμές των σ_η , H_m , $r(H,T)$ ([30], [31])

Πιο πρόσφατα, οι Chondros and Memos [32] επέκτειναν την εργασία των Memos and Tzaniis [30] που αφορούσαν τη συνάρτηση της από κοινού πυκνότητας πιθανότητας των H και T , λαμβάνοντας υπόψη τις μη γραμμικές αλληλεπιδράσεις των κυματισμών, και παρήγαγαν χαρακτηριστικές εικόνες συνάρτησης από κοινού πυκνότητας πιθανότητας των H και T στα ενδιάμεσα και ρηχά νερά για διάφορες εντάσεις των θαλάσσιων καταστάσεων, κατευθύνσεις πρόσπτωσης των κυματισμών, και κλίσεις πυθμένα, χρησιμοποιώντας ένα μοντέλο διάδοσης κυματισμών, τύπου Boussinesq. Σημειώνεται ότι στη μέθοδό τους [32], η κατευθυντικότητα των κυματισμών στα βαθιά νερά λήφθηκε υπόψη, μέσω μίας θεωρητικής έκφρασης υποθέτοντας ανεξαρτησία των H και T από το θ . Στη συνέχεια, η συνάρτηση από κοινού πυκνότητας πιθανότητας των H , T και της κατεύθυνσης των κυματισμών θ στα βαθιά νερά μετατράπηκε σε μία χρονοσειρά ανύψωσης της ελεύθερης επιφάνειας της θάλασσας, ώστε να

χρησιμοποιηθεί από το μοντέλο Boussinesq για την εκτίμηση της συνάρτησης από κοινού πυκνότητας πιθανότητας των H , T και θ σε πιο ρηγά νερά.

2. Κίνητρο, στόχοι και καινοτόμα σημεία της διατριβής

Από τα παραπάνω, συμπεραίνεται ότι εξαιτίας της έλλειψης μακροπρόθεσμων περιβαλλοντικών δεδομένων (π.χ., μετρήσεις, παρατηρήσεις) στη θέση των παράκτιων έργων (που συνήθως συναντάται στα ενδιάμεσα νερά), παρατηρείται μία δυσκολία στην εκτίμηση της μακροπρόθεσμης πιθανοτικής αναπαράστασης των περιβαλλοντικών παραμέτρων στη θέση αυτή. Η πληροφορία αυτή, όπως προαναφέρθηκε, είναι πολύ ουσιαστική για τον σχεδιασμό των παράκτιων κατασκευών. Επιπλέον, η ανάγκη της σημερινής εποχής για την εκτίμηση της αξιοπιστίας των παράκτιων κατασκευών απαιτεί την ανάπτυξη και εφαρμογή μίας πολυπαραμετρικής πιθανοτικής μεθοδολογίας που να χρησιμοποιεί τη συνάρτηση της από κοινού πυκνότητας πιθανότητας των περιβαλλοντικών παραμέτρων φόρτισης των κατασκευών αυτών.

Ως εκ τούτου, ο κύριος στόχος της παρούσας διδακτορικής διατριβής είναι η ανάπτυξη ενός στατιστικού μοντέλου κυματικής διάδοσης έτσι ώστε οι μακροπρόθεσμες κυματικές στατιστικές να μεταφέρονται από τα βαθιά σε πιο ρηγά νερά, δηλ. στη θέση των παράκτιων κατασκευών, και στη συνέχεια η χρησιμοποίηση της πληροφορίας αυτής σε μία πολυπαραμετρική πιθανοτική μεθοδολογία για την εκτίμηση της αξιοπιστίας των παράκτιων κατασκευών. Οι επιμέρους στόχοι καθώς και τα σημαντικότερα καινοτόμα σημεία της παρούσας διατριβής παρατίθενται παρακάτω:

- Η εφαρμογή μίας στατιστικής τεχνικής ώστε να επιτευχθεί μία σημαντική μείωση του όγκου δεδομένων στα βαθιά νερά χωρίς απώλεια των έντονων θαλάσσιων καταστάσεων και της ακρίβειας στον προσδιορισμό της συνάρτησης της από κοινού πυκνότητας πιθανότητας των H_s , T_m και θ_m .
- Η επέκταση της βραχυπρόθεσμης συνάρτησης της από κοινού πυκνότητας πιθανότητας των H και T στα βαθιά νερά για να ενσωματώσει την κατευθυντικότητα των κυματισμών μέσω της χρήσης μίας θεωρητικής σχέσης διασποράς κατευθυντικότητας που εξαρτάται από την κυματική περίοδο και θεωρεί τα H, T, θ εξαρτημένα πιθανοτικά.
- Η μεταφορά των βραχυπρόθεσμων κυματικών στατιστικών, π.χ. κάθε θαλάσσιας κατάστασης, από τα βαθιά σε πιο ρηγά νερά, μέσω μίας τεχνικής κύμα προς κύμα και της εφαρμογής ενός γραμμικού μοντέλου κυματικής διάδοσης.

- Η ολοκλήρωση των βραχυπρόθεσμων με τις μακροπρόθεσμες κυματικές στατιστικές στα ενδιάμεσα νερά με στόχο την εκτίμηση των μακροπρόθεσμων συναρτήσεων πυκνότητας πιθανότητας των H , T , θ και των H_s , T_m , θ_m στη θέση αυτή.
- Η χρησιμοποίηση της στατιστικής ανάλυσης στο σύνολο των θαλάσσιων καταστάσεων και της ανάλυσης ακραίων τιμών βασισμένη σε γεγονότα στην εκτίμηση της πιθανότητας αστοχίας των παράκτιων έργων στη διάρκεια της ζωής τους.
- Η ανάπτυξη μίας πολυπαραμετρικής ανάλυσης αξιοπιστίας μίας παράκτιας κατασκευής, συνδυάζοντας στοχαστικές μεταβλητές με μηδενικό και μη μηδενικό βαθμό επικινδυνότητας, η οποία θα αναφέρεται στο εξής ως μία συνδυασμένη ανάλυση χρονικά-ανεξάρτητων και –εξαρτώμενων μεταβλητών.
- Η ενσωμάτωση της συγκεκριμένης ανάλυσης αξιοπιστίας στο σχεδιασμό των παράκτιων κατασκευών, με αναφορά στο παράδειγμα των συμβατικών κυματοθραυστών με πρανή.

Επιπρόσθετα, σημειώνεται ότι πραγματοποιήθηκαν συγκρίσεις του μοντέλου που χρησιμοποιήθηκε [33], σε επίπεδο βραχυπρόθεσμων θαλάσσιων συνθηκών. Οι συγκρίσεις αυτές αφορούν τόσο τα βαθιά νερά, όπου οι εκτιμήσεις των Memos and Tzanis ([29], [30]) συγκρίθηκαν με πραγματικές μετρήσεις κυματισμών από ωκεανογραφικό πλωτήρα, όσο και τα ενδιάμεσα νερά, όπου οι εκτιμήσεις του γραμμικού μοντέλου διάδοσης συγκρίθηκαν με τα αποτελέσματα ενός γνωστού και εμπορικού μοντέλου Boussinesq (Mike 21 BW/ Mike powered by DHI). Οι συγκρίσεις αυτές ανέδειξαν την περιοχή εγκυρότητας και τους περιορισμούς εφαρμογής του μοντέλου που αναπτύχθηκε.

Στην επόμενη παράγραφο, θα παρουσιαστεί η μεθοδολογία, που υιοθετήθηκε στην παρούσα διατριβή, με έμφαση στα προαναφερόμενα καίρια και καινοτόμα σημεία της.

3. Μεθοδολογία προσέγγισης

Η συγκεκριμένη παράγραφος, η οποία στοχεύει στην περιγραφή της μεθοδολογίας προσέγγισης, έχει την εξής δομή: Αρχικά, θα παρουσιαστεί το γραμμικό μοντέλο κυματικής διάδοσης [33], που ολοκληρώνει με γρήγορο σχετικά τρόπο τις βραχυπρόθεσμες και τις μακροπρόθεσμες κυματικές στατιστικές από τα βαθιά στα ενδιάμεσα νερά. Το συγκεκριμένο μοντέλο θα μπορούσε να χρησιμοποιηθεί στην εκτίμηση του μακροπρόθεσμου κυματικού κλίματος στη θέση των παράκτιων κατασκευών, που παρατηρείται συνήθως στα ενδιάμεσα νερά. Στη συνέχεια, διερευνάται η ικανότητα του γραμμικού μοντέλου να μεταφέρει τη βραχυπρόθεσμη στατιστική πληροφορία από τα βαθιά στα ενδιάμεσα νερά, μέσω της

σύγκρισης των αποτελεσμάτων του με πραγματικές μετρήσεις για τα βαθιά και με τα αντίστοιχα αποτελέσματα ενός εμπορικού και αξιόπιστου μοντέλου τύπου Boussinesq (MIKE 21 BW/ Mike powered by DHI) για τα ενδιάμεσα νερά. Ακολουθεί η ανάλυση αξιοπιστίας μίας παράκτιας κατασκευής, με έμφαση στους συμβατικούς κυματοθραύστες με πρηνή (βλ. π.χ. [34], [35]). Τέλος, παρουσιάζονται χαρακτηριστικά παραδείγματα ανάλυσης αξιοπιστίας και σχεδιασμού συμβατικού κυματοθραύστη με πρηνή και ακολουθεί συζήτηση των αποτελεσμάτων τους.

3.1 Συνδυασμός βραχυπρόθεσμων και μακροπρόθεσμων κυματικών στατιστικών από τα βαθιά στα ενδιάμεσα νερά

Το μοντέλο στοχεύει στο συνδυασμό βραχυπρόθεσμων και μακροπρόθεσμων κυματικών στατιστικών από τα βαθιά στα ενδιάμεσα νερά και έχει αναπτυχθεί από τους Malliouri et al. [33]. Το συγκεκριμένο μοντέλο χρησιμοποιεί τη μακροπρόθεσμη πιθανοτική αναπαράσταση των H_s , T_m , θ_m στα βαθιά νερά, και μέσω της εφαρμογής των βραχυπρόθεσμων κυματικών στατιστικών για κάθε θαλάσσια κατάσταση στα βαθιά νερά, εκτιμάει τις μακροπρόθεσμες κυματικές στατιστικές σε πιο ρηγά νερά. Ειδικότερα, χρησιμοποιώντας α) δεδομένα/μετρήσεις H_s , T_m , θ_m στα βαθιά νερά, β) τις αδιάστατες πιθανοτικές εικόνες των Memos and Tzanis [29], and Tzanis [31] που αφορούν στα βαθιά νερά, γ) μία θεωρητική έκφραση για τη διασπορά κατευθυντικότητας κυματισμών προσαρμοσμένη σε μία στατιστική ανάλυση μεμονωμένων κυματισμών εντός κάθε θαλάσσιας κατάστασης, και δ) μία τροποποίηση της σχέσης του Battjes [36], η βραχυπρόθεσμη συνάρτηση της από κοινού πυκνότητας πιθανότητας των H , T , θ , εντός κάθε θαλάσσιας κατάστασης ή κυματικής καταιγίδας, δύναται να παραχθεί στα βαθιά νερά. Τότε, οι βραχυπρόθεσμες και μακροπρόθεσμες συναρτήσεις της από κοινού πυκνότητας πιθανότητας των H , T , θ θα μπορούσαν να εκτιμηθούν στα ενδιάμεσα νερά, όπως και η μακροπρόθεσμη συνάρτηση της από κοινού πυκνότητας πιθανότητας των H_s , T_m , θ_m , λαμβάνοντας υπόψη τη διάδοση κάθε μεμονωμένου κυματισμού από τα ανοιχτά προς τα πιο ρηγά νερά, σύμφωνα με τη γραμμική κυματική θεωρία.

3.1.1 Τεχνική μείωσης όγκου δεδομένων στα βαθιά νερά

Αρχικά, μπορεί να εφαρμοσθεί μία τεχνική μείωσης του όγκου δεδομένων για να προσαρμοστεί η ανάλυση στις υπολογιστικές δυνατότητες ενός κοινού υπολογιστή. Αυτή μπορεί να επιτευχθεί είτε 1) με τη μέθοδο της υπέρβασης κατωφλίου είτε 2) με τη μέθοδο του στρωματοποιούμενου τυχαίου δείγματος, ή 3) με συνδυασμό των μεθόδων (1) και (2). Η

πρώτη και η τρίτη μέθοδος ενδείκνυνται για την περιγραφή μεσαίων και ακραίων θαλάσσιων καταστάσεων, που αφορούν για παράδειγμα στον σχεδιασμό παράκτιων έργων. Ένας διαχωρισμός ανάμεσα στις δύο αυτές μεθόδους (1) και (3) μπορεί να γίνει με κριτήριο το μέγεθος των αρχικών δεδομένων, το οποίο εξαρτάται από τα έτη που καλύπτουν τα δεδομένα και το χρονικό βήμα ανάμεσα στις διαδοχικές μετρήσεις. Η δεύτερη μέθοδος ενδείκνυται για την περιγραφή θαλάσσιων καταστάσεων χαμηλής και μεσαίας έντασης.

3.1.2 Βραχυπρόθεσμες κυματικές στατιστικές στα βαθιά νερά

Αναφορικά με τις αδιαστατοποιημένες εικόνες των Memos and Tzanis [30] και Tzanis [31], που χρησιμοποιήθηκαν στην παρούσα διατριβή, ο Πίνακας 2 παρουσιάζει τις κλάσεις του H_m , οι οποίες θεωρήθηκαν [33] ότι αντιστοιχούν στην ίδια τυπική απόκλιση της ανύψωσης της ελεύθερης επιφάνειας της θάλασσας σ_η και τον συντελεστή γραμμικής συσχέτισης Pearson μεταξύ των H και T , $r(H,T)$. Ο Πίνακας 2 κατασκευάστηκε ώστε μία αδιάστατη πιθανοτική εικόνα των Memos and Tzanis [30] να αντιστοιχεί σε κάθε θαλάσσια κατάσταση. Επίσης, πιο ακραίες θαλάσσιες καταστάσεις από αυτές του Πίνακα 2 μπορούν να ληφθούν υπόψη με τον τρόπο αυτό, αλλά δεν παρουσιάζονται στην παρούσα διατριβή, καθώς εμφανίζονται σπάνια στη Μεσόγειο.

Πίνακας 2 Κλάσεις του H_m που αντιστοιχούν σε συγκεκριμένη τυπική απόκλιση της ανύψωσης της ελεύθερης επιφάνειας της θάλασσας και συντελεστή συσχέτισης μεταξύ H και T [33]

σ_η (m)	$r(H,T)$	H_m (m)
0.5	0.266	[0.1 - 1.062)
0.6	0.383	[1.062 - 1.185)
0.7	0.485	[1.185 - 1.727)
1.0	0.495	[1.727 - 2.971)
1.5	0.570	[2.971 - 4.368)

3.1.3 Θεώρηση κατευθυντικότητας κυματισμών σε μία ανάλυση κύμα προς κύμα

Στη συνέχεια, θα γίνει αναφορά στο τρόπο που κάθε μεμονωμένος κυματισμός συνδυάζεται με μία κατεύθυνση διάδοσης, εφόσον η μέση κατεύθυνση των κυματισμών είναι γνωστή εκ των προτέρων. Όπως είναι γνωστό, είναι συνήθης πρακτική η κατευθυντικότητα των κυματισμών να λαμβάνεται υπόψη σε μία φασματική ανάλυση, δηλ. στην ανάλυση στην

περιοχή των συχνοτήτων, σύμφωνα με τον ορισμό της κατευθυντικότητας. Ωστόσο, συχνά προκύπτει η ανάγκη να θεωρηθεί η κατευθυντική διασπορά των κυματισμών σε μία ανάλυση κύμα προς κύμα. Για να προχωρήσουμε σε μία τέτοια ανάλυση, οι ακόλουθες υποθέσεις θα πρέπει να ληφθούν αναφορικά με κάθε μία θαλάσσια κατάσταση:

- Τα μεγάλα ύψη κύματος H τείνουν να συνδυάζονται με κατευθύνσεις πιο κοντά στη μέση κατεύθυνση θ_m . Αυτό σημαίνει ότι τα κύματα αυτά παρουσιάζουν μικρότερη κατευθυντική διασπορά, ισχυρίζοντας ότι τα H και θ δεν είναι ανεξάρτητα. Η υπόθεση αυτή βρίσκεται σε συμφωνία με τον Tucker [37], ο οποίος απέδειξε ότι τα σωματίδια του νερού με υψηλότερες ταχύτητες παρουσιάζουν μικρότερο εύρος κατευθυντικής διασποράς γύρω από τη θ_m , σε σύγκριση με σωματίδια μικρότερων ταχυτήτων.

-Εφόσον το ολοκλήρωμα της συνάρτησης κατευθυντικότητας $D(f, \theta)$ ως προς το θ , από $-\pi$ έως π είναι μονάδα, η $D(f, \theta)$ θα μπορούσε να χρησιμοποιηθεί για τον υπολογισμό της δεσμευμένης συνάρτησης πυκνότητας πιθανότητας του θ για δεδομένη συχνότητα f , ή ισοδύναμα για δεδομένη περίοδο κύματος T .

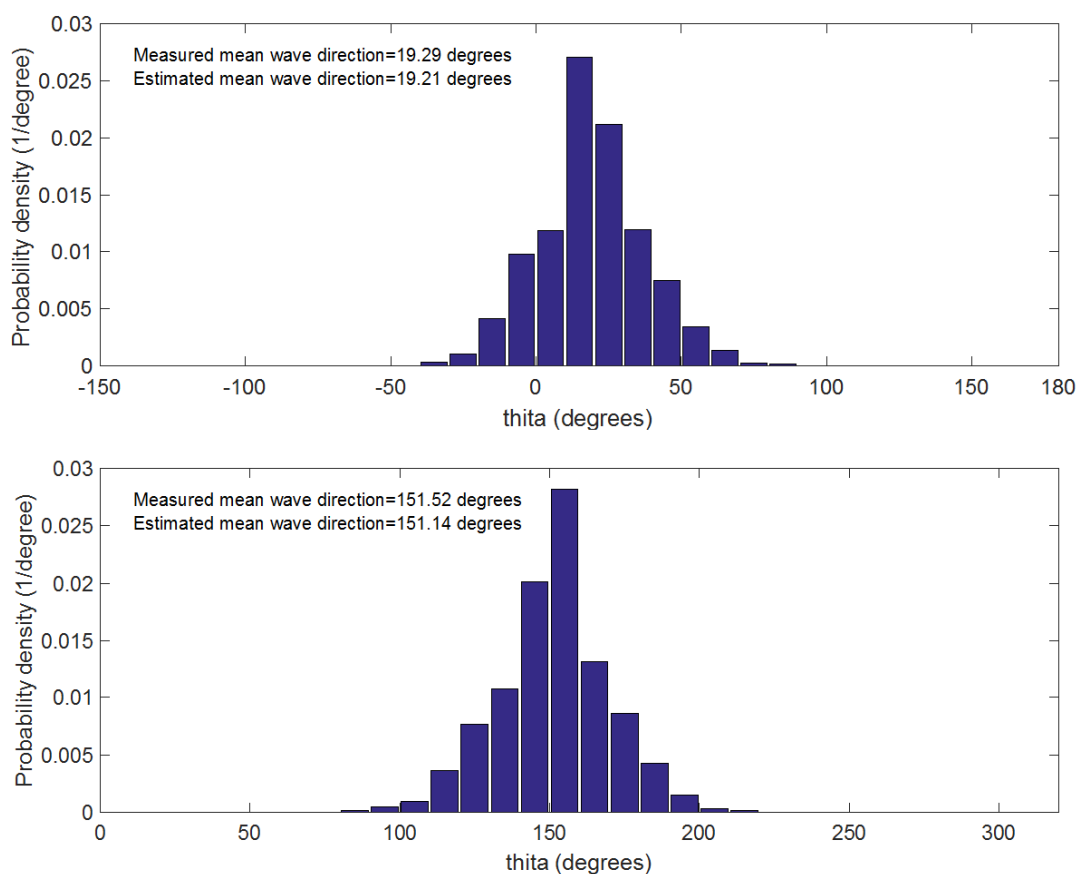
-Συνεπώς, στόχος είναι η εκτίμηση τους εύρους του θ που αντιστοιχεί σε μία κλάση του H , για δεδομένο T . Το εύρος αυτό μπορεί να υπολογιστεί, αρχικά τοποθετώντας όλες τις κλάσεις του H για δεδομένο T σε φθίνουσα σειρά ως προς το H , και ύστερα, μέσω της ακόλουθης εξίσωσης [33]:

$$\int_{\theta_m - x_j}^{\theta_m + x_j} D(f_i, \theta) d\theta = \sum_{n=1}^j \text{freq}(T_i, H_j) / N_i \quad (1)$$

όπου $\text{freq}(T_i, H_j)$ είναι η συχνότητα (ακέραιος αριθμός εμφάνισης) της από κοινού κλάσης του T_i και H_j , και N_i ο συνολικός ακέραιος αριθμός κυμάτων της κλάσης i του T για κάθε H . Επίσης, στην Εξίσωση 1, όπου η άγνωστη μεταβλητή είναι το x_j , η κλάση j του H αντιστοιχίζεται με ένα συγκεκριμένο εύρος του θ , δηλ. $[\theta_m - x_j, \theta_m + x_j]$, όταν η κλάση i της κυματικής συχνότητας f , ή ισοδύναμα του T , θεωρείται σταθερή. Σημειώνεται ότι το δεξί μέρος της εξίσωσης καθορίζει την αθροιστική πιθανότητα της κλάσης j του H με βάση τη φθίνουσα σειρά κατάταξης της κεντρικής τιμής της κλάσης, ενώ το αριστερό μέρος προσδιορίζει την πιθανότητα που σχετίζεται με το συγκεκριμένο εύρος του θ .

-Συνεπώς, κάθε κλάση του H συνδυάζεται με ένα συγκεκριμένο εύρος του θ , για κάθε κλάση του T , και κατ' επέκταση, το ζεύγος T και H που χαρακτηρίζει κάθε μεμονωμένο κύμα μίας θαλάσσιας κατάστασης αντιστοιχεί σε ένα θ εντός του εύρους.

Η εγκυρότητα των παραπάνω υποθέσεων συμπεραίνεται από τα ιστογράμματα πυκνότητας πιθανότητας του θ , τα οποία είναι συμμετρικά γύρω από την μέση κατεύθυνση μίας θαλάσσιας κατάστασης θ_m και από τη σύγκριση της θ_m του ιστογράμματος με την θ_m των μετρήσεων στα βαθιά νερά. Όπως παρατηρείται στην Εικόνα 2, το ιστόγραμμα του θ είναι περίπου συμμετρικό γύρω από την εκτιμώμενη θ_m , η οποία προσεγγίζει ικανοποιητικά την αντίστοιχη μέτρηση.



Εικόνα 2 Εκτιμώμενα ιστογράμματα της κατεύθυνσης των κυματισμών στα βαθιά νερά με διαφορετικές μέσες κατευθύνσεις [33]

3.1.4 Διάδοση κάθε μεμονωμένου κυματισμού από τα βαθιά στα ενδιάμεσα νερά

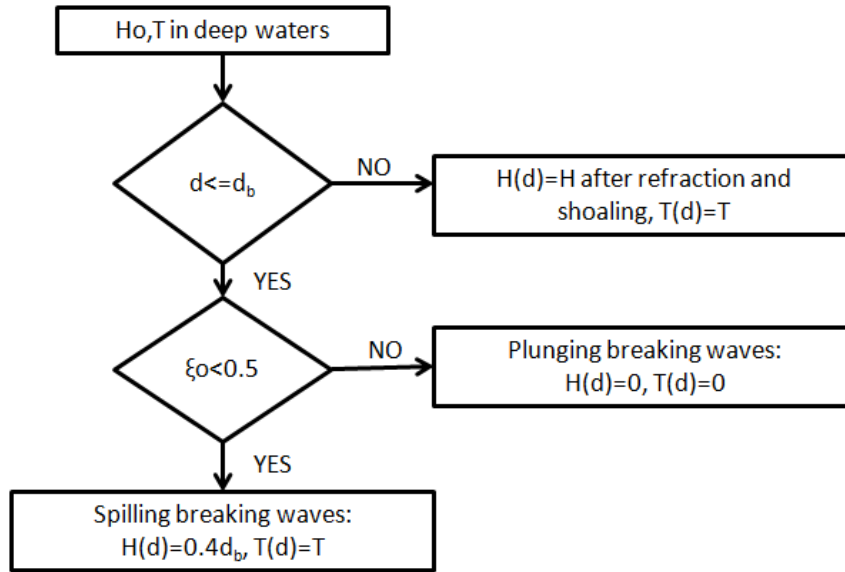
Στην προσέγγιση που ακολουθείται, κάθε μεμονωμένος κυματισμός, καθώς διαδίδεται από τα

βαθιά προς τα ενδιάμεσα νερά, υφίσταται μεταβολή του ύψους, του μήκους και της κατεύθυνσης του, ενώ η περίοδος του παραμένει σταθερή, σύμφωνα με τη γραμμική κυματική θεωρία. Στην παρούσα διατριβή, τέσσερις κυματικοί μηχανισμοί λαμβάνονται υπόψη: η ρήγωση, η διάθλαση, η θραύση, και ο ανασχηματισμός των κυμάτων μετά τη θραύση, ενώ η κλίση του πυθμένα θεωρείται ομοιόμορφη σε όλο το κυματικό πεδίο και ίση με τη μέση κλίση του πυθμένα της εξεταζόμενης περιοχής.

Ειδικότερα, το ύψος κύματος στη θραύση ενός μεμονωμένου κυματισμού καθορίστηκε από την ημι-εμπειρική έκφραση [38], ενώ το βάθος πυθμένα στο σημείο θραύσης υπολογίστηκε από την έκφραση του Weggel [39] με βάση τον δείκτη θραύσης, η οποία βασίστηκε σε εργαστηριακά πειράματα σε μονοχρωματικούς κυματισμούς σε ήπια κλίση πυθμένα. Η έννοια της θραύσης και της εξέλιξης του κυματισμού πριν, εντός, και μετά τη θραύση, που υιοθετήθηκε, παρουσιάζεται στην Εικόνα 3. Σύμφωνα με την Εικόνα 3, όταν ο κυματισμός θραύεται, γίνεται έλεγχος αν πρόκειται για θραύση τύπου “plunging” ή “spilling”. Ο διαχωρισμός αυτός γίνεται βάσει της καμπυλότητας του κυματισμού ξ_0 αναφερόμενης στα βαθιά νερά [40]. Στην πρώτη περίπτωση, ο κυματισμός μετά τη θραύση χάνει εντελώς την κυματομορφή του, ενώ στην περίπτωση της θραύσης τύπου “spilling”, η έννοια της εξέλιξης κατά τη θραύση βασίζεται στη μείωση της κυματικής ενέργειας και της ισοδυναμίας της τελευταίας με αυτή του υδραυλικού άλματος [41]. Ειδικότερα, οι Horikawa and Kuo [42] πραγματοποίησαν εργαστηριακά πειράματα σε θραυόμενους κυματισμούς και παρατήρησαν την ύπαρξη μίας σταθερής ροής ενέργειας, που προσδιορίζει μία κατάσταση όπου ο η θραύση του κυματισμού σταματάει. Χρησιμοποιώντας τη γραμμική κυματική θεωρία, και θεωρώντας ότι το σταθερό ύψος κύματος H_{stable} είναι γραμμική συνάρτηση του βάθους πυθμένα d , δηλ.:

$$H_{stable} = \Gamma d \quad (2)$$

όπου Γ είναι ένας αδιάστατος συντελεστής, ο οποίος τέθηκε ίσος με 0.4 [43].



Εικόνα 3 Περιγραφή της εξέλιξης κάθε μεμονωμένου κυματισμού κατά τη θραύση [33]

3.1.5 Τροποποίηση της σχέσης του Battjes [36]

Η γνώση της μακροπρόθεσμης συνάρτησης από κοινού πυκνότητας πιθανότητας των H και T είναι σημαντική για το σχεδιασμό των υπεράκτιων και παράκτιων κατασκευών, καθώς παρέχει πληροφορία για τα άμεσα φορτία που καταπονούν τις κατασκευές αυτές και δεν περιορίζεται στις χαρακτηριστικές τιμές που αντιπροσωπεύουν ένα σύνολο φορτίων. Η πληροφορία αυτή μπορεί να χρησιμοποιηθεί τόσο στον σχεδιασμό των κατασκευών αυτών αλλά και στην ανάλυση αξιοπιστίας και κοπώσεως τους [33]. Η μακροπρόθεσμη πιθανοτική κατανομή του H αναπτύχθηκε από τον Battjes [36], σαν ένα άθροισμα των στατιστικών όλων των βραχυπρόθεσμων θαλάσσιων καταστάσεων, λαμβάνοντας υπόψη τη συχνότητα εμφάνισης κάθε βραχυπρόθεσμης θαλάσσιας κατάστασης, και παρουσιάζεται παρακάτω:

$$f_{\text{long}}(H) = \frac{\iint f_{\text{short}}(H) \cdot f_{\text{long}}(T_m, H_s) \cdot N \, dH_s \, dT_m}{\iint N \cdot f_{\text{long}}(T_m, H_s) \, dH_s \, dT_m} \quad (3)$$

όπου $f_{\text{short}}(H)$ είναι η βραχυπρόθεσμη κατανομή του H , N είναι ο αριθμός των κυματισμών σε κάθε βραχυπρόθεσμη θαλάσσια κατάσταση που θεωρήθηκε σταθερός, και η $f_{\text{long}}(T_m, H_s)$ αντιστοιχεί στη μακροπρόθεσμη από κοινού κατανομή των H_s και T_m .

Στη συνέχεια, έγιναν δύο σταδιακές τροποποιήσεις της εξίσωσης (3) με στόχο την εκτίμηση της μακροπρόθεσμης από κοινού κατανομής των H και T , αλλά και των H, T, θ , οι οποίες περιγράφονται από τις Εξισώσεις 4 και 5:

$$f_{\text{long}}(T, H) = \frac{\iint f_{\text{short}}(T, H) \cdot f_{\text{long}}(T_m, H_s) \cdot N \, dH_s \, dT_m}{\iint N \cdot f_{\text{long}}(T_m, H_s) \, dH_s \, dT_m} \quad (4)$$

όπου $f_{\text{short}}(T, H)$ είναι η βραχυπρόθεσμη από κοινού κατανομή των T και H , N είναι ο αριθμός των κυματισμών σε κάθε βραχυπρόθεσμη θαλάσσια κατάσταση που θεωρήθηκε σταθερός, και η $f_{\text{long}}(T_m, H_s)$ αντιστοιχεί στη μακροπρόθεσμη από κοινού κατανομή των H_s και T_m .

$$f_{\text{long}}(T, H, \theta) = \frac{\iiint f_{\text{short}}(T, H, \theta) f_{\text{long}}(T_m, H_s, \theta_m) N \, dH_s \, dT_m \, d\theta_m}{\iiint N f_{\text{long}}(T_m, H_s, \theta_m) \, dH_s \, dT_m \, d\theta_m} \quad (5)$$

όπου $f_{\text{short}}(T, H, \theta)$ είναι η βραχυπρόθεσμη από κοινού κατανομή των T, H, θ , N είναι ο αριθμός των κυματισμών σε κάθε βραχυπρόθεσμη θαλάσσια κατάσταση ο οποίος θεωρήθηκε σταθερός, και $f_{\text{long}}(T_m, H_s, \theta_m)$ αντιστοιχεί στη μακροπρόθεσμη από κοινού κατανομή των T_m, H_s , και θ_m . Οι τροποποιήσεις της σχέσης του Battjes [36] βασίζονται στην ίδια λογική και έχουν αποδειχθεί από τους Malliouri et al. [33].

3.1.6 Παραδείγματα εφαρμογής

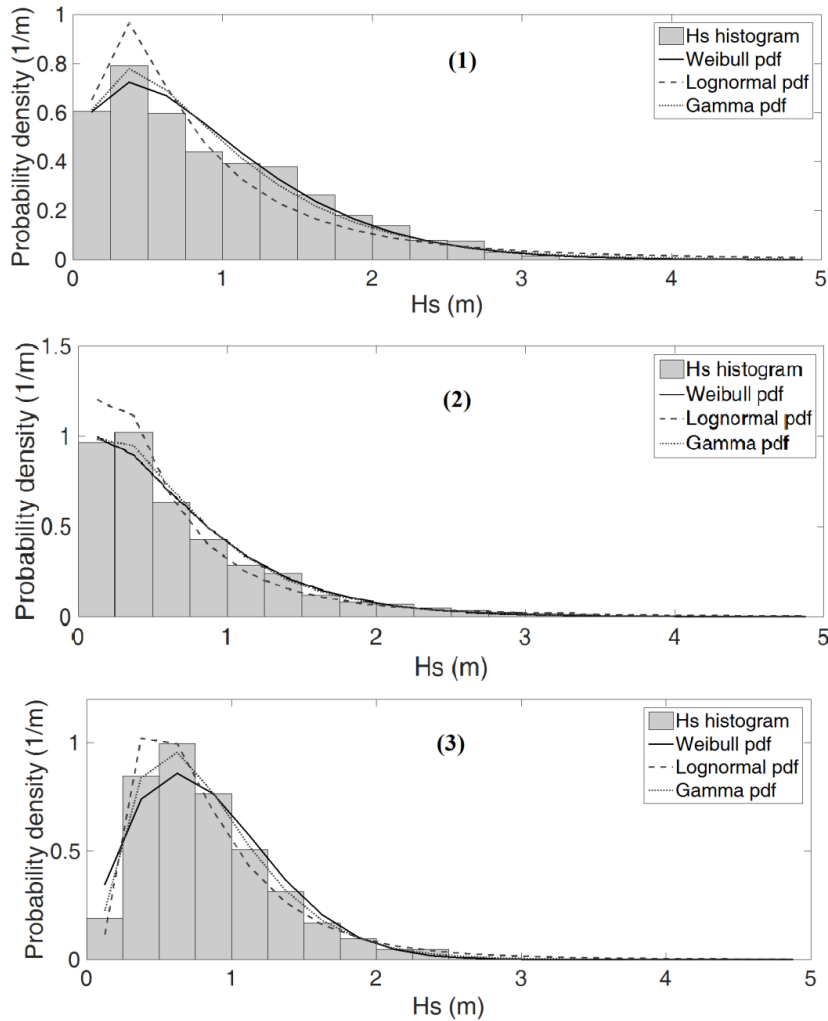
Η προαναφερόμενη μεθοδολογία εφαρμόστηκε σε μετρήσεις T_m, H_s , και θ_m , οι οποίες προήλθαν από 3 ωκεανογραφικούς πλωτήρες που ανήκουν στο σύστημα «ΠΟΣΕΙΔΩΝ» του Ελληνικού Κέντρου Θαλασσίων Ερευνών (ΕΛΚΕΘΕ) [44], [45]. Οι πλωτήρες είναι τοποθετημένοι σε τρεις θέσεις στα βαθιά νερά, δηλ. (37.51 °N, 25.46 °E) στο κεντρικό Αιγαίο στα ανοιχτά της Μυκόνου, (39.96 °N, 24.72 °E) στο βόρειο Αιγαίο στα ανοιχτά του Άθω και (36.25 °N, 25.49 °E) στο νότιο Αιγαίο στα ανοιχτά της Σαντορίνης. Οι τρεις θέσεις των

μετρητικών σταθμών θα αναφέρονται στο εξής σαν Σταθμός M, Σταθμός A, Σταθμός S, αντίστοιχα, και απεικονίζονται στην Εικόνα 4.



Εικόνα 4 Οι θέσεις των τριών μετρητικών σταθμών στο Αιγαίο (Ελλάδα)

Σχετικά με τις πιο κατάλληλες κατανομές για το H_s στα βαθιά νερά, τρεις υποψήφιες κατανομές εξετάστηκαν, ήτοι οι Weibull, Lognormal, και Gamma, και επιλέχθηκε αυτή που αναπαριστά καλύτερα τα δεδομένα για κάθε σταθμό. Οι υποψήφιες κατανομές για το H_s σε συνδυασμό με τα αντίστοιχα ιστογράμματα παρουσιάζονται στην Εικόνα 5. Επίσης, τα μέτρα καλής εφαρμογής (Ευκλείδεια απόσταση) των υποψήφιων περιθώριων κατανομών στα ιστογράμματα του H_s και των μοντέλων δεσμευμένης πιθανότητας στα βαθιά νερά για τους τρεις σταθμούς παρουσιάζονται στον Πίνακα 4.



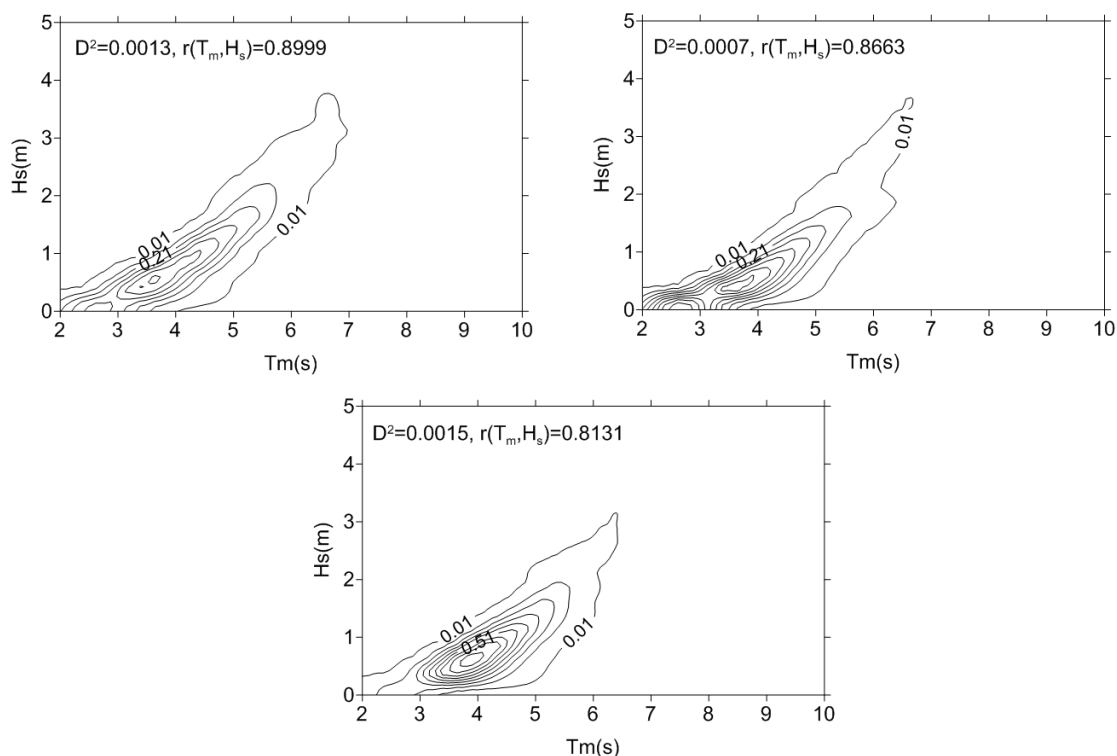
Εικόνα 5 Προσαρμογή των υποψήφιων περιθώριων κατανομών στα ιστογράμματα του H_s στα βαθιά νερά για τους σταθμούς M (1), A (2), και S (3) [33]

Πίνακας 4 Μέτρα καλής εφαρμογής των υποψήφιων περιθώριων κατανομών στα ιστογράμματα του H_s και στα μοντέλα δεσμευμένης πιθανότητας στα βαθιά νερά για τους σταθμούς M (1), A (2), και S (3) [33]

Πηγή δεδομένων	Υποψήφια pdf για το H_s	Ευκλείδεια απόσταση D^2 της $f(H_s)$	Δεσμευμένη pdf για την $T_m H_s$	Συνολική Ευκλείδεια απόσταση
Station M	Weibull	0.0019	Lognormal	0.0013
	Lognormal	0.0056	Lognormal	0.0021
	Gamma	0.0020	Lognormal	0.0013
Station A	Weibull	0.0018	Lognormal	0.0008
	Lognormal	0.0046	Lognormal	0.0014
	Gamma	0.0012	Lognormal	0.0007
Station S	Weibull	0.0039	Lognormal	0.0022

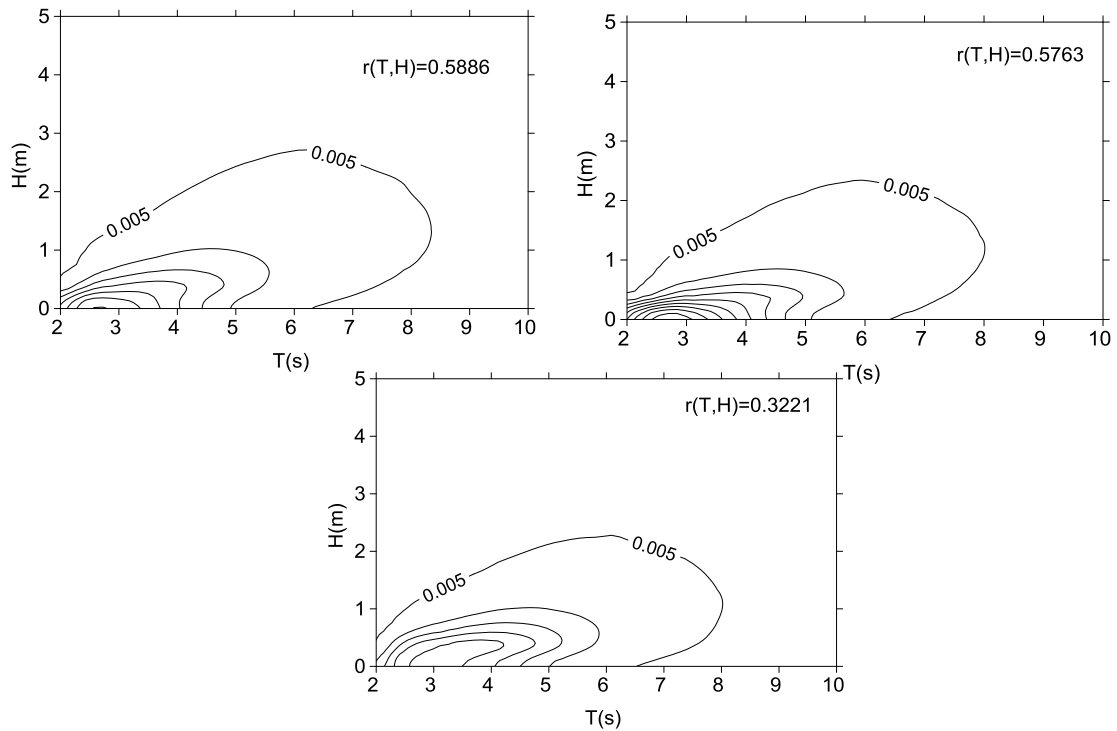
Lognormal	0.0033	Lognormal	0.0020
Gamma	0.0022	Lognormal	0.0015

Όπως φαίνεται στην Εικόνα 6 και στον Πίνακα 4, οι από κοινού πιθανοτικές κατανομές των T_m και H_s , που αναπαριστούν καλύτερα τα δεδομένα T_m και H_s εξήχθησαν από το μοντέλο δεσμευμένης πιθανότητας, το οποίο συνδέεται με την κατανομή Weibull για το H_s για τον σταθμό M και την κατανομή Gamma για το H_s για τους άλλους δύο σταθμούς και την κατανομή Lognormal για το $T_m|H_s$, αφού είχαν τη μικρότερη Ευκλείδεια Απόσταση σε σχέση με τις υπόλοιπες κατανομές που ελέγχθησαν.



Εικόνα 6 Μακροπρόθεσμες συναρτήσεις από κοινού πυκνότητας πιθανότητας των T_m και H_s στα βαθιά νερά για τον σταθμό M (πάνω αριστερά), σταθμό A (πάνω δεξιά), και τον σταθμό S (κάτω) - βήμα καμπύλης ίσης πυκνότητας πιθανότητας = $0.1 \text{ m}^{-1} \text{ s}^{-1}$ [33]

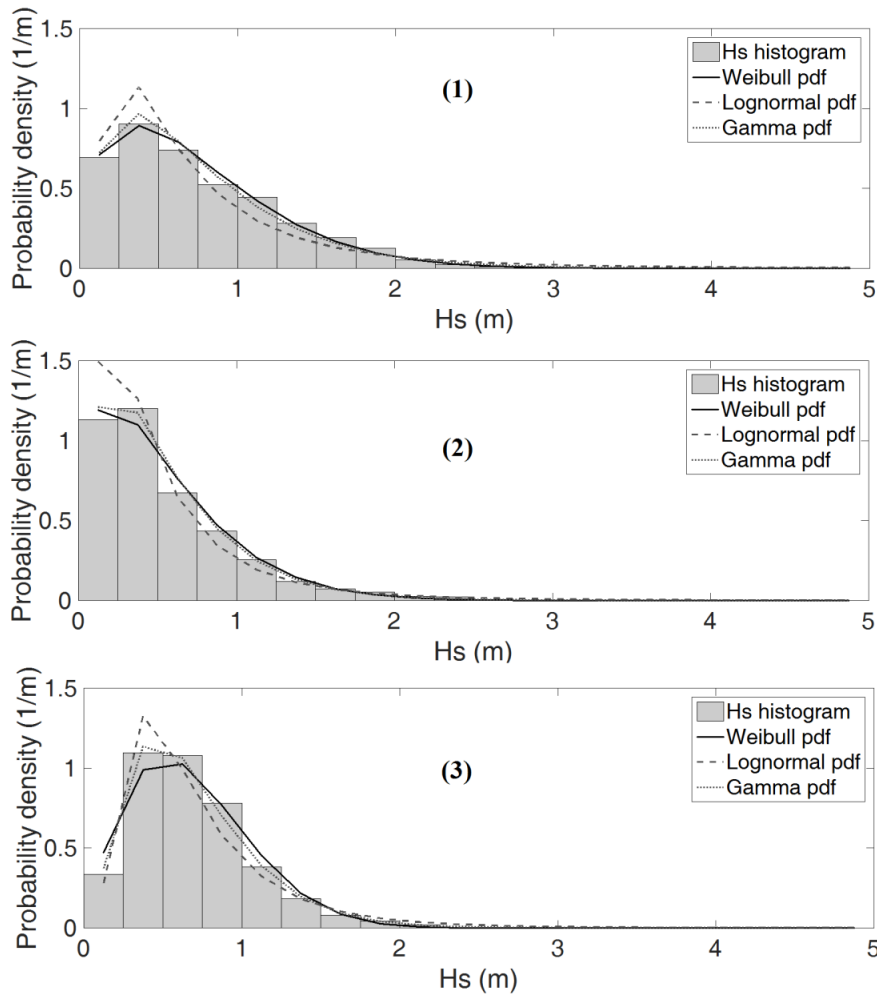
Εφαρμόζοντας τώρα την τροποποιημένη προσέγγιση του Battjes (βλ. Εξίσωση 4), προκύπτουν οι μακροπρόθεσμες συναρτήσεις από κοινού πυκνότητας πιθανότητας των T και H στα βαθιά νερά (βλ. Εικόνα 7). Όπως φαίνεται και από τις Εικόνες 6 και 7, η στατιστική συσχέτιση των T και H είναι μικρότερη από αυτή των T_m και H_s και για τους τρεις σταθμούς.



Εικόνα 7 Μακροπρόθεσμες συναρτήσεις από κοινού πυκνότητας πιθανότητας των T και H στα βαθιά νερά για τον σταθμό M (πάνω αριστερά), σταθμό A (πάνω δεξιά), και τον σταθμό S (κάτω) - βήμα καμπύλης ίσης πυκνότητας πιθανότητας = $0.1m^{-1}s^{-1}$ [33]

Στη συνέχεια, με χρήση της παραπάνω πιθανοτικής πληροφορίας για τα βαθιά νερά, οι μακροπρόθεσμες κυματικές στατιστικές μπορούν να εκτιμηθούν στα ενδιάμεσα νερά. Στην παράγραφο αυτή, οι μακροπρόθεσμες κυματικές στατιστικές θα εκτιμηθούν στο ενδιάμεσο βάθος των 6 m.

Σχετικά με τις πιο κατάλληλες κατανομές για το H_s στο βάθος των 6 m, οι ίδιες υποψήφιες κατανομές εξετάστηκαν για το H_s , όπως και στα βαθιά νερά. Οι υποψήφιες κατανομές για το H_s σε συνδυασμό με τα αντίστοιχα ιστογράμματα παρουσιάζονται στην Εικόνα 8. Επίσης, τα μέτρα καλής εφαρμογής (Ευκλείδεια απόσταση) των υποψήφιων περιθώριων κατανομών στα ιστογράμματα του H_s και των μοντέλων δεσμευμένης πιθανότητας στο βάθος των 6 m για τους τρεις σταθμούς παρουσιάζονται στον Πίνακα 5.

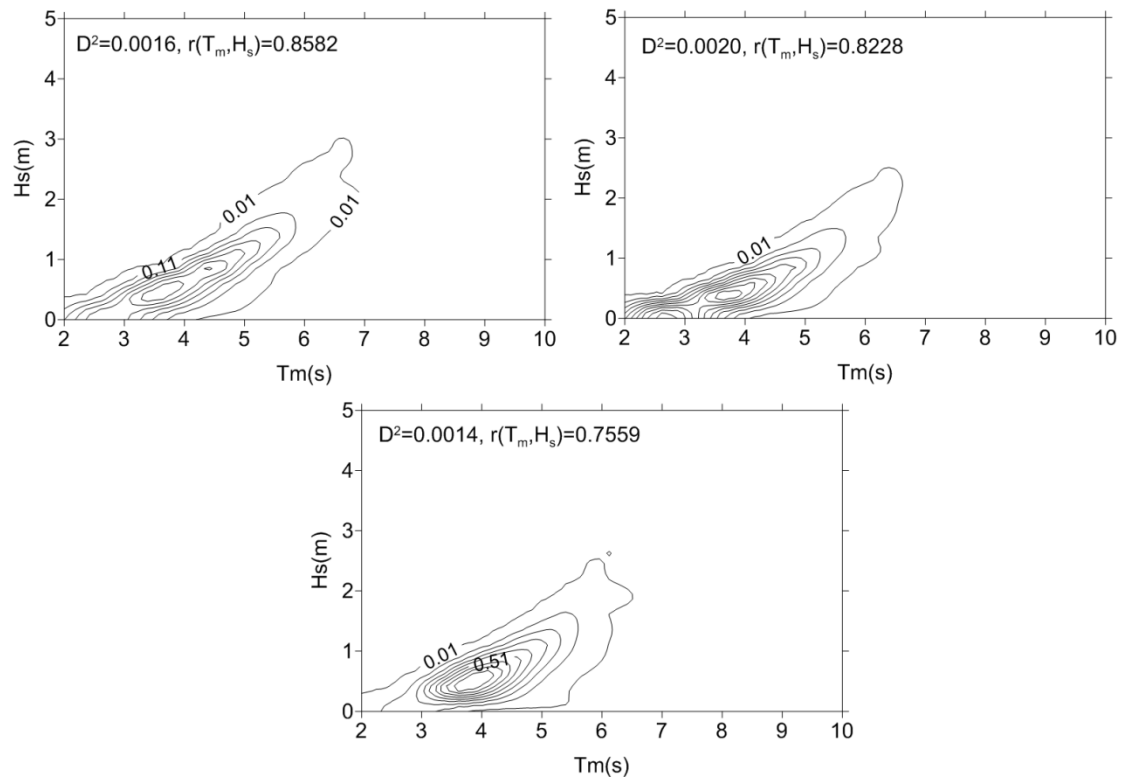


Εικόνα 8 Προσαρμογή των υποψήφιων περιθώριων κατανομών στα ιστογράμματα του H_s στο βάθος των 6 m για τους σταθμούς M (1), A (2), και S (3) [33]

Πίνακας 5 Μέτρα καλής εφαρμογής των υποψήφιων περιθώριων κατανομών στα ιστογράμματα του H_s και στα μοντέλα δεσμευμένης πιθανότητας στα 6 m βάθος για τους σταθμούς M (1), A (2), και S (3) [33]

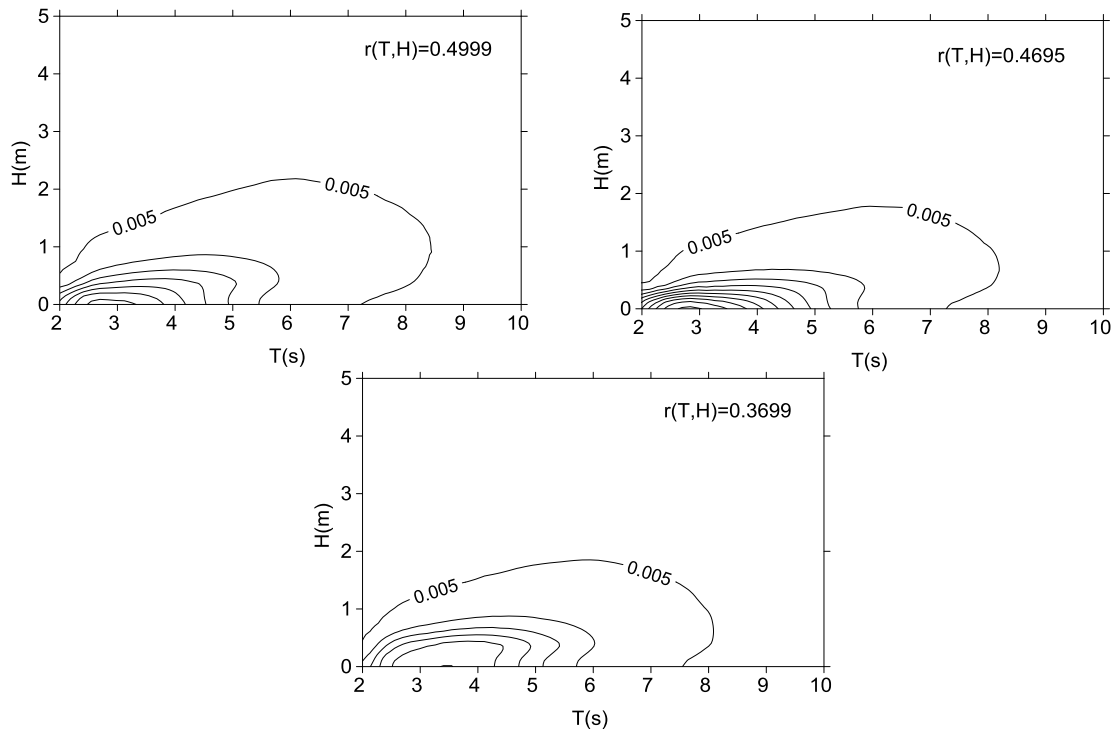
Πηγή δεδομένων	Υποψήφια pdf για το H_s	Ευκλείδεια απόσταση D^2 της $f(H_s)$	Δεσμευμένη pdf για την $T_m H_s$	Συνολική Ευκλείδεια απόσταση
Station M	Weibull	0.0009	Lognormal	0.0016
	Lognormal	0.0068	Lognormal	0.0026
	Gamma	0.0013	Lognormal	0.0017
Station A	Weibull	0.0033	Lognormal	0.0021
	Lognormal	0.0127	Lognormal	0.0035
	Gamma	0.0022	Lognormal	0.0020
Station S	Weibull	0.0026	Lognormal	0.0017
	Lognormal	0.0066	Lognormal	0.0023

Όπως φαίνεται στην Εικόνα 9 και στον Πίνακα 5, οι βέλτιστες από κοινού πιθανοτικές κατανομές των T_m και H_s στο βάθος των 6 m εξήχθησαν από το μοντέλο δεσμευμένης πιθανότητας, το οποίο συνδέεται με την κατανομή Weibull για το H_s για το σταθμό Μ και την κατανομή Gamma για το H_s για τους άλλους δύο σταθμούς και την κατανομή Lognormal για το $T_m|H_s$, σε συμφωνία με τις βέλτιστες κατανομές στα βαθιά νερά. Επίσης, οι επιλεγμένες από κοινού κατανομές για το βάθος των 6 m για κάθε σταθμό παρουσιάζονται στην Εικόνα 9.



Εικόνα 9 Μακροπρόθεσμες συναρτήσεις από κοινού πυκνότητας πιθανότητας των T_m και H_s στο ενδιάμεσο βάθος των 6 m για τον σταθμό Μ (πάνω αριστερά), σταθμό Α (πάνω δεξιά), και τον σταθμό S (κάτω) - βήμα καμπύλης ίσης πυκνότητας πιθανότητας = $0.1 \text{ m}^{-1} \text{ s}^{-1}$ [33]

Οι μακροπρόθεσμες συναρτήσεις από κοινού πυκνότητας πιθανότητας των T και H στο ενδιάμεσο βάθος των 6 m απεικονίζονται στην Εικόνα 10, όπου παρατηρείται ότι και στα ενδιάμεσα νερά η στατιστική συσχέτιση των T και H είναι μικρότερη από αυτή των T_m και H_s και για τους τρεις σταθμούς.



Εικόνα 10 Μακροπρόθεσμες συναρτήσεις από κοινού πυκνότητας πιθανότητας των T και H στο ενδιάμεσο βάθος των 6 m για τον σταθμό M (πάνω αριστερά), σταθμό A (πάνω δεξιά), και τον σταθμό S (κάτω) - βήμα καμπύλης ίσης πυκνότητας πιθανότητας $= 0.1 \text{ m}^{-1}\text{s}^{-1}$ [33]

3.2 Διερεύνηση της περιοχής έγκυρης εφαρμογής του μοντέλου [33]

Οι βραχυπρόθεσμες κυματικές στατιστικές, που λαμβάνονται υπόψη από το μοντέλο των Malliouri et al. [33], αποτελούνται από δύο μέρη. Συγκεκριμένα, το πρώτο μέρος αφορά την ανάλυση μίας θαλάσσιας κατάστασης σε τυχαίους κυματισμούς στα βαθιά νερά χρησιμοποιώντας την αντίστοιχη πιθανοτική πληροφορία για κάθε μία θαλάσσια κατάσταση, και το δεύτερο αφορά τη διάδοση της πιθανοτικής αυτής της πληροφορίας από τα βαθιά στα ενδιάμεσα νερά. Συνεπώς, η ανάδειξη της περιοχής εγκυρότητας του εν λόγω μοντέλου θα επιτευχθεί, ξεχωριστά για τα δύο αυτά μέρη, μέσω απαραίτητων συγκρίσεων με μετρήσεις ή αντίστοιχα αποτελέσματα άλλων αποδεκτών μοντέλων.

3.2.1 Συγκρίσεις στα βαθιά νερά

Σχετικά με την πιθανοτική πληροφορία μίας θαλάσσιας κατάστασης στα βαθιά νερά, η συνάρτηση από κοινού πυκνότητας πιθανότητας των H και T θα πρέπει να παραχθεί, π.χ. μέσω της θεωρητικής συνάρτησης των Longuet-Higgins [24] ή εναλλακτικά των Memos and Tzanis ([29];[30]), στην οποία ενσωματώνεται μία συνάρτηση διασποράς κατευθυντικότητας. Και οι δύο αυτές προσεγγίσεις αναφέρονται σε μη γραμμικούς ανεμογενείς κυματισμούς στα βαθιά νερά. Επίσης, και στις δύο μεθόδους, το ύψος κύματος H θεωρείται ως η υψομετρική

διαφορά της ανύψωσης της ελεύθερης επιφάνειας της θάλασσας από την κορυφή στην κοιλία, και η κυματική περίοδος T ως η κυματική περίοδος μηδενικής διάβασης. Όσον αφορά στη συνάρτηση από κοινού πυκνότητας πιθανότητας των H και T σύμφωνα με τον Longuet-Higgins [24], η οποία είναι κατάλληλη για στενά φάσματα, τα δεδομένα που χρειάζονται για τον σχηματισμό της είναι φασματικές παράμετροι, ήτοι η μηδενική ροπή του ενεργειακού φάσματος, η παράμετρος εύρους φάσματος και η μέση φασματική κυματική περίοδος. Ωστόσο, η συνάρτηση από κοινού πυκνότητας πιθανότητας των H και T των Memos and Tzanis ([29]; [30]) χρησιμοποιεί την τυπική απόκλιση της ανύψωσης της ελεύθερης επιφάνειας της θάλασσας, ή το μέσο ύψος κύματος από την ανάλυση στην περιοχή του χρόνου και παράγει αριθμητικά αποτελέσματα για κυματισμούς στα βαθιά νερά για φάσματα οποιουδήποτε εύρους. Ως εκ τούτου, εντοπίζονται μερικές διαφορές στις δύο προσεγγίσεις ως προς τα δεδομένα που χρησιμοποιούν και την περιοχή εγκυρότητας τους.

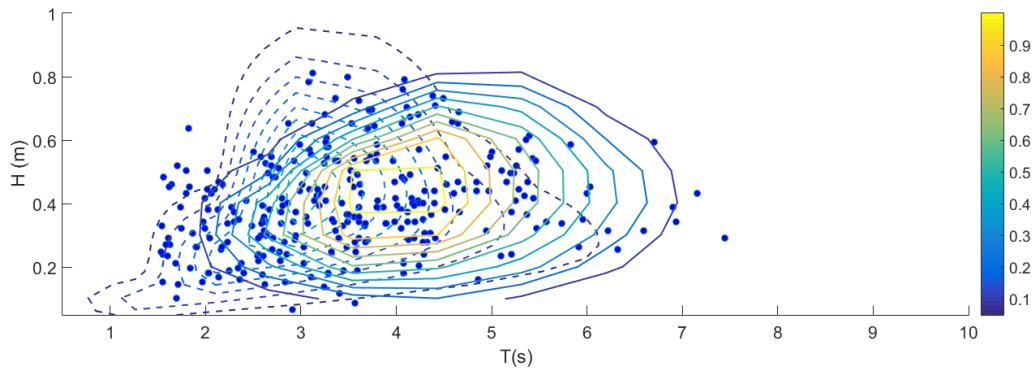
Εφόσον οι δύο μέθοδοι μπορούν να παράγουν διαστατοποιημένα γραφήματα από κοινού πυκνότητας πιθανότητας των H και T ίδιου τύπου, οι δύο μέθοδοι μπορούν να συγκριθούν μεταξύ τους και με κυματικές μετρήσεις στα βαθιά νερά. Οι τελευταίες προήλθαν από τον ωκεανογραφικό πλωτήρα - Σταθμός S (βλ. Εικόνα 4) και μετρούν την ανύψωση της ελεύθερης επιφάνειας της θάλασσας για το χρονικό διάστημα των 17 min ανά 1 Hz κάθε 3 hr.

Στη συνέχεια, μία μέθοδος ανάλυσης στην περιοχή του χρόνου, συγκεκριμένα η μέθοδος μηδενικής-άνω διάβασης, εφαρμόστηκε στη χρονοσειρά των μετρήσεων, ώστε να εκτιμηθούν τα T και H , τα οποία αντιστοιχούν σε κάθε κυματισμό που μετρήθηκε εντός του διαστήματος των 17 min. Επίσης, υπολογίστηκαν οι φασματικές παράμετροι του ίδιου συνόλου μετρήσεων μέσω φασματικής ανάλυσης.

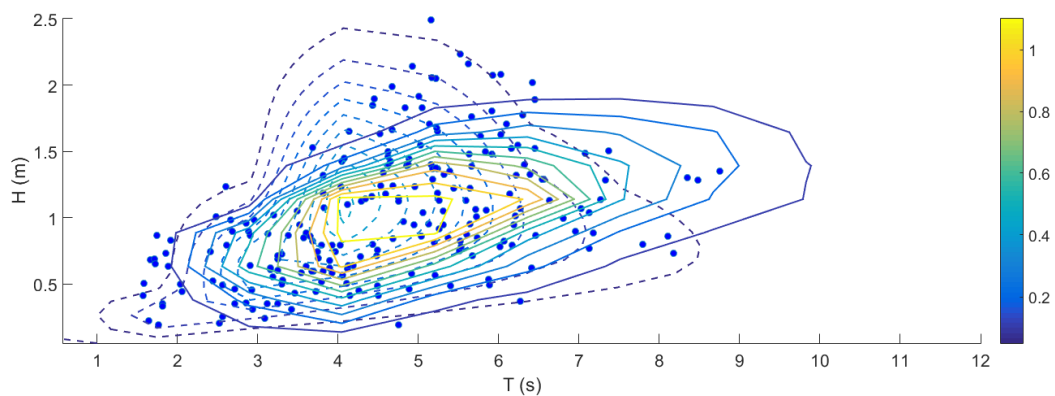
Στην παρούσα διατριβή, εξετάστηκαν τρεις θαλάσσιες καταστάσεις, οι οποίες παρουσιάζονται με αύξουσα σειρά ως προς την ένταση τους. Ειδικότερα, οι συγκρίσεις του διαγράμματος διασποράς των H και T στα βαθιά νερά του σταθμού S για τις τρεις θαλάσσιες καταστάσεις με τα αριθμητικά αποτελέσματα (από κοινού πυκνότητα πιθανότητας των H και T) κατά τον Longuet-Higgins [24] και των Memos and Tzanis [29] απεικονίζονται στις Εικόνες 11 - 13.

Επίσης, παράχθηκε ένας μεγάλος αριθμός τυχαίων δειγμάτων των H και T που αντιστοιχεί στη συνάρτηση από κοινού πυκνότητας πιθανότητας για κάθε μία από τις δύο μεθόδους. Οι στατιστικές κυματικές παράμετροι που εκπροσωπούν τα αποτελέσματα των δύο προσεγγίσεων (ήτοι οι μέσες τιμές από τα δείγματα) και αυτές που προέκυψαν από τις μετρήσεις παρουσιάζονται στον Πίνακα 6. Επιπρόσθετα, στον Πίνακα 7, παρουσιάζεται η σχετική διαφορά των αποτελεσμάτων των δύο μεθόδων από αυτά των μετρήσεων.

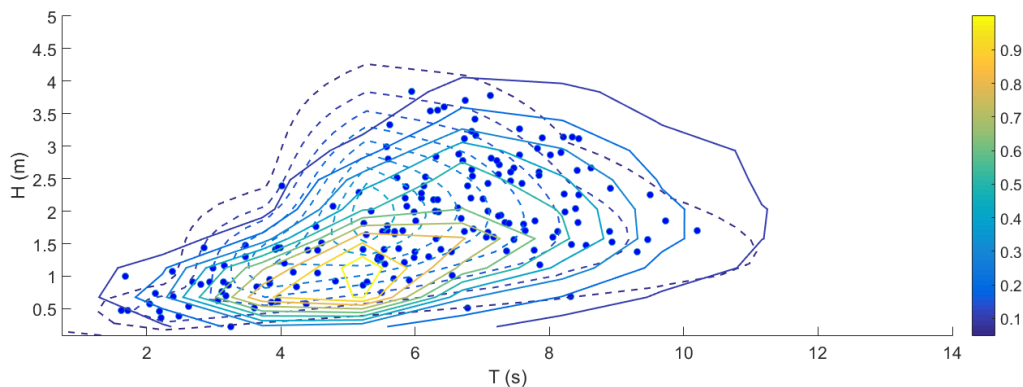
Σημειώνεται ότι οι παράμετροι εύρους φάσματος για τις τρεις θαλάσσιες καταστάσεις, που εξετάστηκαν, κυμαίνονται από 0.33 έως 0.40, και μεταξύ 0.53 και 0.72, αντίστοιχα.



Εικόνα 11 Συγκρίσεις στα βαθιά νερά μεταξύ των κυματικών μετρήσεων (μπλε σημεία) και των αποτελεσμάτων κατά τον Longuet-Higgins [24] (διακεκομμένες γραμμές) και κατά των Memos and Tzanis [29] (συνεχείς γραμμές) για τη θαλάσσια κατάσταση με $H_{1/3}=0.55$ m, $H_m=0.40$ m και $T_m=3.67$ s (βήμα καμπυλών ίσο με 0.05 1/m/s)



Εικόνα 12 Συγκρίσεις στα βαθιά νερά μεταξύ των κυματικών μετρήσεων (μπλε σημεία) και των αποτελεσμάτων κατά τον Longuet-Higgins [24] (διακεκομμένες γραμμές) και κατά των Memos and Tzanis [29] (συνεχείς γραμμές) για τη θαλάσσια κατάσταση με $H_{1/3}=1.56$ m, $H_m=1.01$ m και $T_m=4.62$ s (βήμα καμπυλών ίσο με 0.05 1/m/s)



Εικόνα 13 Συγκρίσεις στα βαθιά νερά μεταξύ των κυματικών μετρήσεων (μπλε σημεία) και των αποτελεσμάτων κατά τον Longuet-Higgins [24] (διακεκομμένες γραμμές) και κατά των Memos and Tzanis [29] (συνεχείς γραμμές) για τη θαλάσσια κατάσταση με $H_{1/3}=2.89$ m, $H_m=1.80$ m και $T_m=5.96$ s (βήμα καμπυλών ίσο με 0.05 1/m/s)

Πίνακας 6 Παράμετροι εύρους φάσματος των τριών θαλασσιών καταστάσεων και συγκρίσεις των στατιστικών κυματικών παραμέτρων μεταξύ μετρήσεων και αυτών που εκτιμήθηκαν από τις προσεγγίσεις

Θαλάσσια Κατάσταση	Δεδομένα/ Αποτελέσματα	Στατιστικές κυματικές παράμετροι			Παράμετροι εύρους φάσματος	
		$H_{1/3}$ (m)	H_m (m)	T_m (s)	ν	ϵ
1	Wave measurements	0.66	0.40	3.54	0.33	0.53
	L-H (1983)	0.76	0.53	3.08		
	M & T (1994)	0.57	0.38	3.90		
2	Wave measurements	1.56	1.01	4.62	0.37	0.65
	L-H (1983)	1.76	1.17	4.19		
	M & T (1994)	1.49	1.04	5.32		
3	Wave measurements	2.89	1.80	5.96	0.40	0.72
	L-H (1983)	2.98	1.96	5.44		
	M & T (1994)	2.86	1.72	6.50		

Πίνακας 7 Σχετική ποσοστιαία διαφορά μεταξύ των αποτελεσμάτων των δύο μεθόδων και αυτών που εξήχθησαν άμεσα από τις μετρήσεις

Θαλάσσια Κατάσταση	Δεδομένα/ Αποτελέσματα	Στατιστικές κυματικές παράμετροι			Παράμετροι εύρους φάσματος	
		$H_{1/3}$ (m)	H_m (m)	T_m (s)	ν	ϵ
1	L-H (1983)	15%	33%	-13%	0.33	0.53
	M & T (1994)	-14%	-5%	10%		
2	L-H (1983)	13%	16%	-9%	0.37	0.65
	M & T (1994)	-4%	3%	15%		
3	L-H (1983)	3%	9%	-9%	0.40	0.72
	M & T (1994)	-1%	-4%	9%		

Όπως παρατηρήθηκε από τις Εικόνες 11-13 και τους Πίνακες 6 και 7, τα αποτελέσματα των δύο προσεγγίσεων διαφέρουν μερικώς μεταξύ τους και με τις μετρήσεις για τις τρεις θαλάσσιες καταστάσεις, οι οποίες περιγράφονται από μη στενά φάσματα. Ειδικότερα, οι στατιστικές παράμετροι που αντιστοιχούν στα αποτελέσματα των Memos and Tzanis ([29]; [30]) προσεγγίζουν με μεγαλύτερη ακρίβεια τις μετρήσεις για τις περισσότερες περιπτώσεις που εξετάστηκαν, σε σύγκριση με του Longuet-Higgins [24]. Μία ευκρινής διαφορά μεταξύ των δύο προσεγγίσεων εντοπίστηκε στη μέση στατιστική κυματική περίοδο, η οποία αφορά στη συγκέντρωση της συνάρτησης της από κοινού πυκνότητας πιθανότητας των H και T κατά τον Longuet-Higgins [24] σε μία γειτονιά γύρω από μία χαρακτηριστική περίοδο (αυτό θα μπορούσε να σχετιστεί με την υπόθεση του στενού φάσματος), ενώ στη μέθοδο των Memos and Tzanis ([29]; [30]) οι κυματισμοί με μεγάλα H τείνουν να έχουν μεγάλες T σε μεγαλύτερο βαθμό από ότι στη μέθοδο του Longuet-Higgins.

3.2.2 Συγκρίσεις στα ενδιάμεσα νερά

Η περιοχή εφαρμογής της γραμμικής θεωρίας είναι ευρεία, καλύπτοντας σχεδόν όλα τα ενδιάμεσα βάθη πυθμένα για τις περισσότερες καμπυλότητες κυματισμών που συναντώνται στην πρακτική της θαλάσσιας μηχανικής και ακτοχημανικής. Στη συγκεκριμένη παράγραφο το γραμμικό μοντέλο κυματικής διάδοσης [33] θα εφαρμοστεί εντός και εκτός των ορίων εφαρμογής της γραμμικής θεωρίας, και θα συγκριθεί με ένα μοντέλο τύπου Boussinesq, από το πακέτο λογισμικό MIKE 21 BW της DHI. Οι συγκρίσεις θα πραγματοποιηθούν με βάση τις χαρακτηριστικές κυματικές παραμέτρους στην περιοχή του χρόνου και των διαγραμμάτων διασποράς του ύψους και της περιόδου κύματος εντός μίας θαλάσσιας κατάστασης.

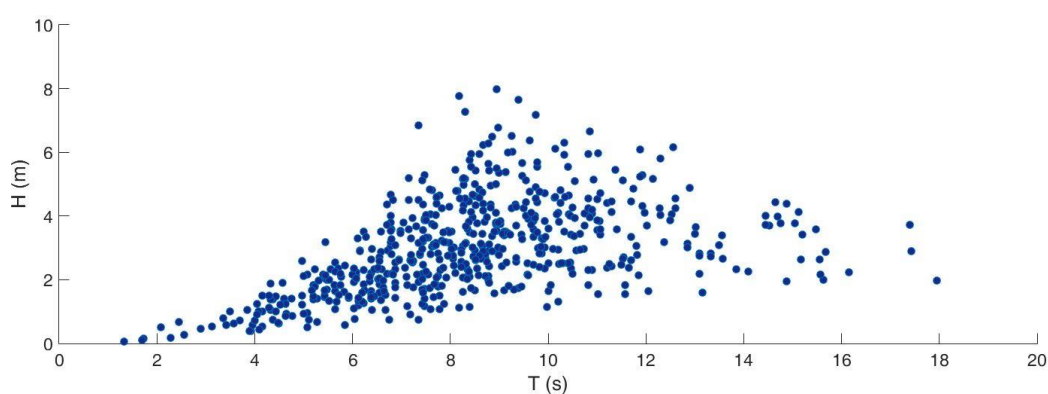
Το πακέτο λογισμικού MIKE 21 BW της DHI στηρίζεται στην αριθμητική επίλυση της διατύπωσης στην περιοχή του χρόνου των εξισώσεων τύπου Boussinesq σύμφωνα με τους Madsen et al. ([46]; [5]; [47]; [48]) και τους Sørensen and Sørensen [49] και Sørensen et al. [6]. Οι εξισώσεις αυτές καθιστούν τα μοντέλα κυματικής διάδοσης ικανά να προσομοιώνουν τη διάδοση μη γραμμικών κατευθυντικών κυματισμών από τα βαθιά στα ρηχά νερά.

Η μεθοδολογία, που υιοθετήθηκε για τη σύγκριση του μοντέλου [33] με το λογισμικό MIKE 21 BW (DHI), παρουσιάζεται παρακάτω. Αρχικά, σημειώνεται ότι στο συγκεκριμένο μοντέλο χρησιμοποιήθηκαν, ως δεδομένα εισόδου, η χρονοσειρά της ανύψωσης της ελεύθερης επιφάνειας, ενώ στο μοντέλο των Malliouri et al. [33] χρησιμοποιήθηκαν οι κυματισμοί όπως παράχθηκαν από την ανάλυση της χρονοσειράς στην περιοχή του χρόνου.

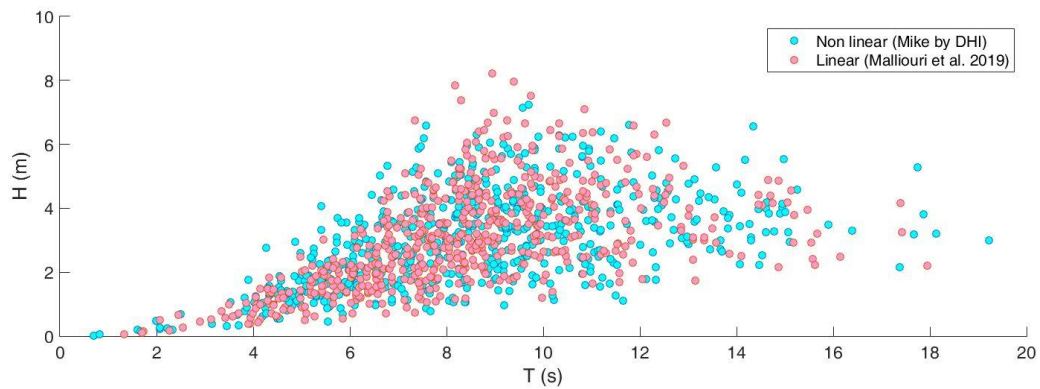
Εφόσον τα δύο μοντέλα θα πρέπει να συγκριθούν υπό κοινές υδραυλικές και οριακές συνθήκες, η ίδια βαθυμετρία και το διάγραμμα διασποράς των H και T χρησιμοποιήθηκαν σαν βάση για τα δύο μοντέλα. Επίσης, οι ίδιοι κυματικοί μετασχηματισμοί λήφθηκαν υπόψη, ήτοι η ρήγωση, η διάθλαση, η θραύση και ο ανασχηματισμός μετά τη θραύση των κυματισμών. Έπειτα, η ανύψωση της ελεύθερης επιφάνειας και οι κυματισμοί μεταφέρθηκαν σε πιο ρηχά νερά. Στη συνέχεια, εφαρμόζοντας τη μέθοδο άνω διάβασης στη χρονοσειρά ανύψωσης της ελεύθερης επιφάνειας, εκτιμήθηκαν το διάγραμμα διασποράς των T και H και οι χαρακτηριστικές κυματικές παράμετροι. Τα αποτελέσματα αυτά συγκρίθηκαν με εκείνα του γραμμικού μοντέλου διάδοσης.

Μία σχετικά έντονη θαλάσσια κατάσταση με κάθετη πρόσπτωση επιλέχθηκε, από τις άλλες 15 θαλάσσιες καταστάσεις που εξετάστηκαν, να παρουσιαστεί στην παρούσα διατριβή, εφόσον θεωρείται πιο σημαντική για το σχεδιασμό των παράκτιων έργων. Η κλίση πυθμένα θεωρήθηκε ίση με 0.10 και στα δύο μοντέλα. Ο χωρικός κάρναβος ήταν ομοιόμορφος με βήμα $\Delta x = \Delta y = 1$ m στις δύο οριζόντιες κάθετες διευθύνσεις x και y .

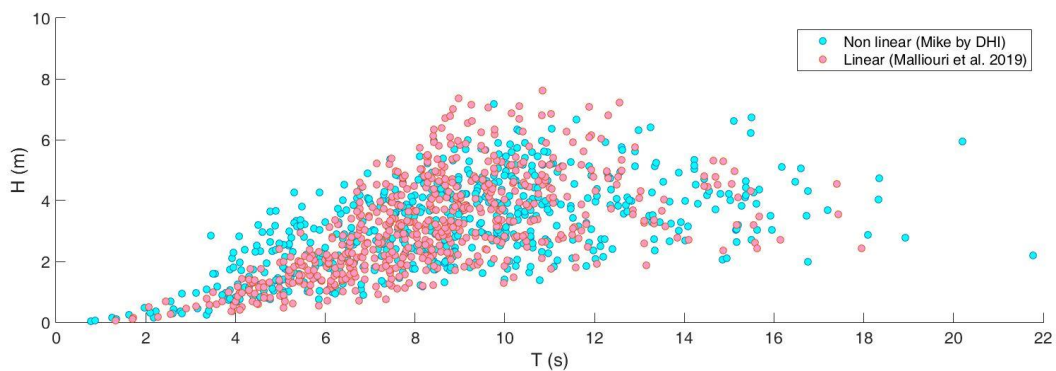
Στην Εικόνα 14 απεικονίζεται το διάγραμμα διασποράς των T και H των δύο μοντέλων στο βάθος των 20.95 m, και στις Εικόνες 15 - 18, τα αποτελέσματά τους για διάφορα ενδιάμεσα βάθη παρουσιάζονται και συγκρίνονται μεταξύ τους. Στον Πίνακα 8 οι χαρακτηριστικές παράμετροι από την ανάλυση στην περιοχή του χρόνου των δύο μοντέλων παρουσιάζονται και συγκρίνονται μεταξύ τους, ενώ στον Πίνακα 9 παρουσιάζεται η σχετική διαφορά των παραμέτρων του γραμμικού μοντέλων ως προς αυτών του μη γραμμικού μοντέλου.



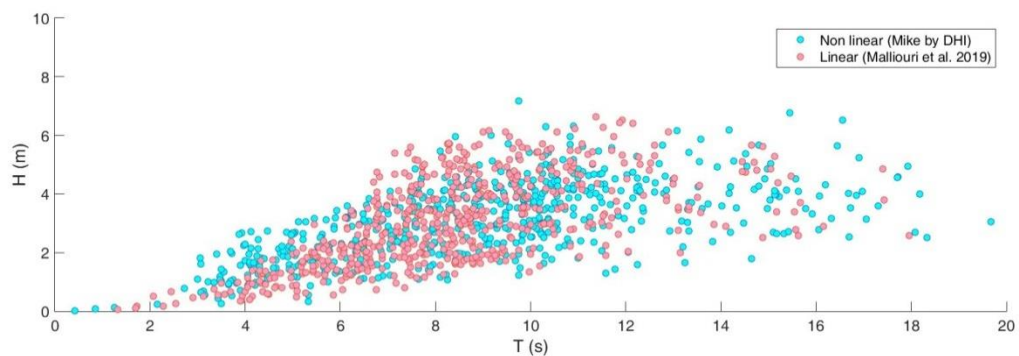
Εικόνα 14 Διάγραμμα διασποράς των T και H που χρησιμοποιήθηκε από τα δύο μοντέλα στο βάθος των 20.95 m



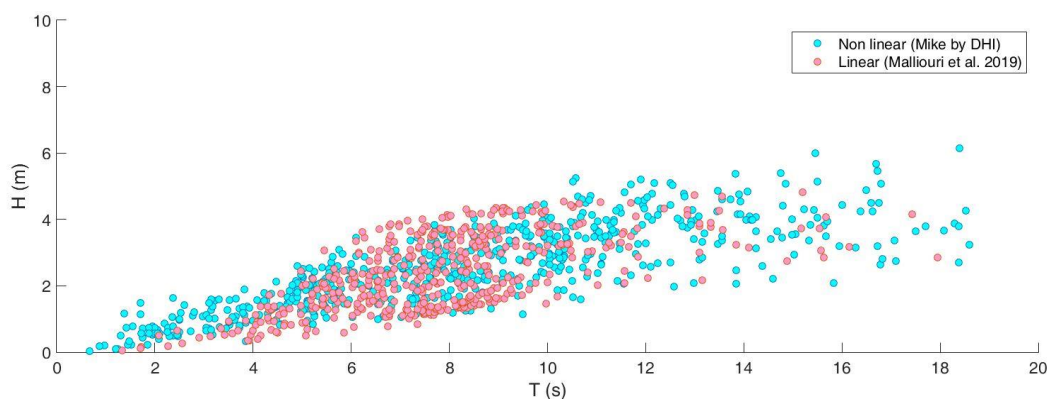
Εικόνα 15 Σύγκριση διαγράμματος διασποράς των T και H του μη γραμμικού μοντέλου (Mike by DHI) με αυτό του γραμμικού μοντέλου διάδοσης στο ενδιάμεσο βάθος των 11.80 m



Εικόνα 16 Σύγκριση διαγράμματος διασποράς των T και H του μη γραμμικού μοντέλου (Mike by DHI) με αυτό του γραμμικού μοντέλου διάδοσης στο ενδιάμεσο βάθος των 7.60 m



Εικόνα 17 Σύγκριση διαγράμματος διασποράς των T και H του μη γραμμικού μοντέλου (Mike by DHI) με αυτό του γραμμικού μοντέλου διάδοσης στο ενδιάμεσο βάθος των 5.70 m



Εικόνα 18 Σύγκριση διαγράμματος διασποράς των T και H του μη γραμμικού μοντέλου (Mike by DHI) με αυτό του γραμμικού μοντέλου διάδοσης στο ενδιάμεσο βάθος των 3.80 m

Κρίνοντας από τα διαγράμματα διασποράς των T και H, τα οποία παρουσιάστηκαν στις παραπάνω εικόνες, οι συγκρίσεις των δύο μοντέλων (γραμμικό v.s. μη γραμμικό) δείχνουν καλή συμφωνία στα περισσότερα ενδιάμεσα βάθη που εξετάστηκαν. Μεγαλύτερες αποκλίσεις μεταξύ των δύο μοντέλων παρατηρήθηκαν στα πιο ρηχά ενδιάμεσα βάθη που εξετάστηκαν (δηλ. στο βάθος των 3.80 m) εξαιτίας των μη γραμμικών αλληλεπιδράσεων των κυματισμών και της θραύσης, οι οποίες είναι πιο έντονες κοντά στην ακτή.

Στους Πίνακες 8 και 9, οι χαρακτηριστικές παράμετροι των αποτελεσμάτων του πακέτου λογισμικού MIKE 21 BW συγκρίνονται με αυτές του μοντέλου των Malliouri et al. [33]. Σημειώνεται ότι εκτός του μέσου ύψους κύματος H_m , του σημαντικού ύψους κύματος $H_{1/3}$, και της μέσης κυματικής περιόδου T_m , παρουσιάζονται, επίσης, το μέσο μήκος κύματος L_m , που εκτιμήθηκε από τη γραμμική εξίσωση διασποράς σε όρους T_m , η μέση καμπυλότητα s_m ($H_{1/3}/L_m$), η οποία εκτιμήθηκε σε όρους $H_{1/3}$ και L_m , και ο αριθμός Ursell, U_r ($(H_{1/3} * L_m^2 / d^3)$) που επίσης εκτιμήθηκε σε όρους $H_{1/3}$ και L_m .

Πίνακας 8 Σύγκριση των χαρακτηριστικών παραμέτρων των αποτελεσμάτων του πακέτου λογισμικού MIKE 21 BW με τις αντίστοιχες παραμέτρους του μοντέλου των Malliouri et al. [33] για κάθετη πρόσπτωση

Model	depth (m)	H_m (m)	$H_{1/3}$ (m)	T_m (s)	L_m (m)	s_m	U_r
MIKE BW	20.95	2.99	4.63	8.40	96.61	$4.79 * 10^{-2}$	4.70
Malliouri et al. 2019	20.95	2.99	4.63	8.40	96.61	$4.79 * 10^{-2}$	4.70
MIKE BW	11.80	3.05	4.69	8.62	82.83	$5.66 * 10^{-2}$	18.36
Malliouri et al. 2019	11.80	3.07	4.81	8.40	80.20	$6.01 * 10^{-2}$	18.83
MIKE BW	7.60	3.17	4.73	8.84	71.33	$6.63 * 10^{-2}$	54.82
Malliouri et al. 2019	7.60	3.15	4.82	8.40	67.27	$7.17 * 10^{-2}$	49.68

MIKE BW	5.70	3.10	4.51	8.97	63.88	$7.06 \cdot 10^{-2}$	99.37
Malliouri et al. 2019	5.70	3.07	4.60	8.39	59.35	$7.75 \cdot 10^{-2}$	89.85
MIKE BW	3.80	2.59	3.96	8.36	49.18	$8.05 \cdot 10^{-2}$	174.52
Malliouri et al. 2019	3.80	2.39	3.68	7.81	45.69	$8.06 \cdot 10^{-2}$	139.97

Πίνακας 9 Σχετική διαφορά των χαρακτηριστικών παραμέτρων των αποτελεσμάτων του μοντέλου των Malliouri et al. [33] ως προς αυτών του MIKE 21 BW για κάθετη πρόσπτωση

d (m)	d/L_m	H_m	H_{1/3}	T_m	L_m	s_m	U_r
11.80	0.22	0.01	0.03	-0.03	-0.03	0.06	0.03
7.60	0.14	-0.01	0.02	-0.05	-0.06	0.08	-0.09
5.70	0.11	-0.01	0.06	-0.07	-0.07	0.10	-0.10
3.80	0.09	-0.08	-0.07	-0.07	-0.07	0.00	-0.20

Όπως εκτιμήθηκε από τους Πίνακες 8 και 9, στα πιο βαθιά ενδιάμεσα νερά (συγκεκριμένα στα βάθη των 11.40 m, 7.60 m, 5.70 m) το H_m , το οποίο εκτιμήθηκε από το γραμμικό μοντέλο διάδοσης κυματισμών, είναι πιο κοντά με αυτό του μη γραμμικού μοντέλου σε σχέση με πιο ρηγά νερά. Οι συγκρίσεις που αφορούν στις υπόλοιπες παραμέτρους είναι εν γένει ικανοποιητικές. Ωστόσο, μεγαλύτερες διαφορές παρατηρούνται στα T_m και L_m , ενώ ακόμα μεγαλύτερες στα s_m και U_r . Όπως ήταν αναμενόμενο, οι αποκλίσεις μεταξύ των παραμέτρων των δύο μοντέλων γίνονται πιο έντονες, όταν οι κυματισμοί εισέρχονται σε πιο ρηγά νερά.

Στην παρούσα διατριβή, εξετάστηκαν, επίσης, και θαλάσσιες καταστάσεις με πλάγια πρόσπτωση. Όσον αφορά την πλάγια πρόσπτωση, παρόμοιες παρατηρήσεις θα μπορούσαν να εξαχθούν όπως με την κάθετη πρόσπτωση, σχετικά με τις παραμέτρους H_m , $H_{1/3}$, T_m , L_m , s_m , U_r . Σχετικά με τη θ_m στην πλάγια πρόσπτωση, παρατηρήθηκε ότι, όσο η γωνία σε σχέση με την κάθετη πρόσπτωση αυξάνεται, η θ_m του γραμμικού μοντέλου διαφέρει σε μεγαλύτερο βαθμό από αυτή που προέκυψε από το πακέτο λογισμικού MIKE 21 BW, ενώ οι υπόλοιπες παράμετροι έδειξαν καλύτερη συμφωνία. Οι διαφορές, σε ένα βαθμό, των δύο μοντέλων ως προς τη θ_m , θα μπορούσαν να αποδοθούν στο γεγονός ότι αυτή αφορά μία στατιστική παράμετρο στην περίπτωση του γραμμικού μοντέλου των Malliouri et al. [33], ενώ στην περίπτωση του MIKE 21 BW η παράμετρος αυτή είναι φασματική και προσδιορίζεται ως η μέση κατεύθυνση του κατευθυντικού φάσματος.

3.3 Ανάλυση αξιοπιστίας συμβατικού κυματοθραύστη με πρανή

Στην παρούσα παράγραφο, παρουσιάζεται μία πλήρως πιθανοτική μεθοδολογία με στόχο την εκτίμηση της αξιοπιστίας των παράκτιων κατασκευών, όπως οι συμβατικοί κυματοθραύστες με πρηνή, βάσει της πιθανοτικής αναπαράστασης παραμέτρων φόρτισης και αντίστασης. Σημειώνεται ότι ένα από τα καινοτόμα σημεία και αντικείμενα της παρούσας διατριβής είναι η εκτίμηση της πιθανότητας αστοχίας των κατασκευών με βάση το μακροπρόθεσμο κυματικό κλίμα στη θέση των έργων, η οποία συνήθως βρίσκεται στα ενδιάμεσα νερά, χρησιμοποιώντας παρατηρήσεις ή μετρήσεις κυματισμών σε πιο βαθιά νερά. Αυτό επιτυγχάνεται μέσω της εφαρμογής ενός στατιστικού μοντέλου κυματικής διάδοσης με στόχο η συνάρτηση από κοινού πυκνότητας πιθανότητας όλων των στοχαστικών μεταβλητών να εκτιμηθεί στη θέση του έργου. Επιπρόσθετα, χρησιμοποιήθηκε η ανάλυση ακραίων τιμών που στηρίζεται σε γεγονότα, και η ανάλυση στις θαλάσσιες καταστάσεις εντός των γεγονότων, σε μία μεθοδολογία εκτίμησης της πιθανότητας αστοχίας των παράκτιων έργων. Επίσης, αποδεικνύεται ότι και οι δύο αυτές προσεγγίσεις μπορούν να ενσωματωθούν στη διαδικασία σχεδιασμού των παράκτιων έργων. Για τον σκοπό αυτό, εφαρμόστηκαν και συγκρίθηκαν μεταξύ τους δύο διαφορετικές μεθοδολογίες, ήτοι η Μέθοδος Άμεσης Ολοκλήρωσης και η Μέθοδος Monte Carlo, χρησιμοποιώντας έναν συνδυασμό μεταβλητών με μηδενικό και μη-μηδενικό βαθμό επικινδυνότητας. Ο συνδυασμός αυτός αναφέρεται εδώ ως μία συνδυασμένη ανάλυση χρονικά μεταβαλλόμενων και χρονικά αμετάβλητων μεταβλητών. Επιπλέον, διερευνάται το κατάλληλο χρονικό βήμα ορισμού της θαλάσσιας κατάστασης εντός των καταιγίδων στην ανάλυση των θαλάσσιων καταστάσεων, θεωρώντας με τον τρόπο αυτό την ιστορία και τη μορφή των κυματικών καταιγίδων-γεγονότων. Τέλος, διερευνάται η επίδραση της θεώρησης περισσότερων στοχαστικών μεταβλητών διαφορετικού τύπου στην εκτιμώμενη πιθανότητα αστοχίας της κατασκευής.

3.3.1 Αρχική προσέγγιση σχεδιασμού βάσει της ανάλυσης ακραίων τιμών στηριζόμενη σε γεγονότα

Μία μονοπαραμετρική ανάλυση ακραίων τιμών βασισμένη σε γεγονότα, η οποία αναφέρεται στο μοντέλο των Αιχμών Άνω Κατωφλίου (Peak Over Threshold) POT, θα χρησιμοποιηθεί εδώ για το $H_{s,p}$, δηλ. το μέγιστο H_s εντός ενός γεγονότος ή αλλιώς μίας κυματικής καταιγίδας, ακολουθώντας το θεωρητικό πλαίσιο, το οποίο εισήγαγαν οι Bernardara et al. [50]. Στη συνέχεια, το $H_{s,p}$ που αναφέρεται σε μία περίοδο επαναφοράς θα αντιστοιχιστεί με τις πιο συχνές τιμές της μέσης κυματικής περιόδου καταιγίδας, storm T_m , και της μέσης κατεύθυνσης καταιγίδας, storm θ_m .

Αρχικά, ομογενοποιούνται τα αρχικά κυματικά δεδομένα, επιτρέποντας με τον τρόπο αυτό τον διαχωρισμό των δεδομένων/ θαλάσσιων καταστάσεων σε ανεξάρτητα μεταξύ τους γεγονότα. Αυτό επιτυγχάνεται με την επιλογή ενός αρχικού κατωφλίου u_1 για το H_s διαχωρίζοντας τις ασθενείς από τις πιο ισχυρές καταιγίδες. Επίσης, επιλέχθηκε μία ελάχιστη περίοδος «ηρεμίας», π.χ. των 6 hr [51], μεταξύ δύο διαδοχικών καταιγίδων, για να εξασφαλίσει ότι τα δύο γεγονότα είναι ανεξάρτητα. Με αυτή τη διαδικασία, προκύπτει το σύνολο των $H_{s,p}$. Σχετικά με την επιλογή του κατωφλίου u_1 , αυτό θα πρέπει να είναι αρκετά υψηλό, ώστε να διακρίνει και να διαχωρίζει δύο διαδοχικές καταιγίδες, αλλά επίσης να είναι πιο χαμηλό από την περιοχή των ακραίων γεγονότων [52].

Το δεύτερο βήμα είναι η επιλογή ενός άλλου κατωφλίου u_2 , υψηλότερου από το u_1 . Η επιλογή του u_2 πρέπει να είναι πιο ακριβής από του u_1 , αφού τα $H_{s,p}$ που υπερβαίνουν το u_2 θα πρέπει να ακολουθούν την ίδια πιθανοτική κατανομή ακραίων τιμών. Αναφορικά με το μοντέλο POT, ο Pickands [53] απέδειξε ότι η πιθανοτική κατανομή ακραίων τιμών μπορεί να προσεγγιστεί από την κατανομή Generalized Pareto (GP) (βλ. επίσης [54]). Αυτό σημαίνει ότι για $H_{s,p} > x_o$, δεδομένου ότι $H_{s,p} > u_2$, ισχύει:

$$\Pr(H_{s,p} > x_o | H_{s,p} > u_2) = \left(1 + \xi \frac{x_o - u_2}{\sigma}\right)^{-1/\xi} \quad (6)$$

όπου: x_o είναι μία τιμή $H_{s,p}$ μεγαλύτερη από το u_2 , $\xi \in (-\infty, +\infty)$ και $\sigma > 0$ είναι οι παράμετροι σχήματος και κλίμακας, αντίστοιχα, της κατανομής.

Οι επιστρεφόμενες τιμές $H_{s,p}$, που αντιστοιχούν σε συγκεκριμένες περιόδους επαναφοράς T_r , εξαγόμενες από το μοντέλο GP παρουσιάζονται παρακάτω:

$$\begin{aligned} H_{s,p-T_r} &= u_2 + \frac{\sigma}{\xi} \left[(T_r \lambda_e)^\xi - 1 \right], \text{ for } \xi \neq 0 \\ H_{s,p-T_r} &= u_2 + \sigma \log(T_r \lambda_e), \text{ for } \xi = 0 \end{aligned} \quad (7)$$

Συνεπώς, η καταιγίδα σχεδιασμού αντιστοιχεί σε μία επιστρεφόμενη τιμή για το $H_{s,p}$, η οποία συνδυάζεται με την πιο πιθανή τιμή της T_m και της θ_m .

Για να εκτιμηθεί, λοιπόν, η πιθανότητα υπέρβασης του $H_{s,p}$ σχεδιασμού στο δείγμα των $H_{s,p}$ των ακραίων γεγονότων στη διάρκεια ζωής του έργου L , η οποία θεωρείται εδώ ως μία ισοδύναμη πιθανότητα αστοχίας $P_{f,e,L}^*$, μπορεί να χρησιμοποιηθεί η παρακάτω εξίσωση:

$$P_{f,e,L}^* = 1 - \left(1 - \frac{1}{\lambda_e T_r} \right)^{\lambda_e L} \quad (8)$$

3.3.2 Πλήρως πιθανοτική ανάλυση αξιοπιστίας εφαρμοσμένη σε ακραία γεγονότα

Η πλήρως πιθανοτική ανάλυση, που παρουσιάζεται παρακάτω, εφαρμόζεται άμεσα στους εκπροσώπους των καταγίδων, δηλαδή είτε στα $H_{s,p}$ των ακραίων γεγονότων, είτε στα H_s της μεθόδου Block Maxima. Για τον σκοπό αυτό, παρουσιάζονται δύο πλήρως πιθανοτικές μέθοδοι αξιοπιστίας, ήτοι η Μέθοδος Άμεσης Ολοκλήρωσης (DIM) και η Μέθοδος Monte Carlo (MCM), εφαρμοσμένη στα ανεξάρτητα $H_{s,p}$ των ακραίων γεγονότων μίας POT ανάλυσης.

3.3.2.1 Μέθοδος Άμεσης Ολοκλήρωσης (DIM)

Η μέθοδος άμεσης ολοκλήρωσης βρίσκεται πιο κοντά θεωρητικά στον προσδιορισμό της πιθανότητας αστοχίας ενός στοιχείου μίας κατασκευής. Βασίζεται στην ολοκλήρωση της συνάρτησης της από κοινού πυκνότητας πιθανότητας σε όλο το πεδίο ορισμού των στοχαστικών μεταβλητών υπό τη συνθήκη ότι το ολοκλήρωμα υπολογίζεται στο χωρίο της αστοχίας.

Σε μία ανάλυση αξιοπιστίας, θα μπορούσαν να εμπλέκονται χρονικά μεταβαλλόμενες αλλά και χρονικά αμετάβλητες μεταβλητές, με την έννοια των παραμέτρων με μηδενικό και μη μηδενικό ρυθμό επικινδυνότητας, οι οποίες παίζουν κάποιο ρόλο στην αξιοπιστία ή στην πιθανότητα αστοχίας μίας παράκτιας κατασκευής $P_{f,e,L}$ κατά τη διάρκεια της ζωής της L . Η συγκεκριμένη πιθανότητα εκτιμάται στο σύνολο των ακραίων γεγονότων. Οι μεταβλητές με μηδενικό ρυθμό επικινδυνότητας, ωστόσο, είναι ανεξάρτητες από την περίοδο αναφοράς L . Στην πράξη, τέτοιες χρονικά αμετάβλητες μεταβλητές μπορούν να θεωρηθούν αυτές που σχετίζονται με την αντοχή/αντίσταση της κατασκευής. Στην περίπτωση του συνδυασμού των δύο αυτών τύπων μεταβλητών, η $P_{f,e,L}$ εκτιμάται μέσω της ακόλουθης εξίσωσης η οποία αναπτύχθηκε εδώ:

$$P_{f,e,L} = \iint_{\Omega(\vec{r},\vec{x})} f_{\vec{R}}(\vec{r}) f_{\vec{X},e,L}(\vec{x}) d\vec{x} d\vec{r} = \int f_{\vec{R}}(\vec{r}) \left(\int_{\Omega(\vec{r},\vec{x})} f_{\vec{X},e,L}(\vec{x}) d\vec{x} \right) d\vec{r} \quad (9)$$

όπου: από εδώ και στο εξής, $f_{\vec{R}}(\vec{r})$ είναι η συνάρτηση της από κοινού πυκνότητας πιθανότητας των μεταβλητών αντίστασης \vec{r} , $f_{\vec{X},e,L}(\vec{x})$ είναι η συνάρτηση από κοινού πυκνότητας πιθανότητας των χρονικά εξαρτώμενων μεταβλητών φόρτισης \vec{x} κατά τη διάρκεια της ζωής του έργου L , και $\Omega(\vec{r},\vec{x})$ είναι το χωρίο αστοχίας, το οποίο προσδιορίζεται από το πεδίο ορισμού όλων των εμπλεκόμενων στοχαστικών μεταβλητών υπό τη συνθήκη ότι η οριακή συνάρτηση σχεδιασμού είναι μικρότερη από το μηδέν, δηλ. για $g(\vec{r},\vec{x}) < 0$.

Στο σημείο αυτό ανοίγει μία παρένθεση: Η συνάρτηση οριακής κατάστασης (limit state function) g του κάθε στοιχείου της κατασκευής προκύπτει από τον τύπο σχεδιασμού του στοιχείου, διαμορφωμένο στην ακόλουθη γενική του μορφή:

$$g = R - A \begin{cases} < 0, & \text{αστοχία} \\ = 0, & \text{οριακή κατάσταση} \\ > 0, & \text{ασφαλής περιοχή} \end{cases} \quad (10)$$

όπου: R η συνάρτηση των παραμέτρων αντίστασης και A η συνάρτηση των παραμέτρων φόρτισης. Συνεπώς, η συνάρτηση οριακής κατάστασης ενός στοιχείου περιγράφει την κατάσταση στην οποία βρίσκεται, και παρουσιάζεται στην παρακάτω εξίσωση:

Κλείνοντας λοιπόν την παρένθεση, προκύπτει ότι:

$$\Omega(\vec{r},\vec{x}) = \{g(\vec{r},\vec{x}) < 0\} \quad (11)$$

Η εφαρμογή της Εξίσωσης 9 στην Εξίσωση 8 συνεπάγεται ότι:

$$P_{f,e,L} = \int f_{\vec{R}}(\vec{r}) \left[1 - \left(1 - \int_{\Omega(\vec{r},\vec{x})} f_{\vec{X},e,ly}(\vec{x}) d\vec{x} \right)^{\lambda_e L} \right] d\vec{r} \quad (12)$$

όπου: $f_{\vec{X},e,ly}(\vec{x})$ είναι η κατά μέσο όρο συνάρτηση της από κοινού πυκνότητας πιθανότητας των \vec{x} που αναφέρεται στην περίοδο αναφοράς του ενός έτους, εξαγόμενη από Y έτη παρατηρήσεων/μετρήσεων. Σημειώνεται ότι οι χρονικά εξαρτώμενες μεταβλητές φόρτισης \vec{x} αποτελούνται από κυματικές παραμέτρους, όπως οι H_s , και T_m , ή άλλες όμοιες, η διακύμανση της στάθμης λόγω μετεωρολογικής παλίρροιας SL, η ταχύτητα των θαλάσσιων ρευμάτων κλπ.

Η πιο συχνή περιβαλλοντική παράμετρος, η οποία είναι ανεξάρτητη από το κυματικό πεδίο και παρουσιάζεται στην παράκτια ζώνη, είναι η διακύμανση της θαλάσσιας στάθμης λόγω της αστρονομικής παλίρροιας (TL). Η μεταβλητή αυτή είναι ντετερμινιστική και εξαρτάται από τον παλίρροιακό κύκλο της περιοχής μελέτης. Παρόλα αυτά, συνδυάζεται τυχαία με τους κυματισμούς, και συνεπώς μπορεί να θεωρηθεί σαν μία τυχαία μεταβλητή. Ωστόσο, η TL δεν είναι στατιστικά συσχετισμένη με τις κυματικές παραμέτρους, αλλά οι τελευταίες, όταν περιορίζονται από το βάθος πυθμένα, εξαρτώνται από τη στάθμη της θάλασσας, η οποία μπορεί να επηρεάζεται έντονα από την αστρονομική παλίρροια, τη μετεωρολογική παλίρροια, κλπ.

Η αστρονομική παλίρροια σχετίζεται κυρίως με τη σχετική θέση της Σελήνης με τη Γη και εξελίσσεται κάθε 50 λεπτά την ημέρα. Οι παλίρροιας, επίσης, μεταβάλλονται εποχιακά, ενώ μικρότερες διακυμάνσεις συμβαίνουν εκτός της χρονικής περιόδου των 19 ετών περίπου [55]. Ως εκ τούτου, δεδομένου ότι η διάρκεια ζωής των περισσότερων παράκτιων έργων κυμαίνεται μεταξύ 20-50 ετών, η αστρονομική παλίρροια μπορεί να θεωρηθεί ως μία χρονικά μη εξαρτώμενη μεταβλητή, και η κατανομή της ανεξάρτητη από την περίοδο αναφοράς. Συνεπώς, η ενσωμάτωση της TL στην Εξίσωση 12 επιτυγχάνεται ως ακολούθως:

$$P_{f,e,L} = \iint f_{\vec{R}}(\vec{r}) f_{TL}(tl) \left[1 - \left(1 - \int_{\Omega(\vec{r},\vec{x},tl)} f_{\vec{X},e,ly}(\vec{x}) d\vec{x} \right)^{\lambda_e L} \right] d\vec{r} dtl \quad (13)$$

όπου: $f_{TL}(tl)$ είναι η συνάρτηση πυκνότητας πιθανότητας της διακύμανση της στάθμης λόγω αστρονομικής παλίρροιας και $\Omega(\vec{r},\vec{x},tl)$ είναι το επεκταμένο χωρίο αστοχίας.

Για την ακριβή εκτίμηση της $P_{f,L}$, τα βήματα ολοκλήρωσης όλων των στοχαστικών μεταβλητών πρέπει να είναι ικανοποιητικά μικρά.

3.3.2.2 Μεταβλητές αντίστασης

Ως μεταβλητές αντίστασης, θεωρούνται εκείνες που σχετίζονται με την αντοχή ή αντίσταση μίας κατασκευής και συνήθως παρουσιάζουν μία διασπορά γύρω από μία χαρακτηριστική τιμή. Στην κατηγορία αυτή ανήκουν παράμετροι, όπως η πυκνότητα των φυσικών ογκολίθων, η πυκνότητα του θαλασσινού νερού, οι γεωμετρικές παράμετροι ή ακόμα και οι παράμετροι των εμπειρικών τύπων σχεδιασμού, οι οποίες προκύπτουν από τη βαθμονόμησή τους βάσει πειραματικών μελετών. Στον πρωταρχικό σχεδιασμό των παράκτιων κατασκευών, οι μεταβλητές αντίστασης εκπροσωπούνται από τις χαρακτηριστικές ή μέσες τιμές τους στους τύπους σχεδιασμού για το κάθε στοιχείο της κατασκευής. Ωστόσο, στον πλήρως πιθανοτικό σχεδιασμό, οι παράμετροι αντίστασης μπορούν και αυτές να ακολουθούν πιθανοτικές κατανομές. Ένας απλός τρόπος να λαμβάνεται υπόψη η μεταβλητότητά τους, και κατά συνέπεια και οι πιθανοτικές τους κατανομές, γίνεται μέσω της θεώρησής τους ως κανονικές κατανομές.

3.3.2.3 Μέθοδος Monte Carlo (MCM)

Στη μέθοδο MCM, χρησιμοποιούνται η πυκνότητα συχνότητας της TL, και οι συναρτήσεις της από κοινού πυκνότητας πιθανότητας των SL, θ_m , T_m , και H_s , με στόχο την παραγωγή ενός τυχαίου δείγματος για κάθε μεταβλητή το οποίο προκύπτει από την πιθανοτική της κατανομή, αλλά, επιπλέον, διατηρώντας τη στατιστική συσχέτιση μεταξύ των στοχαστικών μεταβλητών που παρουσιάζουν σημαντική συσχέτιση. Συνεπώς, η Εξίσωση 13 ισχύει και στη μέθοδο αυτή.

Ένας τρόπος για την παραγωγή του τυχαίου δείγματος της MCM είναι μέσω της αντίστροφης συνάρτησης της αθροιστικής κατανομής, η οποία βασίζεται στην παρακάτω διαδικασία: Κάθε προσομοίωση ξεκινά με την επιλογή ενός τυχαίου πραγματικού αριθμού από μία ομοιόμορφη κατανομή $U(0,1)$. Μέσω του συγκεκριμένου αριθμού (x_i), μπορεί να παραχθεί ένα δείγμα της μεταβλητής (X) χρησιμοποιώντας την αντίστροφη αθροιστική κατανομή της μεταβλητής $F_x^{-1}(x)$ ως εξής:

$$X = F_X^{-1}(X_u) \quad (14)$$

Σημειώνεται ότι η αθροιστική κατανομή της X υπολογίζεται από τη συνάρτηση πυκνότητας πιθανότητας $f_X(x)$ ως εξής:

$$F_X(x) = \int_{-\infty}^x f_X(u) du \quad (15)$$

Επίσης, η μέθοδος βασίζεται στη διεξαγωγή ενός μεγάλου αριθμού προσομοιώσεων N , ένα μέρος των οποίων (N_f) εκφράζει το χωρίο αστοχίας του στοιχείου. Ως εκ τούτου, με την προϋπόθεση ότι ο N είναι ικανοποιητικά μεγάλος θετικός ακέραιος αριθμός,

$$P_f = \frac{N_f}{N} \quad (16)$$

Εάν, λοιπόν, το μέγεθος των δειγμάτων των SL, TL και των μεταβλητών αντίστασης R , που παράγονται από τη μέθοδο MCM, συμβολίζεται με by N_s, N_t, N_r αντίστοιχα, τότε το τελικό αποτέλεσμα της $P_{f,e,L}$ προκύπτει συνδυάζοντας την Εξίσωση 16 με την Εξίσωση 17 ως ακολούθως:

$$P_{f,e,L} = \sum_{N_r} \left(\sum_{N_t} \left[1 - \left(1 - \sum_{N_s} \frac{N_{f,i}}{N} / N_s \right)^{\lambda_e L} \right] / N_t \right) / N_r \quad (8)$$

όπου: $N_{f,i}$ είναι ο αριθμός εμφανίσεων της αστοχίας του i -οστού στοιχείου και N είναι ο συνολικός αριθμός των προσομοιώσεων/ κατατιγίδων.

3.3.2.4 Υπολογίζοντας την πιθανότητα αστοχίας του συστήματος

Ένας απλός τρόπος να υπολογιστεί η πιθανότητα αστοχίας του συστήματος ή αλλιώς η πιθανότητα της ένωσης των ενδεχομένων αστοχίας των στοιχείων του συστήματος, σε περίπτωση σειριακού διαγράμματος αστοχιών, είναι ο έλεγχος όλων των στοιχείων εάν αυτά αστοχούν υπό κοινές συνθήκες φόρτισης. Ένα κατατοπιστικό παράδειγμα, το οποίο αναφέρεται σε ένα σύστημα αστοχιών σε σειρά ενός συμβατικού κυματοθραύστη με πρανή, για την περίπτωση της MCM, παρουσιάζεται στον Πίνακα 10. Στην περίπτωση τώρα της DIM, μπορεί να χρησιμοποιηθεί ο αντίστοιχος Πίνακα 11.

Πίνακας 10 Εκτίμηση της πιθανότητας αστοχίας του συστήματος μέσω της ένωσης των ενδεχομένων αστοχίας των στοιχείων ([34], [56]) για τη μέθοδο MCM

α/α προσομοίωσης θαλάσσιας κατάστασης	Αστοχία προσήνεμου πρανούς	Αστοχία πόδα	Αστοχία Υπήνεμου πρανούς	Αστοχία συστήματος
1	1	0	1	1
2	0	0	0	0
3	0	1	1	1
⋮	⋮	⋮	⋮	⋮
N	1	0	0	1
Σύνολο	$N_{f,s}$	$N_{f,t}$	$N_{f,r}$	N_f

Πίνακας 11 Εκτίμηση της πιθανότητας αστοχίας του συστήματος μέσω της ένωσης των ενδεχομένων αστοχίας των στοιχείων για τη μέθοδο DIM [35]

Από κοινού πιθανότητα παραμέτρων φόρτισης	Αστοχία προσήνεμου πρανούς	Αστοχία πόδα	Αστοχία Υπήνεμου πρανούς	Αστοχία συστήματος
p_1	p_1	0	p_1	p_1
p_2	0	0	0	0
p_3	0	p_3	p_3	p_3
⋮	⋮	⋮	⋮	⋮
p_n	p_n	0	0	p_n
Σύνολο=1	pf_s	pf_t	pf_r	pf

Συνεπώς, σύμφωνα με τη μέθοδο DIM, η πιθανότητα αστοχίας του συστήματος $P_{f,e,L,s}$, π.χ. 3 στοιχείων (όπως στην περίπτωσή μας) σε σειρά, ισούται με:

$$P_{f,e,L,s} = \iint f_{\vec{R}}(\vec{r}) f_{TL}(tl) \left[1 - \left(1 - \int_{g_1(\vec{r},tl,\vec{x}) < 0 \cup g_2(\vec{r},tl,\vec{x}) < 0 \cup g_3(\vec{r},tl,\vec{x}) < 0} f_{\vec{X},e,ly}(\vec{x}) d\vec{x} \right)^{\lambda_e L} \right] d\vec{r} dtl \quad (22)$$

Ομοίως για παράλληλο σύστημα:

$$P_{f,e,L,s} = \iint f_{\vec{R}}(\vec{r}) f_{TL}(tl) \left[1 - \left(1 - \int_{g_1(\vec{r},tl,\vec{x}) < 0 \cap g_2(\vec{r},tl,\vec{x}) < 0 \cap g_3(\vec{r},tl,\vec{x}) < 0} f_{\vec{X},e,ly}(\vec{x}) d\vec{x} \right)^{\lambda_e L} \right] d\vec{r} dtl \quad (23)$$

Κατά αντιστοιχία, στη μέθοδο MCM, η πιθανότητα αστοχίας του συστήματος $P_{f,e,L,s}$, π.χ. 3 στοιχείων (όπως στην περίπτωση μας) σε σειρά, ισούται με

$$P_{f,e,L,s} = \sum_{N_r} \left(\sum_{N_{tl}} \left[1 - \left(1 - \sum_{N_s} \frac{N_f}{N} \right)^{\lambda_e L} \right] / N_{tl} \right) / N_r \quad (24)$$

όπου το N_f προσδιορίζεται από τον Πίνακα 10.

3.3.3 Πλήρως πιθανοτική ανάλυση εφαρμοσμένη στις θαλάσσιες καταστάσεις

Η πλήρως πιθανοτική ανάλυση, που παρουσιάζεται παρακάτω, εφαρμόζεται άμεσα στα διαδοχικά κυματικά δεδομένα με την υιοθέτηση ενός χρονικού βήματος, το οποίο ορίζει τη θαλάσσια κατάσταση. Στην ανάλυση αυτή, οι θαλάσσιες καταστάσεις δεν απαιτείται να είναι ανεξάρτητες μεταξύ τους. Επίσης, με βάση τον σκοπό της ανάλυσης, το χρονικό αυτό βήμα μπορεί να είναι διαφορετικό από το βήμα μέτρησης. Το χρονικό βήμα ορισμού της θαλάσσιας κατάστασης εξαρτάται από το στοιχείο της κατασκευής για το οποίο γίνεται η ανάλυση. Ειδικότερα, το βήμα αυτό, σε μία ανάλυση αξιοπιστίας ενός συμβατικού κυματοθραύστη με πρηνή, συνιστάται να είναι 3 hr, ώστε να αντιστοιχεί σε περισσότερα από 1000 κύματα ανά θαλάσσια κατάσταση, όπως προτείνεται από μία συνήθη συνάρτηση οριακής κατάστασης [57] για τη θωράκιση του προσήνεμου πρηνούς. Η συγκεκριμένη θεώρηση συνδέεται με την ικανότητα της κατασκευής να αντέχει σε μία κυματική καταιγίδα που αποτελείται από ένα

σύνολο από θαλάσσιες καταστάσεις. Η ικανότητα αυτή δεν εγγυάται με τη θεώρηση αυτόνομων βραχέων θαλάσσιων καταστάσεων που οδηγούν σε μικρή ζημιά π.χ. στη θωράκιση, αλλά με τη θεώρηση πιο σημαντικών φορτίσεων, ιδίως όταν οι θαλάσσιες καταστάσεις συνιστούν τμήματα ακραίων κυματικών γεγονότων. Ο λόγος για αυτό είναι ότι μία κατασκευή δεν μπορεί να επιδιορθωθεί εντός ενός ακραίου γεγονότος μεγάλης διάρκειας.

Στην πολυπαραμετρική ανάλυση που εφαρμόζεται στις θαλάσσιες καταστάσεις, οι οποίες συνήθως δίδονται με συγκεκριμένο χρονικό βήμα μεταξύ τους, το μοντέλο δεσμευμένης πιθανότητας χρησιμοποιείται με στόχο να προσαρμόσει διπαραμετρικές κατανομές των H_s και T_m στα διαθέσιμα δεδομένα κάθε κατευθυντικού τομέα, ως ακολούθως:

$$f_{T_m, H_s, \theta_{m_i}}(T_m, H_s, \theta_{m_i}) = f_{\theta_{m_i}}(\theta_{m_i}) f_{H_s | \theta_{m_i}}(H_s | \theta_{m_i}) f_{T_m | (H_s, \theta_{m_i})}(T_m | (H_s, \theta_{m_i})) \quad (25)$$

όπου: $f_{\theta_{m_i}}(\theta_{m_i})$ είναι η πυκνότητα πιθανότητας του i -οστού κατευθυντικού τομέα με κεντρική τιμή την θ_{m_i} και εύρους $d\theta_m$, $f_{H_s | \theta_{m_i}}(H_s | \theta_{m_i})$ είναι η δεσμευμένη συνάρτηση πυκνότητας πιθανότητας του H_s για δεδομένη θ_{m_i} και $f_{T_m | (H_s, \theta_{m_i})}(T_m | (H_s, \theta_{m_i}))$ είναι η δεσμευμένη συνάρτηση πυκνότητας πιθανότητας της T_m δεδομένων των H_s και θ_{m_i} .

Η δεσμευμένη συνάρτηση της από κοινού πυκνότητας πιθανότητας των T_m, H_s $f_{H_s, T_m | \theta_{m_i}}(T_m, H_s | \theta_{m_i})$ για δεδομένο κατευθυντικό τομέα με θ_{m_i} μοντελοποιήθηκε σύμφωνα με τους Mathisen and Bitner-Gregersen [58]. Η $f_{H_s | \theta_{m_i}}(H_s | \theta_{m_i})$ μπορεί με ικανοποιητικό τρόπο να αναπαρασταθεί με μία Weibull κατανομή σε πολλές περιπτώσεις [16], ενώ η $f_{T_m | H_s, \theta_{m_i}}(T_m | (H_s, \theta_{m_i}))$ μπορεί να αναπαρασταθεί από την κατανομή lognormal, της οποίας οι παράμετροι θέσης μ και κλίμακας σ μπορούν να γραφτούν ως συναρτήσεις του H_s / θ_{m_i} , προσαρμοσμένες εδώ για να λαμβάνουν υπόψη και το θ_m , όπως παρακάτω [58]:

$$\begin{aligned} \mu(H_s | \theta_{m_i}) &= a_1 + a_2 H_s^{a_3} \\ \sigma(H_s | \theta_{m_i}) &= b_1 + b_2 \exp(b_3 H_s) \end{aligned}, \quad \theta_m \in \left(\theta_{m_i} - \frac{d\theta_m}{2}, \theta_{m_i} + \frac{d\theta_m}{2} \right) \quad (26)$$

όπου a_1, a_2, a_3, b_1, b_2 , και b_3 είναι σταθερές, οι οποίες προσδιορίζονται από τη βέλτιστη προσαρμογή των καμπυλών της μορφής των Εξισώσεων 26 στα δεδομένα.

3.3.3.1 Μέθοδος Άμεσης Ολοκλήρωσης (DIM)

Στην παρούσα ανάλυση αξιοπιστίας, εάν έχουμε Y έτη μετρήσεων χρονικά εξαρτώμενων μεταβλητών, όπως οι διαδοχικές κυματικές φασματικές μεταβλητές H_s , T_m με ένα σταθερό χρονικό βήμα, οι μεταβλητές αυτές αντιστοιχούν σε Y έτη θεωρώντας στατικές συνθήκες μεταξύ των ετών. Συνεπώς στην ανάλυση αυτή, η δεσμευμένη και η μη δεσμευμένη πιθανότητα αστοχίας του στοιχείου στα Y έτη μπορεί να εκτιμηθεί. Η δεσμευμένη πιθανότητα αστοχίας αναφέρεται στο δείγμα που υπερβαίνει ένα σταθερό κατώφλι. Η μετάβαση της πιθανότητας αστοχίας του στοιχείου από τα Y έτη σε μεγαλύτερη διάρκεια δεν επιτρέπεται καθώς οι τιμές των μεταβλητών αυτών δεν είναι ανεξάρτητες. Συνεπώς, η μη δεσμευμένη πιθανότητα αστοχίας του στοιχείου στα Y έτη εκτιμάται ως ακολούθως:

$$P_{f,Y} = \iint_{\Omega(\vec{r}, \vec{x})} f_{\vec{R}}(\vec{r}) f_{\vec{X},Y}(\vec{x}) d\vec{x} d\vec{r} = \int f_{\vec{R}}(\vec{r}) \left(\int_{\Omega(\vec{r}, \vec{x})} f_{\vec{X},Y}(\vec{x}) d\vec{x} \right) d\vec{r} \quad (27)$$

όπου $f_{\vec{X},Y}(\vec{x})$ είναι η συνάρτηση της από κοινού πυκνότητας πιθανότητας των χρονικά εξαρτώμενων μεταβλητών \vec{x} στην χρονική περίοδο Y .

Η ενσωμάτωση της παλίνρροιας στην παραπάνω εξίσωση οδηγεί στην παρακάτω διατύπωση της πιθανότητας αστοχίας του στοιχείου στα Y έτη:

$$P_{f,Y} = \iint f_{\vec{R}}(\vec{r}) f_{TL}(t) \int_{\Omega(\vec{r}, \vec{x}, t)} f_{\vec{X},Y}(\vec{x}) d\vec{x} d\vec{r} dt \quad (28)$$

3.3.3.2 Μέθοδος Monte Carlo (MCM)

Όσον αφορά στη μέθοδο MCM, η διαδικασία που ακολουθήθηκε στην παρούσα διατριβή περιγράφεται με τα ακόλουθα βήματα: 1) Αρχικά παράγεται ένα δείγμα με τιμές της θ_m που ακολουθούν την κατανομή τους. 2) Στη συνέχεια, για κάθε τιμή της θ_m με βάση την κλάση της, χρησιμοποιείται μία δεσμευμένη αντίστροφη αθροιστική κατανομή της $H_s | \theta_m$ με στόχο την παραγωγή του δείγματος του H_s . Με τον τρόπο αυτό, σε κάθε τιμή της θ_m , αντιστοιχίζεται

μία τιμή του H_s , η οποία καθορίζει τις παραμέτρους της δεσμευμένης αντίστροφης αθροιστικής κατανομής της $T_m|H_s|\theta_m$. Οι συγκεκριμένες παράμετροι είναι συναρτήσεις του H_s . Συνεπώς, χρησιμοποιώντας την Εξίσωση 14, παράγονται N τριάδες των θ_m, H_s, T_m , όπου N είναι ένας αρκετά μεγάλος θετικός ακέραιος αριθμός, ο οποίος θεωρητικά προσεγγίζει τον πληθυσμό τους και επιτυγχάνει τη σύγκλιση της λύσης της μεθόδου.

Συνεπώς, η μη δεσμευμένη πιθανότητα αστοχίας του στοιχείου στα Y έτη με τη μέθοδο Monte Carlo εκτιμάται ως ακολούθως:

$$P_{f,Y} = \sum_{N_r} \left[\sum_{N_d} \left(\sum_{N_s} \frac{N_{f,i}}{N} / N_s \right) / N_d \right] / N_r \quad (29)$$

όπου: $N_{f,i}$ είναι ο αριθμός εμφανίσεων της αστοχίας του i -οστού στοιχείου και N είναι ο συνολικός αριθμός των προσομοιώσεων/ θαλασσιών καταστάσεων.

3.3.3.3 Υπολογίζοντας την πιθανότητα αστοχίας του συστήματος

Σύμφωνα με τη μέθοδο DIM, η πιθανότητα αστοχίας του συστήματος $P_{f,Y,s}$, π.χ. 3 στοιχείων (όπως στην περίπτωση μας) σε σειρά, ισούται με:

$$P_{f,Y,s} = \iint f_{\vec{r}}(\vec{r}) f_{TL}(tl) \int_{g_1(\vec{r},tl,\vec{x}) < 0 \cup g_2(\vec{r},tl,\vec{x}) < 0 \cup g_3(\vec{r},tl,\vec{x}) < 0} f_{\vec{x},Y}(\vec{x}) d\vec{x} d\vec{r} dtl \quad (30)$$

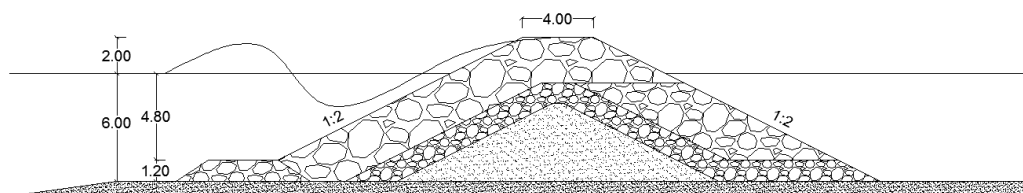
Κατά αντιστοιχία, στη μέθοδο MCM, η πιθανότητα αστοχίας του συστήματος $P_{f,Y,s}$, π.χ. 3 στοιχείων (όπως στην περίπτωση μας) σε σειρά, ισούται με:

$$P_{f,Y,s} = \sum_{N_r} \left[\sum_{N_d} \left(\sum_{N_s} \frac{N_f}{N} / N_s \right) / N_d \right] / N_r \quad (31)$$

όπου το N_f εκτιμάται σύμφωνα με τον Πίνακα 10.

3.4 Παράδειγμα ανάλυσης αξιοπιστίας συμβατικού κυματοθραύστη με πρανή

Στην παρούσα διατριβή, παρουσιάζονται δύο περιπτώσεις εφαρμογής της προαναφερόμενης μεθοδολογίας, με στόχο την εκτίμηση αξιοπιστίας μίας παράκτιας κατασκευής. Η παράκτια κατασκευή που μελετάται είναι ένας συμβατικός κυματοθραύστης με πρανή που βρίσκεται σε βάθος 6 m, του οποίου τα χαρακτηριστικά παρουσιάζονται στην Εικόνα 19. Εφόσον οι κυματοθραύστες σχεδιάζονται συνήθως για αρχική ζημιά και δεν καταστρέφονται αμέσως μετά από μία καταιγίδα, η οριακή κατάσταση σχεδιασμού της υπό μελέτης κατασκευής θεωρήθηκε η οριακή κατάσταση λειτουργικότητας για περιορισμένη ζημιά (Serviceability Limit State - Limited Damage). Επιπρόσθετα, οι περιθώριες περίοδοι επαναφοράς του $H_{s,p}$ που εξετάστηκαν είναι οι περίοδοι των 10 και των 100 ετών και για τα δύο παραδείγματα. Τα δύο αυτά παραδείγματα αναφέρονται σε δύο διαφορετικά σημεία στη Μεσόγειο, το πρώτο αναφέρεται στα ανοιχτά της Μάλαγα (Ισπανία), και το δεύτερο στα ανοιχτά στο κεντρικό Αιγαίο (Ελλάδα). Για λόγους συντομίας, μόνο το πρώτο παράδειγμα θα παρουσιαστεί εδώ.



Εικόνα 19 Μία τυπική διατομή του συμβατικού κυματοθραύστη [35]

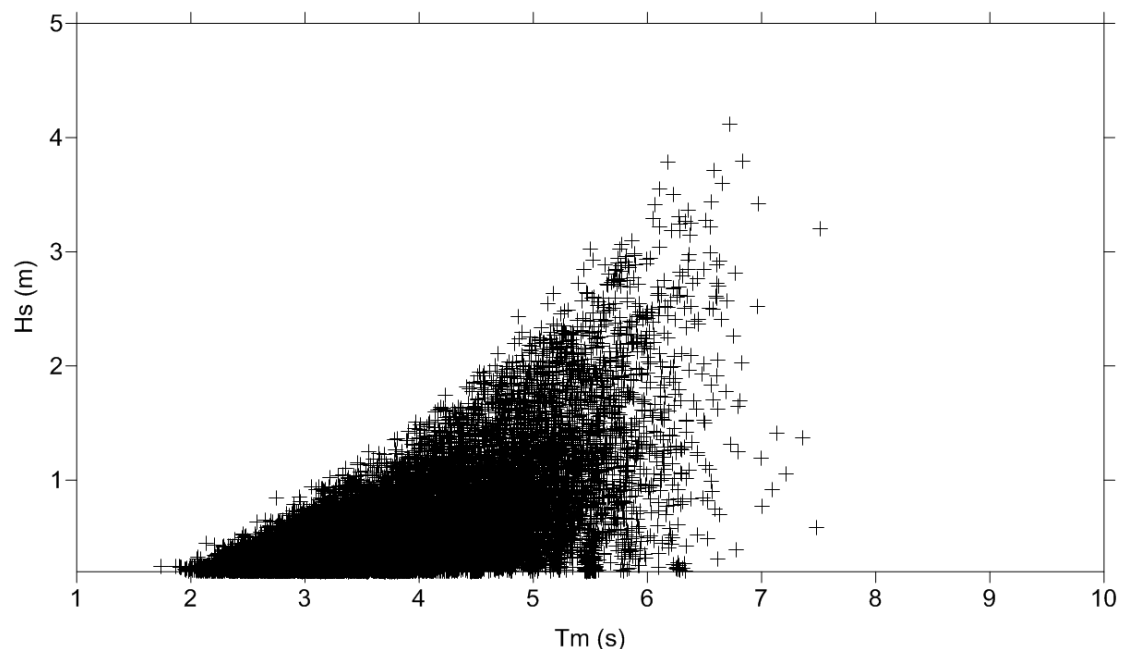
Τα δεδομένα που χρησιμοποιήθηκαν για την περίπτωση της Μάλαγα αφορούν ιστορικά δεδομένα των H_s , T_m , και θ_m που καλύπτουν τη χρονική περίοδο από 2010 έως 2017 και προέρχονται από έναν ωκεανογραφικό πλωτήρα. Η διάρκεια ζωής του έργου θεωρείται ίση με 15 έτη, ώστε να είναι λίγο μεγαλύτερη από τη διάρκεια των μετρήσεων. Ο πλωτήρας είναι τοποθετημένος στα ενδιάμεσα νερά και συγκεκριμένα στο βάθος των 15 m (36.69° N, 4.42° W), κοντά στο λιμάνι της Μάλαγα. Το χρονικό βήμα των κυματικών δεδομένων είναι 1 h. Επίσης, χρησιμοποιήθηκαν μακροπρόθεσμα δεδομένα της θαλάσσιας στάθμης, που καλύπτουν τη χρονική περίοδο από 1992 έως 2019 και προέρχονται από παλιρροιογράφο που βρίσκεται μέσα στο λιμάνι της Μάλαγα (συγκεκριμένα: 36.71° N, 4.42° W). Τα δεδομένα αυτά διαχωρίζονται σε δύο συνιστώσες, δηλ. στην αστρονομική παλίρροια TL και τη μετεωρολογική παλίρροια SL (storm surge).

Όσον αφορά στο διάγραμμα αστοχιών (fault tree), επιλέχθηκε ένα σειριακό διάγραμμα, όπως συνηθίζεται για τις παράκτιες κατασκευές [1], το οποίο αποτελείται από τρεις μεμονωμένους μηχανισμούς αστοχίας: την αστοχία του προσήνεμου πρανούς, την αστάθεια του πόδα, και την αστοχία του υπήνεμου πρανούς εξαιτίας της κυματικής υπερπήδησης. Οι τύποι που χρησιμοποιήθηκαν για το κάθε στοιχείο έχουν αναπτυχθεί από τους Van der Meer [57], Van der Meer et al. [59], and Van Gent and Pozueta [60], αντίστοιχα.

Επίσης, σημειώνεται ότι η επίδραση της πλάγιας πρόπτωσης των κυματισμών στην ευστάθεια αυτών των τριών στοιχείων λήφθηκε υπόψη μέσω της χρήσης του ισοδύναμου H_s κάθετης πρόπτωσης [12].

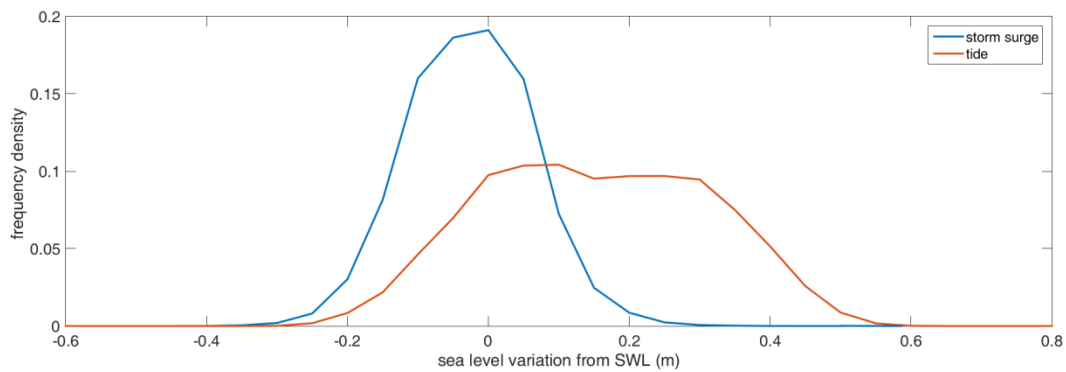
3.4.1 Παρουσίαση δεδομένων

Σχετικά με τη στατιστική συσχέτιση μεταξύ των κυματικών παραμέτρων, ο συντελεστής γραμμικής συσχέτισης Pearson μεταξύ των T_m και H_s εκτιμήθηκε στα 0.68, ενώ παρατηρήθηκαν επιδράσεις της κατεύθυνσης των κυματισμών στην από κοινού κατανομή των T_m και H_s . Το διάγραμμα διασποράς των T_m και H_s των μετρήσεων απεικονίζεται στην Εικόνα 20.



Εικόνα 20 Διάγραμμα διασποράς των μετρήσεων T_m και H_s από τον ωκεανογραφικό πλωτήρα [35]

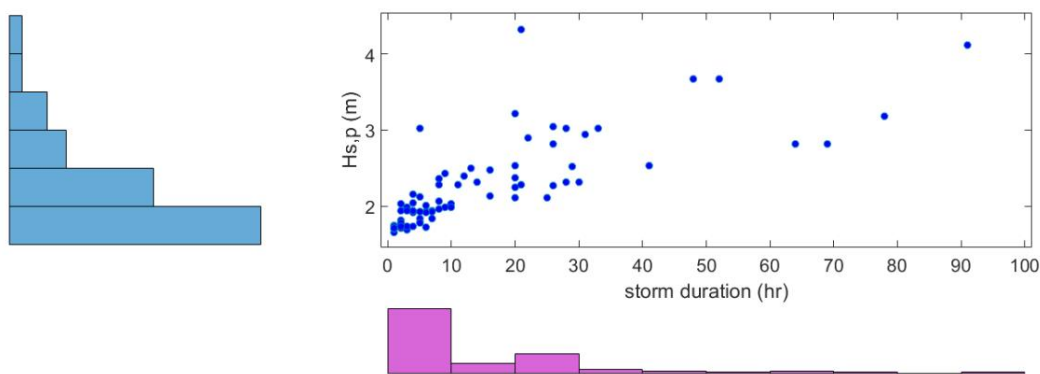
Ο συντελεστής γραμμικής συσχέτισης μεταξύ SL και H_s ισούται με 0.1 περίπου και γι αυτό δεν θεωρήθηκε σημαντικός στην παρούσα μελέτη. Τα ιστογράμματα των TL και SL παρουσιάζονται στην Εικόνα 21, όπως μετρήθηκε από τον παλιρροιογράφο. Όπως παρατηρήθηκε στην Εικόνα 21, η αστρονομική και μετεωρολογική παλίρροια στην περίπτωση της Μάλαγα είναι μικρού εύρους, συνεπώς οι κυματικές παράμετροι μπορούν να θεωρηθούν πιο κρίσιμοι από αυτούς της θαλάσσιας στάθμης για την υπό μελέτη κατασκευή.



Εικόνα 21 Πολύγωνα συχνότητας των TL και SL όπως μετρήθηκαν από τον παλιρροιογράφο [35]

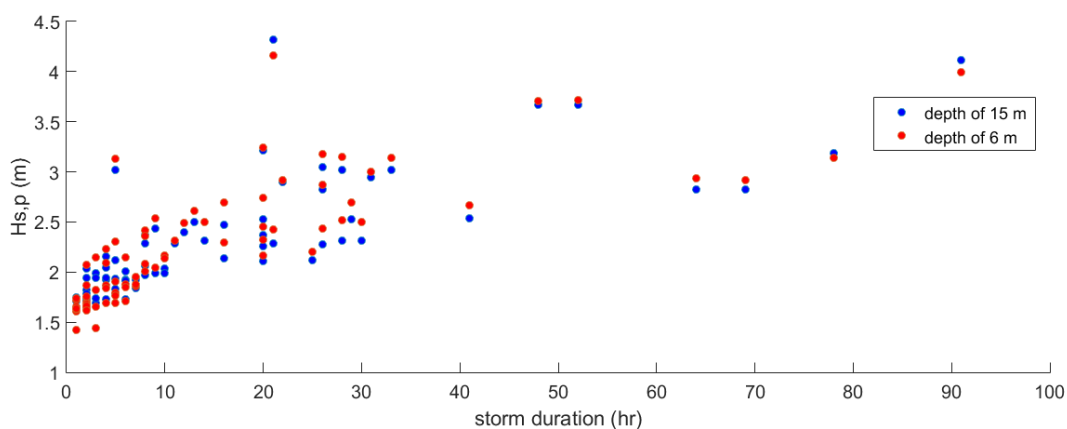
3.4.2 Αναγνώριση ακραίων γεγονότων - καταιγίδων

Αρχικά, επιλέχθηκε ένα κατώφλι u_1 για το H_s διαχωρίζοντας τα ασθενή από τα μεσαία και ακραία γεγονότα του δείγματος. Επίσης, επιλέχθηκε μία ελάχιστη περίοδος ηρεμίας/ύφεσης των 6 hr [51] μεταξύ δύο διαδοχικών καταιγίδων – γεγονότων για να εξασφαλίσει ότι τα δύο γεγονότα είναι ανεξάρτητα μεταξύ τους. Από τη διαδικασία αυτή, προκύπτει το δείγμα των μέγιστων σημαντικών υψών κύματος $H_{s,p}$ κατά τη διάρκεια της κάθε καταιγίδας. Στην παρούσα μελέτη, το αρχικό κατώφλι u_1 ήταν ίσο με 1.65 m, που αντιστοιχεί στο ποσοστημόριο 98.5 των δεδομένων του H_s . Τα ιστογράμματα και το διάγραμμα διασποράς της διάρκειας και του $H_{s,p}$ των ανεξάρτητων γεγονότων παρουσιάζονται στην Εικόνα 22.

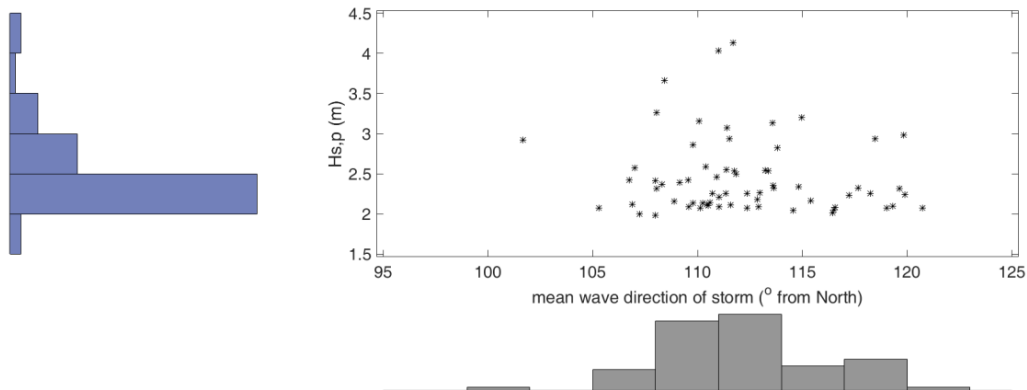


Εικόνα 22 Ιστογράμματα και διάγραμμα διασποράς της διάρκειας και του $H_{s,p}$ των ανεξάρτητων γεγονότων στη θέση του μετρητικού σταθμού

Ο πυθμένας της θάλασσας θεωρήθηκε επίπεδος με κλίση ίση με τη μέση κλίση του, 5%. Συνεπώς, η διακύμανση της θαλάσσιας στάθμης λόγω αστρονομικής και μετεωρολογικής παλίρροιας και τα κυματικά δεδομένα χρειάζονται να μεταφερθούν στη θέση της κατασκευής, δηλ. στο βάθος των 6 m. Στην Εικόνα 23, γίνεται σύγκριση των διαγραμμάτων διασποράς της διάρκειας και του $H_{s,p}$ των ανεξάρτητων γεγονότων στη θέση του μετρητικού σταθμού και στη θέση της κατασκευής. Επίσης, στην Εικόνα 24, παρουσιάζονται τα ιστογράμματα και το διάγραμμα διασποράς του $H_{s,p}$ και της θ_m των γεγονότων στη θέση της κατασκευής, στην οποία φαίνεται ότι οι κατευθύνσεις προέλευσης όλων των γεγονότων αυτών ανήκει στο διάστημα από 100° έως 125° από τον Βορρά και η πιο ακραία καταγίδα, που παρατηρήθηκε στο δείγμα, έχει την κατεύθυνση των 113° από τον Βορρά, η οποία είναι κάθετη στις ισοβαθείς, όπως και στην ακτογραμμή.



Εικόνα 23 Σύγκριση των διαγραμμάτων διασποράς της διάρκειας και του $H_{s,p}$ των ανεξάρτητων γεγονότων στη θέση του μετρητικού σταθμού (μπλε κουκκίδες) και στη θέση της κατασκευής (κόκκινες κουκκίδες)



Εικόνα 24 Ιστογράμματα και διάγραμμα διασποράς των $H_{s,p}$ και θ_m των γεγονότων στη θέση της κατασκευής

Στο επόμενο βήμα, επιλέγεται ένα δεύτερο κατώφλι u_2 υψηλότερο από το u_1 . Σύμφωνα με τα αποτελέσματα των δύο μεθόδων (ήτοι [61], [62]) για την επιλογή του u_2 και κατ' επέκταση των παραμέτρων της κατανομής GP, η τιμή του 2.409 m επιλέγεται για το u_2 , που αντιστοιχεί στη θεώρηση περίπου 3 ακραίων γεγονότων το έτος.

Οι περίοδοι επαναφοράς και οι επιστρεφόμενες τιμές για το $H_{s,p}$ συνδυασμένες με τις πιο πιθανές τιμές της μέσης περιόδου και κατεύθυνσης γεγονότος στη θέση της κατασκευής, οι οποίες επιλέχθηκαν για την αρχική προσέγγιση σχεδιασμού, παρουσιάζονται στον Πίνακα 12.

Πίνακας 12 Περίοδοι επαναφοράς και επιστρεφόμενες τιμές για το $H_{s,p}$ συνδυασμένες με τις πιο πιθανές τιμές της μέσης περιόδου και κατεύθυνσης γεγονότος στη θέση της κατασκευής

Περίοδος επαναφοράς T_r για $H_{s,p}$ (έτη)	$H_{s,p}$ (m)	T_m (s)	Διάρκεια (hr)	θ_m (° από Βορρά)
10	4.03	6.25	3	113
100	4.54	6.58	3	113

Στον Πίνακα 13, παρουσιάζεται το εκτιμώμενο μέσο βάρος των στοιχείων της κατασκευής από τον πρωταρχικό σχεδιασμό για τις δύο περιόδους επαναφοράς του $H_{s,p}$. Επιπλέον, οι πιθανότητες υπέρβασης των $H_{s,p}$ για τα δύο σενάρια κατά τη διάρκεια ενός έτους και κατά τη διάρκεια της ζωής του έργου παρουσιάζονται στον Πίνακα 14.

Πίνακας 13 Μέσο βάρος των μονάδων των στοιχείων της κατασκευής από τον πρωταρχικό σχεδιασμό

T_r for $H_{s,p}$ (years)	Seaside armor units (kg)	Rear-side armor units (kg)	Toe units (kg)
10	5018	1241	379
100	6980	1915	542

Πίνακας 14 Πιθανότητες αστοχίας ανά έτος και κατά τη διάρκεια ζωής του έργου (15 έτη), για τα σενάρια σχεδιασμού $H_{s,p}$ (Malaga)

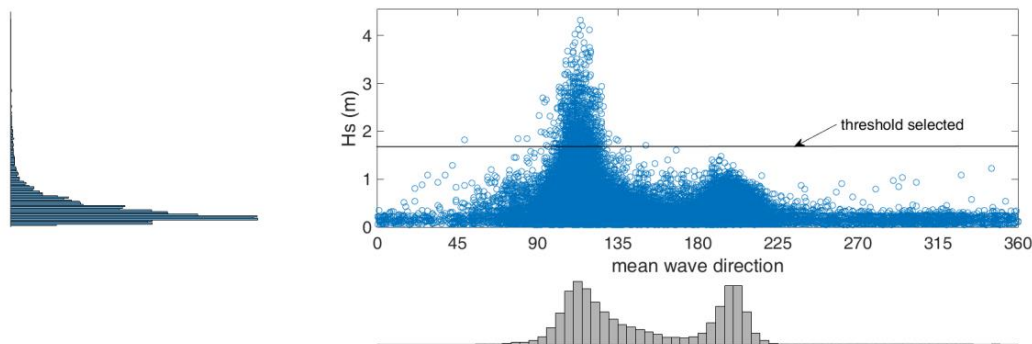
T_r for $H_{s,p}$ (years)	$P_{ex,H_{s,p},e,1y}$	$P_{f,e,L}$
10	$3.20 \cdot 10^{-2}$	$7.82 \cdot 10^{-1}$
100	$3.20 \cdot 10^{-3}$	$1.40 \cdot 10^{-1}$

Σημειώνεται ότι στην παρούσα διατριβή, διεξήχθη μία ανάλυση ακραίων τιμών για μία μεταβλητή βασισμένη σε γεγονότα, και στη συνέχεια οι εξαγόμενες επιστρεφόμενες τιμές της συνδυάστηκαν με τις πιο πιθανές τιμές άλλων μεταβλητών, μέσω των αντίστοιχων διαγραμμάτων διασποράς. Ωστόσο, μία πολυπαραμετρική ανάλυση ακραίων τιμών (π.χ. [63]) συνιστάται για μία πιο ακριβή εκτίμηση των τιμών των λοιπών μεταβλητών. Αυτό δεν επιχειρείται στην παρούσα διατριβή, αφού η ακόλουθη ανάλυση των θαλάσσιων καταστάσεων χρησιμοποιείται για τον πιθανοτικό σχεδιασμό της κατασκευής.

3.4.2 Στατιστική ανάλυση των θαλάσσιων καταστάσεων

Σε αυτό το βήμα, διεξήχθη η στατιστική ανάλυση των διαδοχικών θαλάσσιων καταστάσεων εντός των ακραίων γεγονότων για να ληφθούν ως φορτίσεις στην υπό μελέτη κατασκευή. Αρχικά, το ίδιο κατώφλι εφαρμόστηκε στα δεδομένα του H_s , όπως στην ανάλυση ακραίων τιμών βασισμένη σε γεγονότα, για να φιλτράρει τις πιο σημαντικές και κρίσιμες θαλάσσιες καταστάσεις που θα μεταφερθούν στη θέση της κατασκευής. Με τον τρόπο αυτό, οι πιο κρίσιμες θαλάσσιες καταστάσεις διαχωρίζονται από το συνολικό δείγμα, αλλά επίσης και ο όγκος των δεδομένων και ο υπολογιστικός φόρτος περιορίζεται σημαντικά.

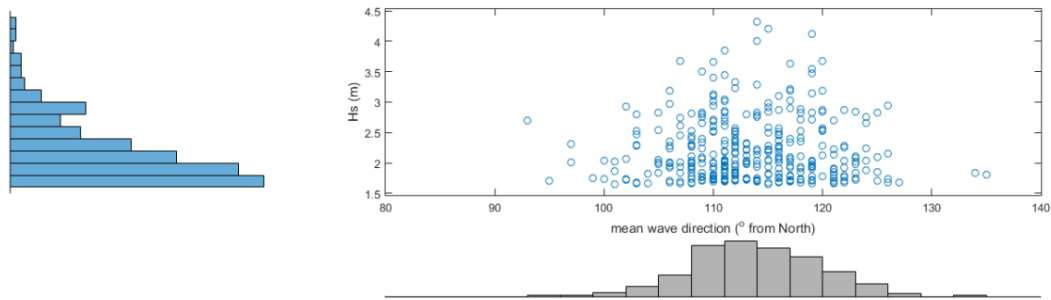
Όπως φαίνεται στην Εικόνα 25, ένα κατώφλι εφαρμόστηκε στα δεδομένα του H_s , με στόχο να φιλτράρει τις πιο σημαντικές θαλάσσιες καταστάσεις που θα μεταφερθούν στη θέση της κατασκευής. Με το συγκεκριμένο τρόπο (δηλ. θέτοντας $H_s > 1.65$ m) το σύνολο των θαλάσσιων καταστάσεων που θα διόδευτεί από το βάθος των 15 m στο βάθος των 6 m αποτελεί το 1.5% του αρχικού δείγματος.



Εικόνα 25 Ιστογράμματα και διάγραμμα διασποράς των H_s και θ_m των θαλάσσιων καταστάσεων στη θέση του μετρητικού σταθμού [35]

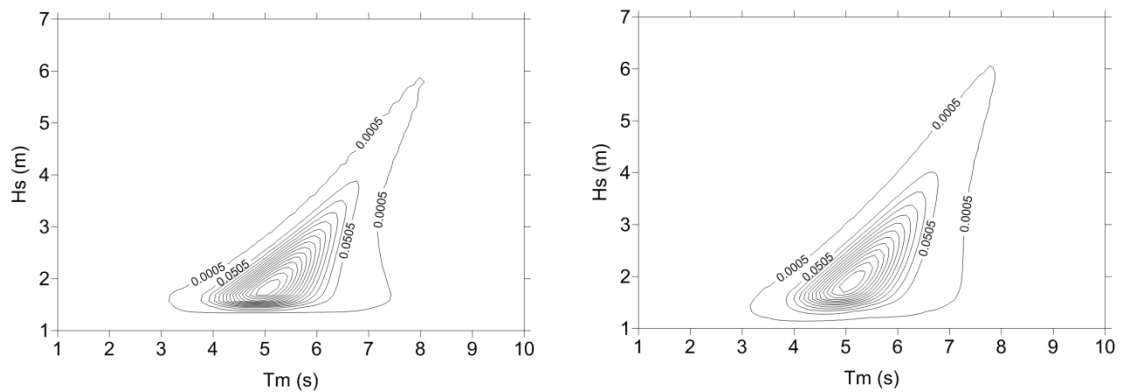
Στη συγκεκριμένη εφαρμογή, χρησιμοποιήθηκε ένα βήμα τριών ωρών που αφορά την αναπαράσταση των θαλάσσιων καταστάσεων στην αξιοπιστία των παράκτιων κατασκευών, έτσι ώστε οι θαλάσσιες καταστάσεις να αντιστοιχούν σε περισσότερο από 1000 κυματισμούς ανά θαλάσσια κατάσταση. Στη συνέχεια, επιλέγεται το μέγιστο H_s σε μία σειρά τριών μονώρων μετρήσεων του H_s εντός μίας καταιγίδας για να αναπαραστήσει τη θαλάσσια κατάσταση.

Εφαρμόζοντας τώρα το ίδιο μοντέλο κυματικής διάδοσης [33] όπως με τις καταιγίδες - γεγονότα, το υποσύνολο των θαλάσσιων καταστάσεων μεταφέρθηκε από το βάθος των 15 m στα 6 m. Τα ιστογράμματα και το διάγραμμα διασποράς των H_s και θ_m που μεταφέρθηκαν στο βάθος των 6 m απεικονίζονται στην Εικόνα 26. Κρίνοντας από την Εικόνα 26, το θ_m αυτών των θαλάσσιων καταστάσεων είναι συγκεντρωμένο σε ένα στενό εύρος κατευθύνσεων, όμοιο με αυτό των καταιγίδων. Συνεπώς, στο σημείο αυτό μπορεί να γίνει η απλοποίηση ότι όλες αυτές οι θαλάσσιες καταστάσεις έχουν κοινή θ_m , που στην περίπτωση της Μάλαγα έχουν κάθετη πρόσπτωση στο έργο.



Εικόνα 26 Ιστογράμματα και διάγραμμα διασποράς των H_s και θ_m του υποσύνολου των θαλάσσιων καταστάσεων στη θέση της κατασκευής

Εφαρμόζοντας, στο σημείο αυτό, το μοντέλο δεσμευμένης πιθανότητας για δύο μεταβλητές, ήτοι H_s και T_m , προκύπτει η δεσμευμένη από κοινού πυκνότητα πιθανότητας των H_s και T_m , δεδομένου ότι οι ληφθείσες θαλάσσιες καταστάσεις ανήκουν στο επιλεγμένο υποσύνολο στη θέση του μετρητικού σταθμού και του έργου. Όπως φαίνεται στην Εικόνα 27, όπου παρουσιάζεται αυτή η σύγκριση, η δεσμευμένη από κοινού πυκνότητα πιθανότητας των H_s και T_m στη θέση της κατασκευής διαφέρει από αυτή του μετρητικού σταθμού, παρά το γεγονός ότι και οι δύο αυτές θέσεις ανήκουν στα ενδιάμεσα νερά.



Εικόνα 27 Δεσμευμένη από κοινού πυκνότητα πιθανότητας των H_s και T_m , δεδομένου ότι οι ληφθείσες θαλάσσιες καταστάσεις ανήκουν στο επιλεγμένο υποσύνολο, στη θέση του μετρητικού σταθμού (αριστερά) και στη θέση της κατασκευής (δεξιά) (καμπύλες ίσης πυκνότητας πιθανότητας με βήμα 0.05 1/s/m)

3.4.3 Εκτιμώντας την πιθανότητα αστοχίας μέσω της DIM και MCM

Εφόσον έναν από τους στόχους της παρούσας διατριβής αποτελεί και η διερεύνηση της επίδρασης διαφόρων τύπων παραμέτρων ως στοχαστικών μεταβλητών στην εκτιμώμενη πιθανότητα αστοχίας της κατασκευής, εξετάστηκαν οι εξής τρεις περιπτώσεις. Αρχικά,

εξετάστηκαν μόνο οι κυματικές παράμετροι, στη συνέχεια οι κυματικές παράμετροι και οι παράμετροι θαλάσσιας στάθμης και τέλος οι προηγούμενες σε συνδυασμό με μία στοχαστική παράμετρο αντίστασης της κατασκευής. Σημειώνεται ότι στην πρώτη περίπτωση οι παράμετροι SL και TL θεωρήθηκαν ίσες με το μηδέν.

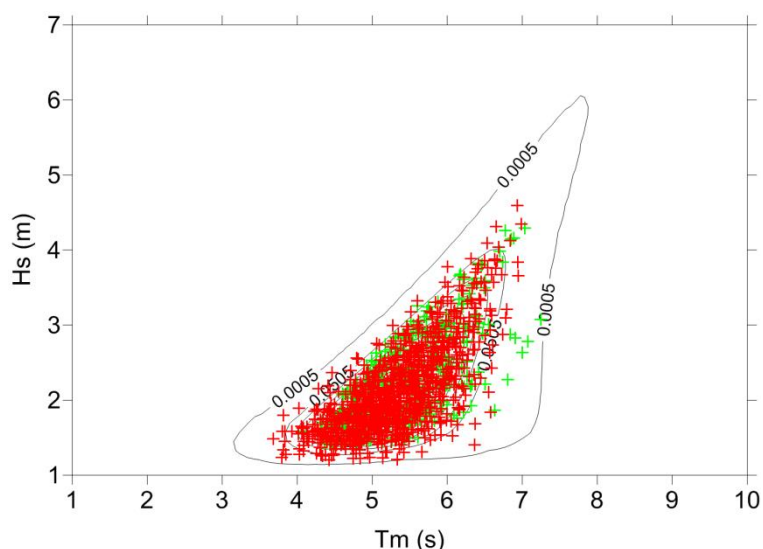
Στην τρίτη περίπτωση, ως στοχαστική μεταβλητή λήφθηκε η πυκνότητα μάζας των φυσικών ογκολίθων. Επειδή η κατανομή της είναι άγνωστη, χρησιμοποιήθηκε για την πιθανοτική της αναπαράσταση μία κανονική κατανομή, της οποίας η μέση τιμή είναι ίση με 2650 kg/m^3 , και η τυπική της απόκλιση ίση με 10 kg/m^3 .

Σημειώνεται ότι δεδομένου ότι η περίπτωση της Μάλαγα αφορά σε μικρές διακυμάνσεις της μετεωρολογικής και αστρονομικής παλίρροιας, η σχέση αλληλεπίδρασης των κυματικών παραμέτρων με τις παραμέτρους στάθμης TL, SL στη θέση της κατασκευής δεν έχει ληφθεί υπόψη.

Όσον αφορά στην εφαρμογή της εξίσωσης 28 μέσω της μεθόδου DIM στη συγκεκριμένη περίπτωση, τα βήματα ολοκλήρωσης d_t και d_s ελήφθησαν ίσα με 0.05 m , και τα dH_s και dT_m ίσα με 0.10 m και 0.10 s , αντίστοιχα, τα οποία θεωρήθηκαν ικανοποιητικά μικρά.

Στη μέθοδο MCM, παράχθηκε ένα τυχαίο δείγμα για κάθε μεταβλητή, το οποίο ακολουθούσε την κατανομή της, αλλά παράλληλα διατηρώντας τη στατιστική συσχέτιση μεταξύ των μεταβλητών με σημαντική συσχέτιση, π.χ. των T_m και H_s . Στην Εικόνα 28, απεικονίζεται το διάγραμμα διασποράς των T_m και H_s στη θέση του έργου, η συνάρτηση από κοινού πυκνότητας πιθανότητας των δύο μεταβλητών, και το δείγμα της μεθόδου MCM, παρουσιάζοντας καλή συμφωνία.

Η επιλογή του συνολικού αριθμού προσομοιώσεων για την κάθε μία παράμετρο εξαρτάται από τη μεταβλητότητα και τον πληθυσμό της. Για παράδειγμα, στη συγκεκριμένη μελέτη ο συνολικός αριθμός προσομοιώσεων για τους κυματισμούς ήταν ίσος με 1500, ενώ για το SL και TL 50, και 20 για τις παραμέτρους αντίστασης, το οποίο συνεπάγεται $7.5 \cdot 10^7$ επαναλήψεις. Από τα παραπάνω, συμπεραίνεται ότι οι υπολογιστικές απαιτήσεις της MCM μπορεί να γίνουν σημαντικά υψηλές.



Εικόνα 28 Σύγκριση του τυχαίου δείγματος της MCM (κόκκινο) με το υποσύνολο του δείγματος στη θέση της κατασκευής (πράσινο) (καμπύλες ίσης πυκνότητας πιθανότητας με βήμα 0.05 1/s/m)

3.4.4 Αποτελέσματα και συζήτηση

Οι προτεινόμενες λύσεις σχεδιασμού που προέκυψαν από την αρχική προσέγγιση σχεδιασμού βάσει των ακραίων γεγονότων στη θέση της κατασκευής γίνονται οι αρχικές λύσεις για την DIM για την πρώτη περίπτωση. Στη συγκεκριμένη περίπτωση, η DIM θεωρεί μόνο τις κυματικές παραμέτρους ως στοχαστικές μεταβλητές (βλ. Πίνακα 15). Όπως παρατηρείται στον Πίνακα 13, τα αποτελέσματα της μεθόδου DIM αφορούν στη δεσμευμένη πιθανότητα αστοχίας της κατασκευής δεδομένης της υπέρβασης καταφλίου και της μη δεσμευμένης πιθανότητάς της στα 8 έτη μετρήσεων. Τα αποτελέσματα της DIM διαφέρουν σε σημαντικό βαθμό από αυτά της αρχικής προσέγγισης σχεδιασμού βάσει ακραίων γεγονότων. Αυτό θα μπορούσε να αποδοθεί στο ότι οι δύο αυτές προσεγγίσεις υπολογίζουν πιθανότητες αστοχίας διαφορετικού τύπου.

Πίνακας 15 Δεσμευμένη και μη δεσμευμένη πιθανότητα αστοχίας του συστήματος/ κατασκευής στα Υ=8 έτη μέσω της DIM για την πρώτη περίπτωση

Περίοδος επαναφοράς για το $H_{s,p}$ (σε έτη)	Δεσμευμένη (Περίπτωση 1)	Μη δεσμευμένη (Περίπτωση 1)
10	$2.42 \cdot 10^{-2}$	$3.97 \cdot 10^{-4}$
100	$6.99 \cdot 10^{-3}$	$1.15 \cdot 10^{-4}$

Επίσης, τα αποτελέσματα της DIM για τις τρεις περιπτώσεις παρουσιάζονται στον Πίνακα 16. Κρίνοντας από τον Πίνακα 16, η πιθανότητα αστοχίας της κατασκευής είναι υψηλότερη στη δεύτερη από ότι στην πρώτη περίπτωση. Προφανώς, αυτό θα μπορούσε να αποφευχθεί, εάν η κατασκευή είχε σχεδιασθεί στην πρώτη περίπτωση για μία υψηλότερη τιμή της αστρονομικής και μετεωρολογικής παλίρροιας. Η βελτιστοποίηση αυτή συνιστάται για τον σχεδιασμό της κατασκευής.

Σχετικά με τη σύγκριση των αποτελεσμάτων των δύο τελευταίων περιπτώσεων, τα αποτελέσματα είναι περίπου ίσα. Αυτό θα μπορούσε να εξηγηθεί από το γεγονός ότι στη δεύτερη περίπτωση η παράμετρος αντίστασης έχει την ίδια τιμή με τη μέση τιμή της παραμέτρου στην τρίτη περίπτωση, και η κατανομή της στην τρίτη περίπτωση είναι συμμετρική γύρω από αυτή τη μέση τιμή.

Πίνακας 16 Μη δεσμευμένη πιθανότητα αστοχίας συστήματος για Y=8 έτη μέσω της DIM για τις τρεις περιπτώσεις

Περίοδος επαναφοράς για το $H_{s,p}$ (σε έτη)	(Περίπτωση 1)	(Περίπτωση 2)	(Περίπτωση 3)
10	$3.97 \cdot 10^{-4}$	$4.03 \cdot 10^{-4}$	$4.05 \cdot 10^{-4}$
100	$1.15 \cdot 10^{-4}$	$1.22 \cdot 10^{-4}$	$1.20 \cdot 10^{-4}$

Στον Πίνακα 17, παρουσιάζεται μία σύγκριση των μεθόδων DIM και MCM για την τρίτη περίπτωση. Ειδικότερα, και τα αποτελέσματα των δύο μεθόδων πλησιάζουν αρκετά, αλλά της MCM είναι λίγο υψηλότερα. Το γεγονός αυτό θα μπορούσε να αποδοθεί στη δυσκολία που πρόεκυψε στη σύγκλιση των αποτελεσμάτων της MCM ως προς τον αριθμό των προσομοιώσεων. Παρά το γεγονός ότι η DIM κρίνεται πιο κατάλληλη στην προκειμένη περίπτωση εκτίμησης αξιοπιστίας της εν λόγω κατασκευής, σε πιο σύνθετα προβλήματα μέθοδοι βασισμένες σε προσομοιώσεις, όπως η MCM, θα μπορούσαν να θεωρηθούν πιο ευέλικτες και αποτελεσματικές.

Πίνακας 16 Μη δεσμευμένη πιθανότητα αστοχίας συστήματος για Y=8 έτη μέσω της DIM και της MCM για την τρίτη περίπτωση

Περίοδος επαναφοράς για το $H_{s,p}$ (σε έτη)	DIM	MCM
10	$4.05 \cdot 10^{-4}$	$4.79 \cdot 10^{-4}$

Τέλος, εκκρεμεί το βήμα της βελτιστοποίησης βάσει της αξιοπιστίας «στόχου», οικονομικών και κοινωνικών κριτηρίων, το οποίο επιβάλλεται για την τελική επιλογή της σχεδιαστικής λύσης της κατασκευής. Το βήμα αυτό δεν θα παρουσιαστεί.

4. Συμπεράσματα

4.1 Περίληψη

Στην παρούσα διατριβή, παρουσιάζεται μία καθολική μεθοδολογία για την εκτίμηση της αξιοπιστίας παράκτιων κατασκευών υπό κυματική φόρτιση, η οποία ξεκινάει από τη συλλογή κυματικών δεδομένων που είναι διαθέσιμα συνήθως στα βαθιά νερά, και καταλήγει στην εκτίμηση της πιθανότητας αστοχίας των κατασκευών αυτών στη διάρκεια της ζωής τους. Σαν δεύτερο βήμα, αναπτύχθηκε και εφαρμόστηκε ένα στατιστικό μοντέλο γραμμικής κυματικής διάδοσης, το οποίο ολοκληρώνει τις βραχυπρόθεσμες με τις μακροπρόθεσμες κυματικές στατιστικές από τα βαθιά στα ενδιάμεσα νερά. Η ικανότητα του στατιστικού μοντέλου γραμμικής κυματικής διάδοσης να παράγει με δόκιμο τρόπο τις βραχυπρόθεσμες κυματικές στατιστικές στα βαθιά και ενδιάμεσα νερά διερευνήθηκε μέσω συγκρίσεων των αποτελεσμάτων με μετρήσεις στα βαθιά νερά και με τα αποτελέσματα ενός εμπορικού και αξιόπιστου μοντέλου τύπου Boussinesq στα ενδιάμεσα νερά. Όσον αφορά την ανάλυση αξιοπιστίας των παράκτιων κατασκευών, παρουσιάζεται μία λεπτομερειακή πιθανοτική ανάλυση, η οποία εστιάζει στην περίπτωση των συμβατικών κυματοθραυστών με πρηνή. Τέλος, εξετάστηκαν παραδείγματα ανάλυσης αξιοπιστίας ενός κυματοθραυστή από δύο σταθμούς στη Μεσόγειο διεκρινίζοντας κάποια από τα σημαντικά θέματα που αφορούν την εκτίμηση αξιοπιστίας των παράκτιων κατασκευών.

4.2 Συνδυάζοντας τις βραχυπρόθεσμες με τις μακροπρόθεσμες κυματικές στατιστικές από τα βαθιά στα ενδιάμεσα νερά

Ένα από τα κυριότερα θέματα του πιθανοτικού σχεδιασμού των παράκτιων κατασκευών αποτελεί η ακριβής περιγραφή του μακροπρόθεσμου κυματικού κλίματος στα ενδιάμεσα νερά, όπου συνήθως κατασκευάζονται τα έργα αυτά. Αυτό είναι και ένα από τα κυριότερα αντικείμενα της παρούσας διατριβής. Η περιγραφή του μακροπρόθεσμου κυματικού κλίματος στα ενδιάμεσα νερά επιτυγχάνεται εδώ μέσω της εφαρμογής μίας τεχνικής μείωσης του

όγκου των δεδομένων στα βαθιά νερά και ενός στατιστικού γραμμικού μοντέλου κυματικής διάδοσης, το οποίο συνδυάζει τις βραχυπρόθεσμες με τις μακροπρόθεσμες κυματικές στατιστικές από τα βαθιά στα ενδιάμεσα νερά και αναπτύχθηκε για το σκοπό αυτό.

Όπως παρατηρήθηκε από τα αποτελέσματα του μοντέλου στα βαθιά και ενδιάμεσα νερά, οι συναρτήσεις από κοινού πυκνότητας πιθανότητας των T_m και H_s στα βαθιά διαφέρουν σε έναν βαθμό από εκείνες που εκτιμήθηκαν για τα ενδιάμεσα νερά. Αυτό οφείλεται στις διεργασίες που λαμβάνουν χώρα στους κυματισμούς που διαδίδονται προς την ακτή, όπως η ρήγωση, η διάθλαση, η θραύση, κλπ. Ωστόσο, παρατηρήθηκε ότι ο τύπος της περιθώριας κατανομής του H_s που αναπαριστούσε καλύτερα τα δεδομένα ήταν ίδιος με αυτόν στα ενδιάμεσα νερά και για τους τρεις σταθμούς, που εξετάστηκαν.

Επίσης, το μοντέλο που αναπτύχθηκε [33], εκτιμά τη μέση στατιστική κατεύθυνση των κυματισμών θ_m , εκτός των H_s και T_m , στα ενδιάμεσα νερά, χρησιμοποιώντας σαν δεδομένα τα H_s , T_m , θ_m στα βαθιά νερά. Αυτό επιτεύχθηκε μέσω μίας εξίσωσης ενσωμάτωσης της κατευθυντικότητας των κυματισμών σε μία στατιστική ανάλυση κύμα προς κύμα. Η εξίσωση αυτή αναπτύχθηκε στα πλαίσια της παρούσας διατριβής. Η εν λόγω προσέγγιση βασίζεται στην υπόθεση ότι μεταξύ των κυματισμών ίδιας κλάσης περιόδου, αυτοί που συνδυάζονται με μεγαλύτερα ύψη κύματος H τείνουν να έχουν κατευθύνσεις πιο κοντά στη θ_m σε σχέση με εκείνα που συνδυάζονται με χαμηλότερα H , υποδεικνύοντας ότι τα H και θ δεν είναι ανεξάρτητα. Αυτή η υπόθεση συμφωνεί με τον Tucker [37].

Επιπρόσθετα, το μοντέλο [33] παρέχει πληροφορία σχετικά με τη μακροπρόθεσμη συνάρτηση από κοινού πυκνότητας πιθανότητας των H , T , θ , όπως και τη μακροπρόθεσμη συνάρτηση από κοινού πυκνότητας πιθανότητας των H_s , T_m , θ_m , στα ενδιάμεσα νερά μέσω τροποποίησης της σχέσης του Battjes [36], η οποία επεκτάθηκε ώστε να θεωρεί, επιπλέον του H , και τα T και θ . Η πληροφορία αυτή είναι σημαντική για πολλές εφαρμογές, όπως είναι η ανάλυση κοπώσεως, και η ανάλυση εκτίμησης αξιοπιστίας των παράκτιων κατασκευών.

4.3 Διερεύνηση της περιοχής έγκυρης εφαρμογής του μοντέλου

Σχετικά με τις βραχυπρόθεσμες κυματικές στατιστικές στα βαθιά νερά που λαμβάνονται υπόψη από το μοντέλο των Malliouri et al. [33], αποδείχθηκε ότι η συνάρτηση της από κοινού πυκνότητας πιθανότητας των T και H μίας πραγματικής θαλάσσιας κατάστασης θα μπορούσε καλά να αναπαρασταθεί από τις αδιάστατες πιθανοτικές εικόνες των Memos and Tzanis ([29]; [30]). Οι εικόνες αυτές αναφέρονται σε μη γραμμικούς κυματισμούς στα βαθιά νερά. Σχετικά με τις βραχυπρόθεσμες κυματικές στατιστικές στα ενδιάμεσα νερά που

λαμβάνονται υπόψη από το μοντέλο των Malliouri et al. [33], οι συγκρίσεις του εν λόγω μοντέλου με το μη γραμμικό μοντέλο τύπου Boussinesq έδειξαν καλή συμφωνία των δύο μοντέλων στη βαθιά και μεσαία ζώνη των ενδιάμεσων νερών, καθιστώντας αυτό ικανό να χρησιμοποιηθεί για το σχεδιασμό πληθώρας παράκτιων κατασκευών.

Επιπλέον, ένα γενικότερο συμπέρασμα εξάγεται από την παρούσα ανάλυση. Αυτό αναφέρεται ότι εντός της προσεγγιστικής περιοχής εφαρμογής της γραμμικής θεωρίας (βλ. π.χ. [64]), ήτοι για $Ur < 40$ και $s_m < 0.04$, το γραμμικό μοντέλο κυματικής διάδοσης των Malliouri et al. [33] δύναται να προσεγγίσει ικανοποιητικά τα αποτελέσματα ενός μη γραμμικού μοντέλου τύπου Boussinesq, όπως αυτό που εμπεριέχεται στο πακέτο λογισμικού MIKE 21 BW. Ωστόσο, το γραμμικό αυτό μοντέλο μπορεί να χρησιμοποιηθεί (π.χ. για το σχεδιασμό παράκτιων κατασκευών) σε μία ευρύτερη περιοχή, η οποία αφορά στη βαθύτερη και μεσαία ζώνη των ενδιάμεσων νερών, ανάντη της ζώνης θραύσης.

4.4 Εξετάζοντας και συγκρίνοντας την ανάλυση στις θαλάσσιες καταστάσεις με την ανάλυση ακραίων τιμών σε γεγονότα

Συνεχίζοντας, αναπτύχθηκε μία πλήρως πιθανοτική μεθοδολογία αξιοπιστίας συμβατικού κυματοθραύστη που αφορά τόσο στην ανάλυση ακραίων τιμών, που στηρίζεται σε γεγονότα, όσο και στην ανάλυση στις θαλάσσιες καταστάσεις. Σημειώνεται ότι η συγκεκριμένη μεθοδολογία διαφοροποιείται σε ένα βαθμό για τις δύο αυτές περιπτώσεις. Αυτό έχει ως αποτέλεσμα στην πρώτη περίπτωση να εκτιμάται η πιθανότητα αστοχίας της κατασκευής κατά τη διάρκεια της ζωής της εκτιμώμενη στο σύνολο των ακραίων γεγονότων. Ωστόσο, στη δεύτερη περίπτωση υπολογίζεται το ποσοστό της περιόδου αναφοράς (π.χ. διάρκειας μετρήσεων) στο οποίο η κατασκευή θα αστοχεί.

Επιπρόσθετα, σημειώνεται ότι και οι δύο προσεγγίσεις μπορούν να ενσωματωθούν σε μία ανάλυση αξιοπιστίας και πιθανοτικού σχεδιασμού των παράκτιων κατασκευών. Στα πλεονεκτήματα της μεθόδου αξιοπιστίας βάσει ακραίων γεγονότων συγκαταλέγεται κυρίως το γεγονός ότι μπορεί να επιτευχθεί εκτίμηση της πιθανότητας αστοχίας της κατασκευής στη ζωή του έργου, στο σύνολο των ακραίων γεγονότων. Ωστόσο, στη συγκεκριμένη προσέγγιση χάνεται ουσιαστική πληροφορία που είναι κρίσιμη για τον σχεδιασμό, καθώς εξετάζονται μόνο οι εκπρόσωποι των γεγονότων, δηλ τα H_{sp} , και δεν μπορεί να υπολογιστεί το ποσοστό της ζωής του έργου στο οποίο η κατασκευή θα αστοχεί.

Αντιθέτως, η μέθοδος αξιοπιστίας, που εφαρμόζεται σε όλες τις θαλάσσιες συνθήκες, αξιοποιεί όλη την κρίσιμη πληροφορία των φορτίσεων στις παράκτιες κατασκευές και δύναται να εκτιμήσει το ποσοστό μίας χρονικής περιόδου αναφοράς στο οποίο η κατασκευή

θα αστοχεί. Το εξαγόμενο αυτό ποσοστό είναι ιδιαίτερα χρήσιμο, καθώς μπορεί να ενσωματωθεί εύλογα σε μία ολοκληρωμένη ανάλυση επικινδυνότητας των παράκτιων κατασκευών, θεωρώντας επίσης οικονομικά και κοινωνικά κριτήρια. Παρόλα αυτά τα θετικά στοιχεία της εν λόγω προσέγγισης, η μέθοδος αξιοπιστίας που εφαρμόζεται σε όλες τις θαλάσσιες συνθήκες δεν μπορεί να μεταφέρει το αποτέλεσμα της αστοχίας από μία περίοδο αναφοράς σε μία άλλη, δηλ. στη ζωή του έργου.

Συμπερασματικά, η ανάλυση αξιοπιστίας που εφαρμόζεται σε όλες τις θαλάσσιες συνθήκες συνιστάται για την ανάλυση αξιοπιστίας και τον σχεδιασμό παράκτιων έργων, όταν η περίοδος των μετρήσεων είναι περίπου ίση ή μεγαλύτερη της ζωής των έργων. Σε άλλες περιπτώσεις, η ανάλυση αξιοπιστίας βάσει ακραίων γεγονότων θα μπορούσε να χρησιμοποιηθεί για τον σχεδιασμό των παράκτιων κατασκευών, λαμβάνοντας ωστόσο υπόψη τα μειονεκτήματά της, και η άλλη προσέγγιση για την ανάλυση λειτουργικότητας των κατασκευών αυτών.

4.5 Εκτίμηση αξιοπιστίας παράκτιων κατασκευών

Αξίζει να σημειωθεί ότι στην πλήρως πιθανοτική μεθοδολογία, που υιοθετήθηκε στην παρούσα διατριβή, η πιθανότητα αστοχίας της κατασκευής (η τελευταία αναφέρεται ως σύστημα) μπορεί να εκτιμηθεί μέσω της θεώρησης της ένωσης των ενδεχομένων αστοχίας των στοιχείων της κατασκευής σε περίπτωση σειριακού διαγράμματος αστοχιών. Επίσης, δύο διαφορετικές πλήρως πιθανοτικές μέθοδοι, ήτοι η Μέθοδος Άμεσης Ολοκλήρωσης και η Μέθοδος Monte Carlo, εφαρμόστηκαν και συγκρίθηκαν μεταξύ τους, χρησιμοποιώντας έναν συνδυασμό μεταβλητών με μηδενικό και μη-μηδενικό βαθμό επικινδυνότητας. Ο συνδυασμός αυτός αναφέρεται εδώ ως μία συνδυασμένη ανάλυση χρονικά μεταβαλλόμενων και χρονικά αμετάβλητων μεταβλητών. Επιπλέον, διερευνήθηκε το κατάλληλο χρονικό βήμα ορισμού της θαλάσσιας κατάστασης στην ανάλυση των θαλάσσιων καταστάσεων, θεωρώντας με τον τρόπο αυτό την ιστορία και τη μορφή των κυματικών καταιγίδων-γεγονότων. Τέλος, διερευνήθηκε η επίδραση της θεώρησης περισσότερων στοχαστικών μεταβλητών διαφορετικού τύπου στην εκτιμώμενη πιθανότητα αστοχίας της κατασκευής.

Εν συντομία, κάποια από τα σημαντικά θέματα στην εκτίμηση της αξιοπιστίας των παράκτιων κατασκευών διευκρινίστηκαν με την παρουσίαση παραδειγμάτων, διαγραμμάτων ροής και μαθηματικών εξισώσεων, που περιγράφουν τη διαδικασία. Ωστόσο, περισσότερα ακόμη θέματα χρειάζεται να αντιμετωπιστούν ώστε οι μηχανικοί να δύνανται να σχεδιάζουν τις εν λόγω κατασκευές ώστε να ικανοποιούν συγκεκριμένα και προκαθορισμένα επίπεδα αξιοπιστίας.

Abstract
Probabilistic Design of Coastal Structures

Dimitra I. Malliouri

National Technical University of Athens
School of Civil Engineering
Department of Water Resources and Environmental Engineering
Laboratory of Harbour Works

Nowadays, more and more researchers and engineers have realized that coastal structures should be designed to meet predefined safety and performance levels, i.e. the reliability level. This can be accomplished by implementing a thorough methodology able to assess accurately the reliability level of a coastal structure, i.e. the probability of failure during its design operating lifetime. The latter should be equal or lower than a predefined allowable failure probability that depends on the consequence class of the structure's failure.

However, due to the lack of long-term environmental data (i.e. measurements, observations, etc.) at the coastal structures' location (commonly in intermediate waters), there is a difficulty in estimating the long-term probabilistic representation of environmental parameters at this location, which is vital for the design of these structures. Besides, since more than one parameter play a significant role in coastal structure's stability, the necessity to develop a multivariate methodology, able to assess accurately a coastal structure's failure probability within its design lifetime via the use of the environmental parameters' joint probability distribution, is derived.

Therefore, the research in the present thesis has been motivated by the abovementioned needs of reliability analysis of coastal structures. Particularly, an overall probabilistic methodology for reliability assessment of coastal structures under wave action is described, which starts from the step of wave data collection referring usually to deep waters, and ends to the estimation of failure probability of coastal structures during their design Lifetime.

In an intermediate step, a statistical linear wave propagation model that integrates short- with long-term wave statistics from deep to intermediate waters has been developed and applied. This is a wave model that uses the long-term wave statistics in deep waters as input data, and via the use of the short-term wave statistics for each sea state in deep waters, estimates the long-term wave statistics in shallower waters. Specifically, by using i) data/measurements of significant wave height H_s , mean wave period T_m , and mean wave direction θ_m e.g. obtained from an oceanographic buoy in deep waters, ii) the dimensionless short-term images by Memos and Tzanis in deep waters, iii) a theoretical expression for wave directionality adjusted in a statistical individual wave analysis, and iv) a modification of Battjes approach, the short-term joint distribution of individual wave height H , period T , and direction θ for every sea state or storm event could be produced in deep waters. Then, the short- and the long-term joint distribution of H , T , θ could be estimated in intermediate waters, as well as the long-term joint probability density function (pdf) of H_s , T_m , θ_m , by considering linear wave transformations of each individual wave, as waves propagate from the open sea towards shallower waters.

The capability of the statistical linear wave propagation model to produce properly the short-term wave statistics in deep and intermediate waters has been investigated via comparisons of its results with measurements in deep waters and the results of a commercial, and well-known for its accuracy, Boussinesq wave propagation model from deep to intermediate waters, respectively. As for the deep water short-term wave statistics considered by the model, it was shown that the joint pdf of individual wave period T and wave height H of a real sea state could be well represented by using the dimensionless probabilistic images by Memos and Tzanis. The latter refer to nonlinear deep water sea waves. Referring to intermediate waters' short-term wave statistics considered by the model, comparisons between the linear wave propagation model and the nonlinear Boussinesq-type model showed good agreement in most of the intermediate water depths examined for both normal and oblique incidence. At the shallower intermediate water depth tested, the results of the two models differed more significantly than in deeper intermediate water depths. Therefore, as it was expected and has been already mentioned, the linear model adopted could cover the deeper and medium zone of intermediate waters and thus could be used for many engineering design purposes.

Also, it is noteworthy that a thorough probabilistic methodology is presented, aiming at estimating the reliability of coastal structures, such as rubble mound breakwaters during their lifetime, based on the probabilistic representation of load environmental and resistance variables. One of the innovative points and main objectives of this study is the estimation of the failure probability of a coastal structure based on the long-term wave climate at the

structure's location, usually met in intermediate waters, using wave observations or measurements in deeper waters. This task is accomplished by applying the abovementioned wave propagation statistical model in order that the joint probability density function of all random load variables be estimated at the structure's location.

Moreover, two thorough probabilistic methodologies, i.e. the event-based extreme value analysis and the reliability analysis applied on all sea conditions, are presented, aiming at estimating the reliability of coastal structures, such as rubble mound breakwaters during their lifetime, based on the probabilistic representation of load environmental and resistance variables. Also, their pros and cons with respect to their outputs and constraints are discussed. The main differences between the two approaches are focused on the fact that the two methods estimate different types of failure probabilities. The first method estimates the failure probability in the sample of extreme events, and the second one the failure probability in the total sample of data. The latter can be translated as the percentage of the structure's lifetime that the structure will be in a failure situation, which can be efficiently incorporated into a risk analysis with consideration of social and economic costs.

The fully probabilistic reliability analysis, applied on all sea conditions, is recommended for reliability and design purposes of coastal structures, when the period of measurements or of data used is close to the lifetime of the structure. In other cases, the extreme event-based method could be used for the design of a coastal structure (e.g. ULS), considering however its cons, and the second method for the operation of the structure (e.g. SLS).

In short, the problem of assessing failure probability of coastal structures was presented and attempted to be solved by giving application examples, flowcharts, and mathematical equations that describe the procedure, focusing on the case of rubble mound breakwaters.

Table of Contents

Εκτενής Ελληνική Περίληψη	i
Abstract	lix
List of Figures	lxix
List of Tables.....	lxxv
1 Introduction	1
1.1 Background, motivation, and research objectives	1
1.2 Innovative points and highlights	5
1.3 Structure of the dissertation.....	6
2 Existing knowledge background	11
2.1 Reliability analysis of coastal structures	11
2.1.1 Breakwater types	11
2.1.2 Components of a conventional rubble mound breakwater	12
2.1.3 Individual failure mechanisms.....	13
2.1.4 System analysis	13
2.1.4.1 Fault tree.....	14
2.1.4.2 Series and parallel failure systems.....	14
2.1.5 Target Reliability.....	17
2.1.5.1 Consequences of damage or failure.....	17
2.1.5.2 Design service life	17
2.1.5.3 Limit states/design situations	18
2.1.5.4 Return period of design sea conditions and encounter/exceedance probability	19
2.2 Reliability of an element	23
2.2.1 Limit state function.....	24
2.2.2 Reliability methods.....	25
2.2.2.1 Deterministic Methods (Level 0).....	25
2.2.2.2 Semi-probabilistic Methods (Level I).....	26
2.2.2.3 Probabilistic Methods with Approximations (Level II).....	29
2.2.2.4 Fully Probabilistic Methods (Level III).....	32
2.3 Probabilistic design process	38

2.3.1	Simplified flow chart of the design process	38
2.3.2	Detailed flow chart of the design process.....	38
2.4	Hydraulic boundary conditions	41
2.4.1	Wave action	42
2.4.1.1	Wave parameters from frequency-domain analysis of a wave record.....	45
2.4.1.2	Wave parameters from time-domain analysis of a wave record.....	58
2.4.2	Marine water level.....	70
2.4.2.1	Mean sea level	71
2.4.2.2	Tidal sea level variations	71
2.4.2.3	Storm surge.....	72
2.4.2.4	Wind set-up	74
2.4.2.5	Wave set-up.....	79
2.4.2.6	Seiches.....	81
2.4.3	Assumptions in predicting wind-driven waves from offshore wind data.....	82
2.5	Estimating long-term wave statistics from analysis of sea states	86
2.5.1	Probability definition and the perspective of statistics	86
2.5.2	Univariate analysis	86
2.5.3	Multivariate analysis	88
2.5.4	Integration of short- with long-term wave statistics	91
2.6	Estimating extreme sea conditions	92
2.6.1	Univariate extreme value analysis.....	92
2.6.1.1	Block maxima method.....	92
2.6.1.2	Peak over threshold method	93
2.6.1.3	Parameters estimation.....	100
2.6.1.4	Best fit selection	101
2.6.2	Multivariate extreme value analysis.....	102
2.6.3	Combining statistics of extreme sea conditions by the the short-term distribution of the maximum wave height.....	105
3	Methodology and results	109
3.1	Integrating short- with long-term wave statistics from deep to intermediate waters 109	
3.1.1	Data reduction technique.....	112

3.1.2	Wave statistics in deep waters	113
3.1.3	Consideration of wave directionality in deep waters.....	115
3.1.4	Transforming wave statistics from deep to intermediate waters	118
3.1.5	Derivation of long-term wave statistics in intermediate waters	120
3.1.6	Examples of application	124
3.1.6.1	Input data	124
3.1.6.2	Data reduction based on a statistical technique	125
3.1.6.3	Results and discussion	128
3.2	Investigating the capability of the linear model	138
3.2.1	Comparisons concerning deep waters	138
3.2.2	Comparisons concerning intermediate waters	141
3.2.2.1	Normal incidence.....	142
3.2.2.2	Oblique incidence.....	146
3.2.3	Determination of the validity domain of the model.....	148
3.2.4	Comparisons with respect to simulation time.....	148
3.3	Reliability analysis of a rubble mound breakwater	150
3.3.1	A short review of structural reliability assessment.....	150
3.3.2	Significant issues in the reliability analysis.....	152
3.3.3	Preliminary design based on an event-based extreme value analysis applied to wave data.....	154
3.3.4	Fully probabilistic event-based reliability analysis	156
3.3.4.1	Time extrapolation of an element's failure probability using time-invariant and time-variant random variables by Direct Integration Method (DIM).....	157
3.3.4.2	Inclusion of sea level variation due to astronomical tide	158
3.3.4.3	Resistance parameters	159
3.3.4.4	Monte Carlo Method (MCM).....	159
3.3.4.5	Assessing failure probability of the system.....	160
3.3.5	Fully probabilistic reliability analysis using all sea conditions	161
3.3.5.1	Sea state multivariate analysis.....	162
3.3.5.2	Data reduction technique for reliability analysis using all sea conditions.	164
3.3.5.3	Assessing an element's failure probability using all sea conditions within storm events by Direct Integration Method (DIM)	166
3.3.5.4	Monte Carlo Method (MCM).....	167

3.3.5.5	Assessing failure probability of the system.....	168
3.3.6	Comparative evaluation of the two fully probabilistic approaches	168
3.3.7	Incorporation of the reliability analysis into a design process	171
3.3.8	Individual failure modes.....	172
3.3.8.1	Seaside armor stability	173
3.3.8.2	Rear-side armor stability	179
3.3.8.3	Toe stability	181
3.3.9	Considering the effect of oblique wave attack in the reliability analysis	182
3.4	Examples of reliability analysis of a rubble mound breakwater.....	183
3.4.1	Define design requirements and structural characteristics	183
3.4.2	Case study off Malaga (Spain)	185
3.4.2.1	Case study description.....	185
3.4.2.2	Identification of storm events at the buoy location (Malaga).....	187
3.4.2.3	Transferring storm events from the buoy to the structure's location (Malaga) 188	
3.4.2.4	Preliminary design based on the design storm events (Malaga).....	190
3.4.2.5	Statistical analysis of sea states at the buoy location (Malaga)	191
3.4.2.6	Transferring the reduced sample of sea states from the buoy to the structure location (Malaga).....	193
3.4.2.7	Sea level parameters at the structure location (Malaga).....	194
3.4.2.8	Assessing failure probability via DIM and MCM (Malaga)	194
3.4.2.9	Results and discussion (Malaga)	196
3.4.2.10	Design of the structure (Malaga).....	198
3.4.3	Case study off Mykonos (Greece).....	200
3.4.3.1	Identification of storm events at the buoy location (Mykonos).....	200
3.4.3.2	Transferring storm events from the buoy to the structure's location (Mykonos)	201
3.4.3.3	Preliminary design based on the design storm events (Mykonos).....	203
3.4.3.4	Statistical analysis of sea states at the buoy's location (Mykonos)	204
3.4.3.5	Transferring the reduced sample of sea states from the buoy to the structure location (Mykonos)	205
3.4.3.6	Assessing structure's failure probability via DIM (Mykonos)	207
3.4.3.7	Design of the structure (Mykonos).....	208
3.4.4	Remarks and recommendations on reliability analysis	210
4	Conclusions and Future Research	215

4.1	Summary and concluding remarks	215
4.1.1	Summary.....	215
4.1.2	Integrating short- with long-term wave statistics from deep to intermediate waters	215
4.1.3	Investigating the capability of the model	216
4.1.4	Using an event-based extreme value analysis and an analysis on all sea conditions	217
4.1.5	Reliability assessment of coastal structures.....	217
4.2	Future research	219
	References	221
	Appendix A. Water wave theories.....	239

List of Figures

Figure 2.1 Cross-sections of various types of rubble mound breakwaters [55]	12
Figure 2.2 Cross-section of a typical rubble mound breakwater [55]	13
Figure 2.3 Failure modes of a rubble mound breakwater with a crest element [65]	13
Figure 2.4 Simplified fault tree of a breakwater [1]	14
Figure 2.5 Series system [1]	15
Figure 2.6 Parallel systems [1]	15
Figure 2.7 The influence of correlation between two failure mechanisms on system failure probability [66].....	16
Figure 2.8. Fault tree of a breakwater protecting a harbor's basin [67]	19
Figure 2.9 Linearization and approximation of the failure surface by a tangent hyperplane at the design point [1].....	29
Figure 2.10 Illustration of the reliability index for a linear failure function of normally-distributed random variables [1].....	31
Figure 2.11 Illustration of the two dimensional jpdf for loading s and resistance r [1]	34
Figure 2.12 Random sample generation step for one variable in MCM [66].....	36
Figure 2.13 MC simulation (according to Schiereck [73]).....	37
Figure 2.14 Simplified flow chart of the design process (according to Everts [56]).....	38
Figure 2.15 Detailed flowchart of the design process for a coastal structure [35] (based on Everts [56]).....	40
Figure 2.16 Hydraulic boundary conditions for coastal structures [55]	42
Figure 2.17 Wave profile in severe seas (a) in deep waters and (b) in shallow waters [10] ...	43
Figure 2.18 Wave profile histogram and the theoretical distribution (a) in deep waters and (b) in shallow waters [10]	44
Figure 2.19 Structure of random sea [75].....	44
Figure 2.20 An approximate instant depiction of free sea surface [86].....	54
Figure 2.21 The Gaussian probability density function and cumulative distribution [1]	63
Figure 2.22 The Rayleigh probability density function and cumulative distribution [1]	64

Figure 2.23 Contours of dimensionless joint probability density function of wave amplitude and period for (a) $v=0.3$ and (b) $v=0.4$ [24].....	67
Figure 2.24 Joint pdfs of H/H_m and T/T_m in deep waters associated with specific values of standard deviation σ_η or correlation coefficient $r(H,T)$ ([31]; [30])	68
Figure 2.25 Variation with time of water level due to astronomical tide and storm surge [55]	71
Figure 2.26 Water level differences for storm surge, storm tide, and a normal (predicted) high tide compared to mean sea level (https://www.al.com/news/index.ssf/2018/09/hurricane_florence_storm_surge.html).....	73
Figure 2.27 Storm tide and its components	74
Figure 2.28 Wind set-up [55]	74
Figure 2.29 Plan (left) and cross-sectional view of the coast [143]	76
Figure 2.30 Dimensionless wind set-up surge versus dimensionless distance of a continental shelf for two cases of dimensionless wind shear stress [143]	79
Figure 2.31 Wave set-up [55].....	80
Figure 2.32 Wind data for the Station of HIOS island in Aegean (Greece).....	85
Figure 2.33 Wind rose diagram for Station of Hios in the Aegean (Greece) estimated from the wind data for the Station of Hios island	85
Figure 2.34 Definition of independent storm events [165]	96
Figure 3.1 Flowchart of the model applied by Malliouri et al. [33]	112
Figure 3.2 Grid of probabilistic calculation (step $d(T/T_m)=d(H/H_m)=0.1$) [193].....	115
Figure 3.3 Estimated histograms of wave direction in two sea states in deep waters with different [33].....	117
Figure 3.4 Description of individual wave evolution through the surf zone adopted [33]....	120
Figure 3.5 The locations of the three oceanographic stations in the Aegean Sea, Greece	124
Figure 3.6 Measured H_s and T_m at M station (2000-2011) [44]; [45]; [33].....	125
Figure 3.7 Comparison of the best fitted distribution of H_s to the new data set against the one derived from the initial dataset, estimated in deep waters (up) and at a depth of 6m (below) at Station M [33]	127
Figure 3.8 Sample of the new dataset of 1500 sea states (T_m and H_s) for Station M [33].....	128

Figure 3.9 Fitting of the candidate marginal distributions to the histogram of H_s data in deep waters for Station M (1), Station A (2), and Station S (3) [33]	129
Figure 3.10 Joint pdf of T_m and H_s in deep waters estimated by applying the Conditional model for Station M (up left), Station A (up right), and Station S (below) - $0.1 \text{ m}^{-1}\text{s}^{-1}$ contour step [33].....	131
Figure 3.11 Long-term joint pdf of T and H in deep waters for Station M (up left), Station A (up right), and Station S (below) - $0.1\text{m}^{-1}\text{s}^{-1}$ contour step [33].....	132
Figure 3.12 Fitting of the candidate marginal distributions to the histogram of H_s data at the depth of 6m for Station M (1), Station A (2), and Station S (3) [33]	133
Figure 3.13 Joint pdf of T_m and H_s at the depth of 6m estimated by applying the Conditional model for Station M (up left), Station A (up right), and Station S (below) - $0.1 \text{ m}^{-1}\text{s}^{-1}$ contour step [33].....	134
Figure 3.14 Long-term joint pdf of T and H at the depth of 6m for Station M (up left), Station A (up right), and Station S (below) - $0.1 \text{ m}^{-1}\text{s}^{-1}$ contour step [33].....	135
Figure 3.15 Probability density of wave direction in a certain sea state propagating from deep to intermediate waters [33].....	137
Figure 3.16 Comparisons in deep waters between wave measurements (blue points) and the results derived by Longuet-Higgins [24] (dotted lines) and by Memos and Tzanis [29] (solid lines) for a sea state with $H_{1/3}=0.55 \text{ m}$, $H_m=0.40 \text{ m}$ and $T_m=3.67 \text{ s}$ (contour step 0.05 1/m/s)	139
Figure 3.17 Comparisons in deep waters between wave measurements (blue points) and the results derived by Longuet-Higgins [24] (dotted lines) and by Memos and Tzanis [29] (solid lines) for a sea state with $H_{1/3}=1.56 \text{ m}$, $H_m=1.01 \text{ m}$ and $T_m=4.62 \text{ s}$ (contour step 0.05 1/m/s)	140
Figure 3.18 Comparisons in deep waters between wave measurements (blue points) and the results derived by Longuet-Higgins [24] (dotted lines) and by Memos and Tzanis [29] (solid lines) for a sea state with $H_{1/3}=2.89 \text{ m}$, $H_m=1.80 \text{ m}$ and $T_m=5.96 \text{ s}$ (contour step 0.05 1/m/s)	140
Figure 3.19 Scatter plot of T and H used by both models at the depth of 20.95 m (normal incidence)	143
Figure 3.20 Scatter plot of T and H obtained by non-linear module (Mike by DHI) compared to the linear wave propagation model at the intermediate depth of 11.80 m (normal incidence)	143

Figure 3.21 Scatter plot of T and H obtained by non-linear module (Mike by DHI) compared to the linear wave propagation model at the intermediate depth of 7.60 m (normal incidence)	143
Figure 3.22 Scatter plot of T and H obtained by non-linear module (Mike by DHI) compared to the linear wave propagation model at the intermediate depth of 5.70 m (normal incidence)	144
Figure 3.23 Scatter plot of T and H obtained by non-linear module (Mike by DHI) compared to the linear wave propagation model at the intermediate depth of 3.80 m (normal incidence)	144
Figure 3.24 The new sample in deep waters derived from the data reduction technique recommended for reliability analysis of coastal structures	166
Figure 3.25 Recommendation on the use of the formulas by Van der Meer [57] and Van Gent et al [217] version [55]	177
Figure 3.26 Design flowchart providing recommendation on the use of the two formulas-sets [220]	178
Figure 3.27 The three-step approach for prediction of erosion at the rear side [60]	179
Figure 3.28 A typical cross section of the rubble mound breakwater [35].....	184
Figure 3.29 Locations of the buoy (red point) and tide gauge (yellow point) near the port of Malaga (Spain)	186
Figure 3.30 Scatter diagram of T_m and H_s measurements obtained from the buoy [35]	186
Figure 3.31 Frequency density polygons of TL and SL as measured by the tide gauge [35]	187
Figure 3.32 Histograms and scatter diagram of $H_{s,p}$ and storm duration at the buoy location (Malaga)	188
Figure 3.33 Histograms and scatter diagram of $H_{s,p}$ and storm T_m at the buoy location (Malaga)	188
Figure 3.34 Histograms and scatter diagram of $H_{s,p}$ and storm θ_m at the buoy location (Malaga)	188
Figure 3.35 Scatter diagram of storm duration and $H_{s,p}$ at the buoy (depth of 15 m) and structure (depth of 6 m) location (Malaga).....	189
Figure 3.36 Histograms and scatter diagram of $H_{s,p}$ and storm θ_m at the structure location (Malaga)	189

Figure 3.37 Histograms and scatter diagram of H_s and θ_m of sea states at the buoy location (Malaga) [35].....	192
Figure 3.38 Histograms and scatter diagram of H_s and θ_m of the subset sea states at the structure location (Malaga).....	193
Figure 3.39 Conditional joint pdf of H_s and T_m , given that sea states belong to the subset selected, concerning the buoy (1) and the structure location (2) (iso-probability density contours step equal to 0.05 1/s/m) (Malaga)	194
Figure 3.40 Frequency density polygons of sea level variation from SWL due to storm surge and tide estimated at the structure location	194
Figure 3.41 Comparison of the random sample generated by Monte Carlo simulation (red) with the transferred reduced data sample (green) to the structure's location (iso-probability density contours step equal to 0.05 1/m/s)	196
Figure 3.42 Histograms and scatter diagram of $H_{s,p}$ and storm duration at the buoy's location (Mykonos)	200
Figure 3.43 Histograms and scatter diagram of $H_{s,p}$ and storm T_m at the buoy's location (Mykonos)	201
Figure 3.44 Histograms and scatter diagram of $H_{s,p}$ and storm θ_m at the buoy's location (Mykonos)	201
Figure 3.45 Scatter diagram of storm duration and $H_{s,p}$ at the buoy's (depth of 140 m) and structure's (depth of 6 m) location (Mykonos).....	202
Figure 3.46 Histograms and scatter diagram of $H_{s,p}$ and storm θ_m at the structure's location (Mykonos)	202
Figure 3.47 Histograms and scatter diagram of $H_{s,p}$ and storm T_m at the structure location (Mykonos)	203
Figure 3.48 Histograms and scatter diagram of H_s and θ_m of sea states at the buoy's location (Mykonos)	205
Figure 3.49 Histograms and scatter diagram of H_s and θ_m of the subset sea states at the structure's location (Mykonos).....	206
Figure 3.50 Conditional joint pdf of H_s and T_m for two directional sectors, given that sea states belong to the subset selected, concerning the buoy's (up) and the structure's location (iso-probability density contours step equal to 0.002) (Mykonos)	207

List of Tables

Table 2.1 Exceedance probability of design return values associated to design lifetime L	22
Table 2.2 Main parameters representative of hydraulic boundary conditions.....	41
Table 2.3 Various sea states associated with specific values of σ_η , $r(H,T)$ and H_m [31]	68
Table 3.1 Classes of H_m assumed to be associated with the same standard deviation of the free surface excursion and correlation coefficient between H and T [33]	114
Table 3.2 Comparison of the Euclidean distances between the best fitted pdf of H_s derived from both the reduced data and the initial data at Station M [33]	127
Table 3.3 Measures of goodness of fit of the candidate marginal distributions for H_s and the corresponding conditional model in deep waters using data from stations M, A, and S [33]	129
Table 3.4 Estimated parameters of the best fitted marginal distribution for H_s in deep waters using data from stations M, A, and S [33].....	130
Table 3.5 Measures of goodness of fit of the candidate marginal distributions for H_s and the corresponding conditional model at the depth of 6m using data from Stations M, A, and S [33]	133
Table 3.6 Estimated parameters of the best fitted marginal distribution for H_s at the depth of 6m using data from Stations M, A, and S [33].....	134
Table 3.7 Relative Frequency and type of wave breaking in deep waters and at the water depth of 6m, for each Station [33].....	136
Table 3.8 Correlation coefficient between T_m and H_s and between T and H in deep waters and at the water depth of 6m, for each Station [33]	136
Table 3.9 Spectral bandwidth parameters of the three sea states tested and comparisons of the statistical wave parameters between wave measurements and those estimated by the two approaches	140
Table 3.10 Relative difference of the two methods' results from those extracted directly from measurements	141
Table 3.11 Comparison of time-domain characteristic parameters estimated by MIKE 21 BW module's results with those by the model by Malliouri et al. [33] for normal incidence.....	145
Table 3.12 Relative difference of Malliouri et al. [33] model's results from those by MIKE 21 BW module for normal incidence	145

Table 3.13 Comparison of MIKE BW module by DHI results with the corresponding ones by the model by Malliouri et al. [33] for oblique incidence ($\theta_m=19.11^\circ$ from normal).....	146
Table 3.14 Relative difference of Malliouri et al. [33] model's results from those by MIKE 21 BW module for oblique incidence ($\theta_m=19.11^\circ$ from normal).....	147
Table 3.15 Comparison of MIKE BW module by DHI results with the corresponding ones by the model by Malliouri et al. [33] for oblique incidence ($\theta_m=42.33^\circ$ from normal).....	147
Table 3.16 Relative difference of Malliouri et al. [33] model's results from those by MIKE 21 BW module for oblique incidence ($\theta_m=42.33^\circ$ from normal).....	147
Table 3.17 Estimation of a series system's failure frequency via consideration of the frequency of union of the elements' failure events ([34]; [56]) for MCM.....	160
Table 3.18 Estimation of a series system's failure probability via consideration of the probability of union of the elements' failure events for DIM	161
Table 3.19 The pros and cons of the event-based and all sea conditions-based reliability methods	169
Table 3.20 Guidelines for selection of damage parameter for armor stone in a double layer [55]	175
Table 3.21 Coefficients for wave run-up predictions [221], [222].....	180
Table 3.22 Structural characteristics of a specific rubble mound breakwater	184
Table 3.23 Return periods and values for $H_{s,p}$ associated with the most probable values of the covariate parameters at the structure's location (depth of 6 m) selected for the preliminary design.....	190
Table 3.24 Median mass of the elements' units estimated by the preliminary design (Malaga)	191
Table 3.25 Equivalent failure probabilities per annum and over structure's Lifetime (15 years), associated to return period of $H_{s,p}$ at the depth of 6 m (Malaga)	191
Table 3.26 Conditional and Unconditional probability of failure of the system during $Y=8$ yr derived from the fully probabilistic reliability method (Direct Integration) applied on all sea conditions for the first case (Malaga).....	197
Table 3.27 System's unconditional probability of failure during $Y=8$ yr derived from fully probabilistic reliability method (Direct Integration) applied on all sea conditions for the three cases considered (Malaga).....	197

Table 3.28 System unconditional failure probability within during Y=8 yr estimated by DIM and MCM (for case 3) (Malaga).....	198
Table 3.29 Median mass of the elements units and system failure probability within Y=8 yr estimated by DIM for the design of the structure (Malaga)	199
Table 3.30 Return periods and values for $H_{s,p}$ associated with the most probable values of the covariate parameters at the structure's location (depth of 6 m) selected for the preliminary design.....	203
Table 3.31 Median mass of the elements' units estimated by the preliminary design (Mykonos)	204
Table 3.32 Equivalent failure probabilities per annum and over structure's Lifetime (15 years), associated to return period of $H_{s,p}$ at the depth of 6 m (Mykonos)	204
Table 3.33 Unconditional probability of failure during Y=12 yr derived from the fully probabilistic reliability method (Direct Integration) applied on all sea conditions for the two cases (Mykonos).....	208
Table 3.34 Median mass of the elements units and system failure probability within Y=12 yr estimated by DIM for the design of the structure (Mykonos)	209

CHAPTER 1

Introduction

1 Introduction

1.1 Background, motivation, and research objectives

Nowadays, more and more researchers and engineers have realized that coastal structures should be designed to meet predefined safety and performance levels, i.e. the reliability level, with due consideration of all uncertainties related to actions, resistance, and design tools. This can be accomplished by implementing a thorough methodology able to assess accurately the reliability level of a coastal structure, i.e. the probability of failure during its operating lifetime. The latter should be equal or lower than a predefined allowable failure probability that depends on the extent of consequences of the structure's failure. Therefore, reliability based design methods should be adopted for coastal structures.

These reliability based design methods for coastal structures are divided into four categories, related to the accuracy in determining the reliability of their elements and the consideration of uncertainties, cited below [1]:

- Deterministic Method (Level 0)
- Semi-Probabilistic Method (Level I)
- Probabilistic Methods with Approximations (Level II)
- Fully Probabilistic Methods (Level III)

It is noted that another category of methods has been also developed. This Level IV method is a risk-based reliability method, which examines the consequences of a coastal structure's failure and the resulting risk. However, this Level IV method is not a part of this PhD research.

Conventional design practice for coastal structures is often deterministic in nature (Level 0), and its reliability is based on the exceedance probability of the design wave load. Specifically, the notion of design wave parameters and especially that of wave height associated with a certain return period is adopted [2].

In addition to the deterministic method, partial factors can be implemented for resistance and load parameters, based on standards [3]. This calculation is classified as a semi-probabilistic (Level I) method. However, this approach does not allow an accurate determination of the reliability of the design. In order to overcome this problem, more advanced probabilistic methods should be applied that consider the uncertainties of all stochastic variables of load and strength of the structure.

Fully probabilistic methods (Level III) belong in this category of advanced probabilistic methods, which consider the joint probability density function of all stochastic variables involved. There are two main methods classified as Level III methods, i.e. the Direct Integration Method (DIM) and Monte Carlo Method (MCM). Another possibility, though less accurate regarding the estimation of the reliability of the design, are methods with approximations (Level II).

It is noted that the probabilistic representation of environmental parameters at the location of the design coastal structures is vital for the reliability based design of these structures. However, there is a lack of long-term environmental data at the location of coastal structures under design making thus difficult to estimate their joint probabilistic density function at this location.

Such data could be measurements of wave parameters, sea level, current velocity etc., which should be collected at the project site. This can be implemented by:

- (i) Measurements at the structure's location for a period of many years. Obviously, such requirement can be rarely met.
- (ii) Measurements of the same type but in deep water if the location of the structure was in shallower water, during a time span ideally of the order of the structure's design operating life. Then, either linear (e.g. [4]) or non-linear ([5]; [6]; [7]) models may be applied to transfer each sea state from deep towards shallower waters.
- (iii) Hindcasting methods for a period of several years ([8]; [1]). Particularly, regarding the long-term wave climate at the structure's location, wind data in the wave generation area (e.g. [9]) can be used to provide this information under a probabilistic framework.

The target of the aforementioned input data collection is to gain a thorough probabilistic representation of the long-term wave climate, sea level conditions, and other environmental parameters, at the structure's location. Referring to the case where measurements are available but in deep waters, it is worth mentioning that non-linear models might be more accurate than linear models, as they account for wave-wave interactions that may play a considerable role in the final outcome depending on water depth; however, non-linear models are quite demanding in terms of computing resources, especially when they have to account for reliability analysis based on fully probabilistic methods.

Information on sea severity is inevitably significant for the design of coastal and marine structures. Specifically, information is necessary not only on the severest sea state expected to occur during the structures' lifetime, but also on the frequency of occurrence of all sea states, the latter being necessary for evaluating more accurately the probability of damage levels and failure of these structures and for ensuring their resilience.

The most commonly available information on sea severity is the probability distribution of significant wave height H_s , which can be estimated from the statistical analysis of data accumulated over several years. "Of course, the greater the number of accumulations, the more reliable the data" [10]. However, nowadays, the role of other wave parameters except for significant wave height in the stability of coastal and marine structures has been also realized (e.g. [11]; [12]). Thus, the information on long-term wave statistics is broadened to a great extent by including, in addition to H_s , wave period, usually the average zero-crossing value of wave periods in a specific sea state T_m , and principal wave direction θ_m .

Furthermore, all core environmental parameters and their statistical correlation should be taken into consideration in a proper manner. An illustrative example of statistical correlation between environmental parameters is that often observed between mean (or peak) wave period and significant wave height, and between wave period and wave height within a sea state, when referring to long- and short-term wave statistics, respectively. Besides, directional effects have been also noticed to long-term wave statistics [13]. Additionally, storm surge and significant wave height are often correlated to some extent.

In order to estimate the joint probability density function (pdf) of H_s and T_m , the study of bivariate distribution models and correlation between the variables is required. One of the first approaches was proposed by Ochi [14], who adopted the bivariate lognormal distribution to represent H_s and T_m , resulting from an exponential transformation of the bivariate normal distribution. This approach although simple to apply, is based on the assumption that the logarithms of the data are normally distributed, and although this may happen for low and moderate values of H_s , it is not applicable for extreme H_s . A bivariate lognormal curve with correction for skewness [15] was an attempt to improve the bivariate lognormal model. Furthermore, a model, based on the marginal distribution of H_s and the conditional distribution of T_p for given H_s , could increase its flexibility and accuracy, and was adopted by Haver [16], and Bitner-Gregersen and Haver [17]. Guedes Soares et al. [18], Lucas and Guedes Soares [19], and Papanikolaou et al. [20] have used a similar model based on the marginal distribution of H_s and the conditional distribution of T_m , referred hereinafter as the conditional model. Other approaches have also been developed for the same purpose (e.g. [21] etc.). However, in the cases examined by Lucas and Guedes Soares [19] and Papanikolaou et al. [20], it was showed that the conditional model represented more accurately H_s and T_m data than the other models tested. Thus, in this thesis the conditional model is used to fit bivariate distributions of H_s and T_m to the available data sets.

Except for the long-term wave statistics, the short-term wave statistics are also necessary for the complete description of individual sea waves. This is due to the significant role that the

joint pdf of wave height (H) and period (T) plays in predicting statistical properties of individual wave characteristics within each sea state.

As far as the short-term joint distribution of wave height H and period T is concerned, Longuet-Higgins [22] was the first to introduce a probabilistic representation of sea waves, by extending the work of Rice [23] on electronic noise, and was able to calculate the joint pdf of H and T for narrow band spectrum. However, a disadvantage of that model was the symmetry of the joint pdf of H and T around some characteristic period, suggesting in this way a zero statistical correlation between the two parameters. Thus, Longuet-Higgins [24] considered the tendency that short-period waves have low heights, whereas high waves tend to be associated to longer periods, as it is observed in real sea states. Other researchers who studied the joint pdf of H and T by considering narrow band spectra were Cavanié et al. [25], Lindgren and Rychlik [26], and Shum and Melville [27].

Furthermore, Memos [28] reviewed the existing results and proposed theoretical approximations valid also for narrow and broad band spectra, known to be a better representation of real sea states than those assuming only narrow band spectra. Besides, Memos and Tzani [29], based on the theoretical approach by Memos [28], produced numerical results of the short-term joint distribution of H and T for deep water waves of any spectral bandwidth. The joint pdf was deduced for various correlation coefficients of H and T, denoted by $r(H,T)$, providing characteristic probabilistic estimates in deep waters. Memos and Tzani [30] extended their previous work by excluding swell from sea waves and the application of a wave breaking criterion in deep waters. The parameters that describe the methodology were the correlation coefficient between H and T, or the standard deviation of free surface elevation, and the representative wave steepness factor.

More recently, Chondros and Memos [32] extended the work of Memos and Tzani [30] concerning the joint pdf of H and T, by taking into account the nonlinear wave-wave interactions, and produced characteristic images of joint pdf of H and T in shallow waters for various storm intensities, wave incidence, and bed slopes, by using a Boussinesq wave propagation model. It is noted that in their method [32], wave directionality in deep waters was considered via the use of a theoretical expression of wave directional spreading, and the joint pdf of H, T, and wave direction θ in deep waters were transformed into time series of surface elevation, in order that the Boussinesq wave propagation model be implemented.

From all the above, it is extracted that due to the lack of long-term environmental data (i.e. measurements, observations, etc.) at the coastal structures' location (commonly in intermediate waters or even in shallow waters in some cases), there is a difficulty in estimating the long-term probabilistic representation of environmental parameters at this location, which is vital

for the design of these structures. Besides, the necessity to develop a multivariate methodology able to assess accurately a coastal structure's failure probability within its design lifetime via the use of the environmental parameters joint probability distribution is derived.

Thus, the prime objective of this research study is to develop a statistical wave propagation model in order that the long-term environmental statistics are transformed from deeper towards shallower waters, i.e. the location of a coastal structure, and then to use those data to apply a multivariate probabilistic design methodology of the structure. The specific research objectives are:

- To apply a statistical technique in order that a considerable data reduction could be made to long-term wave data in deep waters without loss of accuracy, e.g. in determination of the joint distribution of H_s , T_m and θ_m .
- To extend the short-term joint distribution of wave height H and period T in deep waters to incorporate wave directionality via the use of an energy spreading function dependent on wave period.
- To transfer the short-term wave statistics, i.e. of each sea state, from deep to shallower waters.
- To integrate short- with long-term wave statistics in shallower waters in order that the long-term joint pdf of H , T , θ and of H_s , T_m , θ_m be estimated at this location.
- To use a total data sample analysis and an event-based extreme value analysis in a reliability analysis of a coastal structure.
- To develop a combined multivariate structural reliability analysis using variables with zero and nonzero hazard rate, referred here as a combined time-invariant and time-variant analysis.
- To incorporate this reliability analysis into the design of coastal structures, e.g. of rubble mound breakwaters.

1.2 Innovative points and highlights

Some of the most significant innovative points and worth mentioning topics of the present thesis are listed below:

- One of the main issues with probabilistic design of coastal structures is how to properly and correctly describe the intermediate water long-term wave climate. Thus, in this PhD thesis, failure probability of coastal structures is attempted to be estimated based on the long-term wave climate at the structure's location.

- This is accomplished by applying a data reduction technique in deep waters and a statistical linear wave propagation model that integrates short- with long-term wave statistics from deep to intermediate waters, developed for this purpose.
- It is a common practice to consider wave directionality in a spectral wave analysis, as this is in accordance with the definition of wave directionality. However, the need to consider wave directional spreading in a probabilistic wave analysis often arises. The incorporation of wave directionality into a probabilistic wave analysis has been adopted in this study.
- A combined structural reliability analysis, using variables with zero and nonzero hazard rate, has been developed based on the general formulation of a fully probabilistic method.
- A total sample analysis and an event-based extreme value analysis are used in the reliability analysis of a coastal structure, aiming at discussing the differences, and the pros and cons of the two approaches.
- These two approaches have been also incorporated in the probabilistic design of coastal structures.

Additionally, it is noted that comparisons have been made between the statistical model of wave propagation from deep to shallow waters, referring to short-term sea conditions, with wave measurements in deep waters and results in intermediate waters extracted from a Boussinesq wave propagation model (Mike by DHI). These comparisons showed the domain of validity and the limitations of the statistical wave propagation model developed.

1.3 Structure of the dissertation

Referring to the structure of the present thesis, the introductory Chapter 1 is followed by Chapter 2 that presents the existing knowledge background of the reliability analysis of coastal structures, the reliability of a coastal structure's element, and the probabilistic design of coastal structures. Also, in Chapter 2, the hydraulic boundary conditions that need to be determined for the design of a coastal structure are discussed, focusing on the wave action and marine water level change. Besides, a literature review for long-term wave statistics derived from analysis of sea states, and extreme value analysis has been covered.

Chapter 3 presents the methodology adopted and the results derived from the application cases. Specifically, a linear wave propagation statistical model that integrates short- with long-term wave statistics from deep to intermediate water depths will be described. This model could be utilized for estimating long-term wave climate at a coastal structure's location, which is frequently met in intermediate water depths. Secondly, the capability of this

linear model, to transfer the probabilistic information concerning short-term wave statistics, has been investigated by comparing its results with wave measurements in deep waters and the results of the well-known and commercial phase-resolving Boussinesq wave model (MIKE 21 BW/ Mike powered by DHI). The results produced by the latter refer to intermediate water depths. The next section in this chapter refers to the reliability analysis of a coastal structure, focusing on the case of rubble mound breakwaters, and wave loadings. Finally, two illustrative examples of reliability analysis and probabilistic design of rubble mound breakwaters are presented, which are followed by discussion of the results produced. In short, this chapter deals with the existing gap in current practice for the probabilistic representation of long-term wave climate at the structure's location, the use of a total sample analysis and an event-based extreme value analysis in the reliability assessment of a coastal structure, aiming at discussing the differences, the constraints, and the pros and cons of the two approaches.

In Chapter 4, the conclusions drawn from this research work are summarized. Also, some important remarks and results are highlighted, and suggestions for further investigation are displayed.

CHAPTER 2

Existing knowledge background

2 Existing knowledge background

2.1 Reliability analysis of coastal structures

The objective of the reliability analysis of coastal structures is to estimate the probability of a structure to meet predefined safety and performance levels, with due consideration of all uncertainties related to actions, resistance, and design tools. This means that the estimated probability of failure of a coastal structure within its design lifetime should be lower than a predefined allowable failure probability, i.e. the target reliability of the structure.

In this chapter, the reliability analysis of a coastal structure, e.g. a breakwater, is briefly described. Firstly, the different types of breakwaters and an indicative fault tree concerning the case of a rubble mound breakwater will be presented. Then, the parameters that affect the selection of the allowable failure probability or else the target reliability of a coastal structure will be presented.

2.1.1 Breakwater types

Breakwaters are built either for coastal defense or to protect a harbour basin from attack by waves or currents. In the second case, breakwaters generally serve the purpose of providing quiet water conditions for anchorage and mooring of vessels. Rubble mound breakwaters are defined as structures built of quarried rock, usually protected by a cover layer of heavy armour stones or concrete armour units [55].

The different types of breakwaters are presented in Figure 2.1. A conventional rubble mound breakwater is the most commonly used form of a breakwater and has a trapezoidal cross-section. Conventional rubble mound breakwaters with crown wall are mainly used for port protection, and the crown wall often incorporates a roadway, allowing thus access along the breakwater. Regarding the berm breakwater, rock armor units form the seaward slope of the structure. Continuously, three types of a berm breakwater exist, based on the stability of its rock armor units, i.e. the non-reshaping statically shape berm breakwater, the reshaped statically stable berm breakwater, and the dynamically stable reshaping berm breakwater. Besides, low-crested (submerged) breakwaters usually serve the purpose of protection in areas where wave overtopping is acceptable, but wave conditions need to be modified, where horizontal visibility is required, e.g. for aesthetic reasons. Caisson type or vertically composite breakwater is a rubble mound breakwater combined with a caisson placed on top

of the mound. Finally, a horizontally composite breakwater is a combination of a rubble mound with a caisson placed behind the rubble mound seaward protection.

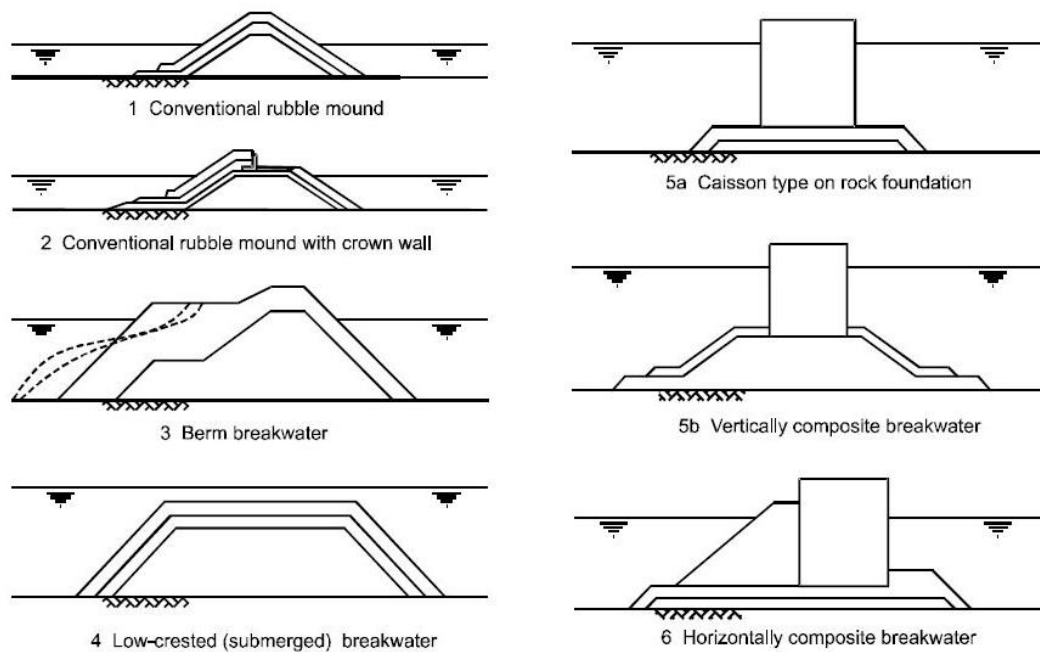


Figure 2.1 Cross-sections of various types of rubble mound breakwaters [55]

2.1.2 Components of a conventional rubble mound breakwater

A typical cross-section of a conventional rubble mound breakwater is shown in Figure 2.2, which indicates its various components. The core of the rubble-mound breakwater is placed on the subsoil and on top of it usually a filter layer is placed, whose properties depend on the grading of the layer on top of it and the governing filter rules [55]. The top layer is the armour layer which is exposed severely to wave action. Besides, a toe is placed to increase the stability of the breakwater and the armour layer. At last, a crest height and width is properly selected, or often a crest element is placed on top of the breakwater, to reduce wave overtopping and increase the stability of the rear-side of the breakwater.

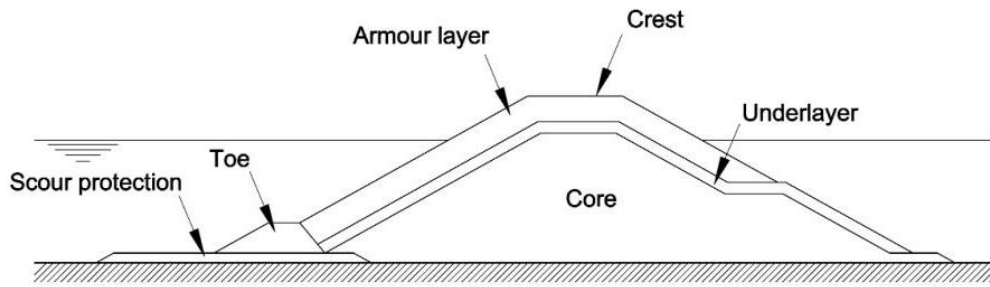


Figure 2.2 Cross-section of a typical rubble mound breakwater [55]

2.1.3 Individual failure mechanisms

To make a proper design of a coastal structure, all the possible failure mechanism should be known and considered. In figure 2.3, an overview is given of the failure mechanisms which can occur in the case of a rubble-mound breakwater with a crest element according to Burcharth [65].

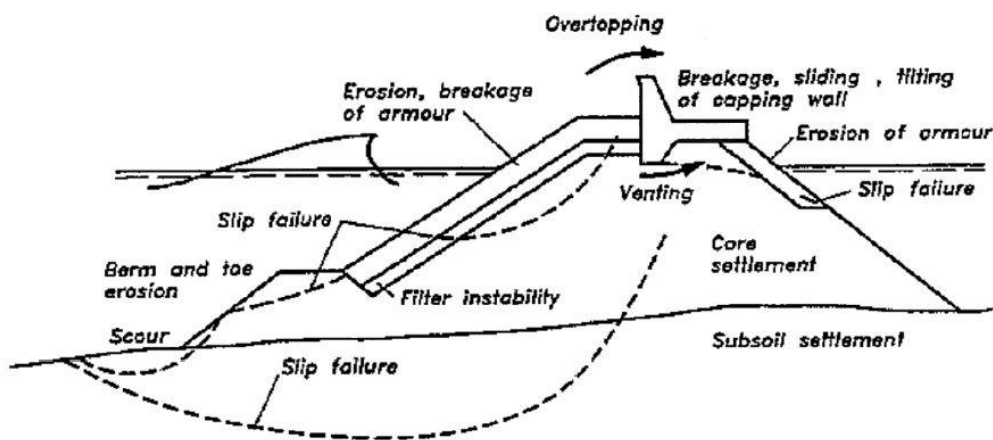


Figure 2.3 Failure modes of a rubble mound breakwater with a crest element [65]

2.1.4 System analysis

To calculate a coastal structure's reliability level, a system analysis is required. The failure probability of a system, e.g. a coastal structure, depends on the failure probability of its individual components, i.e. single failure modes, and on their correlations and inter-linking. A fault tree is often constructed that describes the aforementioned relations. A system can be

split into two types of fundamental systems depending on its fault tree connections, namely series systems and parallel systems.

2.1.4.1 Fault tree

A coastal structure can be regarded as a system of components that can either function or fail under certain conditions. Failure of one component (one mode of failure) may cause the failure of another component and even lead to failure of the system, i.e. the ULS of a rubble mound breakwater, e.g. protecting a harbour. A fault tree describes the interactions, i.e. correlations and linking between the modes of failure and their relation between the failure of a system (e.g. excessive wave transmission over the aforementioned breakwater) and the individual events that lead to this failure [1]. A simplified example of a fault tree of this breakwater is presented in Figure 2.4.

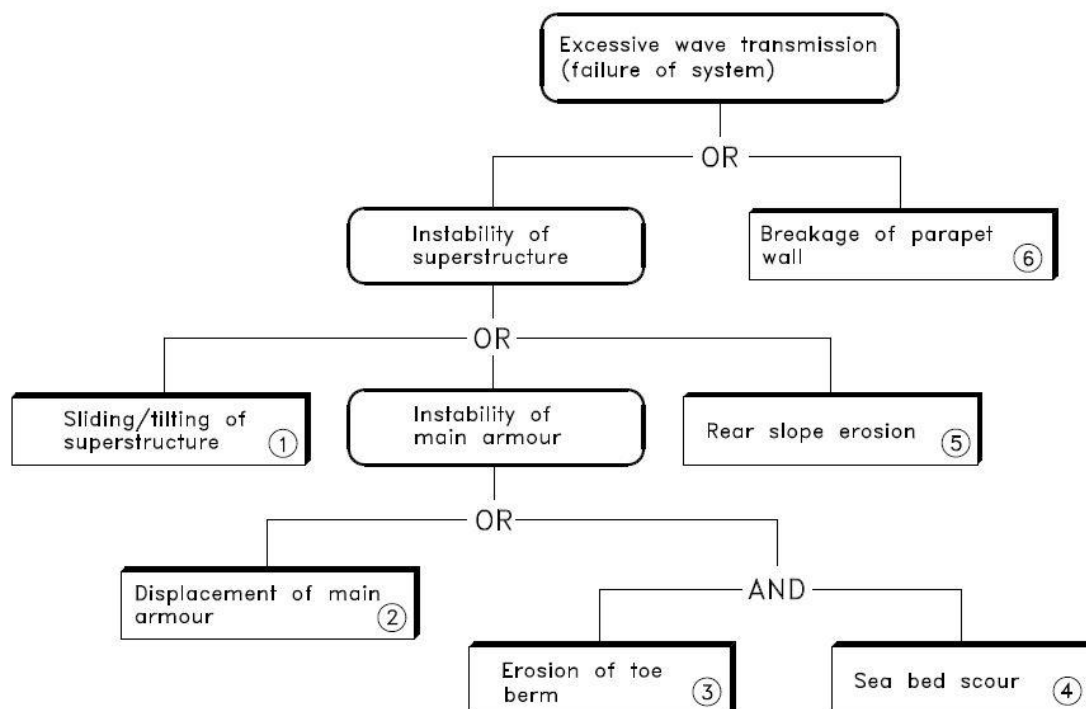


Figure 2.4 Simplified fault tree of a breakwater [1]

2.1.4.2 Series and parallel failure systems

A system can split into two types of fundamental systems, namely series and parallel systems, as illustrated in Figures 2.5 and 2.6 respectively.

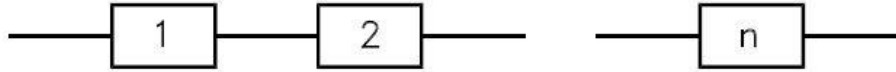


Figure 2.5 Series system [1]

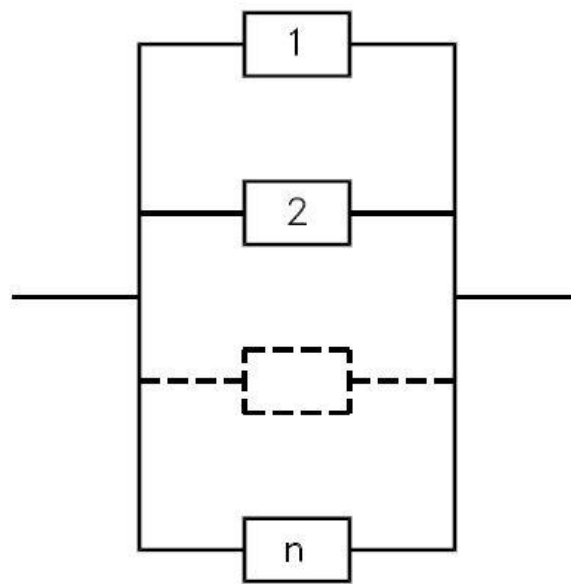


Figure 2.6 Parallel systems [1]

In a series system, failure occurs if any of the elements $i=1,2,\dots, n$ fails and the system failure probability is equal to the probability of the union of the elements' failures. The upper and lower bounds of the failure probability of the series system are:

$$\text{Upper bound: } P_f^U = 1 - (1 - P_{f1})(1 - P_{f2}) \dots (1 - P_{fn}) \quad (2.1)$$

$$\text{Lower bound: } P_f^L = \max[P_{fi}] \quad (2.2)$$

where: $\max[P_{fi}]$, is the largest failure probability among all elements. The upper bound corresponds to no correlation between the failure modes, while the lower bound to full correlation. Equation (1) is sometimes approximated by $P_f^U = \sum_{i=1}^n P_{fi}$, which is applicable only for small P_{fi} , because P_f^U should not be greater than 1.

It is noted that the OR-gates in a fault tree correspond to series components, which are dominant in breakwater fault trees. In fact, the AND-gate, shown in Figure 2.4, is included for illustration purposes, and in reality it should be an OR-gate [1].

In parallel systems failure occurs only if all components fail, thus the system failure probability is equal to the probability of the intersection of the elements failures. The upper bound corresponds to full correlation between the failure elements, and the lower bound to no correlation. The AND-gates in a fault tree represent parallel components.

$$\text{Upper bound: } P_f^U = \min[P_{fi}] \quad (2.3)$$

$$\text{Lower bound: } P_f^L = P_{f1} P_{f2} \dots P_{fn} \quad (2.4)$$

To calculate the upper and lower failure probability bounds for a system, it is practical to decompose the overall system into series and parallel subsystems.

The influence of correlation between two individual failure mechanisms on system failure probability is illustrated in the following diagram referring to the case of a series system.


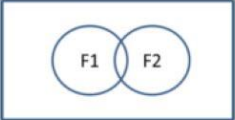
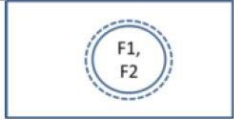
Case	Mutually exclusive	Independent	Dependent
Correlation coefficient. $\rho_{z1,z2} =$	-1	0	1
Venn diagram			
System failure probability $P(F)$	$P(F_1) + P(F_2)$	$P(F_1) + P(F_2) - P(F_1) \cdot P(F_2)$	$\text{Max}(P(F_1), P(F_2))$

Figure 2.7 The influence of correlation between two failure mechanisms on system failure probability [66]

2.1.5 Target Reliability

The target reliability of a coastal structure is the basis of design for the structure under consideration. The parameters that play a significant role in the selection of the structure's target reliability are its potential consequences of damage or failure, the design service life, the limit states/ design situations and the basic variables, which take place in the design formulas of the structure's elements. Therefore, the chosen level of reliability for coastal structures is a function of the consequences of damage or failure, design service life, and return period sea conditions for each limit state.

2.1.5.1 Consequences of damage or failure

The potential consequences of damage and/ or failure of the coastal structure under consideration should be assessed before the design process of the structure. These consequences could be indicatively qualified considering loss of human life or personal injury and also economic, social or environmental impact of the structure's damage or failure.

Furthermore, structures with huge potential consequences of damage or failure should be designed to meet an extremely high target reliability level in order that the exceedance probability of the design actions of the structure be extremely low. This is commonly the case of national scale flood protection structures or structures providing a critical role at a nuclear facility, the damage consequences of which could belong to the highest class if an analogous classification was made. Continuously, normal potential consequences of damage or failure could be attributed to flood protection structures protecting small areas/ populations, e.g. embankments or breakwaters, whilst the lowest class could be attributed to structures with no significant economic, social or environmental protection role.

From the above, it is concluded that the higher the potential consequences of a coastal structure's damage or failure, the higher its target reliability level or the lower allowable probability of failure, and vice versa.

2.1.5.2 Design service life

The design service life, or design lifetime of a coastal structure should be selected at the beginning of the design process.

Port infrastructure including breakwaters for ports of nationally significant strategic or economic value or infrastructure for regional flood defense or coast protection are considered the most permanent of coastal structures. A common design lifetime attributed to this category could be 100 years. However the most commonly used design lifetime is that of 50 years, which refers to port infrastructure for commercial and industrial ports including reclamation, shore protection, breakwaters or infrastructure for local flood defenses or coast protection.

Lower design lifetimes than those associated to the aforementioned categories could be selected for more temporary or replaceable structures.

2.1.5.3 Limit states/design situations

As far as the unacceptable wave action is concerned, four different states of coastal structures can be distinguished. Specifically, limit states used for breakwater design are states, beyond which the structures no longer satisfy the requirements, and can be distinguished in ULS (Ultimate Limit States), FLS (Fatigue Limit States), PLS (Progressive collapse Limit States) and SLS (Serviceability Limit States). Ultimate limit states are concerned with safety for people (to prevent human loss or injury) and structural collapse (or states immediately prior to collapse). Serviceability limit states are associated with damage that is likely to adversely affect the durability or functioning of the structure or comfort of users and are distinguished as reversible or irreversible.

A breakwater can have several functions, the most common of which is the protection of a certain coastal area against severe wave attack that can cause beach erosion or harbor basin protection against wave attack. The first case refers to detached breakwaters, while in the second case the main objective of the breakwater is to maintain the downtown of the harbor due to unacceptable wave attack to a requested minimum.

In the present thesis, only the ULS and the SLS are presented. The former is assumed to happen under extreme marine conditions and is a state where the breakwater is damaged and loses its structural integrity, while the latter is a state where the breakwater is not seriously damaged but leads to port downtime. Considering the Ultimate Limit State of a coastal structure, extrapolation of the marine variables to high enough return periods has to be performed.

An overview of these two limit states of a breakwater in relating to the port downtime is presented in Figure 2.8.

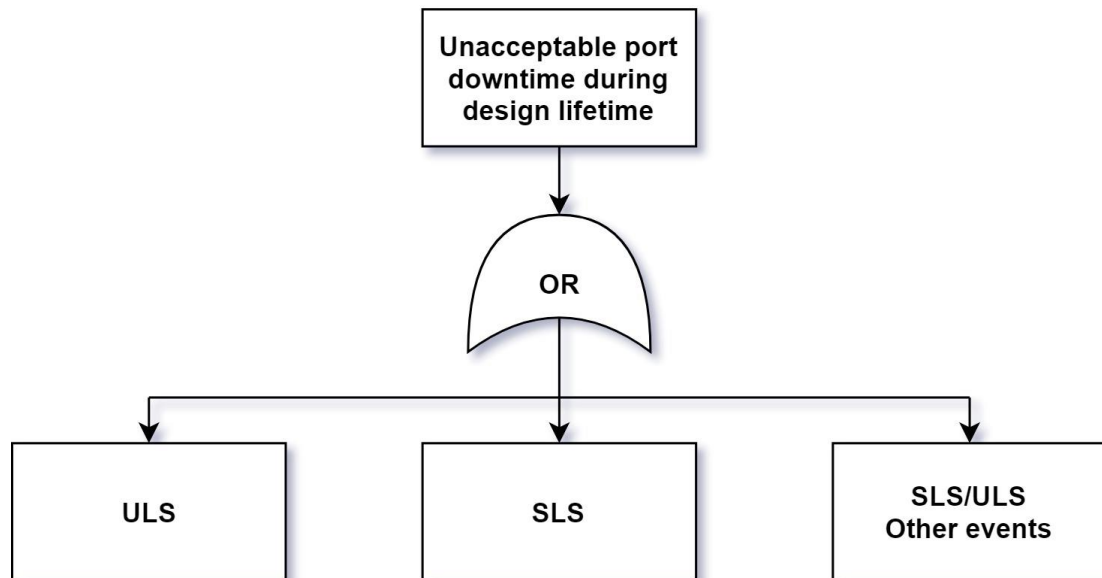


Figure 2.8. Fault tree of a breakwater protecting a harbor's basin [67]

2.1.5.4 Return period of design sea conditions and encounter/exceedance probability

Based on the potential consequences of damage and/ or failure of a coastal structure under consideration and its predefined design service life, the appropriate return period should be used for estimating environmental sea conditions associated with design events for the design limit state. As it is expected, the higher the consequences of damage or failure and the design lifetime of a coastal structure, the higher the return period that should be selected. The three parameters (i.e. consequences of failure, design lifetime, and return period) determine the exceedance probability of the design sea conditions within the structure's lifetime, which is directly related to the system's failure probability especially in deterministic design.

Return values of environmental sea conditions associated to certain return periods are extracted from an extreme data value analysis applied to observations or measurements of environmental parameters. Assuming time-dependent environmental parameters (e.g. wave parameters, sea level, currents etc.) and stationary long-term conditions, a time-variant analysis should be performed in order that the exceedance probability of the design sea conditions be estimated within the design lifetime, denoted by L .

In such an analysis, if we had Y years of observations/ measurements, the encounter probability of a design sea condition extracted from the dataset, i.e. the probability that this condition will be exceeded once in the mean within Y years, is equal to the average encounter probability of this condition within 1 year. In deterministic design, the latter is usually considered as the average failure probability of 1 year denoted by $P_{f,e,1y}^*$ referred to the sample of extreme events. This may be extrapolated to larger time periods such as the design lifetime of the structure L by assuming independent failure events from one year to another [1], [2]. The latter means that $P_{f,e,1y}^*$ is dependent on Y , but its value does not depend on the particular years that are included in the dataset. The aforementioned extrapolation can be accomplished by the following expressions, concerning the extreme sample:

$$P_{f,e,L}^* = 1 - \left(1 - P_{f,e,1y}^*\right)^L \quad (2.5)$$

This expression is based on the following relation [2] written in a more illustrative form here ([35]):

$$F_{X,e}^L(x_o) = P_L(x < x_o, x \in \text{extreme}) = \left(F_{X,e}^{1y}(x_o)\right)^{N_{e,L}} \quad (2.6)$$

where: $F_{X,e}^L(x_o)$ and $F_{X,e}^{1y}(x_o)$ are the average conditional cumulative probabilities of an extreme event x_o ¹ within L , and 1 year, respectively, estimated in the sample of extreme events, extracted from Y years of observations, and $N_{e,L}$ is the independent trials within L , i.e. the independent extreme events during L .

Therefore, by considering Eq. 2.6, it is concluded that Eq. 2.5 implies that the number of extreme events considered per year is only one, which is commonly the maximum observation of each year, i.e. $N_{e,L} = L$. However, Eq. 2.5 can be written in its general expression as follows:

¹ As an extreme event is considered the annual maximum observation or one that exceeds a relatively high threshold.

$$P_{f,e,L}^* = 1 - \left(1 - P_{f,e,1y}^*\right)^{\lambda_e L} \quad (2.7)$$

where: λ_e is the number of extreme observations considered per year of observations, i.e. $N_{e,L} = \lambda_e L$.

By using the notion of return periods, Eq. 2.6 and Eq. 2.8 can be written respectively as follows:

$$P_{ex,e,L}^* = 1 - \left(1 - \frac{1}{T_r}\right)^L \quad (2.8)$$

$$P_{ex,e,L}^* = 1 - \left(1 - \frac{1}{\lambda_e T_r}\right)^{\lambda_e L} \quad (2.9)$$

where: $P_{ex,e,L}^*$ is the exceedance probability of the return sea conditions that correspond to return period T_r .

Continuously, by applying Eq. 2.9, the exceedance probabilities of different return periods associated to different design lifetimes are presented in Table 2.1. For example, if the return period of 100 years is selected for the design of a coastal structure, whose design lifetime is 50 years, then the exceedance probability of the return sea conditions is expected to be 0.39. This exceedance probability is high enough given that a considerably extreme sea condition, that of 100 years, is selected for the design. This contradiction could be attributed to the fact that this probability is extracted from the average failure probability of 1 year estimated from the extreme sample of observations/measurements.

Also, it is recommended that regarding the extrapolation of data, aiming at getting the best possible estimates of extreme conditions at desired return periods, often the data must be extrapolated to probabilities beyond the record length Y to match design return periods. Extrapolation beyond 2-3 times the data record length should be avoided if possible [1], e.g. 30 years of data should be used for estimating return values of 60-90 years or less.

Table 2.1 Exceedance probability of design return values associated to design lifetime L

Return period T_r (years)	Design lifetime L (years)					
	2	5	10	25	50	100
2	0.75	0.97	1.00	1.00	1.00	1.00
5	0.36	0.67	0.89	1.00	1.00	1.00
10	0.19	0.41	0.65	0.93	0.99	1.00
25	0.08	0.18	0.34	0.64	0.87	0.98
50	0.04	0.10	0.18	0.40	0.64	0.87
100	0.02	0.05	0.10	0.22	0.39	0.63
200	0.01	0.02	0.05	0.12	0.22	0.39

It is noted that, theoretically, the return period used in deterministic design refers to dependent (joint probability) sea conditions, e.g. of waves and water-levels and/or currents, where clear evidence exists that a modest or a significant degree of correlation is expected. However, when no correlation is expected, or in some cases where the structure response is not to be sensitive to combined sea actions, the independent sea action may be used, e.g. wave action only.

2.2 Reliability of an element

The reliability based design methods for coastal structures are divided into four categories, related to the accuracy in determining the reliability (or failure probability) of the element design and the consideration of all involved uncertainties (see section 1.1).

Conventional design practice for coastal structures, such as breakwaters, is often deterministic in nature, and its reliability is based on the exceedance probability of the design sea condition, defined by the wave load. In this approach, the notion of design wave parameters and especially that of significant wave height (H_s) associated with a certain return period, e.g. the expectation (mean) value of the 100-year return period extreme event, is adopted. The resistance of the structure is treated in a deterministic manner, and the exceedance probability of the design load is identical with the exceedance probability of the damage associated to this design load. This is attributed to the fact that most of the available design formulas give the relationship between wave characteristics and some structural response, i.e. armour damage, wave overtopping, run-up etc. [1]. Thereafter, it is noted that the deterministic design approach, classified as Level 0, is based on an extreme value analysis. However, all the uncertainties involved in the element design are not taken into consideration.

Moreover, all coastal structure design formulas are semi-empirical, since they have derived from experiments and the estimation of the formulas' parameters is based mainly on central fitting to model test results. Thus, the often considerable scatter in test results is not taken into account in general. This leads to the fact that the mean or a characteristic value is applied in the design formulas for the resistance parameters, and not a lower fractile, as is usually used in other engineering problems [1]. Therefore, the only contribution to a safety margin in the design process is the selection of a certain return period for the design load, which is a considerable step towards a fully probabilistic design.

In addition to the deterministic method, partial safety factors can be implemented for resistance and load, based on standards [3]. This calculation is classified as semi-probabilistic (Level I) method. However, this approach often results in overdesign of the structure and does not allow accurate determination of the reliability of the design. In order to overcome this problem, more advanced probabilistic methods must be applied that consider the uncertainties of all stochastic variables of load and strength of the structure.

Fully probabilistic methods or Level III methods belong in this category of the advanced probabilistic methods, which consider the actual probabilistic distribution of all stochastic variables involved. When statistical correlation between the stochastic variables does exist, it

can be considered by these methods. Another possibility, though less accurate regarding the estimation of the reliability of the design, are methods with approximations or Level II methods. They generally transform correlated and non-normally distributed variables into uncorrelated and standard normal distributed variables, and reliability indices are used as measures of the reliability of the structure [1].

2.2.1 Limit state function

The reliability of an element depends on the safety margin between the strength (i.e. resistance R) and the load (or action A). The limit state function describes the relation between resistance and load of an element.

In general, the reliability function of an element is formulated as follows:

$$g = R - A \quad (2.10)$$

where: as it has been aforementioned, R stands for strength and A for action. Both are functions of several stochastic variables:

$$R = R(X_1, X_2, \dots, X_m) \quad (2.11)$$

$$A = A(X_{m+1}, X_{m+2}, \dots, X_n) \quad (2.12)$$

Therefore, the limit state function describes the state of the element, as presented in the following relation:

$$g = g(X_1, X_2, \dots, X_n) = g(\vec{X}) = \begin{cases} < 0, & \textit{failure} \\ = 0, & \textit{limit state} \\ > 0, & \textit{no failure (safe region)} \end{cases} \quad (2.13)$$

Thus, the probability of failure of the element (P_f) is defined by Eq. 2.14 and the reliability of the element (R_f) by Eq. 2.15.

$$P_f = Prob(g < 0) = Prob(A > R) \quad (2.14)$$

$$R_f = 1 - P_f \quad (2.15)$$

2.2.2 Reliability methods

The four categories of the reliability methods, based on the accuracy of the structural reliability estimation, are described in the following paragraphs.

2.2.2.1 Deterministic Methods (Level 0)

A deterministic calculation method uses nominal values of the basic variables. Often a global safety factor is applied to deal with the unknown uncertainties in the basic variables and to provide a safety margin between strength and load. Thus, the reliability inequality is formulated as:

$$R_{nom} \geq \gamma A_{nom} \quad (2.16)$$

The formula by Van der Meer [57] for surging waves and deep waters can be used as an example to describe a global safety factor, presented in the following equation:

$$\Delta D_{n50} P^{-0.13} \left(\frac{S_d}{\sqrt{N}} \right)^{0.2} \sqrt{\cot \alpha} \xi_m^P \geq H_s / c_s \quad (2.17)$$

where: H_s is the significant wave height of the design storm of a certain return period or probability of exceedance within the structure lifetime, Δ the relative buoyant density, D_{n50} the nominal stone diameter, P the notional permeability of the structure, S_d the damage level factor, N the number of waves, α the armor slope, ξ_m the surf similarity parameter based on the mean wave period, and c_s is a constant for surging waves.

To ensure the structure's reliability, a global safety factor is included in the Van der Meer [57] formula via the parameter c_s , which is often a mean value with 95% confidence interval. Thus, the limit state function is not close to zero, but has a safety margin between strength and load.

2.2.2.2 *Semi-probabilistic Methods (Level I)*

This section presents the partial safety factors developed by PIANC [3], Burcharth [68] and Burcharth and Sørensen [69]. This calculation is based on standards and partial safety factors are implemented for strength (γ_r) as well for load (γ_A) via the following relation, creating by this way a safety margin for the reliability of the element:

$$\frac{R_{nom}}{\gamma_r} \geq \gamma_A A_{nom} \quad (2.18)$$

The partial safety factors (γ_i) are related to characteristic values of the stochastic variables ($X_{i,ch}$), and are usually larger than or equal to 1. The magnitude of γ_i reflects the uncertainty of the parameter X_i and the relative importance of the latter in the limit state function [1]. A large value of γ_i , e.g. $\gamma_{H_s} = 1.4$, indicates a relatively large sensitivity of the element's reliability or the corresponding failure probability to significant wave height, H_s , while a γ_i close to 1 indicates negligible sensitivity, and thus the partial safety factor should be omitted.

An illustrative example of this method will be presented considering the Hudson formula [70] for rock armor layer. Specifically, the partial safety factors can be applied to each parameter (load or resistance) or to a combination of parameters, i.e. overall coefficients. The limit state function, determined by Hudson design formula, which must be greater than or equal to 1, referring to the case of partial safety factors applied to each parameter involved is given by:

$$G = \frac{A_{ch}}{\gamma_A} \frac{\Delta_{ch}}{\gamma_\Delta} \frac{D_{n,ch}}{\gamma_D} \left(K_D \frac{\cot \alpha}{\gamma_{\cot \alpha}} \right)^{1/3} - \gamma_{H_s} H_{s,ch} \geq 0 \quad (2.19)$$

Continuously, if the partial safety factors are applied to a combination of parameters, there might be only γ_{H_s} , and γ_Z related to the first term on the right part of Eq. 2.20. Therefore, the design equation leading to a safety domain of the element would become:

$$G = \frac{1}{\gamma_Z} A_{ch} \Delta_{ch} D_{n,ch} (K_D \cot \alpha)^{1/3} - \gamma_{H_s} H_{s,ch} \geq 0 \quad (2.20)$$

Equations 2.19 and 2.20 are equivalent. However, Eq. 2.20 is simpler than Eq. 2.19. The values of these partial safety factors are different for each design formula and are determined according to PIANC [3] via the following equations:

$$\gamma_{H_s} = \frac{H_s^{T_{P_f}}}{H_s^{T_L}} + \sigma_{F_{H_s}} \left[1 + \left(\frac{H_s^{3T_L}}{H_s^{T_L}} - 1 \right) k_\beta P_f \right] + \frac{k_s}{\sqrt{P_f N}} \quad (2.21)$$

$$\gamma_Z = 1 - (k_\alpha \ln k_\beta P_f) \quad (2.22)$$

where: $H_s^{T_L}$ is the central estimate for H_s with a return period equal to the lifetime of the structure T_L (which in average is exceeded once every T_L years, $H_s^{T_{P_f}}$ is the central estimate for H_s with a return period based on the allowable probability of failure during the structure's lifetime, and $H_s^{3T_L}$ stands for the central estimate for H_s associated with a return period equal to three times the lifetime of the structure. Continuously, P_f is the allowable probability of

failure during the structure's lifetime T_L , N is the number of wave data on which the extreme value wave analysis is based. Besides, the coefficient k_s depends on the type of the mechanism of failure and is found by optimization [3], $\sigma'_{F_{H_s}}$ declares the quality of measured wave data, i.e. high quality and low quality wave data could be represented by $\sigma'_{F_{H_s}}$ equal to 0.05 and 0.20, corresponding to accelerometer buoy and Fetch diagram estimates respectively. The middle term of the right-hand side of Equation 2.21 takes into account the model uncertainty related to the quality of wave measurements. This is accomplished by implying a multiplicative stochastic variable F_{H_s} assumed to be normally distributed with a mean value of 1.0 and a standard deviation of $\sigma'_{F_{H_s}}$.

Finally, the coefficients k_α and k_β have been derived by optimization for each failure mechanism and design formula by PIANC [3].

The partial safety factor for the load variable given in Equation 2.21 consists of three terms. The first term estimates the partial safety coefficient given that no statistical uncertainty and measurements errors are present in H_s . This term signifies the encounter probability of the design significant wave height during the structure's lifetime, caused by the nature's vagaries. This is expressed by the central estimate of H_s for a certain return period, given a certain extreme value distribution for storms, e.g. a Weibull probability distribution [71].

The last term stands for the statistical uncertainty of the estimated extreme probability distribution of H_s . The latter depends on the number of wave data considered. In case that H_s has not derived from wave statistics, then the last term is omitted and the second term accounts for the inherent uncertainty.

In short, according to PIANC [3], partial safety factors are calibrated with the following input:

- Design Lifetime T_L (=20, 50 or 100 years)
- Acceptable probability of failure P_f (=0.01, 0.05, 0.10, 0.20, or 0.40)
- Coefficient of variation $\sigma'_{F_{H_s}}$ (=0.05 or 0.20)
- Deep or shallow water conditions

Wave loads determined with or without hydraulic model tests

Besides, the partial safety factors are as follows:

- A load partial safety factor γ_{H_s} to be applied to H_s^T
- A partial safety factor γ_Z to be used to the combination of the mean values of the resistance parameters in the design equation.

It is noted that the element's probability of failure cannot be calculated precisely via this design process, since it is selected a priori, and is defined as the allowable probability of failure of the element during the structure's Lifetime P_f . This drawback can lead to underestimation or overestimation of the design structure's elements characteristics.

2.2.2.3 Probabilistic Methods with Approximations (Level II)

Another possibility of estimating the reliability of an element is to use a level II method which is a probabilistic method with approximations. In the present thesis, only the concept of this method will be presented, since its calculation is based on a rather iterative and complex process, making thus Level II methods difficult to apply, especially if the random variables are non-normal and statistical correlated. Besides, only the first-order reliability methods (FORM) will be briefly described here. In these methods, the failure surface is approximated by a tangent hyperplane at the design point (see Figure 2.9). However, the second-order reliability methods (SORM) are considered more precise, but calculations are more complex than in FORM. Specifically, a quadratic approximation to the failure surface is used in SORM.

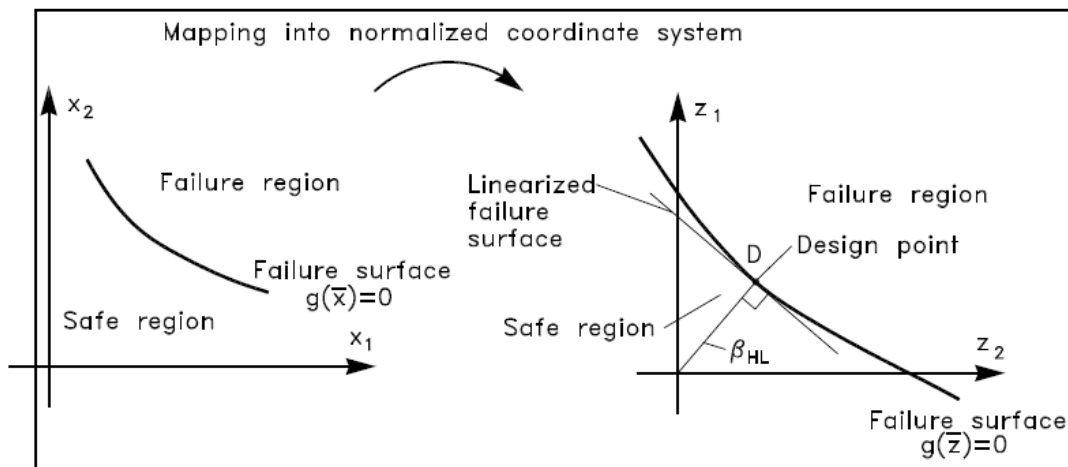


Figure 2.9 Linearization and approximation of the failure surface by a tangent hyperplane at the design point [1]

Regarding the type of the failure function and the distributions of random variables three different cases of FORM methods can be distinguished, which are listed below in order of increasing complexity:

- Linear failure functions of normally-distributed random variables
- Nonlinear failure functions of normally-distributed random variables
- Nonlinear failure functions of non-normal random variables

It is noted that for correlated random variables, the transformation into non-correlated random variables should be performed before normalization.

In the first case, which is the simplest one compared against the other two cases, the failure function for a single mode of failure, given by Equation 2.11, is estimated using only the mean values and standard deviations of the loading $A(x)$ and resistance $R(x)$. If $A(x)$ and $R(x)$ are assumed to be independent normally distributed random variables with known means and standard deviations, the linear failure function is also normally distributed with mean value:

$$\mu_g = \mu_R - \mu_A \quad (2.23)$$

and standard deviation:

$$\sigma_g = \sqrt{(\sigma_R^2 + \sigma_A^2)} \quad (2.24)$$

The quantity $(g - \mu_g) / \sigma_g$ will be unit standard normal, and consequently the failure probability of the element is estimated as follows:

$$P_f = \text{Prob}(g \leq 0) = \int_{-\infty}^0 f_g(x) dx = \Phi\left(\frac{0 - \mu_g}{\sigma_g}\right) = \Phi(-\beta) \quad (2.25)$$

where:

$$\beta = \frac{\mu_g}{\sigma_g} \quad (2.26)$$

is referred to as the reliability index [72], since it is a measure of the failure probability and consequently of the reliability of the element. The reliability index is the inverse of the coefficient of variation, and can be defined as the distance (in terms of standard deviation) from the most probable value of g (in this case the mean value) to the failure surface, $g=0$ (see Figure 2.10).

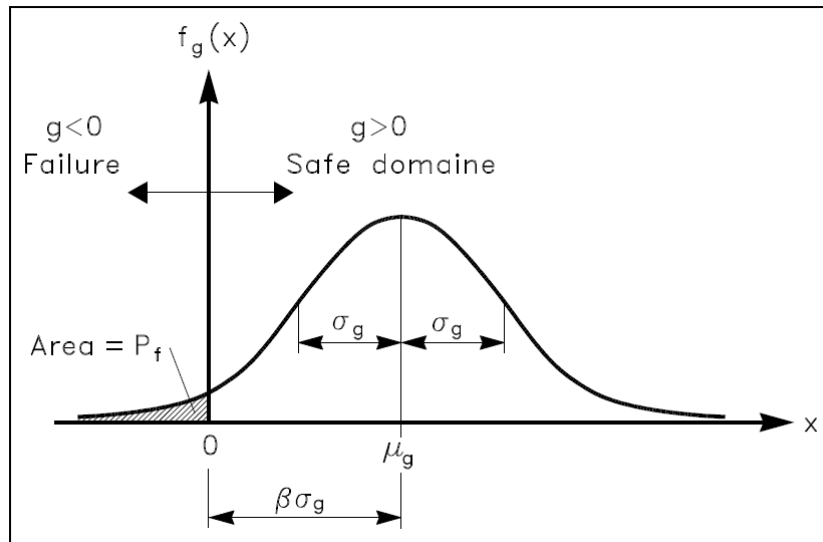


Figure 2.10 Illustration of the reliability index for a linear failure function of normally-distributed random variables [1]

It is noted that if $A(x)$ and $R(x)$ are normally distributed and correlated, then Equation still holds, but the standard deviation of the linear failure function is given by

$$\sigma_g = \sqrt{(\sigma_R^2 + \sigma_A^2 + 2\rho_{RA}\sigma_R\sigma_A)} \quad (2.27)$$

where ρ_{RA} is the linear correlation coefficient between $A(x)$ and $R(x)$:

$$\rho_{RA} = \frac{Cov(R, A)}{\sigma_R \sigma_A} \quad (2.28)$$

where $Cov(R, A)$ is the covariance between $A(x)$ and $R(x)$.

As it has been aforementioned, the calculation of the reliability of an element becomes rather complex in the other cases listed above, and consists of a number of transformations, e.g. of nonlinear failure functions to equivalent linearized ones, of uncorrelated non-normal random variables to equivalent normal ones, etc. However, due to the difficulties that may arise during the reliability calculation process and to the probable loss of accuracy during these transformations, Level II methods will not be adopted in the present thesis and thus will not be further analysed here.

2.2.2.4 Fully Probabilistic Methods (Level III)

When a fully probabilistic method is applied, the failure probability of an element can be calculated accurately and is directly linked to the reliability of the element. There are two main methods classified as Level III methods, the Direct Integration Method (DIM) and Monte Carlo Method (MCM), which will be described below.

Direct Integration Method (DIM)

The core problem of DIM is the exact estimation of the joint pdf of all stochastic variables involved. Given that the marginal pdfs of the variables considered are known, the calculation of the joint pdf of the variables is necessary, only if these variables are correlated, otherwise the joint pdf is equal to the multiplication product of the marginal pdfs of the variables.

In case of correlated variables, an efficient way to capture their correlation is to apply the conditional probability model in order to calculate the jpdf. The said model can be illustrated by the following probability law applied indicatively to two variables, e.g. two wave load

variables that are correlated, and can be also applied to more than two correlated variables as well:

$$f_{X_1, X_2}(x_1, x_2) = f_{X_1|X_2}(x_1 | x_2) f_{X_2}(x_2) \quad (2.29)$$

where $f_{X_1, X_2}(x_1, x_2)$ is the jpdf of the stochastic variables X_1, X_2 , $f_{X_1|X_2}(x_1 | x_2)$ is the conditional pdf of X_1 given X_2 , and $f_{X_2}(x_2)$ is the marginal pdf of X_2 .

Given that $f_{\vec{X}}$ is the joint pdf of all stochastic variables involved, i.e. of the vector $\vec{X} = (X_1, X_2, \dots, X_n)$, Equation 2.14 can be expressed by:

$$P_f = \int_{g(\vec{x}) < 0} f_{\vec{X}}(\vec{x}) d\vec{x} \quad (2.30)$$

Note that if only two variables $R(r)$ and $A(a)$ are taken into consideration, the above Equation reduces to:

$$P_f = \iint_{R \leq A} f_{R,S}(r, a) dr da \quad (2.31)$$

which is illustrated in Figure 2.11.

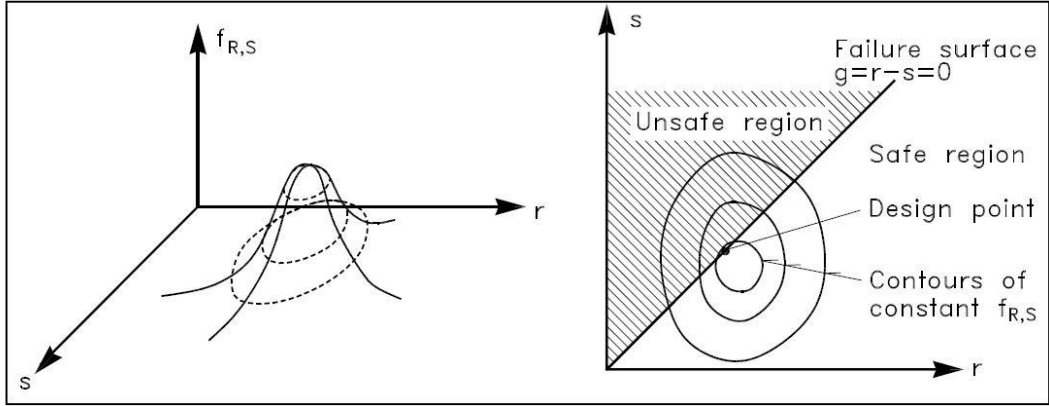


Figure 2.11 Illustration of the two dimensional jpdf for loading s and resistance r [1]

If more than two variables are involved, the joint pdf of the stochastic variables cannot be described as a surface, and the problem becomes multidimensional. Thus, Eq. 2.31 is given by the n -fold integral:

$$P_f = \iint \dots \int_{R \leq A} f_{X_1, X_2, \dots, X_n}(x_1, x_2, \dots, x_n) dx_1 dx_2 \dots dx_n \quad (2.32)$$

If all variables can be assumed independent, their jpdf is equal to the product of all marginal probability density functions (pdfs) and then Equation 2.32 can be simplified to:

$$P_f = \iint \dots \int_{R \leq A} f_{X_1}(x_1) f_{X_2}(x_2) \dots f_{X_n}(x_n) dx_1 dx_2 \dots dx_n \quad (2.33)$$

If only two independent variables are considered, Equation 2.33 reduces to:

$$P_f = \iint_{R \leq A} f_R(r) f_A(a) dr da \quad (2.34)$$

which by partial integration can be written as a single integral:

$$P_f = \int_0^{\infty} F_R(x) f_A(x) dx \quad (2.35)$$

where F_R is the cumulative distribution for resistance/strength R . Since negative resistance is not meaningful, $-\infty$ has been replaced by 0 in the above equation.

It should be noted that the computational requirements of DIM are very demanding especially if the number of stochastic variables, n , is greater than 5 [1].

Monte Carlo Method (MCM)

This method is based on a large number of simulations N , a part of which (N_f) leads to element's failure. Thus, it is assumed that provided N is a high enough number,

$$P_f = \frac{N_f}{N} \quad (2.36)$$

NOTE: N should be sufficiently large for P_f to attain acceptable convergence.

One way (e.g. inverse CDF method) to generate the random sample for each variable is described here. Specifically, each simulation starts by drawing a random number from a uniform probability density function $U(0,1)$. Through this number (x_u), a sample of the variable (X) can be produced by the latter's inverse cumulative distribution function $F_x^{-1}(x)$ as follows:

$$X = F_x^{-1}(X_u) \quad (2.37)$$

The cumulative distribution function of X is calculated from its probability density function $f_X(x)$ as follows:

$$F_X(x) = \int_{-\infty}^x f_X(u) du \quad (2.38)$$

Function $F_X(x)$ is linked to P_f of Equation 2.36 by letting $f_X(x)$ become multidimensional to represent the joint probability density function $f_{\vec{X}}(\vec{x})$ of Eq. 2.30. Evaluation of function $g(\vec{x})$ should then be performed to assess the failure domain $\Omega(\vec{x}) = \{g(\vec{x}) < 0\}$ in order to apply Equation 2.36.

In Figure 2.12, the random sample generation process of the variable X , and the inverse cumulative distribution of which is denoted by $F_X^{-1}(x)$, is depicted.

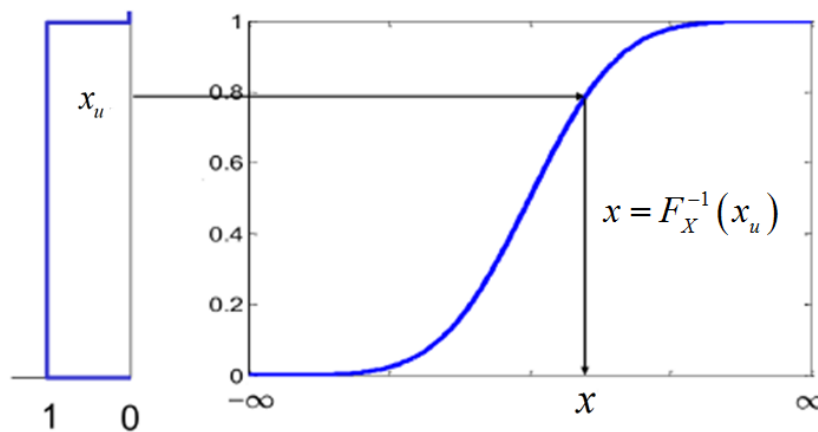


Figure 2.12 Random sample generation step for one variable in MCM [66]

The procedure of Monte Carlo simulation after the random sample generation for each variable is presented in the following diagram (see Figure 2.13).

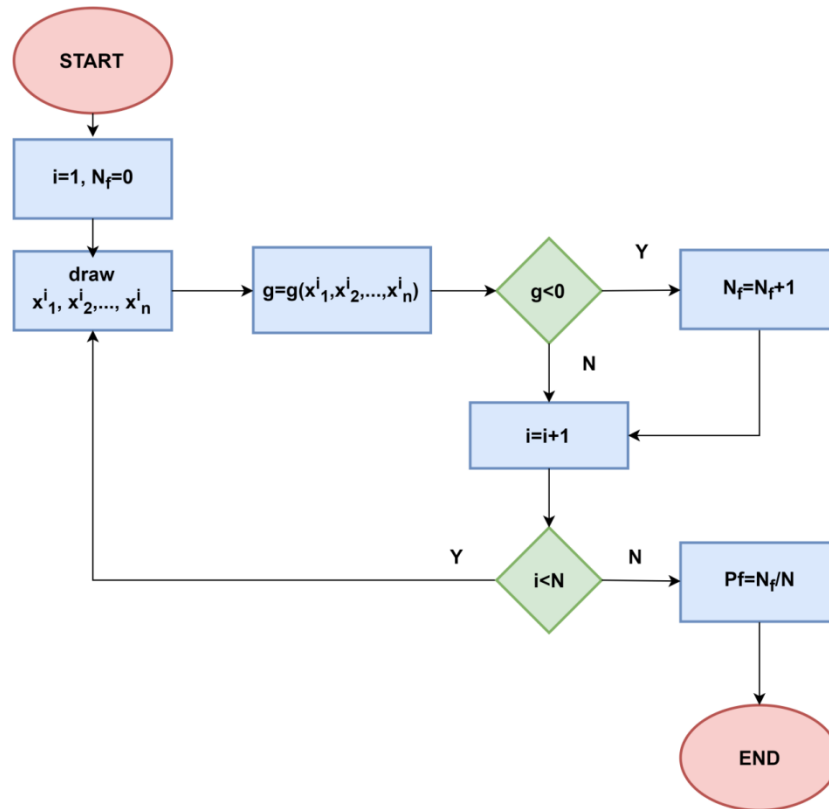


Figure 2.13 MC simulation (according to Schiereck [73])

Despite the fact that MC simulation is relatively simple, its computational demands increase, when more stochastic variables are involved and the total number of simulations N is very large. Besides, MC procedure becomes more complex and difficult to apply when correlation between variables is considered.

2.3 Probabilistic design process

In this section, an overview is given of the probabilistic design of coastal structures. Firstly, a simplified flow chart of the design process and then a more detailed one are presented.

2.3.1 Simplified flow chart of the design process

In Figure 2.14, a simplified diagram for the probabilistic design process of marine coastal structures is presented. Firstly, the design requirements and the environmental boundary conditions are defined; secondly the design parameters are determined for preliminary (deterministic) and fully probabilistic design method. It is noted that the preliminary, i.e. deterministic, design is important for the beginning of the probabilistic design method, since the first one provides the latter with the initial solution, which will then be used for the more accurate calculation of the system reliability.

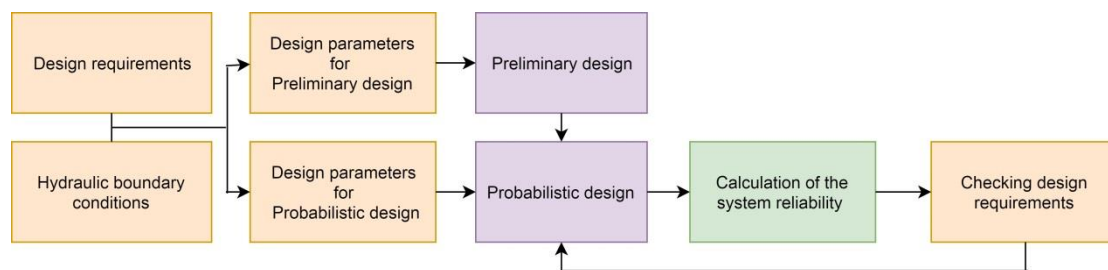


Figure 2.14 Simplified flow chart of the design process (according to Everts [56])

As it can be observed in the above Figure (Figure 2.14), the three final steps develop an iterative procedure which ends only if the predefined design requirements are met.

2.3.2 Detailed flow chart of the design process

In Figure 2.15, a more detailed diagram of the design process is presented. Firstly, the design requirements need to be specified for the limit state, e.g. Ultimate Limit State (ULS) and the Serviceable Limit State (SLS), e.g. the structure's Lifetime and the allowable probability of failure during the design lifetime, of a coastal structure. Then, the fault tree that describes the linking of failure mechanisms has to be constructed in a proper manner. The boundary

conditions, determined next, can be subdivided in hydraulic, geotechnical and geometric, etc. The mean or characteristic values of the structure's resistance/strength parameters, or their probability distributions, should also be specified in order that both boundary conditions and the structural properties be used for preliminary or probabilistic design, respectively.

Preliminary (deterministic) design uses deterministic input variables and a deterministic or a semi-probabilistic design method. Then, the preliminary design is subjected to a fully probabilistic reliability method, like Monte Carlo and Direct Integration Method. As noted in Figure 2.15, preliminary (deterministic) design is the basis for the fully probabilistic method, since the first uses the same variables as the latter, and can provide an initial solution, which will be checked via the probabilistic design method. However, instead of the deterministic input variables of the preliminary design, a fully reliability method uses the joint probability distribution of all these variables, now being stochastic ones. Thus, their marginal pdfs and the correlation between variables are taken into consideration in a fully probabilistic design process.

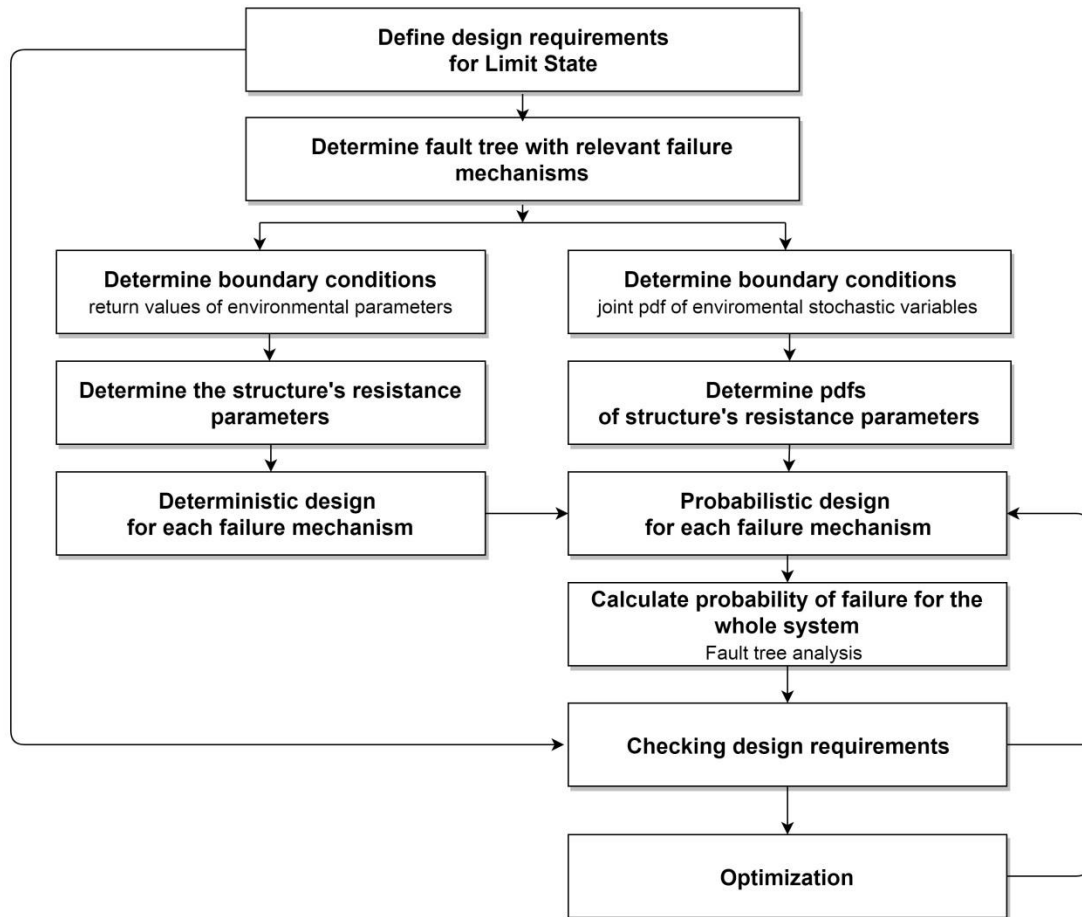


Figure 2.15 Detailed flowchart of the design process for a coastal structure [35] (based on Everts [56])

Before the total reliability of the system can be determined, the correlation and linking between the failure mechanisms should be considered. Then, after the reliability of whole system is calculated, the estimated reliability level is subjected to control over the design requirements. If the design requirements are met, further optimization can be made considering economic cost aspects.

2.4 Hydraulic boundary conditions

In this section, all the necessary environmental boundary conditions that need to be determined for the design of a coastal structure will be discussed. Apart from the environmental boundary conditions, there are also other boundary conditions like the geometric limitations that are imposed on the design structure.

The category of environmental boundary conditions consists of hydraulic and geotechnical boundary conditions. The latter are not within the scope of the present thesis.

The hydraulic boundary conditions define the load actions upon a coastal structure which are the sea conditions (i.e. wave actions and sea level). Some main load parameters associated to their units in SI system are presented in Table 2.2.

Table 2.2 Main parameters representative of hydraulic boundary conditions

Load parameters	Symbol	Units
Significant water height	$H_{1/3}$, H_s	m
2% wave height	$H_{2\%}$	m
Mean wave period	T_m	s
Principal wave direction relative to North	θ_m	°N
Spectral significant wave height	H_{mo}	m
Spectral peak wave period	T_p	s
Energy period	T_e	s
Water depth	d	m
Water level variation due to tide	TL	m
Water level variation due to storm surge	SL	m

Usually, coastal structures are built in intermediate water depths, i.e. $0.05 < d/L_m < 0.5$, where d is the water depth and L_m the mean wave length of a sea state at the structure's location. This means that the hydraulic parameters, presented in the Table 2.2, must be determined at the structure's location.

Hydraulic boundary conditions are caused either by meteorological forcing (winds, waves, storms surges etc.) or by astronomical forcing (tides), or by seismic forcing (tsunamis). The principal relationships between the above forces are shown in the Figure 2.16.

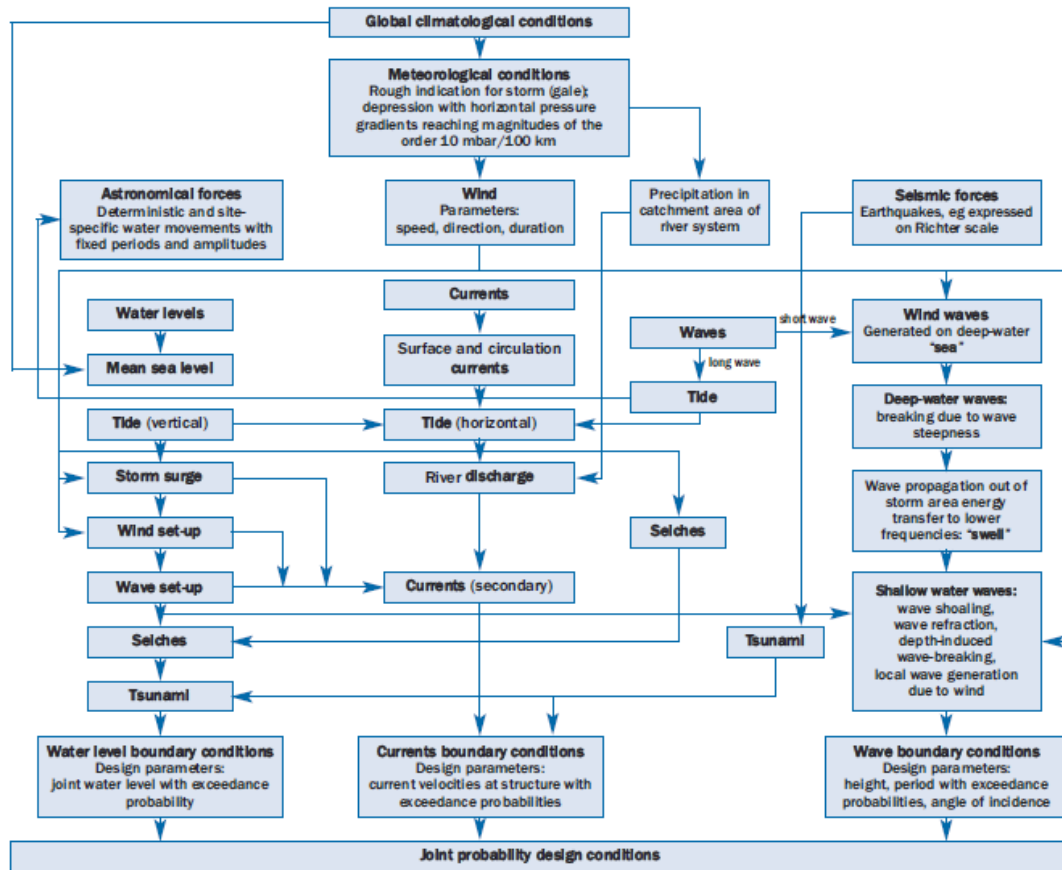


Figure 2.16 Hydraulic boundary conditions for coastal structures [55]

An example of combined loading includes water level and wave conditions determining the required armor units and the required crest level of an emerged breakwater or a seawall.

Two main categories of hydraulic boundary conditions (i.e. wave and water level boundary conditions) are considered in the present thesis and will be described in the following sections.

2.4.1 Wave action

Wind-generated ocean waves change randomly with time, i.e. both wave height and period vary randomly from one cycle to another. Their period ranges from 1 s to 30 s. Waves tend to break when the wave steepness exceeds a certain limit. Besides, it is often observed that during propagation of wind-generated waves from one location in the ocean to another in deep waters, far away from the wind field that generated the waves, swell waves propagate not necessarily at the local wind direction and are longcrested and their frequency spectrum is very narrow-banded.

As waves move inshore, depth-induced wave transformations take place and a more distinct difference in the wave profile can be observed. Referring to severe seas, as shown in Figure 2.17, the wave profile in deep water the wave profile in deep water is somewhat symmetrical relative to the mean water level, while in shallow waters peaks are much sharper than troughs, and the order of magnitude of the peaks is higher than that of the troughs.

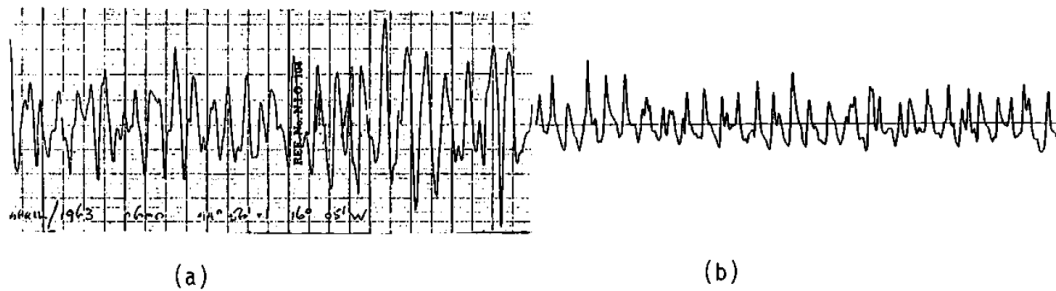


Figure 2.17 Wave profile in severe seas (a) in deep waters and (b) in shallow waters [10]

In probabilistic approach, wave profile in deep waters is characterized as a Gaussian random process, since the sea surface displacement from its mean value can be represented by a normal probability distribution (see Figure 2.18a). This was first found by Rudnick [74] who analyzed measured data obtained in the Pacific Ocean. Furthermore, Pierson et al. [75], based on the central limit theorem, presented an illustrative sketch (shown in Figure 2.19), which indicates that ocean waves consist of an infinite number of monochromatic, or else sinusoidal, waves having the same height but different frequencies and directions.

On the other hand, depth-limited waves follow a non-Gaussian random process, as seen in Figure 2.18b. However, waves in relatively shallow waters may be considered as a Gaussian random process if the sea severity is very mild [10].

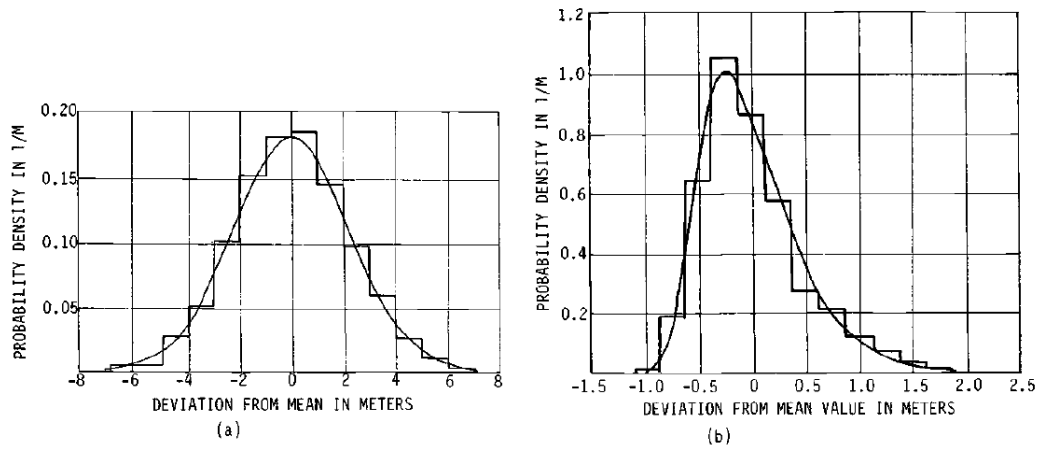


Figure 2.18 Wave profile histogram and the theoretical distribution (a) in deep waters and (b) in shallow waters [10]

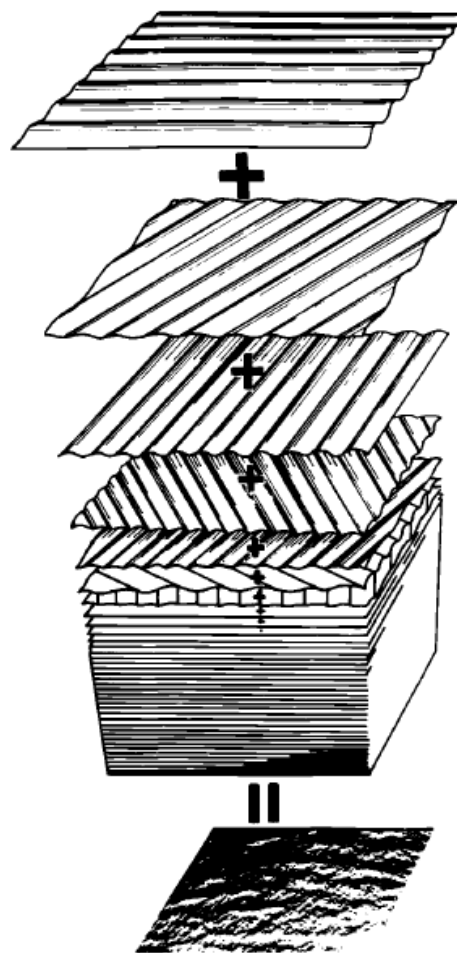


Figure 2.19 Structure of random sea [75]

Wave parameters can be determined either from a frequency-domain or a time-domain analysis of a wave record. These two categories of the analysis will be described next.

2.4.1.1 Wave parameters from frequency-domain analysis of a wave record

A detailed structure of wind waves and swell can be extracted from the frequency-domain analysis of a wave record. In this analysis, wave spectra are used to represent the total wave (potential and kinetic) energy at a certain location in the ocean, which is an accumulation of the energy of all waves propagating from various directions.

Waves as a Gaussian random process

In reality, only the major part of wind-generated wave energy does propagate in the wind direction [10]. Continuously, there is a directional spread of the energy which should be taken into consideration in the frequency-domain analysis of a wave record. Therefore, the notion of the directional spectral density function has been adopted denoted by $S(f, \theta)$. Continuously, if the time average of wave energy at any frequency interval df and directional interval $d\theta$ is equal to $1/2\rho g\alpha_j^2$, where α_j is a positive random variable, and by ignoring ρg , it can be written:

$$S(f, \theta)df d\theta = 1/2\alpha_j^2 \quad (2.39)$$

The time average of the total energy of waves of all frequencies and propagating from various directions is given by:

$$\sum_{\Delta f} \sum_{\Delta \theta} \frac{1}{2} \alpha_j^2 = \int_{-\pi}^{\pi} \int_0^{\infty} S(f, \theta) df d\theta \quad (2.40)$$

Wave spectral formulations

There are many formulations of wave spectra proposed (e.g. [76]; [77]; [78]; [79]; [80]; [81] etc.) used in engineering applications, which are based on wind speed, significant wave height, wave period, etc. Some of them will be briefly presented below:

Referring to the case of fully developed seas, a widely used spectrum for wave hindcasting and forecasting is developed by Pierson and Moskowitz [82] given by:

$$S_{PM}(f) = \frac{0.0081g^2}{(2\pi)^4 f^5} \exp\left[-0.74\left(\frac{2\pi U_w f}{g}\right)^{-4}\right] \quad (2.41)$$

where: U_w is the wind speed at 19.5 m above mean sea level. As seen in Eq. 2.41, the Pierson-Moskowitz spectral formulation is based on a single parameter, the wind speed.

Another spectral formulation is the JONSWAP spectrum, which is based on an extensive wave measurement program known as the Joint North Sea Wave Project carried out in the North Sea Sylt Island in 1968 and 1969 [83]. The spectrum represents fetch-limited wind-generated seas, thus wind speed and fetch length are input variables to this formulation:

$$S_{JONSWAP}(f) = \frac{ag^2}{(2\pi)^4 f^5} \exp\left[-1.25\left(\frac{f}{f_p}\right)^{-4}\right] \gamma^{\exp\left[\frac{\left(\frac{f}{f_p}-1\right)^2}{2\sigma^2}\right]} \quad (2.42)$$

$$\text{where: } f_p = 3.5 \left[\frac{g^2 F}{U_{10}} \right]^{-0.33}, \quad (2.43)$$

$$a = 0.076 \left[\frac{gF}{U_{10}} \right]^{-0.22} \quad (2.44)$$

$1 \leq \gamma \leq 7$, called the peak-shape parameter (with the mean value of 3.3), and

$$\begin{aligned} \sigma &= 0.07, \quad \text{for } f \leq f_p \\ \sigma &= 0.09, \quad \text{for } f > f_p \end{aligned} \quad (2.45)$$

The TMA spectral formulation has been proposed by Bouws et al. [84] as an extension of the JONSWAP spectrum so that it can be applied to wind generated seas in finite water depths, based on the similarity law shown by Kitaigorodskii et al. [85]. The TMA spectral formulation is given by:

$$S_{TMA}(\omega, d) = S_{JONSWAP}(\omega) \Phi(\omega^*, d) \quad (2.46)$$

where $\Phi(\omega^*, d) = \frac{1}{f(\omega^2)^{\frac{1}{2}}} \left[1 + \frac{K}{\sinh K} \right]^{-1}$ is the Kitaigorodskii depth function and

$$\omega^* = \omega \sqrt{\frac{d}{g}}, \quad f(\omega^*) = \tanh^{-1} [k(\omega^*)d], \quad K = 2(\omega^*)^2 f(\omega^*) \quad (2.47)$$

where: k is the wave number.

Directional spectra

Wave spectrum represents energy distributed not only in the range of frequency, but also in the range of direction. This type of spectrum is called the directional wave spectrum $S(f, \theta)$ and can be expressed as the product of the frequency wave spectrum $S(f)$ and the directional spreading function $D(f, \theta)$, where f is the frequency in Hz. The directional spectrum $S(f, \theta)$ is the general form of a wave spectrum, while the frequency spectrum $S(f)$ is the integral of

$S(f, \theta)$ with respect to θ . The term f denotes the frequency and θ is the azimuth measured from some fixed axis of direction. Next, it can be written:

$$S(f, \theta) = S(f)D(\theta | f) \quad (2.48)$$

and

$$\int_{-\pi}^{\pi} D(\theta | f) d\theta = 1 \quad (2.49)$$

Regarding the units of wave spectra, the frequency wave spectrum $S(f)$ has the dimension of m^2s or equivalent units, since it expresses the wave energy density (being divided by the unit weight of water) in the frequency domain. The directional spreading function $D(f|\theta)$ expresses the wave energy density in the directional domain at a specific frequency f , dependent on the wave energy density at that frequency. Thus, the directional spreading function has no dimensions and its integration over the full range of azimuth is set at unity for every frequency.

Estimation of wave directional spreading from data

In order to obtain information on wave directionality, different types of instruments are currently available for measuring the directional characteristics of wave energy in the ocean or in laboratory basins. They can be divided into the following groups, depending on the number and the type of their signals [86]:

(1) gauge arrays: In principle, these probes can be set up at any location of the wave field and may be identical, e.g. surface elevation probes or of various types. However, there are limitations to deploying such arrays in deep water depths, since when instruments are mounted on an offshore fixed structure they should be placed outside the area of influence of the supporting structures. Such a requirement is difficult to achieve, making deployment costly.

(2) single-point devices: They measure simultaneously several wave properties at a single location. The most widely known such device is the heave-pitch-roll buoy, which measures the sea surface elevation (heave) and two orthogonal slopes of sea-surface that produce pitch and roll [87]. An even more sophisticated single-point system is the cloverleaf buoy, which records the sea surface elevation, its slopes in two orthogonal directions and the curvature of the sea surface in these two directions [88].

(3) subsurface instruments: The simplest instruments in this category are high resolution pressure transducers which measure the pressure fluctuations due to the surface waves. Acoustic Doppler current profilers (ADCPs) are used for measurements of ocean currents and waves in coastal environments and can resolve the directional properties of ocean surface waves ([89]; [90]).

(4) remote-sensing systems: These techniques include aerial stereo-photography techniques and microwave radars [91] and allow the measurement of ocean wave fields with both high resolution and large coverage. Topography of the surface has been retrieved, using stereo-photographic data, by observing scenes perpendicular to the still surface, by Shemdin et al. [92], but in their case the observed scales are of limited extent, while those considered in airborne stereoscopy used by Holthuijsen [93] are rather large. Digital photography is now an opportunity to collect quantitative sea surface data more easily. As for the radar wave measurements, their main advantage is that the acquisition of active radar data is independent of daylight and cloud conditions. They are therefore believed to be most suited for operational use, as well as for many ongoing scientific investigations [94].

There have been developed many methods for estimating the wave directional spreading from data. The most commonly acknowledged methods for practical use are the maximum likelihood method, the maximum entropy method and the Bayesian approach method.

Maximum likelihood method (MLM)

This method, introduced by Capon *et al.* [95] in seismic wave detection and then extended by several authors (e.g. [96]; [97]), is based on the assumption that the estimate of directional spreading function $D_{\text{MLM}}(f, \theta)$ may be expressed as a linear combination of the cross spectra:

$$D_{\text{MLM}}(f, \theta) = \frac{1}{E_{\text{MLM}}(f)} \sum_{m,n} a_{mn}(f, \theta) G_{mn}(f) \quad (2.50)$$

where: $E_{MLM}(f)$ is the frequency spectrum estimated by MLM, which is equal to the average of the auto-spectra at each pole, $a_{mn}(f, \theta)$ is a coefficient as a function of frequency and angle of propagation, and $G_{mn}(f)$ is the cross power spectrum between the wave properties of the m-th and the n-th probe.

The MLM estimate $D_{MLM}(f, \theta)$ may be seen as the convolution product of the actual directional spreading function $D(f, \theta)$ by a window function $w(\theta, \theta')$, as described by the following relationship:

$$D_{MLM}(f, \theta) = \int_0^{2\pi} D(f, \theta') w(\theta, \theta') d\theta' \quad (2.51)$$

$$\text{where: } w(\theta, \theta') = \sum_{m,n} a_{mn}(f, \theta) H_m(f, \theta') H_n^*(f, \theta') \quad (2.52)$$

with $H_m(f, \theta') = H_n^*(f, \theta') = 1$ for probes of free surface elevation, as in this case, where $H_m(f, \theta')$, is the transfer function from water surface elevation to the m-th wave property and $H_n^*(f, \theta')$ is the conjugate of the transfer function from water surface elevation to the n-th wave property.

The $D_{MLM}(f, \theta)$ will best approach the actual directional spreading function $D(f, \theta)$, as the window function tends towards a Dirac function $\delta(\theta, \theta')$.

The estimate that best satisfies the previous condition is found to be ([96]):

$$D_{MLM}(f, \theta) = \frac{\kappa}{\sum_{m,n} H_m(f, \theta') \cdot G_{mn}^{-1}(f) H_n^*(f, \theta')} \quad (2.53)$$

In the above expression $G_{mn}^{-1}(f)$, stands for the elements of the inverse of the cross spectral matrix and κ is determined from the condition that the integral of the MLM estimate over $[0, 2\pi]$ should be equal to 1.

Finally, the estimate of the directional wave spectrum is then given by the basic relationship:

$$S_{\text{MLM}}(f, \theta) = D_{\text{MLM}}(f, \theta) E_{\text{MLM}}(f) \quad (2.54)$$

where $S_{\text{MLM}}(f, \theta)$ is the estimate of the directional spectrum.

Maximum entropy method (MEM)

This method is based on the definition of Shannon [98] for entropy χ :

$$\chi = - \int_0^{2\pi} D(f, \theta) \ln(D(f, \theta)) d\theta \quad (2.55)$$

Entropy χ is maximized under certain constraints given by the cross-spectra. The application to single-point systems or gauge arrays was described by Kobune and Hashimoto [99], Nwogu *et al.* [100] and Nwogu [101]. This entropy definition is different from the one used by other authors (e.g. [102]) which generally appears to be less powerful.

Kobune and Hashimoto [99] applied the MEM for estimating directional wave energy spreading from a heave-pitch-roll buoy. In this case, the input data are three timeseries, one corresponding to surface elevation and the other two to orthogonal surface slopes at the probe location. By maximizing the entropy in Equation 2.55, the following estimated spreading function by MEM was derived [10]:

$$D_{\text{MEM}}(f, \theta) = \exp \left[-\lambda_0 - \sum_{j=1}^4 \lambda_j a_j(\theta) \right] \quad (2.56)$$

where:

$$\lambda_0 = \ln \int_0^{2\pi} \exp \left[-\sum_{j=1}^4 \lambda_j a_j(\theta) \right] d\theta \quad (2.57)$$

and the Lagrangian multipliers λ_j , dependent on f and θ , are determined from a Fourier series expansion of the energy spreading function and $a_j(\theta)$ coefficients.

By expressing $D_{\text{MEM}}(f, \theta)$ in terms of Fourier series and applying some constraints in its coefficients the following expression is arrived at:

$$\int_0^{2\pi} [\beta_i - a_i(\theta)] \times \exp \left[-\sum_{j=1}^4 \lambda_j a_j(\theta) \right] d\theta = 0 \quad (2.58)$$

For $i=1,2,3,4$, where the coefficients β_i are written in the form:

$$\beta_i = \int_0^{2\pi} D_{\text{MEM}}(f, \theta) a_i(\theta) d\theta \quad (2.59)$$

The unknown Lagrangian multipliers λ_j in Equation 2.56 can then be obtained after solving Equation 2.57.

Note that if we consider only $j=1$ and 2 , the estimated spreading function coincides with the formula proposed by Borgman [103] and Equation 2.56 becomes then:

$$D_{\text{MEM}}(f, \theta) = \exp[-\lambda_0 - \lambda_1 \cos \theta - \lambda_2 \sin \theta] \quad (2.60)$$

Hence, from here on, the MEM corresponding to $j=1, 2, 3$ and 4 will be denoted as MEM – 4λ , while the MEM corresponding to only $j=1$ and 2 , as MEM – 2λ .

-The approximate technique [86]

At this point, the proposed approximate technique will be described, based on a simple alternative calculation of two orthogonal slopes of surface elevation, which was involved in the MEM [86]. Actually, the whole concept was to estimate the wave properties that a heave-pitch-roll buoy records, using data measured by three surface elevation probes set up at an appropriate location.

It is known that the motion of a rigid body, such as a floating buoy in sea water, has six degrees of freedom: three translations and three rotations. However for this analysis only three of them are required, i.e. heave, pitch and roll (see e.g. [104]). Assume that the curved surface, in Figure 2.20, represents the free sea surface and points (1), (2), (3) are three points that belong to it and form a right angle on a horizontal projection. Therefore, when plane O1'3' coincides with the still water surface, then

$$z(1) = \eta(1),$$

$$z(2) = \eta(2),$$

$$z(3) = \eta(3),$$

where: $\eta(1)$ is the measurement of free sea surface displacement at point (1), etc.

Continuously, the free surface elevation and its two slopes in orthogonal directions, at point (2), can be calculated at any time through the following relations, provided Δx and Δy are small enough quantities:

$$\text{Heave} \quad : \quad \eta(2)$$

$$\text{Pitch} \quad : \quad \frac{\Delta \eta}{\Delta y}(2) = \frac{\eta(3) - \eta(2)}{y(3) - y(2)} = \frac{\eta(3) - \eta(2)}{\Delta y} \quad (2.61)$$

$$\text{Roll} \quad : \quad \frac{\Delta \eta}{\Delta x}(2) = \frac{\eta(1) - \eta(2)}{x(1) - x(2)} = \frac{\eta(1) - \eta(2)}{\Delta x} \quad (2.62)$$

The above relations calculate approximately the wave properties that a heave-pitch-roll buoy delivers, if the distances Δx and Δy are adequately small for the estimation of sea surface's slopes.

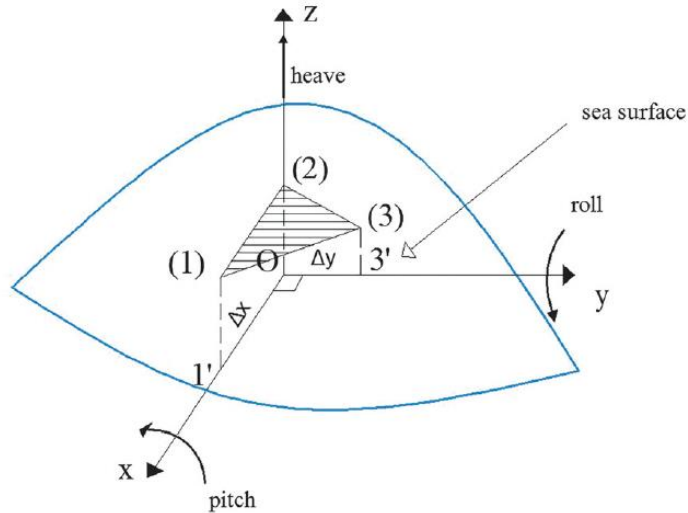


Figure 2.20 An approximate instant depiction of free sea surface [86]

The approximate technique, by using an array of three probes, is close to the concept employed by Benoit and Teisson [105], who, however, used an array of four probes. The said technique employs probes of the same type, i.e. of surface elevation, and requires the minimum number of gauges. Besides, the measurement of the surface elevation is available at the triangle vertex, where the directional spectrum is finally estimated, in contrast to the method with four probes, in which the surface elevation at the point of the final estimation is calculated as an average of the four probes' measurements.

Formulation of the wave energy directional spreading function

A first approach was performed by Pierson et al. [106] who introduced the following directional spreading function, which has often been used for design of marine structures due to its simplicity:

$$D(\theta) = \frac{2}{\pi} \cos^2 \theta, \quad -\frac{\pi}{2} < \theta < \frac{\pi}{2} \quad (2.63)$$

Borgman [103] proposed the following formula which is called the circular normal probability distribution:

$$D(\theta) = \frac{1}{2\pi I_0(a)} \exp[a \cos(\theta - \theta_0)] \quad (2.64)$$

where a is a positive constant, θ_0 is the angle of propagation of the predominant wave energy, and $I_0(\)$ is the modified Bessel function of zero order. This formula agrees with the first approximation of the directional spreading function by Kobune and Hashimoto [99] estimated via Maximum Entropy Method.

Longuet-Higgins et al. [107] proposed that $D(\theta/f)$ is proportional to an even-numbered power of half of the directional angle. That is,

$$D(\theta/f) = \left| \cos\left(\frac{1}{2}(\theta - \bar{\theta})\right) \right|^{2s} G(s) \quad (2.65)$$

where $\bar{\theta}$ is the mean direction of energy spreading estimated via the following relation:

$$\bar{\theta} = \tan^{-1} \frac{\int_{-\pi}^{\pi} S(f) \sin \theta \, d\theta}{\int_{-\pi}^{\pi} S(f) \cos \theta \, d\theta} \quad (2.66)$$

and $G(s)$ is a normalizing factor determined from the condition that the integration of $D(f, \theta)$ from $-\pi$ to π with respect to θ is unity. This yields:

$$G(s) = \frac{2^{2s-1} (\Gamma(s+1))^2}{\pi \Gamma(2s+1)} \quad (2.67)$$

where $\Gamma(\cdot)$ represents the Gamma function.

Thus, Longuet-Higgins et al. [107] showed that the $D(\theta|f)$ can be presented as follows:

$$D(\theta|f) = \left| \cos\left(\frac{1}{2}(\theta - \bar{\theta})\right) \right|^{2s} \frac{2^{2s-1} (\Gamma(s+1))^2}{\pi \Gamma(2s+1)} \quad (2.68)$$

where the parameter s is a positive integer which controls the degree of concentration of energy around the mean value $\bar{\theta}$. In reality, s depends on frequency, wind speed, and fetch length. Mitsuyasu et al. [88] carried out further analysis for evaluating the value of s and proposed the frequency dependency of the spread parameter s as follows:

$$s = \begin{cases} s_{\max} (f/f_p)^5 & : f \leq f_p \\ s_{\max} (f/f_p)^{-2.5} & : f > f_p \end{cases} \quad (2.69)$$

where f_p is the peak spectral frequency.

Mitsuyasu et al. [88] formulated the maximum value of spreading parameter s_{\max} as a function of the state of wind-wave growth. Goda and Suzuki [108] proposed values of s_{\max} equal to 10, 25 and 75 for wind waves, swell with short decay distance, and swell with long decay distance, respectively. The proposed s_{\max} values are still employed in many case studies.

From analysis of measured data, Hasselmann et al. [109] propose the same formula given in Eq. 2.69, but the s value in this equation is substituted by s_I -value written as below:

$$s_1 = \begin{cases} (9.77 \pm 0.43) (f / f_m)^{-(2.33 \pm 0.06) - (1.45 \pm 0.45)(U/c_m - 1.17)} & , \text{ for } U \geq c_m \text{ and } f > f_m \\ (6.97 \pm 0.83)(f / f_m)^{4.06 \pm 0.22} & , \text{ for } U \geq c_m \text{ and } f > f_m \end{cases} \quad (2.70)$$

where: U is the wind speed, c_m is the wave celerity at the modal frequency f_m . The s_1 -value by Hasselmann et al. [109] derived from an extensive analysis of directional data obtained in the North Sea (JONSWAP site).

Wave spectrum parameters

By assuming that a wave spectrum is narrow-banded, and therefore obeys the Rayleigh probability distribution (Longuet-Higgins [110], [111], [24]), its n -th moment is estimated as the integral over frequency of the spectral density function multiplied by the n -th power of the frequency, either expressed in hertz (cycles per second) as:

$$m_n(f) = \int_0^{\infty} f^n S(f) df \quad (2.71)$$

or expressed in circular frequency (radians/second) as:

$$m_n(\omega) = \int_0^{\infty} \omega^n S(\omega) d\omega \quad (2.72)$$

where $n=0, 1, 2, 3, \dots$

Since $\omega = 2\pi f$, the relationship between the two moment expressions is:

$$m_n(\omega) = (2\pi)^n m_n(f) \quad (2.73)$$

Using this definition, the spectral significant wave height for a Rayleigh distribution [110]

may be approximated by:

$$H_{m_0} \approx 4\sqrt{m_0} \quad (2.74)$$

The period associated to the largest energy per frequency is known as the spectral peak wave period T_p and the mean period T_m and energy period T_e can be approximated by:

$$T_m = \frac{m_0}{m_1} \quad (2.75)$$

$$T_e = \frac{m_{-1}}{m_0} \quad (2.76)$$

An approximation of zero-crossing mean wave period is estimated by:

$$T_z = \sqrt{\frac{m_0}{m_2}} \quad (2.77)$$

Two parameters are frequently used concerning the spectral bandwidth, ν and ε . Both of them range from 0 to 1. When these parameters tend to zero, i.e. $\nu \ll 1$ and $\varepsilon \ll 1$, the wave spectra are narrow-banded, while if they tend to unity, the spectra are broad-banded. The spectral band width parameters can be approximated by spectral moments by:

$$\nu = \sqrt{\frac{m_0 m_2}{m_1^2} - 1} \quad (2.78)$$

$$\varepsilon = \sqrt{1 - \frac{m_2^2}{m_0 m_4}} \quad (2.79)$$

2.4.1.2 Wave parameters from time-domain analysis of a wave record

Wind-generated sea waves are essentially random in time and space. Heights and periods of individual waves in a short time span, which can represent a sea state, vary randomly over

wide ranges. It is necessary to define individual waves with some criterion and calculate characteristic individual wave heights and periods in a statistical manner in the time domain analysis. The zero-upcrossing or zero-downcrossing method is the standard technique to define individual waves, in which the two successive upcrossing or downcrossing points of the wave surface profile with the mean water level (zero-level) mark the start and the end of one individual wave, respectively. The significant wave height determined from this analysis is the mean value of the highest one-third waves denoted by $H_{1/3}$. Besides, other characteristic wave heights can be determined from the same analysis, e.g. $H_{1/10}$ and $H_{2\%}$ etc.

Except for characteristic wave height, other characteristic wave parameters are also used to describe a sea state. These parameters are usually the mean wave period T_m and the principal wave direction θ_m , defined as the mean value of individual wave periods and azimuths measured from some fixed axis of direction within a sea state, respectively.

It is noted that there is not a unique definition of wave period; it can be defined as the time interval between either two neighboring wave crests or troughs. Another common definition of wave period is the time interval between successive upcrossing points, or downcrossing points, of the wave surface profile with mean water level, called as zero up-crossing period, or zero down-crossing period, respectively.

Both zero-upcrossing and zero-downcrossing methods yield similar mean values of wave parameters [1]. There seems to be some preference for zero-downcrossing method [112], since it has been suggested that its definition of wave height, as the vertical distance from a wave trough to wave crest, may be better suited for extreme waves.

As it is aforementioned, the analysis of individual waves from a wave record is generally made for a short time span of twenty minutes or so. Furthermore, the length of the time span is also determined by the Fourier transforms which will then be made on the raw recordings for the production of the spectrum. Also, it is chosen in order that the requirement of a short duration, to guarantee the constancy of sea state during the recording time period, and that of a long duration, to have a sufficient number of waves necessary for reliable estimates of significant wave height and other characteristic wave parameters, be met at the same time.

The statistical analysis of individual waves within a sea state provides information on short-term wave statistics, while the statistical analysis of sea states covering a period of some decades yields the long-term description of wave conditions at a particular site, called the long-term wave climate.

As for short-term wave statistics, since the individual waves within a sea state are extracted from the time-domain analysis of a wave record, the probability distribution or probability density function (pdf) of wave parameters can be estimated. The pdf f_X of a random variable X is most commonly associated with an absolutely continuous univariate distribution, and it applies:

$$\Pr(a \leq X \leq b) = \int_a^b f_X(x) dx \quad (2.80)$$

Hence, if F_X is the cumulative distribution of X (cdf), then

$$F_X(x) = \int_{-\infty}^x f_X(u) du \quad (2.81)$$

and if f_X is continuous at x :

$$f_X(x) = \frac{dF_X(x)}{dx} \quad (2.82)$$

In simple words, the term $f_X(x)dx$ can be considered as the probability of X within this interval of dx .

The most commonly used probability distribution in the study of random ocean waves are the Gaussian (see Figure 2.21) and Rayleigh (see Figure 2.22) distributions suited for describing the short-term statistics of surface elevation and wave height, respectively, mainly in deep waters. It is noted that the Rayleigh distribution satisfies the condition of narrow band spectra, but seems to represent wave height satisfactory also for non narrow spectra. The Gaussian pdf is defined as:

$$p(x) = \frac{1}{\sigma_x \sqrt{2\pi}} e^{-\left(\frac{(x-\mu_x)^2}{2\sigma_x^2}\right)} \quad (2.83)$$

where μ_x is the mean of x and σ_x the standard deviation. As it is aforementioned, the Gaussian cumulative distribution $P(x)$ is the integral of $p(x)$. Since a closed form of this interval is not possible, Gaussian distribution is often considered as the normal distribution (e.g. [113]) written as:

$$p(x) = N(\mu_x, \sigma_x) \quad (2.84)$$

and

$$P(x) = \Phi\left(\frac{x - \mu_x}{\sigma_x}\right) \quad (2.85)$$

For zero mean and unit standard deviation, the Gaussian pdf and cdf reduces to standard normal pdf $p(x)$ and cdf $\Phi(x)$, respectively, written as below:

$$p(x) = \frac{1}{\sqrt{2\pi}} e^{-\left(\frac{x^2}{2}\right)} \quad (2.86)$$

$$\Phi(x) = \int_0^x p(y) dy \quad (2.87)$$

where the last integral is the *error function*.

- Wave height distribution

In engineering practice, the main interest is attracted by the wave height distribution rather than the surface elevation. Continuously, if wave energy is concentrated in a very narrow range of wave frequencies (or periods), and therefore the maxima of the wave profile coincide with wave crests and the minima with the troughs (this is termed a narrow-band condition), wave heights could be represented by the following Rayleigh distribution ([110]; [22]; [24]). The Rayleigh pdf and cdf are presented in Eqs 2.88 and 2.89:

$$p(H) = \frac{2H}{H_{rms}^2} e^{-\left(\frac{H^2}{H_{rms}^2}\right)} \quad (2.88)$$

$$P(H) = 1 - e^{-\left(\frac{H^2}{H_{rms}^2}\right)} \quad (2.89)$$

where:

$$H_{rms} = \sqrt{\frac{1}{N} \sum_{i=1}^N H_i^2} \quad (2.90)$$

in which H_i is the ordered individual wave heights in a wave record.

Various estimates of characteristic wave heights may then be obtained [1]:

$$\begin{aligned} H_{1/3} &\approx 4.00\sqrt{m_0} = 1.416H_{rms} \\ H_{1/10} &= 1.27H_{1/3} = 1.80H_{rms} = 5.091\sqrt{m_0} \\ H_{1/100} &= 1.67H_{1/3} = 2.36H_{rms} = 6.672\sqrt{m_0} \\ H_{\max} &= 1.86H_{1/3} \quad (\text{for } 1000 \text{ wave cycles in the record}) \end{aligned} \quad (2.91)$$

where: m_0 is the zero moment of wave spectrum.

The most probable maximum wave height related to H_{rms} assuming N waves in a wave record is estimated [110] by:

$$H_{max} = \left[\sqrt{\log N} + \frac{0.2886}{\sqrt{\log N}} - \frac{0.247}{(\log N)^{3/2}} \right] H_{rms} \quad (2.92)$$

It has been observed that deep wave height measurements from different oceans closely follow a Rayleigh distribution ([114]; [115]; [116]; [117]). However, studies of shallow-water wave records indicate the wave height histograms at these depths deviate from the Rayleigh, and other distributions seem to follow them better [118]; [119]; [120]. This is attributed to the bathymetric effects combined with non-linear wave-wave interactions that play a significant role in shallow-water depths.

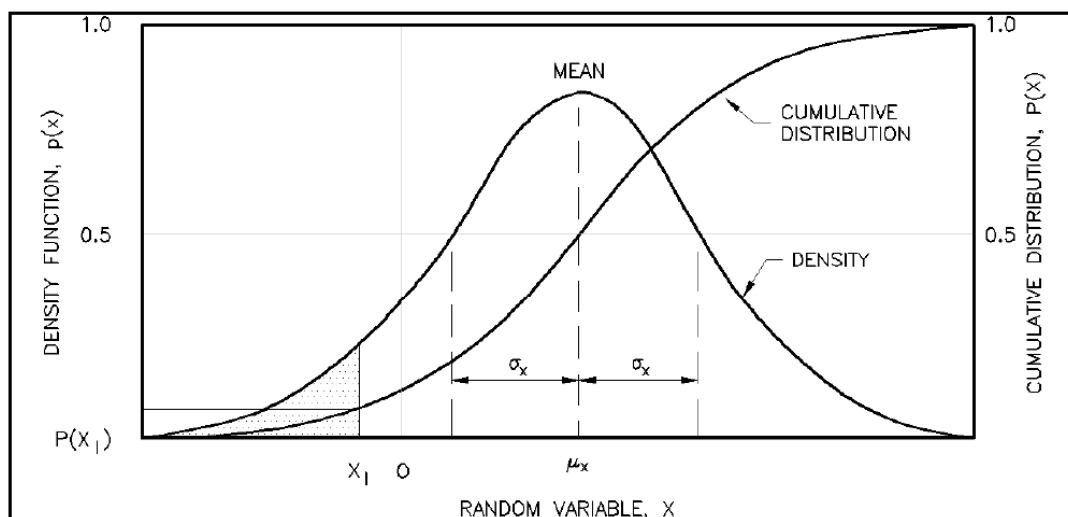


Figure 2.21 The Gaussian probability density function and cumulative distribution [1]

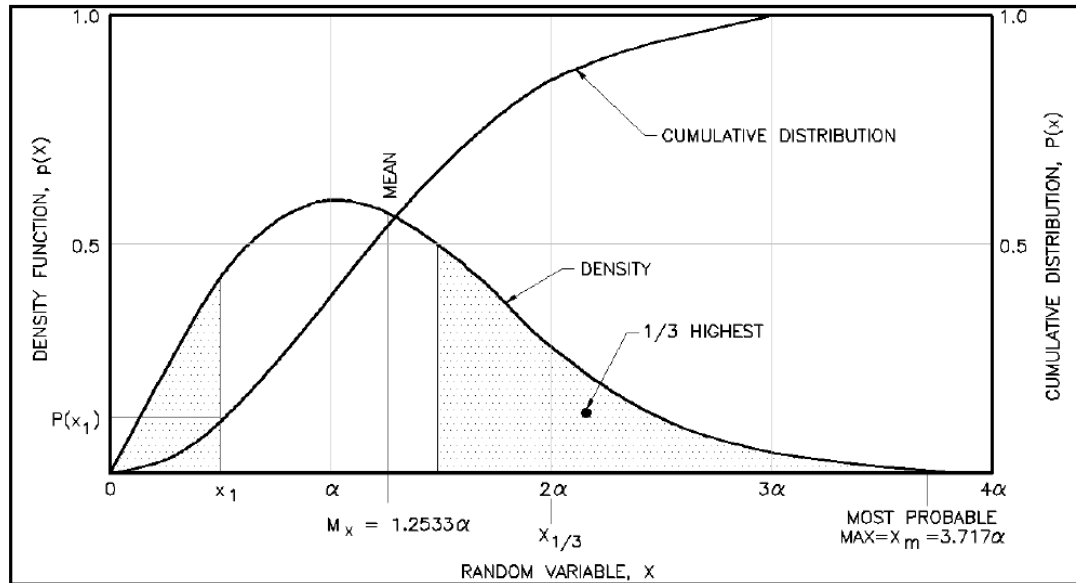


Figure 2.22 The Rayleigh probability density function and cumulative distribution [1]

- Wave period distribution

Longuet-Higgins [121] and Bretschneider [122] derived the probabilistic distribution of wave period assuming that the wave period squared follows a Rayleigh distribution. This distribution is very similar to the normal distribution with a mean period by:

$$T_{0,1} = \frac{m_0}{m_1} \quad (2.93)$$

where the moments are defined in terms of cyclic frequency.

The probability density function of wave period according to Longuet-Higgins [121] is given by:

$$p(\tau) = \frac{1}{2(1+\tau^2)^{3/2}} \quad (2.94)$$

where $\tau = \frac{T - T_{0,1}}{\nu T_{0,1}}$ and ν is the spectral width parameter, which will be defined later. This pdf is symmetric about its maximum value at $\tau = 0$, and is similar to the normal distribution with a mean value equal to $T_{0,1}$. In general, the distribution for wave period is narrower than that of wave height and its spread lies mainly in the range of 0.5 to 2.0 times the mean wave period [1].

According to Bretschneider [122], the pdf of wave period is given by:

$$p(\tau) = 2.7 \frac{T^3}{T_m} e^{(-0.675\tau^4)} \quad (2.95)$$

where: $\tau = \frac{T}{T_m}$ and T_m is the mean wave period.

- Joint distribution of wave height and period

Since wave height H and period T are somehow correlated, the following relation that estimates their joint pdf using only the marginal pdfs of H and T is inappropriate for ocean waves:

$$p(H, T) = p(H)p(T) \quad (2.96)$$

Specifically, as far as the short-term joint distribution of wave height H and period T is concerned, Longuet-Higgins [22] was the first to introduce a probabilistic representation of sea waves, by extending the work of Rice [23] on electronic noise, and was able to calculate the joint pdf of H and T for narrow band spectrum. However, a disadvantage of that model was the symmetry of the joint pdf of H and T around some characteristic period, suggesting in this way a zero statistical correlation between the two parameters. Thus, Longuet-Higgins [24] considered the tendency that short-period waves have low heights, whereas high waves tend to be associated to longer periods, as it is observed in real sea states.

Particularly, assuming waves to be a Gaussian and a narrow-band random process, whose spectrum is concentrated in the vicinity of the mean frequency, the dimensionless joint pdf of wave amplitude and period is written by:

$$f(\xi, \eta) = L \frac{1}{v\sqrt{2\pi}} \left(\frac{\xi}{\eta}\right)^2 \exp\left\{-\frac{\xi^2}{2} \left[1 + \left(1 - \frac{1}{\eta}\right)^2 \frac{1}{v^2}\right]\right\} \quad (2.97)$$

where:

$\xi = \rho / \sqrt{m_0}$ is the dimensionless amplitude

$\eta = T / T_m$ is the dimensionless wave period

$T_m = 2\pi / \bar{\omega} = 2\pi m_0 / m_1$ is the mean wave period

$$v = \sqrt{\frac{m_0 m_2}{m_1^2} - 1}$$

and $L = 1 + \frac{v^2}{4}$ is a normalization required so that the integration of joint pdf over the entire sample becomes unity.

Thus, the previous expression can be rewritten by:

$$f(\xi, \eta) = \left(1 + \frac{v^2}{4}\right) \frac{1}{v\sqrt{2\pi}} \left(\frac{\xi}{\eta}\right)^2 \exp\left\{-\frac{\xi^2}{2} \left[1 + \left(1 - \frac{1}{\eta}\right)^2 \frac{1}{v^2}\right]\right\} \quad (2.98)$$

where $0 < \xi < \infty$ and $0 < \eta < \infty$.

It is noted that the original expression differs slightly from the above expression. The first is given below by defining the dimensionless wave amplitude as $r = \rho / \sqrt{2m_0}$:

$$f(r, \eta) = \left(1 + \frac{v^2}{4}\right) \frac{2}{v\sqrt{\pi}} \left(\frac{r}{\eta}\right)^2 \exp\left\{-\frac{r^2}{2} \left[1 + \left(1 - \frac{1}{\eta}\right)^2 \frac{1}{v^2}\right]\right\} \quad (2.99)$$

where $0 < r < \infty$ and $0 < \eta < \infty$.

In Figure 2.23, the contours of dimensionless joint probability density function of wave amplitude and period for $v=0.3$ and $v=0.4$. The results by Longuet-Higgins [24] showed good agreement with field data provided the spectrum is narrow banded and has a single peak [123]. Other researchers who studied the joint pdf of H and T by considering also narrow band spectra were Cavanié et al. [25], Lindgren and Rychlik [26], and Shum and Melville [27]. Besides, most of the researchers make the definition of wave period by the successive maxima and not on the basis of zero up- or down-crossing of surface elevation. The latter has broad application in engineering practice.

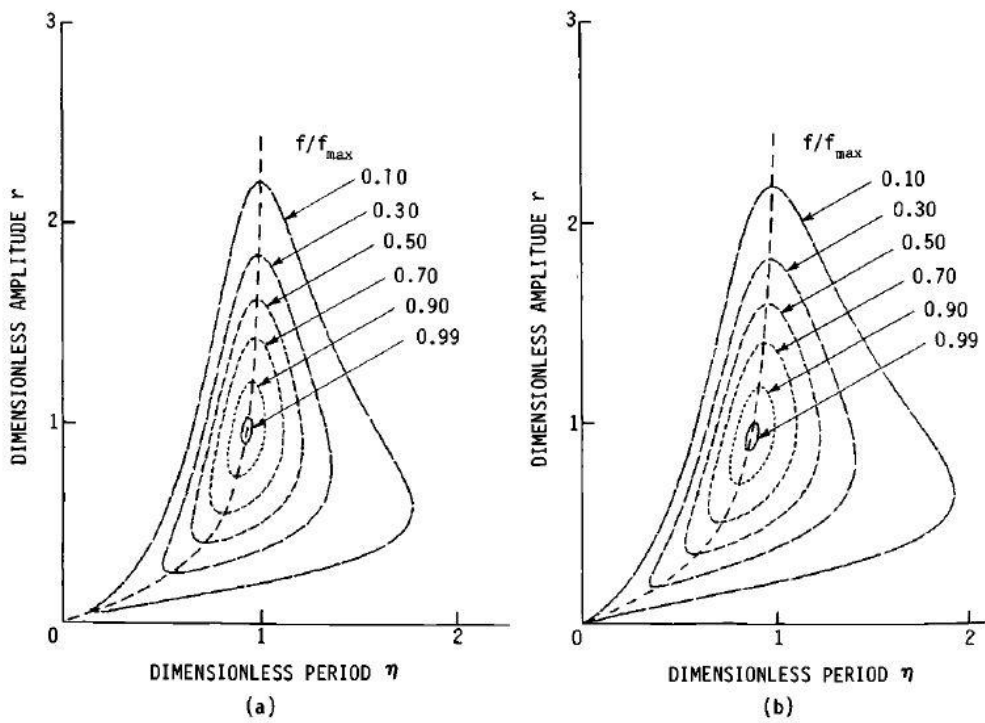


Figure 2.23 Contours of dimensionless joint probability density function of wave amplitude and period for (a) $v=0.3$ and (b) $v=0.4$ [24]

However, Memos [28] reviewed the existing results and proposed theoretical approximations, valid also for narrow and broad band spectra, known to be a better representation of real sea states than those assuming only narrow band spectra, and used the definition of wave period

based on zero-crossing of surface elevation. Particularly, Memos and Tzanis [29], based on the theoretical approach by Memos [28], produced numerical results of the short-term joint distribution of H and T for deep water waves of any spectral bandwidth, based on the assumptions of ergodicity and normal distribution of free surface elevation. Their joint pdf was deduced for various correlation coefficients of H and T , denoted by $r(H,T)$, providing characteristic probabilistic estimates in deep waters. Memos and Tzanis [30] extended their previous work by excluding swell from sea waves and the application of a wave breaking criterion in deep waters. The parameters that describe their methodology were the correlation coefficient between H and T , or the standard deviation of free surface elevation, and the representative wave steepness factor.

Table 2.3 contains indicative values of mean wave height H_m , associated with the standard deviation of sea surface elevation, σ_η , and the linear correlation coefficient $r(H,T)$ [31]. Moreover, indicatively, three graphs derived from the methodology by Memos and Tzanis [30] and Tzanis [31] are presented in Figure 2.24.

Table 2.3 Various sea states associated with specific values of σ_η , $r(H,T)$ and H_m [31]

Standard Deviation σ_η	Correlation Coefficient $r(H,T)$	Mean Wave Height H_m
0.5m	0.266	1.020m
0.6m	0.383	1.103m
0.7m	0.485	1.266m
1.0m	0.495	2.187m
1.5m	0.570	3.755m

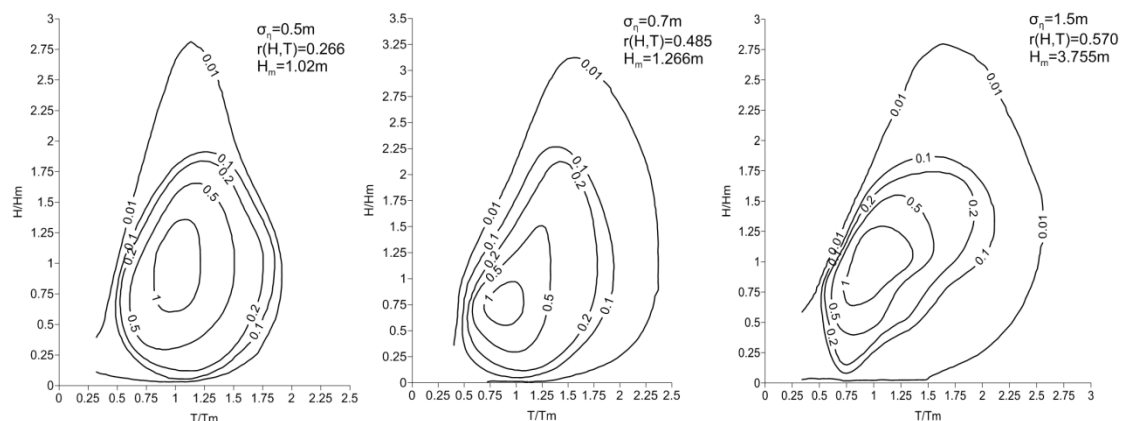


Figure 2.24 Joint pdfs of H/H_m and T/T_m in deep waters associated with specific values of standard deviation σ_η or correlation coefficient $r(H,T)$ ([31]; [30])

A detailed review concerning the wave parameters probabilistic distributions was made by Soares [124]. Improvement of Longuet-Higgins [24] Gaussian models was made by Stansell et al. [125] by proposing some new marginal and joint pdfs of wave envelope and local wave period. Furthermore, Zhang et al. [126] investigated the differences between marginal and joint pdf of wave parameters produced by the linear theoretical model by Longuet-Higgins [24] and the empirical ones, derived from waves produced in wave basins.

- Probabilistic wave parameters in shallow waters

In shallow waters, the solid boundary of the sea bottom plays a significant role in wave transformations, such as wave refraction, shoaling, breaking, and wave-wave interactions that make the estimation of wave parameters probabilistic distributions more complicated than in deep waters.

As far as the probabilistic distribution of wave height in shallow waters is concerned, Collins [127], Mase and Iwagaki [128], and Dally and Dean [129] proposed a method for estimating this distribution by applying a monochromatic individual wave model for shoaling and breaking. Dally [130]; [131] and Kuriyama [132] also contributed to this approach. Glukhovskiy [133] and Klopman [134] proposed a pdf for wave heights that considers the impact of depth-limited wave breaking on the distribution, by making the exponent of the Rayleigh distribution an increasing function of the ratio of wave height towards the water depth.

Battjes and Groenendijk [135] derived wave probabilistic distributions on shallow foreshores by analyzing laboratory data and proposed generalized empirical parameterizations as a function of local energy, water depth and bottom slope. Myrhaug and Fouques [136] provided a joint distribution of wave height and surf similarity parameter (or else Iribarren number) for individual waves within a sea state via the use of the joint pdf of wave height and wave steepness by Myrhaug and Kjeldsen [137] representing Norwegian continental shelf data.

Regarding the joint pdf of wave height and period in intermediate and shallow waters, Chondros and Memos [32] extended the work of Memos and Tzani [30] concerning the joint pdf of H and T , by taking into account the nonlinear wave-wave interactions, and produced characteristic images of joint pdf of H and T in shallow waters for various storm intensities, wave incidence, and bed slopes, by using a Boussinesq wave propagation model [7]. It is

noted that in their method [32], wave directionality in deep waters was also considered [138] via the use of a theoretical expression of wave directional spreading, and the joint pdf of H , T , and wave direction θ in deep waters were transformed into time series of surface elevation, in order that the Boussinesq wave propagation model be implemented.

2.4.2 Marine water level

Marine water level is important since:

- most instances of coastal flooding and/or coastal structures' damage occur during high water levels
- wave transmission and wave overtopping on marine and coastal structures depend on the Still Water Level (SWL)
- a coastal area or a structure may be exposed to different risks of vulnerability depending on SWL
- wave conditions also depend on SWL since wave height is limited in a different way by different water depths.
- wave forces upon coastal structures are usually affected by SWL
- the overall water level regime affects coastal structures' construction and maintenance.

The existing water level consists of different components, which should be considered during a structure's design process. Apart from the astronomical forcing (i.e. tide), rare seismic forcing (i.e. tsunami), there are also several meteorological effects, causing water level variations to be considered. The latter consist of storm surge, wind set-up, wave set-up etc.

Besides, sea level rise due to climate change affects SWL at a long-term level, and should also be considered especially when a coastal structure lifetime is significantly large.

Usually, the most important components of water level at any moment are the astronomical tide and the storm surge [55]. The former is cyclical with a period that depends on the relative significance of astronomical forces at a particular location (e.g. along the Atlantic European coasts tide lasts 12 hr and 26 min on average) and the latter occurs randomly, as an individual event with duration of approximately half a day to one day, peaking about mid-way [55].

The variation with time of water level due to astronomical tide and storm surge is depicted in Figure 2.25.

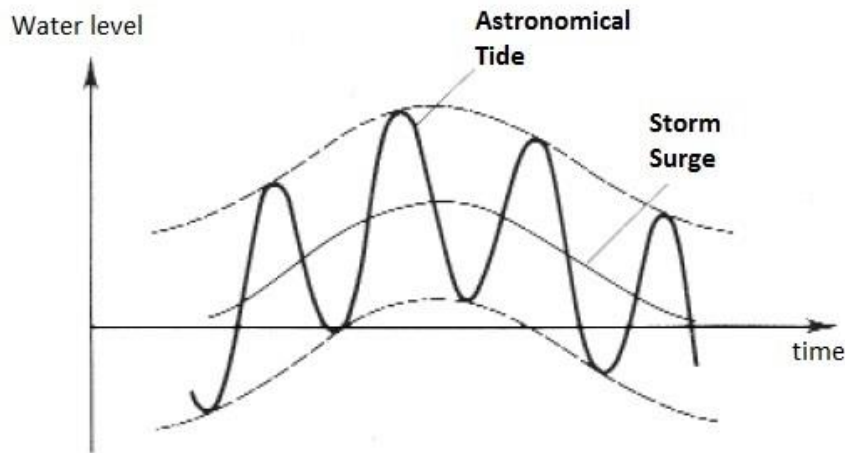


Figure 2.25 Variation with time of water level due to astronomical tide and storm surge [55]

2.4.2.1 Mean sea level

For coastal waters open to the open sea, the mean water level can be taken as a site-specific constant related to the mean sea level (MSL) of the oceans. For example, in some areas, like the eastern Mediterranean Sea, the MSL varies slightly, according to the time of the year, in a more or less predictable manner. Specifically, sea level changes vary between 0.05 m and 0.15 m, whereas in the rest of the Mediterranean Sea differences up to 0.30 m may be observed in some locations [55].

2.4.2.2 Tidal sea level variations

Tides are mainly generated by the gravitational attractions of the Moon and Sun, which are proportional to their masses and the inverse square of their distances from the Earth. Despite that the mass of the moon is much smaller than the Sun, the moon is closer to the earth; consequently it has a greater impact on tides compared against the Sun. Besides, near full moon and new moon, the Sun and Moon act in the same direction giving thus higher tides, i.e. spring tides.

The orbits of the Moon around the Earth and of the Earth around the Sun are not circular. Therefore, tides appear seasonal variations, and obtain their maximum amplitude of the year at the spring and autumn equinoxes, i.e. when the Sun crosses the equator and night and day are everywhere of equal duration [55]. Minor variations also occur during an 18.6 year period due to the variable angular disposition of the Sun and the Moon. This time period is, in

the vast majority of coastal structures, well below the design service life of the structures. Hence, this variable is not included in the environmental factors that influence the modification of the failure occurrence with time.

As it is aforementioned, the driving forces of tides are astronomical. This means that tide is entirely predictable, or otherwise that the tidal ranges and currents prediction is deterministic. Continuously, it must be noted that tides belong to long waves and they are amplified in shallow waters and estuaries due to resonance phenomena and shoaling effects. Specifically, the tidal range, which is equal to twice the tidal amplitude, is generally less than a meter in the open ocean and may increase considerably in shallow water areas, i.e. the continental shelf. Large tidal amplifications are observed, e.g. in bays along the coasts of England and Wales (spring tidal range of up to 12 m), in the bay of Fundy, Canada (spring tidal range of up to 13 m), and around Saint-Malo in Normandy, France (spring tidal range of up to 14 m), whereas a 3-4 m spring tidal range is common in the southern North Sea [55].

Besides, Coriolis' force plays a significant role in explaining the large tidal ranges differences between different locations. Particularly tide amplitude is zero at amphidromic points (i.e. the further away from the amphidromic point, the higher the tide will be) and tidal wave propagates around amphidromic points counter-clockwise in the northern hemisphere, while the tidal circulation in the southern hemispheres of the oceanic basins occurs clockwise.

2.4.2.3 Storm surge

Meteorological forces, namely atmospheric pressure and wind, may also affect sea level during storms. This section focuses on atmospheric pressure effects, because the wind driven effects on sea level (i.e. wind set-up) are described in the following section.

Sea level varies depending also on the weather conditions. Pressure and wind effects are often combined during storms generating long waves, called storm surges, with a characteristic time-scale of several hours to one day and a wavelength that varies between 150 and 800 km [55]. In practice, the storm tide level term is used to include the astronomical tide (see Figures 2.26, 2.27) and often and other meteorological effects.

Continuously, atmospheric pressure has a direct influence on the sea level. Specifically, high atmospheric pressure exerts a force on the surroundings and results in water movement, i.e. high atmospheric pressure over a sea area corresponds to low sea level and conversely low

atmospheric pressure (a depression) results in higher sea levels. This is called the inverse barometer effect [139].

The atmospheric pressure is 1013.25 hPa in normal conditions. Since atmospheric pressure normally varies between 950 hPa and 1050 hPa during a year and a deviation of 1 hPa in atmospheric pressure results in change in water level by approximately 1cm, the expected variation in sea level due to air pressure is between +63 cm and -37 cm around mean sea level. This atmospheric pressure effect on sea level is described by the following formula:

$$\Delta P = \Delta h \rho g \quad (2.100)$$

where: ΔP represents atmospheric pressure difference from normal conditions (i.e. 1013.25 hPa), Δh is the corresponding change of seawater level due to pressure, ρ is the density of seawater, and g is the gravity acceleration.

In accordance to tidal long waves, the height of long waves caused by storm surges may increase considerably as a result of amplifications due to shoaling in the nearshore zones.

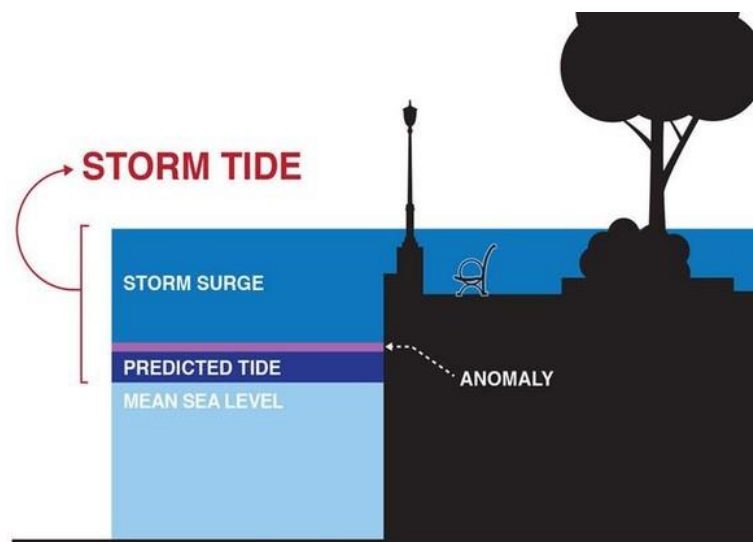


Figure 2.26 Water level differences for storm surge, storm tide, and a normal (predicted) high tide compared to mean sea level

(https://www.al.com/news/index.ssf/2018/09/hurricane_florence_storm_surge.html)

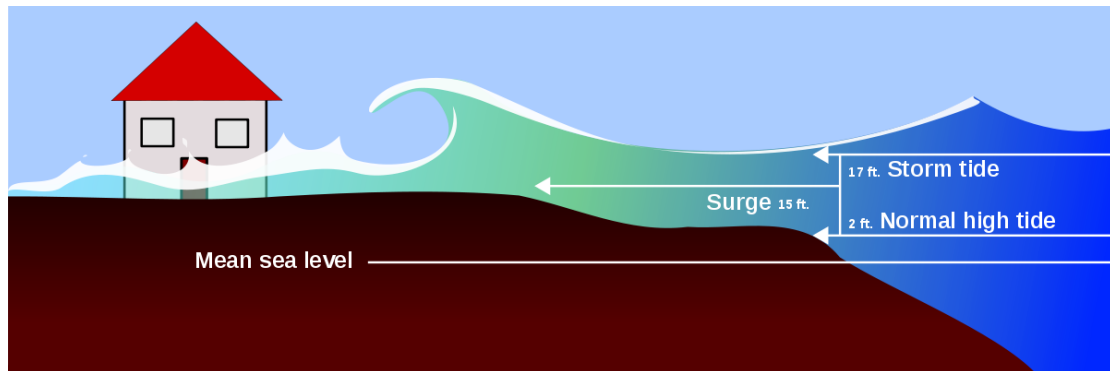


Figure 2.27 Storm tide and its components

(https://en.wiktionary.org/wiki/storm_tide)

2.4.2.4 Wind set-up

Shear stress exerted by wind on seawater surface causes a slope in the water surface (see Figure 2.28) and consequently wind set-up and set-down occur at downwind and upwind boundaries [55].

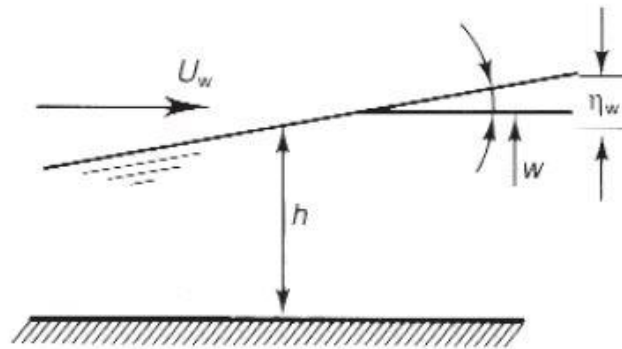


Figure 2.28 Wind set-up [55]

The long wave equations can be used to describe the change in seawater level induced by wind blowing over bodies of water such as a continental shelf [140] or a lake. Although the wind stress is usually very small, its effect, when integrated over a large body of water, can be significantly increased.

The wind stress acting on the water surface is represented as:

$$\tau_w = \rho k \mathbf{W} |\mathbf{W}| \quad (2.101)$$

where: ρ is the mass density of water, \mathbf{W} the wind speed vector at a reference elevation of 10 m, and k is a friction of order 10^{-6} . Numerous studies have been made for k (see [141]) and one of the more widely used sets of results is that of Van Dorn [142]:

$$k = \begin{cases} 1.2 \times 10^{-6}, & |\mathbf{W}| \leq W_c \\ 1.2 \times 10^{-6} + 2.25 \times 10^{-6} \left(1 - \frac{W_c}{|\mathbf{W}|}\right), & |\mathbf{W}| > W_c \end{cases} \quad (2.102)$$

where $W_c = 5.6$ m/s.

For a bottom profile with straight and parallel bottom contours, and the wind blows at an angle θ to the coast normal (see Figure 2.29), then the offshore wind shear stress is $\tau_{w_x} = |\tau_w| \cos \theta$. The wind-induced gradient of the still water surface, along the x-axis (taken normal to the shoreline) can be computed via the following Equation:

$$\frac{\partial \eta}{\partial x} = \frac{n}{\rho g (h + \eta)} \tau_{w_x} \quad (2.103)$$

The factor n lumps the effect of the bottom friction in the wind shear stress. This factor is greater than 1, and typical values are 1.15 to 1.30 [118].

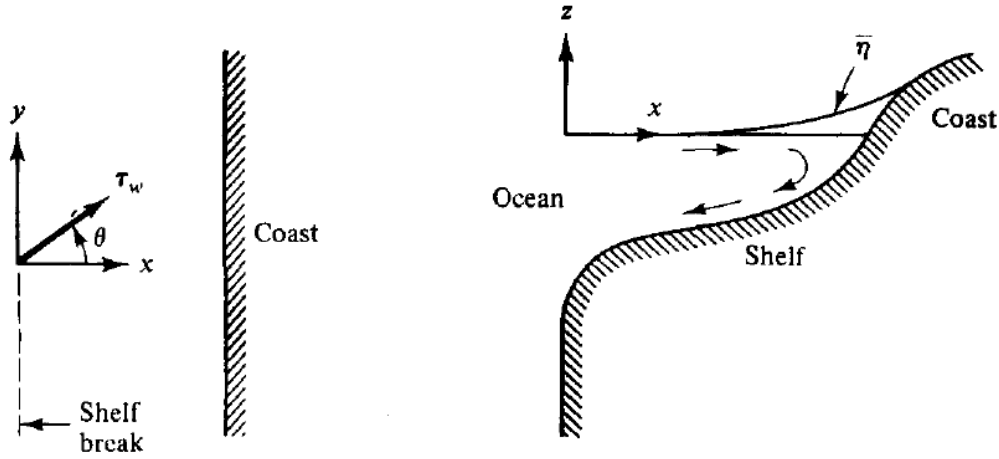


Figure 2.29 Plan (left) and cross-sectional view of the coast [143]

Two examples of bottom profiles are presented below aiming at calculating the wind set-up due to a constant and uniform wind (τ_{w_x} is not a function of x) blowing over a continental shelf of width l . The first case (a) is that of a constant depth, h_o and the second one (b) is that

h is a linear function of x : $h = h_o \left(1 - \frac{x}{l}\right)$.

(a) The governing equation (Eq. 2.104) can be written as:

$$(h + \eta) \frac{\partial \eta}{\partial x} = \frac{n \tau_{w_x}}{\rho g} \quad (2.104)$$

Since h is not a function of x , solving of Eq. 2.105 through integration gives:

$$(h + \eta)^2 = \frac{2n \tau_{w_x} x}{\rho g} + C \quad (2.105)$$

To evaluate the constant C of the integration, the wind set-up is assumed to be zero in deep waters, i.e. at $x=0$. Thus, after substitution for C , Eq. 2.106 is written as:

$$(h + \eta)^2 = \frac{2n\tau_{w_x} x}{\rho g} + h_o^2 \quad (2.106)$$

or

$$\eta(x) = +\sqrt{\frac{2n\tau_{w_x} x}{\rho g} + h_o^2} - h_o \quad (2.107)$$

and in dimensionless form:

$$\frac{\eta(x)}{h_o} = +\sqrt{1 + \frac{2Ax}{l}} - 1 \quad (2.108)$$

where $A = \frac{n\tau_{w_x} l}{\rho g h_o^2}$ a ratio of shear to hydrostatic forces [143].

(b) For a plane sloping bottom, the governing Eq. 2.104 can be rewritten as:

$$(h + \eta) \frac{\partial(h + \eta)}{\partial x} - (h + \eta) \frac{dh}{dx} = \frac{n\tau_{w_x}}{\rho g} \quad (2.109)$$

Separation of variables and evaluating C as before leads to:

$$x = l \left[\left(1 - \frac{h + \eta}{h_o} \right) - A \ln \left(\frac{\frac{h + \eta}{h_o} - A}{1 - A} \right) \right] \quad (2.110)$$

or in dimensionless form:

$$\frac{x}{l} = \left(1 - \frac{h + \eta}{h_o}\right) - A \ln \left(\frac{\frac{h + \eta}{h_o} - A}{1 - A} \right) \quad (2.111)$$

These two solutions (Equations 2.109 & 2.112) are plotted in Figure 2.30 showing the effect of the bottom to the wind set-up. It is clear from both equations and Figure 2.33 that the sloping bottom causes an increase in the wind set-up compared against the flat bottom. Particularly, the governing Eq. 2.104 indicates that for a given wind stress, the water surface slope depends on the local water depth in such a way that the water surface slope is greater in shallower waters.

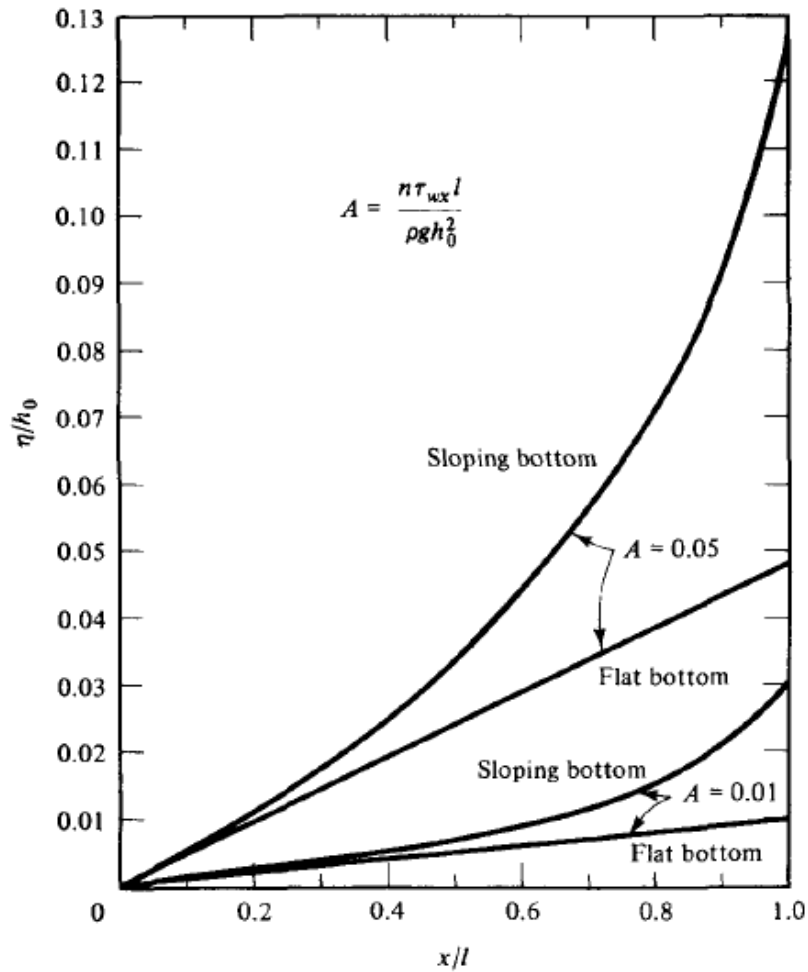


Figure 2.30 Dimensionless wind set-up surge versus dimensionless distance of a continental shelf for two cases of dimensionless wind shear stress [143]

2.4.2.5 Wave set-up

Wave set-up is mainly caused by energy dissipation caused by water depth-induced breaking of incoming waves (see Figure 2.31) and is localized near the shoreline. For a plane sloping bottom (straight and parallel contours), regarding 1D situation, the gradient of the wave set-up η (m) along the x axis (taken normal to the shoreline) can be computed via the following equation:

$$\frac{\partial \eta}{\partial x} = -\frac{1}{\rho g (h + \eta)} \frac{\partial S_{xx}}{\partial x} \quad (2.112)$$

where S_{xx} (N/m) is the component of the radiation stress tensor normal to the coast which is estimated considering the linear wave theory as below:

$$S_{xx} = \frac{1}{8} \rho g H^2 \left[\frac{1}{2} + \frac{2kd}{\sinh(2kd)} \right] \quad (2.113)$$

where H is the wave height, k is the corresponding wave number (rad/m), and $d = h + \eta$ is the actual water depth.

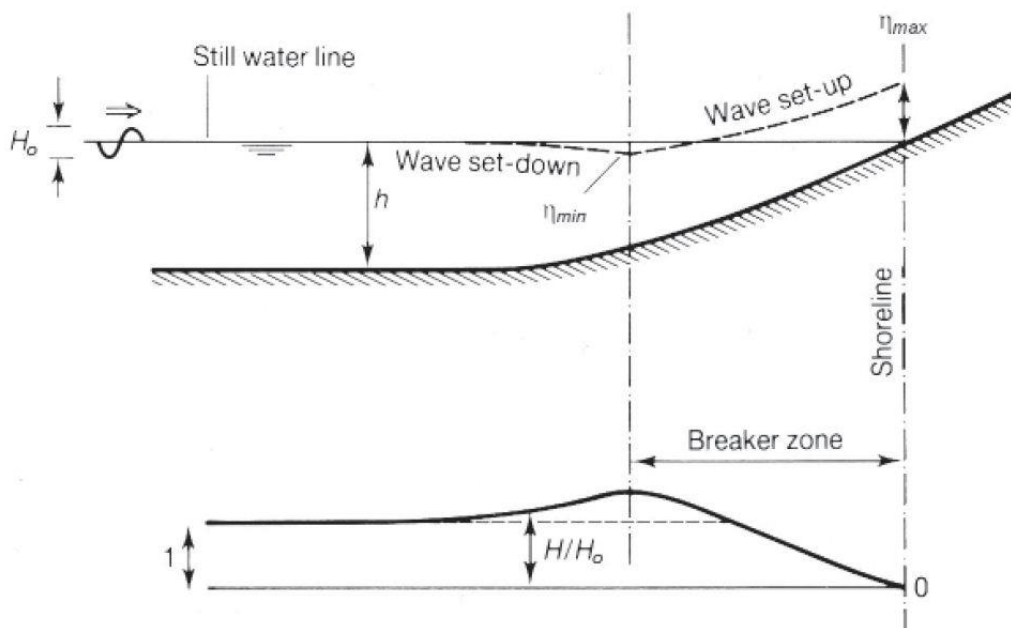


Figure 2.31 Wave set-up [55]

Using linear wave theory for normally incident regular waves, Battjes [144] derived a first estimate of wave set-up at the shoreline. The following equation estimates the wave set-up:

$$\eta_{max} = 0.3\gamma_{br}H_b \quad (2.114)$$

where γ_{br} is the breaker index or maximum wave height to water depth ratio, and H_b is the wave height at the breaker line for regular waves.

For the case of a planar beach, Bowen et al. [145] used the shallow water linear wave theory for the radiation stress, used the approximate relation $H = \gamma_{br}(h + \eta)$ in the surf zone and derived the following relation for the wave set-up:

$$\eta - \eta_b = \frac{1}{K}(h_b - h) \quad (2.115)$$

$$\text{where } K = 1 + \frac{8}{3\gamma_{br}^2} \quad (2.116)$$

Besides, Goda [4] proposed a chart, according to which the shoreline set-up can be estimated for uniformly beaches (slope varying from 1/100 to 1/10) as a function of H_o'/L_o , where H_o' is the equivalent deep water significant wave height obtained from the actual deep water significant wave height corrected for refraction effects.

2.4.2.6 Seiches

Seiches are standing wave oscillations caused by some excitation mechanism and trapped by the general geometry and bathymetry of a water domain like a harbour basin or a lake. Harbour oscillations are long period waves, since their periods vary between 2 min and 40 min. Vertical motions are generally small in contrast to horizontal motions. Oscillations are most damaging when their period coincide with a natural resonant period of the basin.

Seiches are normally observed in completely enclosed water bodies, e.g. lakes and closed seas. Regarding the simplest case, which corresponds to a rectangular closed basin of width, l , and constant water depth, h , the standing wave oscillations occur when the ratio of l to half of the wavelength L is an integer, as written below:

$$l = nL/2 \text{ with } n = 1, 2, 3, \dots \quad (2.117)$$

If the shallow water approximation is used in the dispersion relationship, the periods of seiches T_n can be estimated by the following equation [55]:

$$T_n = \frac{2l}{n\sqrt{gh}} \text{ with } n = 1, 2, 3, \dots \quad (2.118)$$

In a similar way, for a semi-enclosed basin, the periods of seiches T_n are obtained by the system of the following two equations:

$$l = L/4 + nL/2 \text{ with } n = 0, 1, 2, 3, \dots \quad (2.119)$$

$$T_n = \frac{4l}{(2n+1)\sqrt{gh}} \text{ with } n = 0, 1, 2, 3, \dots \quad (2.120)$$

2.4.3 Assumptions in predicting wind-driven waves from offshore wind data

The process of wave generation by wind can be explained by combining the resonance model developed by Phillips [146] and the shear flow model developed by Miles [147]. This topic will not be further analyzed here, since is not within the scope of the present thesis.

There are three wave conditions that can be estimated by using simplified wave predictions [148]. The first occurs when the wind blows with a constant velocity and direction over a certain fetch length for sufficient time for the waves to travel the entire fetch length. In this situation, wave characteristics will only depend on the fetch length and wind velocity. These wave conditions are known as fetch-limited, and it is assumed that steady state wave conditions are achieved for that fetch length [1]. If the wind duration is less than the required time for the waves to travel the fetch length, the wave conditions will depend on duration, and such wave conditions are described as duration-limited. Wind blowing for an unlimited duration over an unlimited distance will have a limited fetch length, beyond which the waves

do not continue to grow. This limiting condition is called a fully developed sea, and the rate of energy input to the waves from the wind is balanced with dissipation by wave breaking and turbulence [1].

It is noted that in the followings sections, SI units will be used in all equations presented.

The general equation for fetch-limited wave development for short fetches can be derived by combining the JONSWAP growth law for the peak frequency, an equation for the fully developed frequency, and an assumption that the group velocity of a local wave field is approximately equal to 0.85 times the spectral peak's group velocity [1]. Consequently, the duration required for waves crossing a fetch length of X under a wind speed u to become fetch-limited is given by:

$$t_{x,u} = 77.23 \frac{X^{0.67}}{u^{0.34} g^{0.33}} \quad (2.121)$$

Referring to the case of wave growth with fetch, the following equations provide estimations of the energy - based significant wave height H_{m0} , and peak period T_p , based on wind speed, and fetch:

$$\frac{gH_{m0}}{u_*^2} = 4.13 \cdot 10^{-2} \left(\frac{gX}{u_*^2} \right)^{1/2} \quad (2.122)$$

and

$$\frac{gT_p}{u_*} = 0.651 \left(\frac{gX}{u_*^2} \right)^{1/3} \quad (2.123)$$

$$C_D = \frac{u_*^2}{U_{10}^2} \quad (2.124)$$

$$C_D = 0.001(1.1 + 0.035U_{10}) \quad (2.125)$$

where:

X is a straight line fetch distance under the wind blows

C_D is the drag coefficient

U_{10} is the average wind speed at 10 m above the mean water level, and

u_* is the friction velocity

Assuming fully developed wave conditions, the following equations can be used to provide estimates of H_{m0} , and T_p :

$$\frac{gH_{m0}}{u_*^2} = 2.115 \cdot 10^2 \quad (2.126)$$

$$\frac{gT_p}{u_*} = 2.398 \cdot 10^2 \quad (2.127)$$

Equations governing duration limited wave conditions can be obtained by converting duration t into an equivalent fetch given by:

$$\frac{gX}{u_*^2} = 5.23 \cdot 10^{-3} \left(\frac{gt}{u_*} \right)^{3/2} \quad (2.128)$$

The equivalent fetch X estimated from Eq. 2.129 can then be substituted into the equations (Eqs 2.123 and 2.124) referring to fetch-limited wave conditions in order that duration-limited estimates of H_{m0} and T_p be obtained.

Indicatively, in Figure 2.32 an example of wind data for the Station of XIOS island in Aegean (Greece) is presented, as provided by the Hellenic National Meteorological Service. Figure 2.33 depicts the wind rose diagram extracted from the wind data, presented in Figure 2.32. These data could be used for wind-driven wave predictions in deep waters.

HELLENIC NATIONAL METEOROLOGICAL SERVICE
 DIRECTION OF CLIMATOLOGY
 SECTION OF STATISTICAL CLIMATOLOGY
 CLIMATOLOGICAL DATA BASE

D A T C L I M

STATION XIOS 706
 LATITUDE 38° 21' N LONGITUDE 26° 09' E ALTITUDE OF BAROMETER 3.8 METERS
 PERIOD 1973-1997

ANNUAL FREQUENCY (PER CENT) OF WIND DIRECTION AND FORCES IN BEAUFORT SCALE
 FROM OBSERVATIONS 06H, 12H, 18H GMT
 MONTH -00 YEAR -00

BEAUF	N	NE	E	SE	S	SW	W	NW	CALM	SUM
0									38.066	38.066
1	.033	.022	.011	.011	.066	.033	.011	.033		.220
2	1.849	.583	.122	.484	1.563	.429	.143	.385		5.568
3	11.701	2.367	.154	.892	4.920	.737	.341	.594		21.706
4	10.710	2.796	.066	.374	2.323	.495	.132	.363		17.259
5	6.318	1.805	.033	.121	1.233	.253	.022	.066		9.851
6	2.928	.881	.011	.022	.550	.088	.011	.011		4.502
7	1.189	.407	.011	.011	.264	.055	.011	.011		1.959
8	.455	.209	.011	.011	.055	.033	.011	.011		.836
9	.011	.022	.000	.000	.000	.000	.000	.000		.033
10	.000	.000	.000	.000	.000	.000	.000	.000		.000
>11	.000	.000	.000	.000	.000	.000	.000	.000		.000
SUM	35.234	9.092	.429	1.926	10.974	2.123	.682	1.474	38.066	100.000

Figure 2.32 Wind data for the Station of HIOS island in Aegean (Greece) (Hellenic National Meteorological Service)

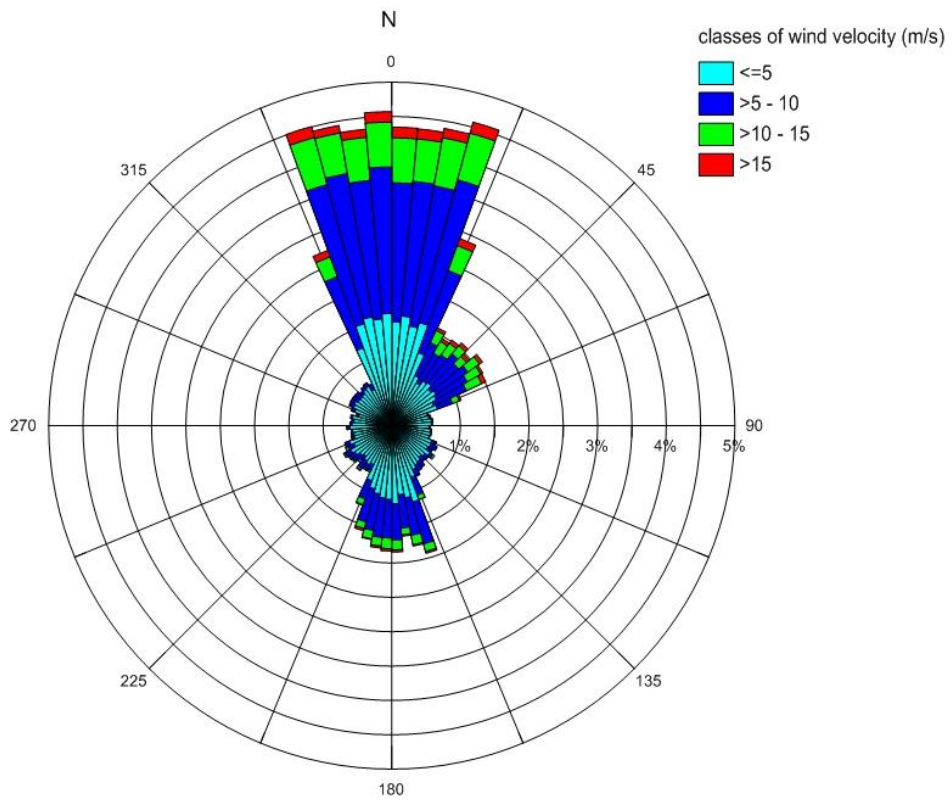


Figure 2.33 Wind rose diagram for Station of Hios in the Aegean (Greece) estimated from the wind data for the Station of Hios island

2.5 Estimating long-term wave statistics from analysis of sea states

2.5.1 Probability definition and the perspective of statistics

It is noted that the statistical method adopted in the present thesis is the classical perspective of statistics, i.e. the Frequentist. Frequentist statistics calculates the probability of an event as its proportion in the long run of an experiment (i.e. the experiment is theoretically repeated infinite number of times under the same conditions to obtain the outcome). An alternative approach to the problem of statistics is the Bayesian inference, which use Bayes theorem to combine the prior probabilities and the likelihood from the data to get the posterior probability of an event. Bayesian probability is an interpretation of the concept of probability, in which, instead of frequency of some phenomenon, probability is interpreted as reasonable expectation [149] representing a state of knowledge [150] or as quantification of a personal belief [151].

2.5.2 Univariate analysis

Information on the statistical representation of sea severity is vital for the design of marine systems and coastal structures. Referring to sea severity, all sea conditions are taken into consideration and not only the severest storm expected to occur during a marine system/coastal structure's lifetime [10]. The statistical analysis of all sea conditions is especially necessary for evaluating fatigue loadings and the cumulative damage of the system.

The most commonly available information on sea severity is the probability distribution of one variable, the significant wave height H_s , which can be estimated from the statistical analysis of data accumulated over several years [33].

In fact, there is no scientific basis for selecting a specific distribution for H_s . This is because, wave measurements are site specific and sea severity depends on the geographical location where the data are obtained, the water depth, wind direction, frequency of occurrence of storms, etc., [10]. Thus, various probability distribution functions (pdfs) have been proposed which appear to best fit various observed datasets. These include the lognormal distribution [14], the three-parameter Weibull distribution ([152]; [58]), the Gamma distribution [153] etc. In general, the lognormal distribution represents well the greater part of data, but diverges from the data for extreme H_s which are critical for the design of marine and coastal structures. Specifically, the lognormal cumulative distribution often diverges to unity much slower than the data of H_s . Another general trend observed on the statistical distribution of H_s is that large

significant wave heights can well be represented by the Weibull distribution, but approximately 30 percent of the lower part of the dataset fails to follow [10].

Another attempt to find an appropriate distribution for the total range of H_s data was made by Ochi [154], who found from the statistical analysis of H_s data that the cumulative distribution of the standardized generalized gamma distribution is nearly equal to the lognormal distribution up to 0.90, but the former converges to unity much faster than the latter. Thus the generalized gamma distribution seemed to represent the total dataset much better than the lognormal distribution in his study.

The parameters of these distributions are selected so that the likelihood function or the log-likelihood function is maximized.

The lognormal pdf is defined as follows:

$$f(x; \mu, \sigma) = \frac{1}{\sigma \cdot x \cdot \sqrt{2\pi}} \cdot \exp\left\{-\frac{[\ln(x) - \mu]^2}{2 \cdot \sigma^2}\right\}, \quad x > 0 \quad (2.129)$$

where: μ is a location parameter and σ is a scale parameter, i.e. the mean value and the standard deviation of $\ln(x)$.

The 3-parameter Weibull pdf is defined as follows:

$$f(x; \alpha, \beta, \gamma) = \frac{\beta}{\alpha} \left(\frac{x - \gamma}{\alpha}\right)^{\beta-1} \exp\left[-\left(\frac{x - \gamma}{\alpha}\right)^\beta\right] \quad (2.130)$$

where: α , β , and γ are the scale, shape, and location parameter respectively. For $\gamma = 0$, Eq. 2.131 simplifies to Eq. 2.132, i.e. the 2-parameter Weibull pdf:

$$f(x; \alpha, \beta) = \frac{\beta}{\alpha} \left(\frac{x}{\alpha}\right)^{\beta-1} \exp\left[-(x/\alpha)^\beta\right] \quad (2.131)$$

The γ parameter of the 3-parameter Weibull distribution is regarded as a constant and known beforehand.

Another candidate pdf for H_s is the 2-parameter Gamma distribution defined as follows:

$$f(x; \alpha, \beta) = \frac{1}{\beta^\alpha \Gamma(\alpha)} x^{\alpha-1} \exp(-x/\beta), \quad x > 0, \alpha > 0, \beta > 0 \quad (2.132)$$

where: α is a shape parameter, β is a scale parameter, and Γ is the Gamma function.

The pdf of the generalized gamma distribution (non-standardized form) is as follows:

$$f(x; \lambda, c, m) = \frac{c}{\Gamma(m)} \lambda^{cm} x^{cm-1} \exp[-(\lambda x)^c] \quad (2.133)$$

where: Γ is the Gamma function.

2.5.3 Multivariate analysis

Nowadays, the role of other variables except for H_s in the stability of coastal and marine structures has been realized, necessitating a multivariate analysis that involves a number of variables. In particular, the joint effect of H_s and T_m on those structures' stability has been realized (e.g. [11]; [155]). Thus, the information on long-term wave statistics is broadened to a great extent by including, in addition to wave height, wave period, usually the average zero-crossing value of wave periods in a specified sea state, denoted by T_m .

In order to estimate the joint pdf of H_s and T_m , the study of bivariate distribution models and correlation between the variables is required. One of the first approaches was proposed by Ochi [14], who adopted the bivariate lognormal distribution to represent significant wave heights and average zero-crossing periods, resulting from an exponential transformation of

the bivariate normal distribution. This approach although simple to apply, is based on the assumption that the logarithms of the data are normally distributed, and although this may happen for low and moderate values of H_s , it is not applicable for extreme sea states. The joint pdf of this model can be written as:

$$f(H_s, T_m) = \frac{0.5}{H_s T_m \pi \delta_{H_s} \delta_{T_m} \sqrt{1-\rho^2}} \exp \left\{ -\frac{0.5}{1-\rho^2} \left[\frac{(\log T_m - \lambda_{T_m})^2}{\delta_{T_m}^2} - \frac{2\rho(\log T_m - \lambda_{T_m})(\log H_s - \lambda_{H_s})}{\delta_{H_s} \delta_{T_m}} + \frac{(\log H_s - \lambda_{H_s})^2}{\delta_{H_s}^2} \right] \right\} \quad (2.134)$$

in which $\lambda_{H_s}, \lambda_{T_m}, \delta_{H_s}, \delta_{T_m}$ are the location and scale parameters of the marginal pdfs of H_s, T_m respectively [156] and ρ is their linear correlation coefficient. All of the parameters mentioned here are estimated using the Maximum Likelihood estimation procedure.

A bivariate lognormal curve with correction for skewness [15] was an attempt to improve the bivariate lognormal model, when there is clear evidence of skewness in the log transformed data of H_s . The pdf of the bivariate log-normal model with correction of skewness is:

$$f(H_s, T_m) = \frac{0.5}{H_s T_m \pi \delta_{H_s} \delta_{T_m} \sqrt{1-\rho^2}} \exp \left\{ -\frac{0.5}{1-\rho^2} \left[\frac{(\log T_m - \lambda_{T_m})^2}{\delta_{T_m}^2} - \frac{2\rho(\log T_m - \lambda_{T_m})(\log H_s - \lambda_{H_s})}{\delta_{H_s} \delta_{T_m}} + \frac{(\log H_s - \lambda_{H_s})^2}{\delta_{H_s}^2} \right] \right\} \quad (2.135)$$

$$\exp \left\{ 1 - \frac{k_{H_s}}{6} \left[3(\log H_s - \lambda_{H_s}) - (\log H_s - \lambda_{H_s})^3 \right] \right\}$$

where: k_{H_s} is the skewness coefficient for $\log H_s$ [156].

Furthermore, a model, based on the marginal distribution of H_s and the conditional distribution of T_p for given H_s , could increase its flexibility and accuracy, and was adopted by

Haver [16], and Bitner-Gregersen and Haver [17]. Guedes Soares et al. [18], Lucas and Guedes Soares [19], Papanikolaou et al. [20], and Malliouri et al. [33] have used a similar model based on the marginal distribution of H_s and the conditional distribution of T_m , referred hereinafter as the conditional model. Other approaches have also been developed for the same purpose (e.g. [21] etc.). However, in the cases examined by Lucas and Guedes Soares [19] and Papanikolaou et al. [20], it was showed that the conditional model represented more accurately H_s and T_m data than the other models tested. Thus, in the present thesis the conditional model is used to fit bivariate distributions of H_s and T_m to the available data sets, written as below:

$$f(H_s, T_m) = f(T_m|H_s)f(H_s) \quad (2.136)$$

where $f(T_m|H_s)$ is the conditional pdf of T_m given H_s , and $f(H_s)$ is the marginal distribution of H_s . Moreover, it was shown by Mathisen and Bitner-Gregersen [58], Guedes Soares et al. [18], and Lucas and Guedes Soares [19], that $f(T_m|H_s)$ can be modeled by a lognormal probability distribution, i.e.,

$$f(T_m | H_s) = \frac{1}{\sigma(H_s) \cdot T_m \cdot \sqrt{2\pi}} \cdot \exp\left\{-\frac{[\ln(T_m) - \mu(H_s)]^2}{2 \cdot [\sigma(H_s)]^2}\right\} \quad (2.137)$$

where, according to Mathisen and Bitner-Gregersen [58], the parameters of the conditional lognormal pdf can be written as functions of H_s as below:

$$\begin{aligned} \mu(H_s) &= a_1 + a_2 H_s^{a_3} \\ \sigma(H_s) &= b_1 + b_2 \exp(b_3 H_s) \end{aligned} \quad (2.138)$$

where a_1, a_2, a_3, b_1, b_2 , and b_3 are constants determined from fitting of the curves described by Eq. 2.139 to the data.

Furthermore, information on wave directionality is also important in representing accurately wave fields, since wind wave energy spreads over various directions, though the major part of the energy may propagate in the wind direction. Also, it is known that wave forces on maritime structures, computed assuming that the wave system is unidirectional, are not only overestimated but the associated coupled responses induced by waves propagating from other directions are also disregarded [10]. Besides, according to Laface et al. [13], it is important, for several marine applications, to consider directionality during storms in order to determine the long-term statistics for any directional sector.

2.5.4 Integration of short- with long-term wave statistics

The statistical properties of waves accumulated over a long period of time are of great interest and importance e.g. for the design of coastal and marine structures. The knowledge on the joint distribution of individual wave height H and period T of each short-term sea state over a long period of time provides vital information for the evaluation of the wave loads on these structures. In this way, information can be provided on the direct loadings towards the structures and not only on the representative loadings which come from the statistical analysis of the first, as in the case of the joint distribution of H_s and T_m [33]. This information can be very useful for the design of these structures. The long-term statistics of individual wave height or the long-term pdf of H was developed by Battjes [36], as an accumulation of the statistics for all short-term sea conditions, considering the frequency of occurrence of each short-term sea state. According to his approach, the long-term pdf of H is defined as:

$$f_{\text{long}}(H) = \frac{\iint f_{\text{short}}(H) \cdot f_{\text{long}}(T_m, H_s) \cdot N \, dH_s \, dT_m}{\iint N \cdot f_{\text{long}}(T_m, H_s) \, dH_s \, dT_m} \quad (2.139)$$

where $f_{\text{short}}(H)$ is the short-term pdf for H , N is the number of waves in each short-term sea state that is considered constant, and $f_{\text{long}}(T_m, H_s)$ corresponds to the long-term pdf of H_s and T_m .

2.6 Estimating extreme sea conditions

Preliminary or deterministic design of coastal structures is based on the extreme value analysis of their environmental loadings. In this approach, appropriate return periods of the environmental parameters need to be specified, typically of 100 years or sometimes of 1000 years or even more, in order to meet the reliability requirements. However the uncertainties associated with long return period criteria are usually large, as the available data (from measurements and/or hindcasts) usually cover a relatively small period [157].

2.6.1 Univariate extreme value analysis

Univariate extreme value analysis theory includes models for block maxima (Block Maxima Method) and models for exceedances over an appropriately selected high threshold (Peak over Threshold – POT method). In the following paragraphs, the two methods will be described.

2.6.1.1 Block maxima method

Block Maxima Method uses the Generalized Extreme Value (GEV) distribution, which combines the Gumbel, Fréchet, and Weibull families into its one family. The cumulative distribution function (cdf) of GEV is written as below ([54]; [158]):

$$G(x) = \exp \left[- \left(1 + \xi \frac{x - \mu}{\sigma} \right)^{-1/\xi} \right] \quad (2.140)$$

defined on the set: $\left\{ x : 1 + \xi \frac{x - \mu}{\sigma} > 0 \right\}$, for location parameter $\mu \in (-\infty, +\infty)$, scale parameter $\sigma > 0$, and shape parameter $\xi \in (-\infty, +\infty)$. The subset of the GEV family when $\xi \rightarrow 0$ leads to the Gumbel family, with cumulative distribution:

$$G(x) = \exp \left[- \exp \left(- \frac{x - \mu}{\sigma} \right) \right], \quad -\infty < x < +\infty \quad (2.141)$$

The parameters of the GEV can be estimated using different techniques, i.e. the maximum likelihood estimation procedure, and the method of L-moments [159].

As far as the return periods and the corresponding return values are concerned, if the annual maxima are GEV distributed with parameters σ, μ , and ξ , the return period $T_r = 1/p$, where p is the annual exceedance probability is defined by:

$$\begin{aligned} 1-p &= \exp\left[-\left(1+\xi\frac{x-\mu}{\sigma}\right)^{-1/\xi}\right], \text{ for } \xi \neq 0 \\ 1-p &= \exp\left[-\exp\left(-\frac{x-\mu}{\sigma}\right)\right], \text{ for } \xi = 0 \end{aligned} \quad (2.142)$$

so that the corresponding return value is:

$$\begin{aligned} x_p &= \mu - \frac{\sigma}{\xi} \left\{ 1 - \left[-\log\left(1 - \frac{1}{T_r}\right) \right]^{-\xi} \right\}, \text{ for } \xi \neq 0 \\ x_p &= \mu - \sigma \log\left[-\log\left(1 - \frac{1}{T_r}\right) \right], \text{ for } \xi = 0 \end{aligned} \quad (2.143)$$

It is noted that in order to extrapolate the annual exceedance probability p , estimated in the sample of annual maximum observations, to longer reference period than one year, Eq. 2.6 could be used by substituting $P_{f,1y,e}^*$ with p .

2.6.1.2 Peak over threshold method

Referring to modeling from the perspective of peaks over threshold, Pickands [160] showed that the conditional cumulative distribution $F_u(x)$ of a random variable X , of a continuous

cumulative distribution F , given exceedances $X > u$ of a sufficiently high threshold u , can be approximated by a Generalized Pareto distribution, which is written as below (see also [54]):

$$\begin{aligned} F_u(x) &= \frac{F(x) - F(u)}{1 - F(u)} = \Pr(X \leq x | X > u) \\ &= 1 - \left[1 + \frac{\xi}{\sigma}(x - u) \right]^{-1/\xi}, \quad \text{for } \xi \neq 0 \end{aligned} \quad (2.144)$$

and

$$\begin{aligned} F_u(x) &= \frac{F(x) - F(u)}{1 - F(u)} = \Pr(X \leq x | X > u) \\ &= 1 - \exp\left(-\frac{x - u}{\sigma}\right), \quad \text{for } \xi = 0 \end{aligned} \quad (2.145)$$

where: threshold $u \in (-\infty, +\infty)$, scale parameter $\sigma > 0$, and shape parameter $\xi \in (-\infty, +\infty)$, $1 + \xi \frac{x - u}{\sigma} > 0$. When $\xi > 0$, the distribution has a heavy and unbounded tail and belongs to Fréchet domain, which means that its tail is not exponentially bounded, and extreme values have a higher probability than in distributions with exponential or higher tails. Continuously, when $\xi < 0$, the distribution implies a finite upper bound on the right (extreme area) by $x_{\max} = u + \sigma / \xi$ [52] and belongs to the Weibull domain of attraction. Finally, when $\xi = 0$, the distribution is the exponential one.

Since the GP distribution is an asymptotic law, its threshold must be high enough. However, the higher the threshold, the greater the uncertainties, because the amount of data left is smaller [52].

We have now considered that the exceedances of a sufficiently high threshold follow the GP distribution. Also, it is noted that the storm occurrence follows a Poisson distribution with parameter λ , which is equal to the mean number of storms per year. Therefore, the GP-Poisson model is adopted, and thus a Poisson distribution should be fitted to the data.

Poisson distribution

It is noted that the Poisson distribution is a discrete probability distribution that expresses the probability of a given number of occurrence of events in a fixed interval of time or space, if these events occur with a known constant mean rate and independently of the time since the last event [161]. The probability mass function of the variable X that follows the Poisson distribution [162]:

$$f(k, \lambda) = \Pr(X = k) = \frac{\lambda^k e^{-\lambda}}{k!} \quad (2.146)$$

where:

e is the Euler's number ($e=2.71828\dots$)

$k!$ is the factorial of k

The positive real number λ is equal to the expected value of X , i.e. the mean value, and its variance:

$$\lambda = E(X) = \text{Var}(X) \quad (2.147)$$

Steps of POT Analysis

(1) The first step is to extract homogenous data from buoy measurements or hindcast data, etc. Such homogenization could be the separation of data/sea states into independent wave systems, the separation in directional sectors or the seasonal analysis of those data [52]. According to Mathiesen et al. [163], homogenization may be the most important step in the extreme value theory analysis.

(2) The second step is the extraction of storm peaks from the homogenous sea states (selected at step 1). To do this, we take into account that the POT assumptions of independent and identically distributed data should be satisfied. Firstly, a threshold u_1 for H_s is selected to

select weak and strong storms from the dataset extracted at step 1. Besides, a minimum calm period between two consecutive storms should be selected to ensure that their storm peaks are independent (see Figure 2.34). For example, according to Li et al. [164], the minimum time interval between two successive storms was set at 6 hours, i.e. any two storms with time interval less than 6 hours were considered as one storm event. Therefore, the dataset of the maximum significant wave heights $H_{s,p}$ is derived from this procedure. Referring to the selection of u_1 , it should be high enough to distinguish and separates two consecutive storms, but also low enough to be below the extreme area [52].

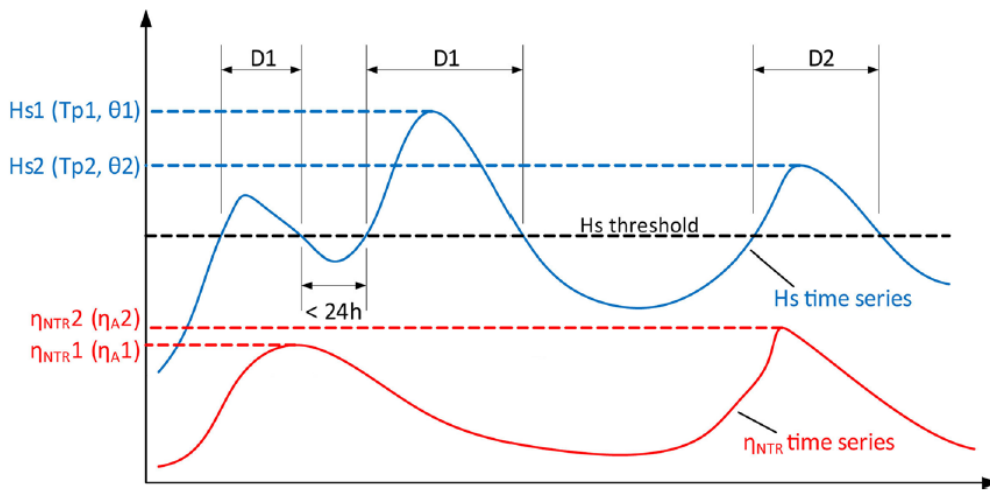


Figure 2.34 Definition of independent storm events [165]

(3) The third step is the selection of another threshold u_2 higher than u_1 . The selection of u_2 needs to be more precise than that of u_1 , since the storm peaks above u_2 should follow the same extreme probability distribution. Using the properties of GP distribution (if storm peaks follow a GP distribution) to determine u_2 , two different methodologies are commonly used. Precisely, an appropriate threshold u_2 value could be selected by examining the domain of stability of the shape parameter ξ , and the stability of modified scale parameter $\sigma^* = \sigma - \xi u_2$ or the linearity of the scale parameter σ of the GP distribution with respect to u_2 (see e.g. [61]). The domain of stability is the interval of u_2 where the shape and modified shape parameters remain roughly constant, or the interval of u_2 where the shape parameter remains constant and the scale parameter a linear function of u_2 . The second procedure for threshold selection is to search for the domain of threshold u_2 where the mean residual life plot is approximately linear in u_2 [62]. The mean residual life plot is defined as the locus of points:

$$\left\{ u_2, \frac{1}{n_e} \sum_{i=1}^{n_e} (x_i - u_2) : u_2 < x_{\max} \right\} \quad (2.148)$$

where: x_i is i -th observation that exceeds u_2 and x_{\max} is the largest of $X > u_2$.

In both methods, the interest is focused on the highest domain of stability (firstly mentioned method) or of linearity (secondly mentioned method), since this belongs to the extreme area/asymptotic domain. Moreover, the lowest value of this highest domain is the most appropriate, as does not limit the amount of data that is needed to be kept as large as possible to ensure reliable estimates of return values, extracted from the GP-distribution fitting to the dataset.

Thus, if n_e is number of observations (e.g. of $H_{s,p}$) that exceed u_2 and Y is the number of years of observations, then the mean value of the Poisson distribution λ is equal to:

$$\lambda = \frac{n_e}{Y} \quad (2.149)$$

Furthermore, Mazas and Hamm [52] recommend that λ should stand approximately between 2 and 5, i.e. if Y is low a value around 5 is more appropriate, whilst if Y is relatively large (around 40-50 years) a value close to 2 is more advisable.

The second and third steps of over-threshold modelling of environmental time series, which were introduced by Bernardara et al. [50], provide a relevant event-based framework that stems from the standard practice that the analyst generally deals with a time series of discrete observations of a variable at a given time step, while the conventional tools provided by the extreme value theory assume that the dataset is independent and identically distributed [63]). Each event or else storm extracted from the dataset has a duration and other characteristic parameters such as $H_{s,p}$ mentioned above, or average mean wave period T_m of storm, average significant wave height $H_{s,m}$ of storm, etc.

It is noted that this event-based framework for over-threshold modelling of environmental time series has been also used for multivariate analysis by Mazas and Hamm [63].

Alternative distributions

There are also some other models for describing exceedances x of a threshold u , e.g. fitting the conditional distribution $F_u(x)$, i.e. the conditional cumulative distribution of a random variable X given exceedances $X > u$ of a sufficiently high threshold u , with $F_u(x)$ given by the Weibull cumulative distribution, written as below.

$$F_u(x) = 1 - \exp\left[-\left(\frac{x-u}{\beta}\right)^\alpha\right] \quad (2.150)$$

where: $u \in (-\infty, +\infty)$, $\alpha, \beta > 0$, $x > u$ and the Gumbel cumulative distribution;

$$F_u(x) = \exp\left\{-\exp\left[-\left(\frac{x-u}{\beta}\right)\right]\right\} \quad (2.151)$$

for $u \in (-\infty, +\infty)$, $\beta > 0$.

For example, fitting using the Weibull distribution implies that the distribution is unbounded on the right hand side, whilst the use of the GP distribution avoids this constraint. For this reason, fitting using Weibull and GP distributions is expected to give similar estimates for return values associated with return periods of the order of that of the sample, but different estimates for longer return periods [157].

However, some researchers recommend the GP form for $F_u(x)$ based on the goodness of fit alone (e.g. [166]) and many others based on theoretical considerations (e.g. [160]; [62]).

Unconditional POT distribution

The unconditional cumulative distribution F of peaks over threshold is written as:

$$F(x) = (1 - p_{u_2}) + p_{u_2} F_{u_2}(x) \quad (2.152)$$

where, p_{u_2} is the exceedance probability of the threshold u_2 .

Return values of H_s and encounter probabilities

It is a standard practice to interpret extreme value models in terms of quantiles or return levels. Thus, suppose a GP distribution with parameters σ and ξ is a suitable model for exceedances of a threshold u by a variable X , then for $X > u$ it applies [62]:

$$\Pr(X > x | X > u) = \left[1 + \frac{\xi}{\sigma}(x - u) \right]^{-1/\xi}, \quad \text{for } \xi \neq 0 \quad (2.153)$$

which follows that:

$$\Pr(X > x) = \zeta_u \left[1 + \frac{\xi}{\sigma}(x - u) \right]^{-1/\xi}, \quad \text{for } \xi \neq 0 \quad (2.154)$$

where: $\zeta_u = \Pr(X > u)$. Hence, the level x_m that is exceeded on average once every m observations is the following equation:

$$\zeta_u \left[1 + \frac{\xi}{\sigma}(x_m - u) \right]^{-1/\xi} = \frac{1}{m} \quad (2.155)$$

and thus,

$$x_m = u + \frac{\sigma}{\xi} \left[(m\zeta_u)^\xi - 1 \right] \quad (2.156)$$

If $\xi = 0$, we have:

$$x_m = u + \sigma \log(m\zeta_u) \quad (2.157)$$

To provide return values on an annual scale, the T_r -return level x_{T_r} , where T_r is the return period in years, is expressed as follows:

$$\begin{aligned} x_{T_r} &= u + \frac{\sigma}{\xi} \left[(T_r \lambda \zeta_u)^\xi - 1 \right], \text{ for } \xi \neq 0 \\ x_{T_r} &= u + \sigma \log(T_r \lambda \zeta_u), \quad \text{for } \xi = 0 \end{aligned} \quad (2.158)$$

where λ is the number of extreme observations per year, defined by Eq. 2.160.

To connect with the previous theory, the threshold mentioned in this section denotes the threshold u_2 , thus $u = u_2$ here.

2.6.1.3 Parameters estimation

Mathiesen et al. [163] mentioned three methods for the estimation of the extreme distributions' parameters: least squares methods, the method of moments, and the Maximum Likelihood Estimator (MLE). The most efficient and handy method is to use the MLE, which maximizes the likelihood function of the fit, defined by:

$$L(X_1, \dots, X_N | \theta) = \prod_{i=1}^N f_\theta(X_i; \theta) \quad (2.159)$$

where, f_θ is the joint density function (with parameter θ) at the sample observations X_i . Also, the log-likelihood function is usually used, since it is much easier to be estimated:

$$l(X_1, \dots, X_N | \theta) = \sum_{i=1}^N \ln(f_\theta(X_i; \theta)) \quad (2.160)$$

2.6.1.4 Best fit selection

Once several candidate distributions are fitted to the data, the best fit should be determined. For this purpose, objective Bayesian criteria are used. The first one is the Bayesian Information Criterion (BIC), also known as the Schwarz Criterion [167], which minimizes the bias between the unknown “real” model and the fitted model. Assuming that the sample size N is large enough, BIC is given by:

$$\text{BIC} = -2 \ln L + k_p \ln N \quad (2.161)$$

where: L is the likelihood of the fit, and k_p is the number of the parameters of the distribution tested.

The second criterion is the closely related Akaike Information Criterion (AIC) that provides the best compromise between bias and variance [168]. Therefore it can be interpreted as the sum of two terms (the first term is the bias and the second one is the variance) given below:

$$\text{AIC} = -2 \ln L + 2k_p \quad (2.162)$$

For both BIC and AIC, it is recommended to select the distribution that provides the lowest criteria. Most of the time, both criteria give the same result. If not, it is recommended to select the distribution that provides the most conservative return values [52].

2.6.2 Multivariate extreme value analysis

In accordance with long-term wave statistics of all sea conditions (sea severity), extreme sea conditions should also be specified jointly by adopting a joint extremal analysis. For example, wave climate can be described in terms of sea state variables, such as significant wave height H_s , spectral peak wave period T_p , or mean zero-crossing wave period T_m , and/or wave direction, and thus a multivariate analysis should be adopted. Due to the statistical correlation between those variables, e.g. between H_s and T_m , and the fact that physical arguments apply, we are interested in extreme values of H_s , and associated values for T_m at the extreme value of H_s . In this case, the conditional model by Haver [16] could be applied, but when no such physical arguments apply, other more complex models should be applied.

Besides, availability of met-ocean data allows the effect of heterogeneity of extremes with respect to direction and location to be considered in estimation of design criteria [169]. Jonathan and Evans [170] review statistical modelling of extremes for the design of marine structures, capturing covariate effects in extreme sea states developing design criteria. There is a large body of statistical literature incorporating modelling of covariate effects in extreme value analysis (e.g. see [171]; [172]).

Furthermore, in a multivariate extreme value analysis the asymptotic form of the multivariate distribution cannot be derived directly or theoretically in contrast to univariate EV theory using the Block Maxima or Peak over Threshold methods. Therefore there is a need to estimate the tail behavior of the multivariate distribution of the sample, based on the sample alone ([157]). For this purpose, there have been developed four possible approaches: the extremal dependence models, parametric models, conditional extremes models, and max-stable models.

The extremal dependence models introduce the different forms of extremal dependence, which are the asymptotic dependence, asymptotic independence and perfect asymptotic independence. Besides, a large number of parametric models have been developed based on the form of their extremal dependence (e.g. [173]; [174]; [175]; [176]; [177]). Furthermore, conditional models (e.g. [16]; [178]) provide the basis for modeling for all forms of extremal dependence. Multivariate max-stable models are also attractive, since they provide the basis for spatial extremes models.

Referring at this point to the two different classes of joint tail behaviour that have very different implications: i.e. asymptotic independence suggesting that extreme events are unlikely to occur together, and asymptotic dependence implying that extreme events can occur simultaneously, Kereszturi et al. [179] developed good diagnostics to identify the

appropriate dependence class. It is vital to have such diagnostics of good quality, since if variables are asymptotically independent, incorrectly assuming their asymptotically dependence can lead to overestimation of the joint risk of extreme events, and hence to overdesign of offshore structures [179].

Modeling dependence using Copula models

The joint cumulative distribution F of random variables x_1, x_2, \dots, x_p may be written as [180]:

$$F(x_1, x_2, \dots, x_p) = C(F_1(x_1), F_2(x_2), \dots, F_p(x_p)) \quad (2.163)$$

where F_1, F_2, \dots, F_p are univariate marginal cumulative distributions and C is a p -dimensional cumulative distribution, known as copula, defined in the domain $[0,1]^p$. The copula C is uniquely determined from well-behaved distributions F , and in this case it can be written that:

$$C(u_1, u_2, \dots, u_p) = F(F_1^{-1}(u_1), F_2^{-1}(u_2), \dots, F_p^{-1}(u_p)) \quad (2.164)$$

for $\{u_1, u_2, \dots, u_p\} \in [0,1]^p$ and F_i^{-1} is the inverse cumulative distribution of the i -th variable.

Referring to the case of two dimensional copulas, three one-parameter Archimedean copulas could be used, namely the Clayton, the Frank, and the Gumbel, characterized by lower tail dependence, no tail dependence, and strong upper tail dependence, respectively. The copula function for each case is defined by [181]:

$$C_{clayton}(u_1, u_2) = (u_1^{-a} + u_2^{-a} - 1)^{-1/a} \quad (2.165)$$

$$C_{frank}(u_1, u_2) = -\frac{1}{a} \ln \left[1 + \frac{(e^{-au_1} - 1)(e^{-au_2} - 1)}{e^{-au_1} - 1} \right] \quad (2.166)$$

$$C_{gumbel}(u_1, u_2) = \exp \left\{ - \left[(-\ln u_1)^a + (-\ln u_2)^a \right]^{1/a} \right\} \quad (2.167)$$

where a is the dependence parameter, which ranges in $(0, \infty)$ for the Calyton, in $-\ln(-\infty, \infty) / \{0\}$ for the Frank, and in $[1, \infty)$ for the Gumbel copula.

Except for the Archimedean copulas, the bivariate Student's t copula could be utilized, which is an Elliptical copula [182], written as follows:

$$C_t(u_1, u_2) = t_{v,a}(t_v^{-1}(u_1), t_v^{-1}(u_2)) \quad (2.168)$$

where, $t_{v,a}$, with a ranging in $[0, 1]$, and ν is the degrees of freedom, is the bivariate distribution that corresponds to the univariate t Student distribution t_ν [182]:

$$t_{v,a}(x_1, x_2) = \int_{-\infty}^{x_1} \int_{-\infty}^{x_2} \frac{1}{2\pi\sqrt{1-\alpha^2}} \left(1 + \frac{s^2 + t^2 - 2ast}{\nu(1-\alpha^2)} \right)^{\frac{\nu+2}{2}} ds dt \quad (2.169)$$

The dependence parameter a of the copula functions could be estimated by the method by Joe and Xu [183].

As in the univariate extreme value analysis the most appropriate marginal distribution is selected that represents the data better than all other candidate marginal distributions, also in the multivariate extremal analysis the most appropriate copula function is selected among the aforementioned copula functions. To do this, Galiatsatou and Prinos [184] implemented the parametric bootstrap procedure by Genest et al. [185].

Selection of design events

In multivariate extreme value theory, the joint return period can be estimated from the joint exceedance probability of a pair of events e.g. given by Bender et al [181]:

$$T_{x_1, x_2} = \frac{1}{\Pr(X_1 > x_1 \cap X_2 > x_2)} = \frac{1}{1 - F_1(x_1) - F_2(x_2) + C(u_1, u_2)} \quad (2.170)$$

It is noted that an infinite number of combinations of the variables u_1, u_2 corresponds to each joint return period [184]. Thus, to overcome the problem of selecting a design event represented by two variables, Salvadorey et al. [186] proposed the most likely design event method, i.e. with the highest probability density among others of the same iso-probability contour [187]:

$$(u_1, u_2) = \arg \max_{T_{x_1, x_2}} f_{x_1, x_2}(F_1^{-1}(u_1), F_2^{-1}(u_2)) \quad (2.171)$$

where f_{x_1, x_2} is the joint probability density function of the two variables X_1, X_2 and F^{-1} is the inverse cumulative distribution.

Therefore, the design values x_1, x_2 can then be estimated using the inverse marginal cumulative distributions:

$$x_1 = F_1^{-1}(u_1), x_2 = F_2^{-1}(u_2) \quad (2.172)$$

2.6.3 Combining statistics of extreme sea conditions by the the short-term distribution of the maximum wave height

Good estimation of extremes of individual wave height H and of maximum wave height H_{\max} on some spatio-temporal domain, are essential for the design and assessment of marine and coastal structures [188]. There is a large literature related to this subject. A part of this literature consists of a variety of research studies motivated by observations and laboratory measurements. As noted in section 2.4.1.2, the distribution of H in deep waters has been

modelled using the Rayleigh distribution [110] and the Weibull distribution [189]. Also, Tayfun [114] generalised the asymptotic model of Boccotti [190] to include the effects of higher order non-linearities. Other studies are focused on the intermediate and shallow water short-term distribution of H and H_{max} . Some of them are indicatively cited here, see e.g. [135]; [191]; [119]; [120]; [188].

Thus, by combining statistics of individual waves during storm events with the statistics of extreme events, information on the maximum loadings upon marine and coastal structures can be obtained. This information is vital for the reliability assessment and design of those structures.

CHAPTER 3
METHODOLOGY AND RESULTS

3 Methodology and results

In this chapter, the methodology developed and adopted in the present PhD thesis is presented and described. Firstly, a linear wave propagation model that integrates short- with long-term wave statistics from deep to intermediate water depths will be described. This model could be utilized for estimating the long-term wave climate at a coastal structure's location, which is frequently met in intermediate water depths. Secondly, the capability of this linear model, to transfer the probabilistic information concerning short-term wave statistics, will be investigated by comparing its results with wave measurements in deep waters and the results of the well-known and commercial phase-resolving Boussinesq wave model (MIKE 21 BW / Mike powered by DHI). The results produced by the latter refer to intermediate water depths. The next section deals with the reliability analysis of a coastal structure, focusing on the case of rubble mound breakwaters, and wave loadings. Finally, two illustrative examples of reliability analysis and probabilistic design of a rubble mound breakwater are presented, followed by discussion of the results produced.

3.1 Integrating short- with long-term wave statistics from deep to intermediate waters

The model that will be described here has been developed by Malliouri et al. [33]. This is a wave model that uses long-term wave statistics in deep waters as input data, and via the use of the short-term wave statistics for each sea state in deep waters, estimates the long-term wave statistics in shallower waters. Specifically, by using i) data/measurements of significant wave height H_s , mean wave period T_m , and mean wave direction θ_m e.g. obtained from an oceanographic buoy in deep waters, ii) the dimensionless short-term images by Memos and Tzani [29], and Tzani [31] in deep waters, iii) a theoretical expression for wave directionality adjusted in an individual wave statistical analysis, and iv) a modification of Battjes approach [36], the short-term joint distribution of individual wave height H , period T , and direction θ for every sea state or storm event could be produced in deep waters. Then, the short- and the long-term joint distribution of H , T , θ could be estimated in intermediate waters, as well as the long-term joint probability density function of H_s , T_m , θ_m , by considering linear wave transformation of each individual wave, as waves propagate from the open sea towards shallower waters.

The analysis refers to short-crested waves, thus wave directionality was accounted for in deep water wave input. It is noted that if there is not a wave probe array or an appropriate buoy (e.g. heave-pitch-roll buoy [107]), cloverleaf buoy [192], etc.), to evaluate wave directionality, and only the mean wave direction is available, an established theoretical spreading function could be applied. Besides, the nonlinear wave-wave interactions' effects have not been taken into account in the present analysis. However, the effect of non-linear wave-wave interactions to wave transformations as waves move inshore has been investigated in section 3.2, by comparing the linear wave propagation model developed with a nonlinear one.

A quite similar attempt was made by Chondros [193], and Chondros and Memos [32], but there are some significant differences between the approach by Malliouri et al. [33] and the approach adopted by them. As for the similarities, both approaches utilized the short-term dimensionless probabilistic images by Memos and Tzani [30] and Tzani [31], incorporated wave directionality in deep waters in a probabilistic manner via the use of a theoretical expression, and used a wave propagation model to transfer the short-term probabilistic information from deep to shallower waters. However, the main differences between these two approaches are focused on:

- the theoretical expression implemented for the incorporation of wave directionality: Chondros [193], and Chondros and Memos [32] used the expression by Pierson et al. [106] that was not dependent on wave period and assumed independence of wave and period from direction, whilst in Malliouri et al. [33] approach the directional spreading function [107], used in a probabilistic expression derived by Malliouri et al. [33], is a function of wave frequency/period. Besides, in their approach, Malliouri et al. assumed dependence of wave height, period and direction.
- the wave propagation model applied: Chondros [193] and Chondros and Memos [32] developed a 2DH highly non-linear Boussinesq-type wave model to propagate sea surface timeseries generated by the probabilistic images by Memos and Tzani [30] in deep waters, thus considering non-linear wave-wave interactions, and hence estimating short-term wave statistics of H/H_m , T/T_m in intermediate and shallow waters. However, Malliouri et al. [33] developed an easier and faster statistical linear wave propagation model to transfer the same probabilistic images from deep to intermediate only waters but neglecting non-linearities in intermediate water depths.
- the output of the analysis: The main interest of the study by Chondros [193] and Chondros and Memos [32] was focused on short-term wave statistics in intermediate and shallow waters, while in the study by Malliouri et al. [33] the accumulation of all

short-term wave statistics for each sea condition considered leads to the long-term wave statistics in intermediate waters.

Therefore, the need to use a linear wave propagation model stemmed from the constraint of non-linear wave propagation models, like Boussinesq-type models, that are significantly more time-consuming than linear models, and also from the fact that the model used should be implemented for a large number of sea states that represent the long-term wave climate. The latter is vital for applying fully probabilistic, reliability or design, methods for coastal structures.

In Figure 3.1 the flowchart of the model by Malliouri et al. [33] applied in the present thesis is depicted consisting of five steps. The first step is optional and could be applied when the computational requirements exceed computer capacities. Continuously, step 1 contains the data reduction technique and the generation of a representative reduced sample of offshore long-term data.

In step 2, the appropriate offshore dimensionless probabilistic image by Memos and Tzani [30] is selected that corresponds to each sea state, based on the value of mean wave height H_m or the standard deviation of surface elevation σ_n etc. Moreover, the multiplication of the coordinates of the offshore dimensionless probabilistic image by T_m and H_m leads to the dimensionalization of the image.

In step 3, for every sea state of the long-term wave data sample, a sample of H and T pairs can be estimated, by randomly generating an integer number of groups of H and T between the limits of each joint class, equal to the new frequency of each class. Then wave directionality is taken into consideration, with the mean wave direction θ_m known a priori, and groups of H, T and θ are obtained.

Then, for every sea state a linear wave propagation model is applied for each individual wave of the dataset characterized by offshore H, T and θ parameters. Therefore, these individual wave parameters are estimated in intermediate waters, and statistical analysis of all individual waves within the sea state can lead to the characteristic statistical parameters of the sea state, i.e. T_m and H_m , H_s , θ_m , in intermediate waters.

In the final step, the accumulation and statistical analysis of all transferred individual waves and sea states in intermediate waters enables the estimation of the long-term joint probability density function of H_m , H_s , θ_m , and also of H, T, and θ .

These five steps will be further analyzed in the next paragraphs.

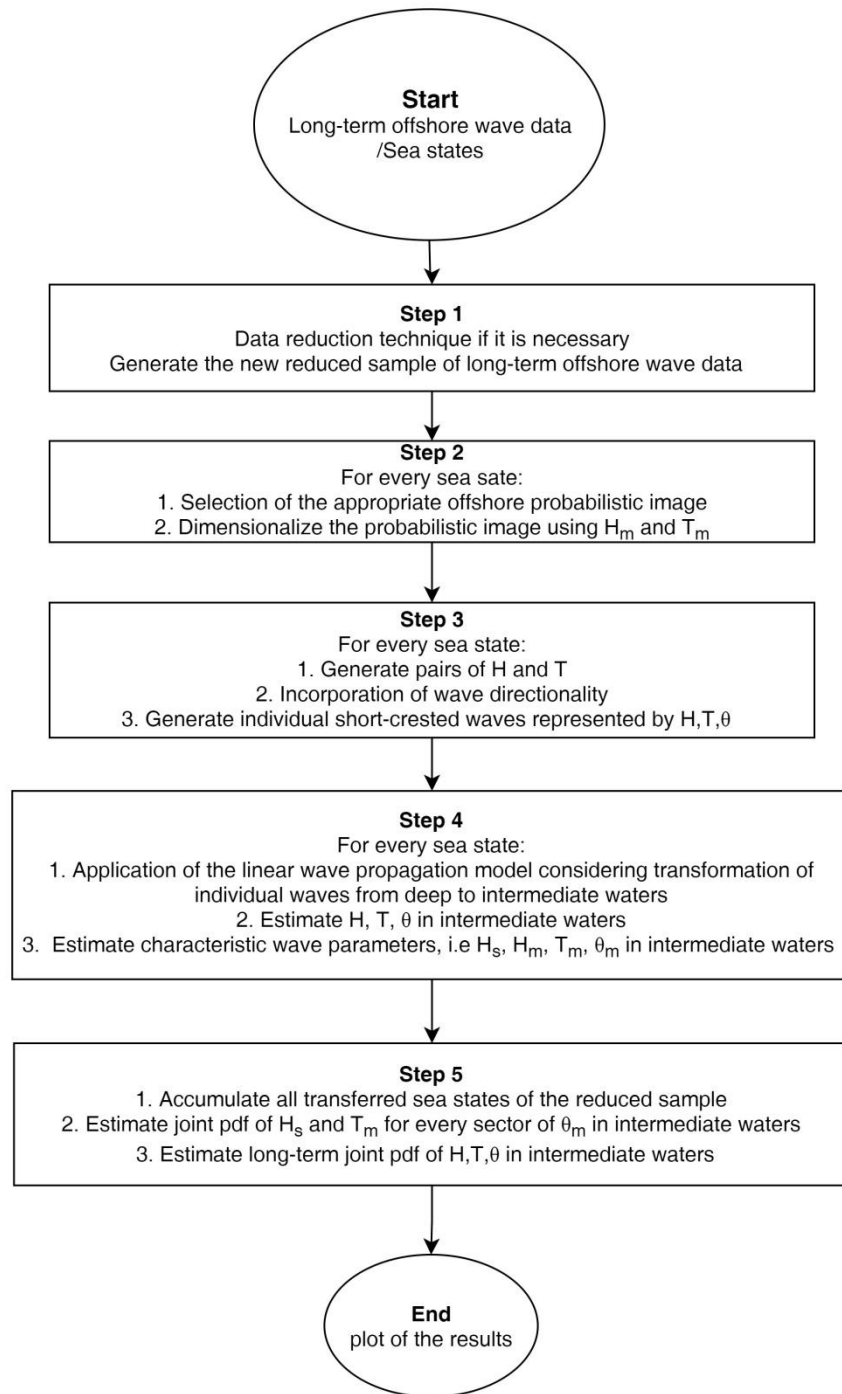


Figure 3.1 Flowchart of the model applied by Malliouri et al. [33]

3.1.1 Data reduction technique

The aim of the data reduction technique is to reduce that long-term wave data and could be applied if the computational requirements by using the total dataset exceed the existing

computer capacities, as noted above. This technique can be summarized in the following five steps:

- (1) Calculation of the total number of sea states in the dataset (denoted by N_d) in deep waters.
- (2) Grouping of the initial data into joint classes of θ_m , H_s , T_m , and estimation of the number of occurrence (frequency) of each joint class.
- (3) Selection of the reduced sum of data of the new dataset (denoted by M_d) to optimize computational demands.
- (4) Calculation of the new frequencies of the joint classes of the new dataset by rounding to the nearest integer the product of the initial frequencies of each joint class by M_d , divided by N_d .
- (5) To obtain the new dataset of H_s , T_m , and θ_m , a sample of M_d sea states can be estimated, by generating an integer number of groups of H_s , T_m , and θ_m between the limits of each joint class, equal to the new frequency of each class (step 4).

The accuracy of the artificial sample depends on the bin size of the joint classes, which should be adequately small, and the total sum of the reduced sample M_d that should be adequately large. These two conditions make the probabilistic distribution, fitted to the random sample generated, able to represent the real population and also avoid elimination of the most extreme and rare events in the artificial sample. Also, it is recommended that the reduced sample M_d should not contain less than 10-15% of the population of the initial sample N_d .

3.1.2 Wave statistics in deep waters

When referring to short- and long-term wave statistics, the joint probability density function of H , T , θ of individual waves within a sea state, which is representative of a time period (e.g. of 3hrs), and the joint probability density function of H_s , T_m , θ_m , which covers a time period of some decades (e.g. of 40 years), are meant respectively.

As it has been mentioned above, the dimensionless short-term probabilistic images by Memos and Tzanis [30] and Tzanis [31] have been used in the present thesis. Table 3.1 has been derived from Table 2.3, and presents the classes of mean wave height H_m assumed to be associated with the same standard deviation of the free surface excursion σ_η and the Pearson correlation coefficient between H and T $r(H,T)$. It is noted that Table 3.1 has been constructed by Malliouri et al. [33] in order that an existing dimensionless probabilistic image in deep waters developed by Memos and Tzanis [30] be attributed to every sea state, represented by

these parameters. More extreme sea states than the last line of the table could also be included but have not been presented here, since they are rarely met in the Mediterranean Sea.

Table 3.1 Classes of H_m assumed to be associated with the same standard deviation of the free surface excursion and correlation coefficient between H and T [33]

Standard Deviation σ_η (m)	Correlation Coefficient $r(H,T)$	Mean Wave Height H_m (m)
0.5	0.266	[0.1 - 1.062)
0.6	0.383	[1.062 - 1.185)
0.7	0.485	[1.185 - 1.727)
1.0	0.495	[1.727 - 2.971)
1.5	0.570	[2.971 - 4.368)

Similarly to Chondros [193], digitization of iso-probability density curves yields the coordinates of each pair of H/H_m and T/T_m along with their respective probability density function. A sufficiently low discretization step $d(T/T_m)=d(H/H_m)=0.1$ is then chosen in order that relative frequency $fr\left(\frac{T}{T_m}, \frac{H}{H_m}\right)$ be calculated at each node (Figure 3.2):

$$fr\left(\frac{T}{T_m}, \frac{H}{H_m}\right) \cong f_{\frac{T}{T_m}, \frac{H}{H_m}}\left(\frac{T}{T_m}, \frac{H}{H_m}\right) d\left(\frac{T}{T_m}\right) d\left(\frac{H}{H_m}\right) \quad (3.1)$$

where $f_{\frac{T}{T_m}, \frac{H}{H_m}}$ is the joint pdf of $\frac{T}{T_m}, \frac{H}{H_m}$.

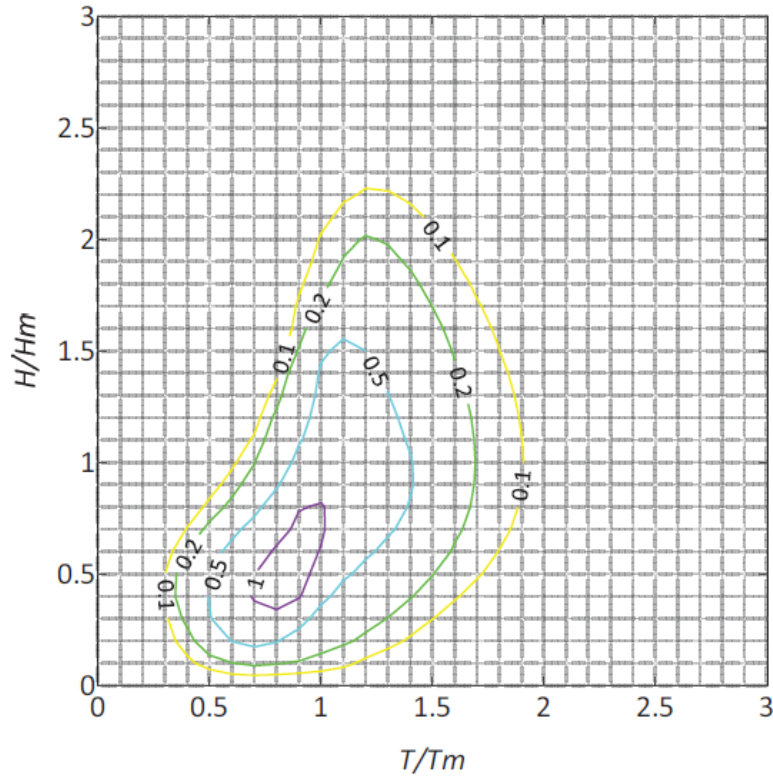


Figure 3.2 Grid of probabilistic calculation (step $d(T/T_m)=d(H/H_m)=0.1$) [193]

Then, an appropriate selection of an adequately large number N (of the order of a few thousands) of individual waves is selected to represent a probabilistic image by Memos and Tzani [30], and the number of occurrence attributed to the (i,j) cell of the Figure 3.2 is estimated by rounding to the nearest integer the multiplication product as of the cell's frequency $f_{i,j}$ by N , as follows:

$$n_{i,j} = \text{round}(f_{i,j}N) \quad (3.2)$$

To obtain the sample of individual waves within a sea state, $n_{i,j}$ pairs of H and T can be estimated for every cell (i,j) , by generating $n_{i,j}$ uniformly distributed random numbers between the limits of i -th class for T , and $n_{i,j}$ uniformly distributed random numbers between the limits of j -th class for H .

3.1.3 Consideration of wave directionality in deep waters

In this section, the methodology by Malliouri et al. [33] is presented aiming at associating each individual wave within a sea state with a certain azimuth angle of propagation. As it is aforementioned, the mean wave direction for each sea state is known.

It is a common practice to consider wave directionality in a spectral wave analysis, as this is in accordance with the definition of wave directionality. However, the need to consider wave directional spreading in an individual wave analysis often arises. To proceed with this consideration, the following assumptions should be made with respect to every sea state:

- The classes of higher values of H tend to have directions closer to θ_m ; that is, they show less directional spread, suggesting that H and θ are not independent. This assumption is in agreement with Tucker [37], who proved that the larger values of the magnitude of the resultant water particle velocity under directional waves show less directional spread around θ_m , compared with lower values.

- Since the integration of $D(f, \theta)$ from $-\pi$ to π with respect to θ is unity, $D(f, \theta)$ could be used for the estimation of the conditional probability distribution of θ for given f , or equivalently T . This also suggests that the number of waves should be large enough in order that all waves within a certain T -rank would cover the whole range of wave directions determined by the directional spreading function $D(f, \theta)$, associated to the T -rank.

- Specifically, this can be accomplished by estimating the range of θ that corresponds to each class of H for a given T . This range can be computed, by, firstly, arranging all classes of H for a given T in decreasing order of H , and, then, via the following equation [33]:

$$\int_{\theta_m - x_j}^{\theta_m + x_j} D(f_i, \theta) d\theta = \sum_{n=1}^j \text{freq}(T_i, H_j) / N_i \quad (3.3)$$

where $\text{freq}(T_i, H_j)$ is the frequency (number of occurrence) of the bivariate class of the i -th T and j -th H and N_i is the total number of waves of the i -th class of T for every H . Besides, in the above equation, in which the unknown variable is x_j , the j -th class of H is associated with a certain range of θ , i.e. $[\theta_m - x_j, \theta_m + x_j]$, when the i -th class of f , or equivalently of T , is considered fixed. It is noted that the right part of the above equation determines the cumulative probability of the j -th class of H based on the ranking position of the H classes in

decreasing order from the H class central value, and the left part determines the probability referred to this unique range of θ .

-Therefore, for a fixed class of T, each class of H is combined with a certain range of θ . Then, each pair of T and H of an individual wave in this specific sea state corresponds to a random value of θ within this range.

The validity of the above assumptions can be concluded by checking whether the histogram of θ in a sea state is symmetric around θ_m and by comparing the measured θ_m with the estimated θ_m , computed as the statistical mean direction of all individual waves considered. As can be noticed in Figure 3.3, the histogram of θ is approximately symmetric around θ_m and the estimated θ_m is satisfactorily close to the measured θ_m in both sea states with different measured θ_m in deep waters.

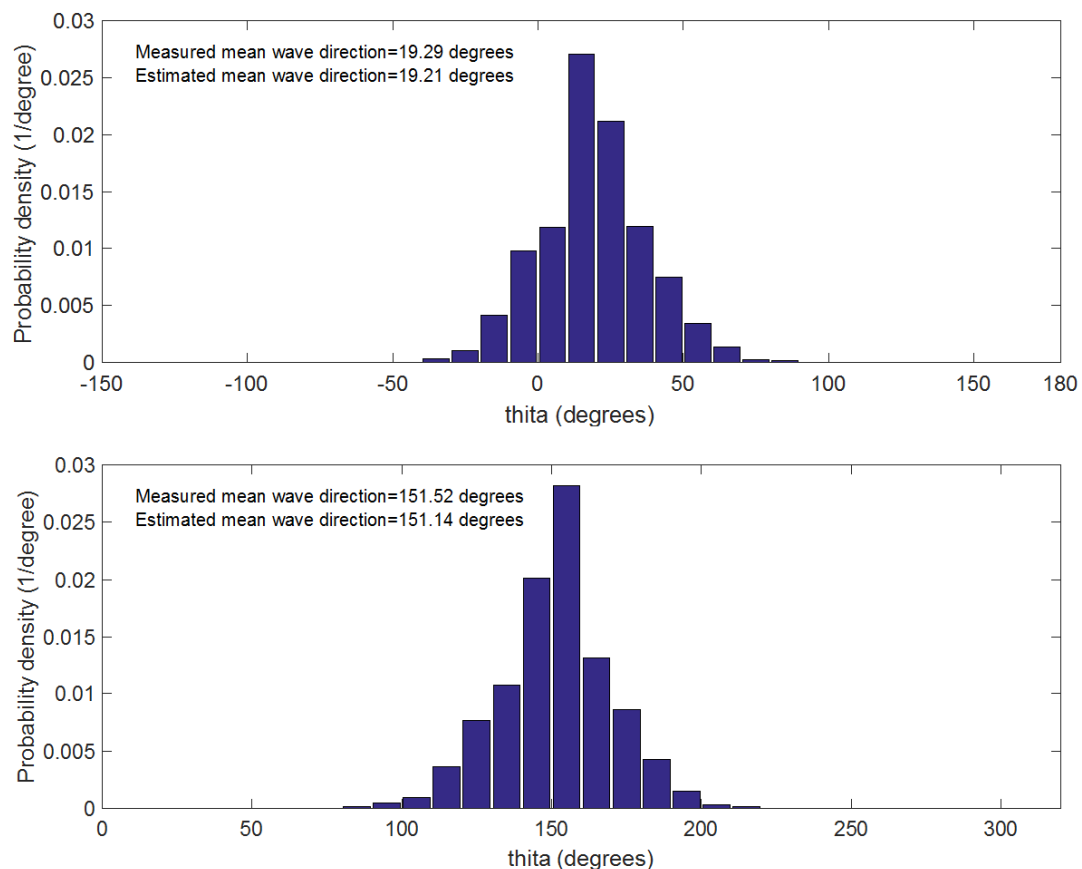


Figure 3.3 Estimated histograms of wave direction in two sea states in deep waters with different [33]

3.1.4 Transforming wave statistics from deep to intermediate waters

The height of each individual wave is modified as the latter propagates from deep into shallower waters, while the wave period is assumed to be constant according to linear wave theory. In the present study, four wave processes have been taken into account; wave shoaling, wave refraction, wave breaking, and wave reforming after breaking. These processes are considered for all individual waves, since H , T , and θ of each individual wave within a sea state are known in deep waters, derived from the aforementioned methodology. Moreover, the coastal slope is considered uniform and equal to a representative mean bed slope. In this step, an individual wave shoaling and a refraction process were applied, and a wave breaking criterion was adopted. Hence, Snell's law was used here concerning the refraction process, the shoaling process selected is described in terms of Stokes first order wave theory, while the breaking wave height associated to each individual wave height H is determined by the semi-empirical expression by Komar and Gaughan [38] derived from linear wave theory:

$$\frac{H_b}{H_o} = 0.56 \left(\frac{H_o}{L_o} \right)^{-1/5} \quad (3.4)$$

where H_o is the individual wave height in deep waters, H_b is the individual breaking wave height, and L_o is the individual wave length in deep waters. Regarding the depth of each individual wave breaking, this is estimated by the expression of Weggel [39] for the breaker index γ_b , based on laboratory data on monochromatic wave breaking on smooth, plane slopes, i.e.:

$$\gamma_b = \frac{H_b}{d_b} = b(m) - a(m) \frac{H_b}{gT^2} \quad (3.5)$$

where

$$a(m) = 43.8 [1 - \exp(-19m)] \quad (3.6)$$

$$b(m) = \frac{1.56}{1 + \exp(-19.5m)} \quad (3.7)$$

where: d_b is the depth at breaking, m is the bed slope, and g is the gravitational acceleration. Referring to H_b and d_b , it is noted that a number of expressions (e.g. [194]; [195]; [196]) have been proposed for their estimation, but most of these equations are hampered by two obstacles. First, the breaker depth is usually required to compute its wave breaking height, and vice versa, and second, the equations consider either the deep water wave height to wavelength ratio or the sea bed slope, but not both [197].

The concept of individual wave breaking and evolution before, in, and after the surf zone, adopted here, is described in the flowchart presented in Figure 3.4. According to this, when wave breaking occurs, waves are then examined whether they are plunging or spilling breaking waves. This distinction between plunging and spilling breakers is made by considering the surf similarity parameter ξ_o , based on the offshore wave height and deep water wave length [40]. In the case of plunging breakers, waves lose their wave forms totally after breaking, thus waves are then excluded from the total set of H and T data. Regarding the spilling breakers, the concept of wave evolution in the surf zone is based on the decay of the wave energy in the surf zone and the equivalence between the energy decay in a spilling breaking wave and that of a hydraulic jump [41]. In particular, Horikawa and Kuo [42] conducted laboratory tests on breaking waves and determined the existence of a stable energy flux, which defines a state at which waves no longer break. Using linear wave theory and assuming that the stable wave height H_{stable} is a linear function of water depth d , i.e.

$$H_{stable} = \Gamma d \quad (3.8)$$

where Γ is a dimensionless coefficient, Dally et al. [43] determined that Γ is 0.4 for achieving minimum error to the data of Horikawa and Kuo [42]. Therefore, the wave evolution in the surf zone after an incipient spilling breaking is based on H_{stable} . As for wave period, it remains equal to the corresponding one in deep waters.

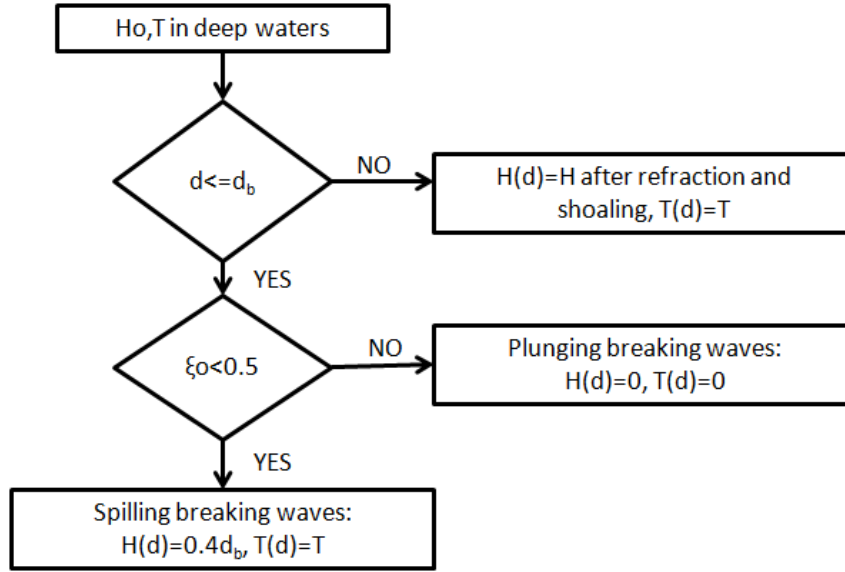


Figure 3.4 Description of individual wave evolution through the surf zone adopted [33]

3.1.5 Derivation of long-term wave statistics in intermediate waters

Long-term wave statistics could be defined those described by the characteristic wave parameters, i.e. T_m , H_s , θ_m , and also by the direct loading parameters H , T , θ , derived from the statistical analysis of wave data accumulated over several years. In case of lack of those data at the location of interest (this is often in intermediate waters, when referring to coastal structures), wave data observed in deep waters could be used and transferred at this location using linear or non-linear wave propagation models.

As for the long-term joint distribution of the characteristic parameters, i.e. T_m , H_s , θ_m in intermediate waters, a simple and proper manner to derive this three-parameters' joint distribution is to apply the conditional model described previously, using the transferred long-term wave data of T_m , H_s , θ_m at this location.

As far as the calculation of the long-term joint distribution of the direct loading parameters H and T is concerned, the main concept is that the short-term pdf $f_{\text{short}}(H)$ in Eq. 2.140 by Battjes [36] can be replaced by the joint short-term pdf $f_{\text{short}}(T, H)$, presented in the following equation:

$$f_{\text{long}}(T, H) = \frac{\iint f_{\text{short}}(T, H) \cdot f_{\text{long}}(T_m, H_s) \cdot N \, dH_s \, dT_m}{\iint N \cdot f_{\text{long}}(T_m, H_s) \, dH_s \, dT_m} \quad (3.9)$$

where $f_{\text{short}}(T,H)$ is the short-term joint probability density function of T and H , N is the average number of waves in each short-term sea state, which is assumed to be constant, and $f_{\text{long}}(T_m, H_s)$ corresponds to the long-term joint pdf of T_m and H_s . This can be proved via the following process:

The number of occurrence of the cell (i,j) of the short-term wave statistics associated to the i -th class of wave period, T_i , and the j -th class of the wave height, H_j , in the k -th sea state, for adequately small ΔT and ΔH is approximately calculated as:

$$n_{ijk}(T_i, H_j) = f_{\text{kshort}}(T_i, H_j) \cdot \Delta T \cdot \Delta H \cdot N_k \quad (3.10)$$

where N_k represents the total number of waves in the k -th sea state, ΔT and ΔH are the bin widths of the classes of T and H respectively.

The number of occurrences of the k -th sea state, for adequately small ΔT_m and ΔH_s , is estimated as:

$$m_k(T_m, H_s) = f_{\text{klong}}(T_m, H_s) \cdot \Delta T_m \cdot \Delta H_s \cdot M \quad (3.11)$$

where M is the total number of sea states, $f_{\text{klong}}(T_m, H_s)$ represents the long-term joint pdf of T_m and H_s at the k -th sea state, and ΔH_s , ΔT_m are the bin widths of the classes of H_s and T_m respectively.

The total number of occurrences of T_i and H_j , taking into consideration the number of occurrences of the k -th sea state in the long-term wave statistics, is computed as:

$$N_{ijk}(T_i, H_j) = n_{ijk}(T_i, H_j) \cdot m_k(T_m, H_s) \quad (3.12)$$

$$= \overbrace{f_{\text{kshort}}(T_i, H_j) \cdot \Delta T \cdot \Delta H \cdot N_k}^{\text{number of occurrence of } T_i \text{ and } H_j \text{ in the sea state } k} \cdot \overbrace{f_{\text{klong}}(T_m, H_s) \cdot \Delta T_m \cdot \Delta H_s \cdot M}^{\text{number of occurrence of sea state } k}$$

Subsequently, the total number of occurrences of T_i and H_j , taking into consideration the total number of sea states, M , is computed as:

$$N_{ijtotal} = \left\{ \begin{array}{l} f_{1short}(T_i, H_j) \cdot \Delta T \cdot \Delta H \cdot N_1 \cdot f_{1long}(T_m, H_s) \cdot \Delta T_m \cdot \Delta H_s \cdot M \\ + f_{2short}(T_i, H_j) \cdot \Delta T \cdot \Delta H \cdot N_2 \cdot f_{2long}(T_m, H_s) \cdot \Delta T_m \cdot \Delta H_s \cdot M \\ \dots\dots\dots \\ \dots\dots\dots \\ \dots\dots\dots \\ + f_{Mshort}(T_i, H_j) \cdot \Delta T \cdot \Delta H \cdot N_M \cdot f_{Mlong}(T_m, H_s) \cdot \Delta T_m \cdot \Delta H_s \cdot M \end{array} \right\} \quad (3.13)$$

The total number of individual waves that comprise the total number of sea states M , is given by the following equation:

$$N_{total} = \left\{ \begin{array}{l} N_1 \cdot f_{1long}(T_m, H_s) \cdot \Delta T_m \cdot \Delta H_s \cdot M \\ + N_2 \cdot f_{2long}(T_m, H_s) \cdot \Delta T_m \cdot \Delta H_s \cdot M \\ \dots\dots\dots \\ \dots\dots\dots \\ \dots\dots\dots \\ + N_M \cdot f_{Mlong}(T_m, H_s) \cdot \Delta T_m \cdot \Delta H_s \cdot M \end{array} \right\} \quad (3.14)$$

The long-term relative frequency of T_i and H_j is given by the following equation:

$$fr_{long}(T_i, H_j) = \frac{N_{ijtotal}}{N_{total}} \quad (3.15)$$

and the long-term joint pdf of T_i and H_j is then expressed as:

$$f_{long}(T_i, H_j) = \frac{fr_{long}(T_i, H_j)}{\Delta T \cdot \Delta H} = \frac{N_{ijtotal}}{N_{total} \cdot \Delta T \cdot \Delta H} \quad (3.16)$$

By substituting Eqs 3.13 and 3.14 in Eq. 3.16 and deleting the short- and long-term spatial and time steps, i.e. ΔH , ΔH_s and ΔT , ΔT_m (since they all appear in the numerator and the denominator of the fraction in the second part of Eq. 3.16), the following relation is derived:

$$f_{\text{long}}(T_i, H_j) = \frac{f_{\text{1short}}(T_i, H_j) \cdot N_1 \cdot f_{\text{1long}}(T_m, H_s) + \dots + f_{\text{Mshort}}(T_i, H_j) \cdot N_M \cdot f_{\text{Mlong}}(T_m, H_s)}{N_1 \cdot f_{\text{1long}}(T_m, H_s) + \dots + N_M \cdot f_{\text{Mlong}}(T_m, H_s)} \quad (3.17)$$

Eq. 3.17 can also be written as:

$$f_{\text{long}}(T_i, H_j) = \frac{\sum_{k=1}^M f_{\text{kshort}}(T_i, H_j) \cdot N_k \cdot f_{\text{klong}}(T_m, H_s)}{\sum_{k=1}^M N_k \cdot f_{\text{klong}}(T_m, H_s)} \quad (3.18)$$

which is similar to the modified equation of Battjes, i.e. Eq. 3.9. However, in Eq. 3.18, the total number of waves in each sea state N_k is not assumed to be constant. If the latter is regarded as constant, as in our case, Eqs 3.9 and 3.18 are equivalent.

In a similar way, regarding the long-term joint distribution of H , T , and θ , Eq. 3.9 can be replaced by:

$$f_{\text{long}}(T, H, \theta) = \frac{\iiint f_{\text{short}}(T, H, \theta) f_{\text{long}}(T_m, H_s, \theta_m) N dH_s dT_m d\theta_m}{\iiint N f_{\text{long}}(T_m, H_s, \theta_m) dH_s dT_m d\theta_m} \quad (3.19)$$

where $f_{\text{short}}(T, H, \theta)$ is the short-term joint probability density function of T , H , and θ , N is the average number of waves in each short-term sea state, assumed to be given, and $f_{\text{long}}(T_m, H_s, \theta_m)$ corresponds to the long-term joint pdf of T_m , H_s , and θ_m .

3.1.6 Examples of application

3.1.6.1 Input data

The aforementioned methodology that will be presented has been applied [33] to measured data of relative frequencies of T_m , H_s , and θ_m , obtained from 3 oceanographic buoys that belong to the POSEIDON Marine Monitoring Network operating under the responsibility of the Hellenic Centre of Marine Research (HCMR), see Soukissian and Chronis [44], Soukissian et al. [45]. These buoys were located at three locations in deep waters, i.e.: (37.51 °N, 25.46 °E) in the central Aegean off Mykonos island; (39.96 °N, 24.72 °E) in the northern Aegean off Athos; and (36.25 °N, 25.49 °E) in the southern Aegean off Santorini island. These locations referred to hereinafter as Station M, Station A, and Station S, respectively, are depicted in Figure 3.5.



Figure 3.5 The locations of the three oceanographic stations in the Aegean Sea, Greece

Furthermore, the interval between successive measurements is 3 h and the wave measurements cover the period from 1.1.2000 to 12.31.2011. It is noted that, in principle, a long-term analysis requires longer time series that must cover more than few decades.

However, often the data are extrapolated to probabilities beyond the record length, i.e. 2-3 times the record length [1].

Regarding the wave measurements at M station, each pair of T_m and H_s represents a sea state, while the total number of sea states is 24946. The scatter diagram of T_m and H_s is presented in Figure 3.6.

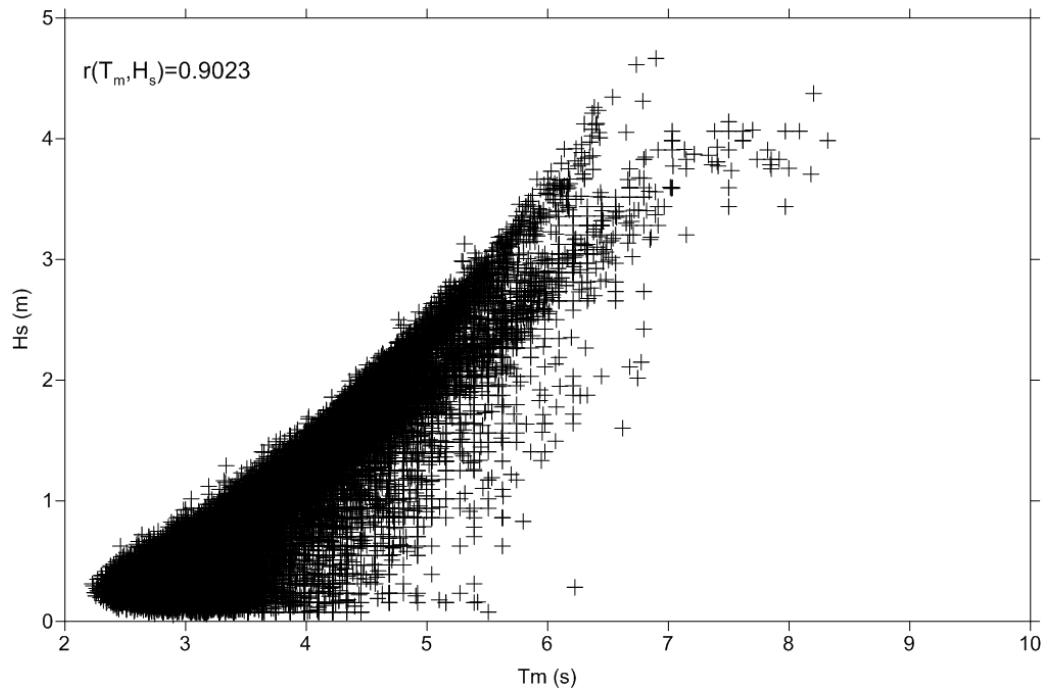


Figure 3.6 Measured H_s and T_m at M station (2000-2011) [44]; [45]; [33]

The correlation coefficient $r(T_m, H_s)$ between T_m and H_s is equal to 0.9023, suggesting a strong correlation. This was expected, since only wind waves and not swell have been considered. The exclusion of swell was made directly by the buoy. Therefore, there was no need to apply another swell exclusion criterion to this set of data.

3.1.6.2 Data reduction based on a statistical technique

It is noted that the dataset was organized in classes of equal width (i.e. $\Delta H_s=0.25\text{m}$, $\Delta T_m=0.25\text{s}$, $\Delta\theta_m=20^\circ$), and then the class frequencies were modified in order that the total sum of the data be reduced from 24,946 to 1500 sea states, by maintaining, though, as much as possible the relative frequency of each class. The methodology developed here, in

compliance with the statistical method named “Stratified random Sampling” [198], for producing the reduced dataset of 1500 sea states, is summarised in the following steps:

- 1) Calculation of the total sum of sea states of the initial data set (e.g. 24,946 sea states for Station M);
- 2) Grouping of the initial data set into joint classes of T_m , H_s , and θ_m , and estimation of the frequency of each joint class;
- 3) Selection of the reduced sum of sea states of the new dataset;
- 4) Calculation of the new frequencies of the joint classes of the new dataset by rounding to the nearest integer the product of the initial frequencies of each joint class by the reduced sum of data (i.e. 1500) divided by the initial sum of sea states (i.e. 24,946);
- 5) To obtain the new dataset of T_m , H_s , and θ_m , a sample of 1500 sea states was estimated, by generating a number of groups of T_m , H_s , and θ_m , between the limits of each class, linearly related to the frequency of each joint class.

It is noted that the reduced total sum of sea states of the new dataset, selected in step 3 should be satisfactorily high. However, due to the rounding process, described in step 4, the low initial frequencies of the higher, and therefore, rare H_s may get zero values in the new dataset. Nevertheless, this shortcoming may be overlooked, if the fitted H_s pdf to the new dataset is representative of the initial data set. Therefore, this requirement should be checked before the selection of the reduced sum of sea states of the new dataset in step 3. This process has been adopted here and in Figure 3.7 the best fitted distribution of H_s to the new dataset is compared against the one derived from the initial dataset, estimated in deep waters and at the depth of 6m. As it can be seen from Figure 3.7, the dataset reduced by the technique described previously can form a solid framework where best-fit exercises can be credibly developed.

In Table 3.2, the Euclidean distance between the best fitted pdf of H_s derived from the original dataset and the initial data, as well as the Euclidean distance between the best fitted pdf of H_s derived from the new dataset and the initial data, have been estimated and compared. From the last column of Table 2, it is observed that the best fitted pdf of H_s derived from the new dataset can satisfactorily represent the initial data, since in deep waters its Euclidean distance from the initial dataset is improved, and at the depth of 6m the Euclidean distance is slightly higher compared against the best fitted pdf to the initial dataset.

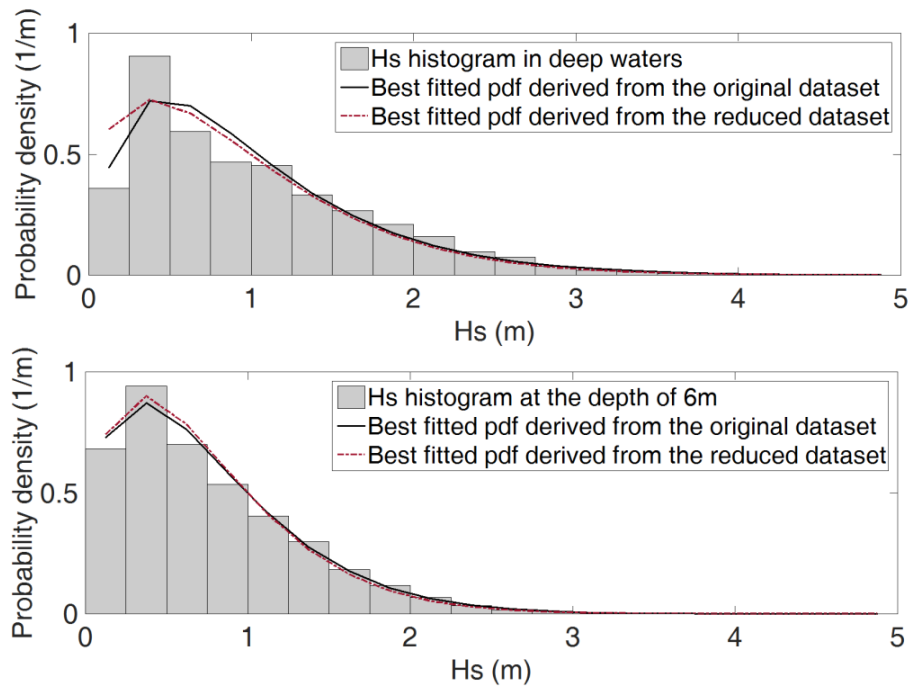


Figure 3.7 Comparison of the best fitted distribution of H_s to the new data set against the one derived from the initial dataset, estimated in deep waters (up) and at a depth of 6m (below) at Station M [33]

Table 3.2 Comparison of the Euclidean distances between the best fitted pdf of H_s derived from both the reduced data and the initial data at Station M [33]

Depth (m)	Euclidean distance D^2		Relative difference [(2)-(1)]/(1)
	Initial data	Reduced data	
	(1)	(2)	
140	0.00186	0.00169	-0.091
6	0.00091	0.00098	0.077

In this way, the reduced dataset can satisfactorily substitute the extensive raw data. The new sample generated is depicted in Figure 3.8. The correlation coefficient $r(T_m, H_s)$ in the new dataset, is equal to 0.8999, i.e. very close to that of the raw data. This new data set in deep waters has been used as input data in the present methodology. Therefore, the computational demands have been significantly reduced (by almost 17 times) without altering to a great extent the information on the relative frequencies of the grouped raw data.

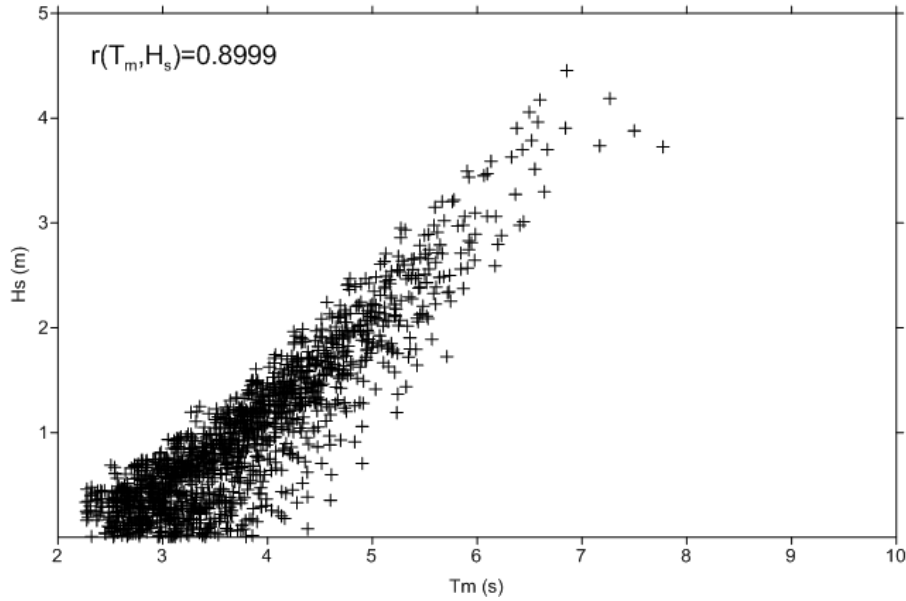


Figure 3.8 Sample of the new dataset of 1500 sea states (T_m and H_s) for Station M [33]

It is highly recommended that when such a data reduction technique has to be applied for a reliability analysis of coastal structures to reduce computational cost, a relatively high threshold should be applied to filter the most significant sea states that should be transferred to the structure's location (see section 3.3.5.2).

3.1.6.3 Results and discussion

Deep waters

Regarding the most appropriate marginal distribution for H_s in deep waters, three candidate distributions, namely the Weibull, the Lognormal, and the Gamma pdfs, have been examined aiming at selecting the one that best represents the histogram of H_s . These candidate distributions for H_s along with the corresponding histogram are depicted in Figure 3.9. In order to select the most appropriate marginal distribution for H_s , two goodness of fit measures have been estimated, the Euclidean distance between each marginal distribution for H_s and H_s data, and the Euclidean distance between the joint probability distribution of T_m and H_s and T_m and H_s joint data. As it has been already mentioned, the joint probability distribution of T_m and H_s is associated with the marginal distribution for H_s and the conditional distribution for $T_m|H_s$, which follows a Lognormal distribution. These two measures of goodness of fit are presented in Table 3.3. The parameters of the best fitted pdf to H_s data for each Station are presented in Table 3.4.

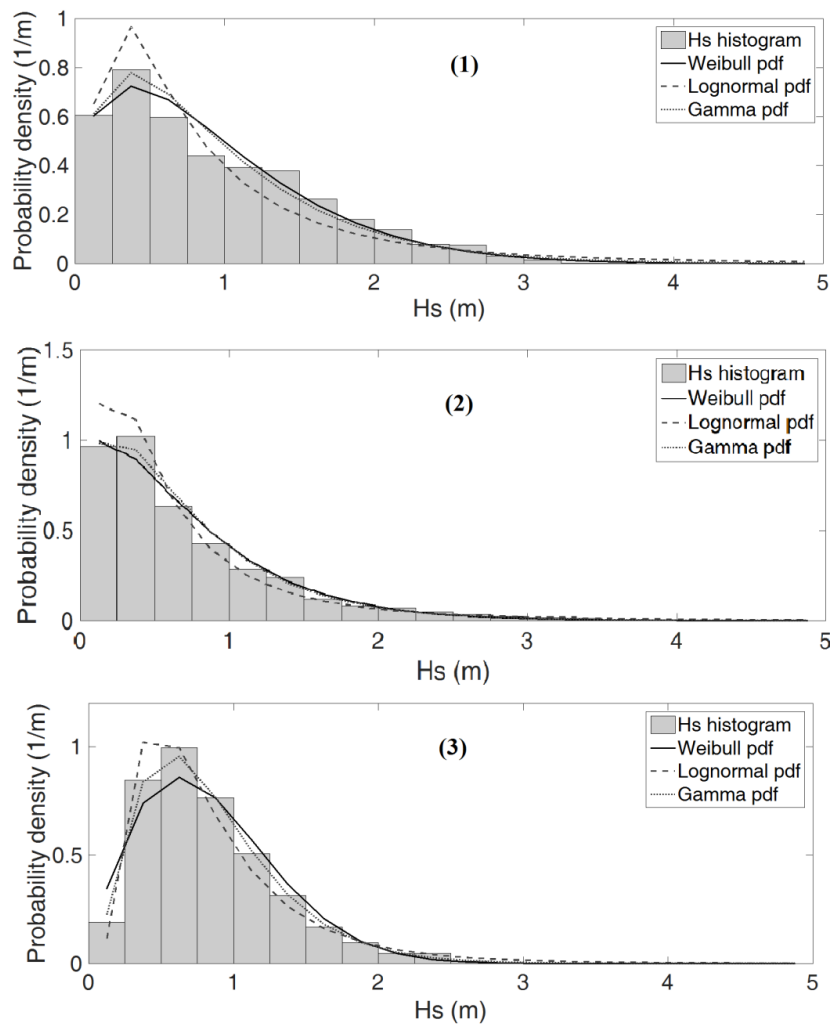


Figure 3.9 Fitting of the candidate marginal distributions to the histogram of H_s data in deep waters for Station M (1), Station A (2), and Station S (3) [33]

Table 3.3 Measures of goodness of fit of the candidate marginal distributions for H_s and the corresponding conditional model in deep waters using data from stations M, A, and S [33]

Data Source	Candidate pdf for H_s	Euclidean distance D^2 of $f(H_s)$	Conditional pdf for $T_m H_s$	Total Euclidean distance
Station M	Weibull	0.0019	Lognormal	0.0013
	Lognormal	0.0056	Lognormal	0.0021
	Gamma	0.0020	Lognormal	0.0013
Station A	Weibull	0.0018	Lognormal	0.0008
	Lognormal	0.0046	Lognormal	0.0014
	Gamma	0.0012	Lognormal	0.0007
Station S	Weibull	0.0039	Lognormal	0.0022

Lognormal	0.0033	Lognormal	0.0020
Gamma	0.0022	Lognormal	0.0015

Table 3.4 Estimated parameters of the best fitted marginal distribution for H_s in deep waters using data from stations M, A, and S [33]

Data Source	Best fitted marginal distribution for H_s	Shape parameter	Scale parameter
Station M	Weibull pdf	1.3517	1.0122
Station A	Gamma pdf	1.4243	0.4957
Station S	Gamma pdf	3.0138	0.2789

As it is shown in Figure 3.9 and Table 3.3, the joint distributions of T_m and H_s that best represent the T_m and H_s data are derived from the conditional model associated with combinations of a Weibull pdf for H_s for Station M and a Gamma distribution for H_s for the other two Stations and a Lognormal conditional distribution for $T_m|H_s$, since they have the lowest Euclidean distance compared to the other distributions tested. The joint pdfs of T_m and H_s are presented in Figure 3.10.

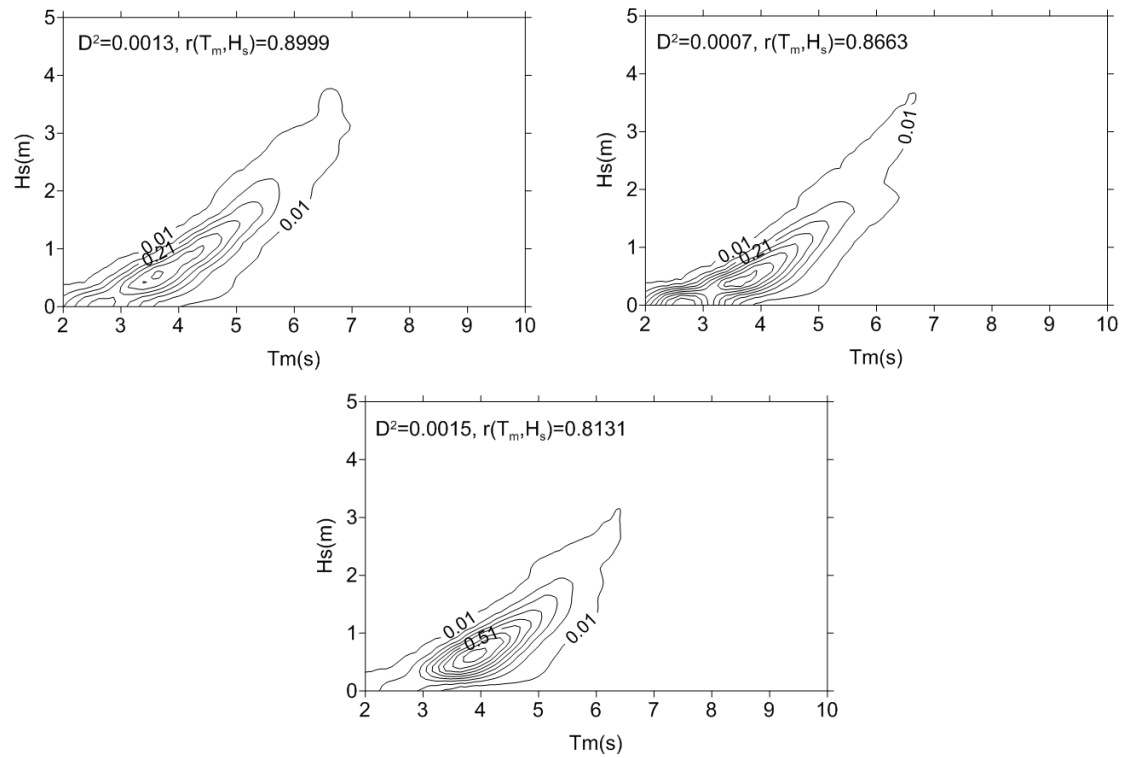


Figure 3.10 Joint pdf of T_m and H_s in deep waters estimated by applying the Conditional model for Station M (up left), Station A (up right), and Station S (below) - $0.1 \text{ m}^{-1}\text{s}^{-1}$ contour step [33]

By applying the modified Battjes approach, the long-term joint distribution of T and H in deep waters is obtained for each Station; see Figure 3.11. The correlation coefficient between T and H is smaller than that of T_m and H_s at the same location for the three Stations. This indicates that the correlation between T_m and H_s is greater than the correlation between H and T .

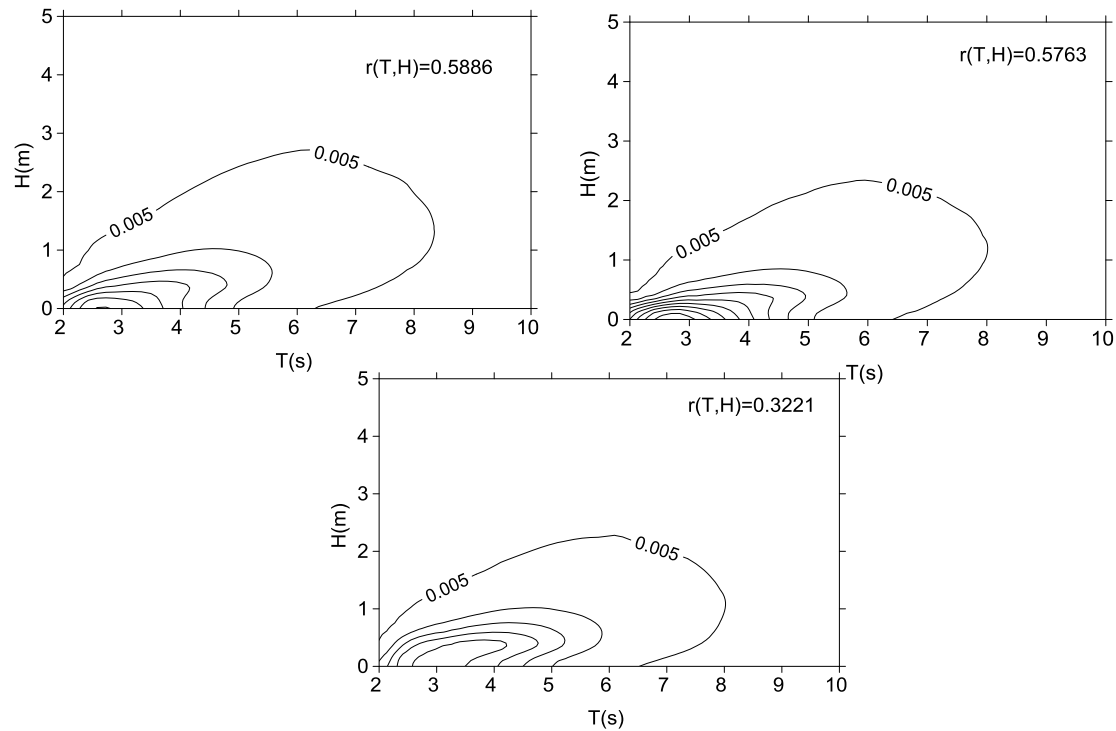


Figure 3.11 Long-term joint pdf of T and H in deep waters for Station M (up left), Station A (up right), and Station S (below) - $0.1\text{m}^{-1}\text{s}^{-1}$ contour step [33]

Intermediate waters

As it has been noted above, the long-term and short-term wave statistics in deep waters have been used in order that the long-term wave statistics be estimated in intermediate waters. In this section, the long-term wave statistics are estimated at the depth of 6m following the aforementioned methodology. This water depth corresponds to intermediate waters with respect to the wave length associated to the statistically mean T_m .

Regarding the most appropriate marginal distribution for H_s at the depth of 6m, the same three candidate marginal distributions presented above have been examined, in similarity to deep waters. The candidate marginal distributions for H_s and the corresponding histogram at the depth of 6m are depicted in Figure 3.12. The two measures of goodness of fit for each marginal and bivariate model are presented in Table 3.5.

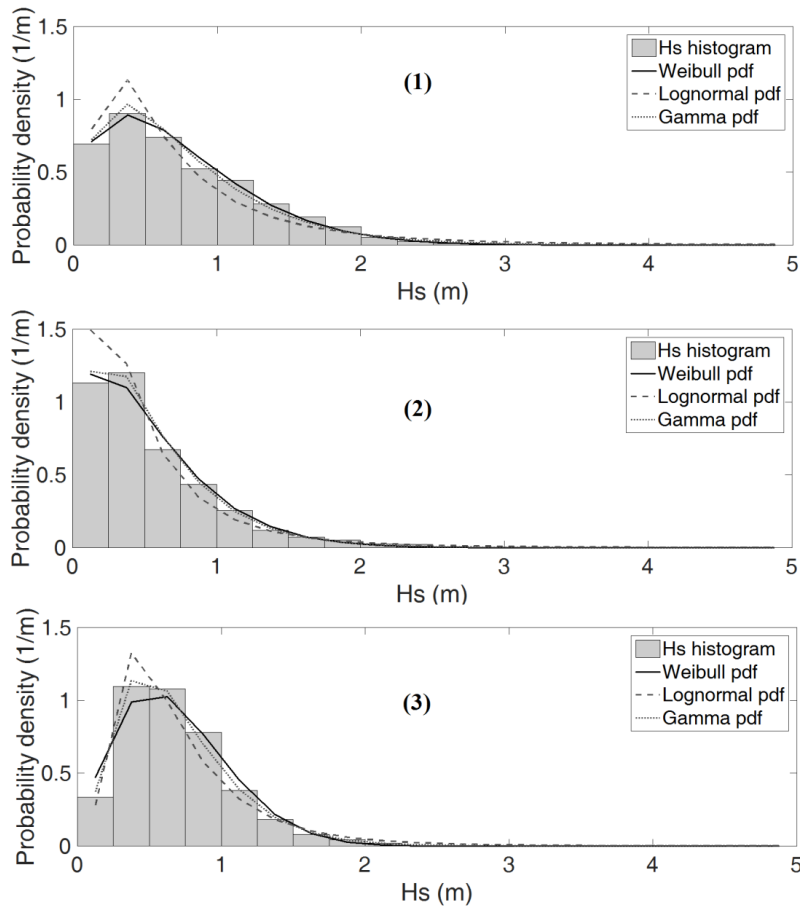


Figure 3.12 Fitting of the candidate marginal distributions to the histogram of H_s data at the depth of 6m for Station M (1), Station A (2), and Station S (3) [33]

Table 3.5 Measures of goodness of fit of the candidate marginal distributions for H_s and the corresponding conditional model at the depth of 6m using data from Stations M, A, and S [33]

Data Source	Candidate pdf for H_s	Euclidean distance D^2 of $f(H_s)$	Conditional pdf for $T_m H_s$	Total Euclidean distance
Station M	Weibull	0.0009	Lognormal	0.0016
	Lognormal	0.0068	Lognormal	0.0026
	Gamma	0.0013	Lognormal	0.0017
Station A	Weibull	0.0033	Lognormal	0.0021
	Lognormal	0.0127	Lognormal	0.0035
	Gamma	0.0022	Lognormal	0.0020
Station S	Weibull	0.0026	Lognormal	0.0017
	Lognormal	0.0066	Lognormal	0.0023
	Gamma	0.0007	Lognormal	0.0014

As it is shown in Figure 3.12 and Table 3.5, the joint distributions of T_m and H_s that best represent the T_m and H_s data for all three Stations are derived from the conditional model associated with combinations of a Weibull pdf for H_s for Station M and a Gamma pdf for H_s for the other two Stations and a Lognormal conditional distribution for $T_m|H_s$, in similarity with the best fitted pdfs for H_s in deep waters. The parameters of the best fitted pdf to H_s data for each Station are presented in Table 3.6. The joint pdfs of T_m and H_s for each Station are presented in Figure 3.13.

Table 3.6 Estimated parameters of the best fitted marginal distribution for H_s at the depth of 6m using data from Stations M, A, and S [33]

Data Source	Best fitted marginal distribution for H_s	Shape parameter	Scale parameter
Station M	Weibull pdf	1.4150	0.8159
Station A	Gamma pdf	1.7476	0.2857
Station S	Gamma pdf	2.9828	0.2321

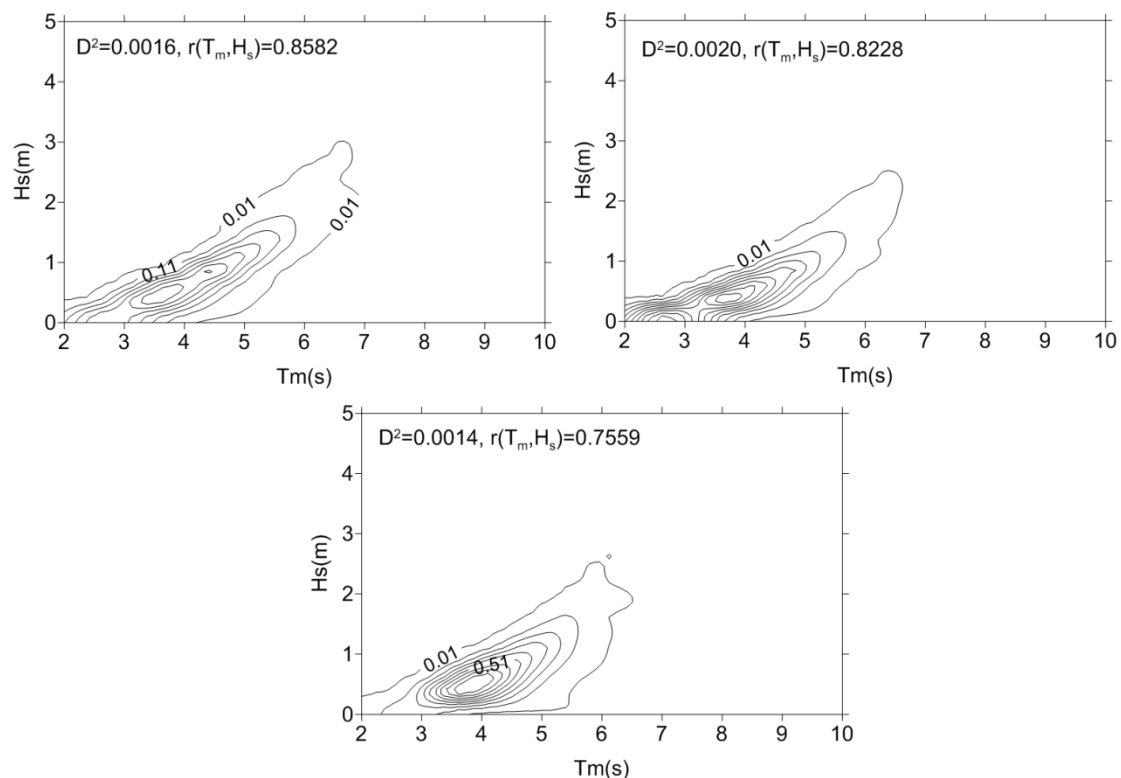


Figure 3.13 Joint pdf of T_m and H_s at the depth of 6m estimated by applying the Conditional model for Station M (up left), Station A (up right), and Station S (below) - $0.1 \text{ m}^{-1}\text{s}^{-1}$ contour step [33]

The joint long-term distribution of T and H at 6m depth for each Station, computed by applying the modified Battjes approach, is depicted in Figure 3.14. The correlation coefficient between T and H is again smaller than that of T_m and H_s at the same location for the three Stations in accordance with deep waters.

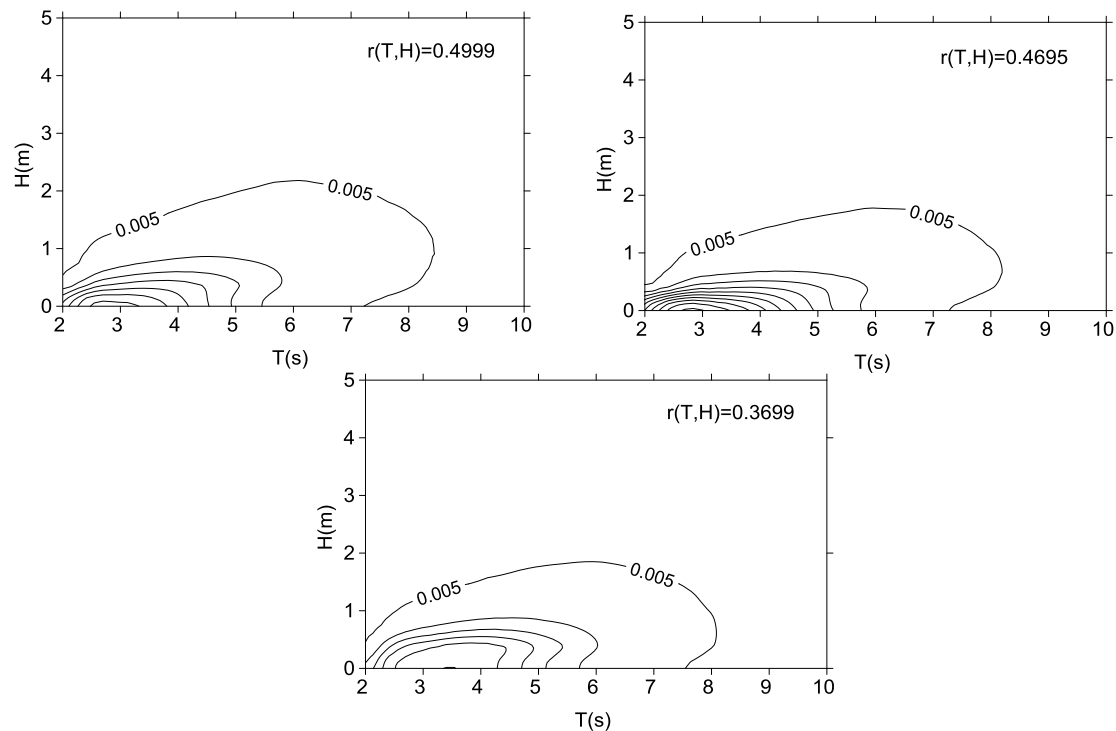


Figure 3.14 Long-term joint pdf of T and H at the depth of 6m for Station M (up left), Station A (up right), and Station S (below) - $0.1 \text{ m}^{-1}\text{s}^{-1}$ contour step [33]

It is noted that the long-term joint pdfs of T_m and H_s and those of T and H presented in the above diagrams are of great significance for the calculation of coastal structures. Firstly, they are the basis for the computation of extreme sea conditions at desired return periods and the extrapolation of the data to probabilities beyond the record length to match desired return periods. The design of coastal structures based on the extreme conditions at design return periods is deterministic. However, nowadays, it is widely accepted that the fully probabilistic design gives more thorough insight in the relations and correlations between the variables, the failure behaviour and the probability of damage of these structures than deterministic and lower probabilistic design methods, by using the total joint distribution of T_m and H_s of all sea states. Moreover, the long-term joint distribution of T and H can be used in order that direct wave loadings of the structures and their probabilities of occurrence be estimated within the structures' lifetime. This information is important for the design of coastal structures to

ensure their stability and resilience. Thus, via this methodology, the necessary tools can be provided for the deterministic and probabilistic calculation of coastal structures.

In table 3.7, some statistics concerning the wave breaking and its type are presented at each depth, where it is observed that the number of breaking waves towards the total number of individual waves is increased as wave propagate from deep towards intermediate waters. Besides, in this case of 0.07 uniform bed slope, only spilling breakers appear at the depth of 6m for all Stations.

Table 3.7 Relative Frequency and type of wave breaking in deep waters and at the water depth of 6m, for each Station [33]

Data Source	Depth (m)	Number of breaking waves towards total number of waves	Number of plunging breakers towards total number of waves	Number of spilling breakers towards total number of waves
Station M	140	-	-	-
	6	4.69×10^{-6}	-	4.69×10^{-6}
Station A	220	-	-	-
	6	1.03×10^{-5}	-	1.03×10^{-5}
Station S	320	-	-	-
	6	5.07×10^{-6}	-	5.07×10^{-6}

In Table 3.8 the correlation coefficients between i) T_m and H_s and ii) T and H in deep waters and at the water depth of 6m, for each Station are presented. $r(T_m, H_s)$ and $r(T, H)$ vary significantly between deep and intermediate waters. In general, $r(T_m, H_s)$ reduces from deep to intermediate waters for all Stations. Similarly, $r(T, H)$ seems to reduce from deep to intermediate waters for Stations M and A in contrast to Station S. Besides, both correlation coefficients are higher in the case of Station M and A than those of Station S for all depths.

Table 3.8 Correlation coefficient between T_m and H_s and between T and H in deep waters and at the water depth of 6m, for each Station [33]

Data Source	Depth (m)	$r(T_m, H_s)$	$r(T, H)$
Station M	140	0.90	0.59
	6	0.86	0.50
Station A	220	0.87	0.58

	6	0.82	0.47
Station S	320	0.81	0.32
	6	0.76	0.37

Indicatively, the wave direction pdf is presented at various water depths for one of the sea states. The angular pdf in deep waters has been estimated via the methodology presented in section 3.1.3, while the corresponding pdf in shallower waters has been estimated by applying the refraction process to each individual wave. This has been applied for all considered sea states in deep waters within the analyzed datasets. From Figure 3.15, it can be seen that as waves propagate from deep to shallower waters, the pdf becomes narrower, and the mean wave direction tends to come closer to the perpendicular to the iso-depths, as expected [32].

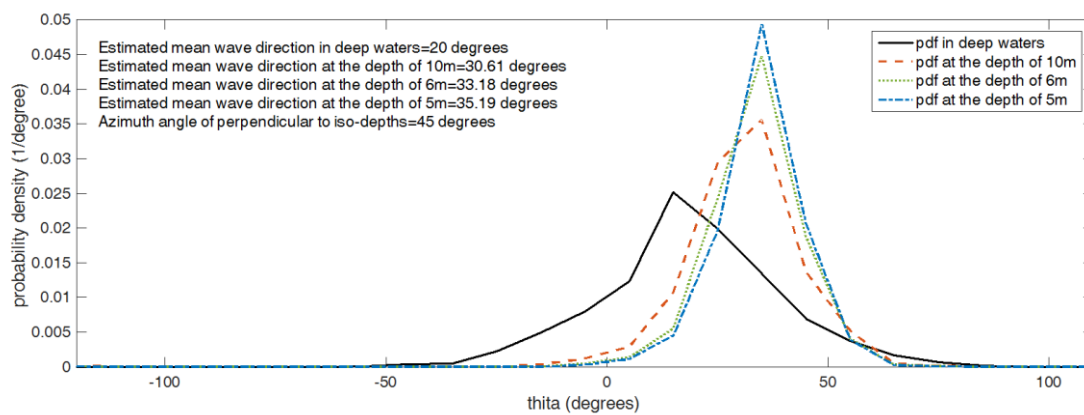


Figure 3.15 Probability density of wave direction in a certain sea state propagating from deep to intermediate waters [33]

In this way, significant information can be provided for the design of marine and coastal structures. As mentioned before, the consideration of directional waves is more realistic and, also, results in lower extreme forces upon the structures when compared against the uni-directional case. The latter is very important since it can lead to a more economical but not less safe design of these structures.

3.2 Investigating the capability of the linear model

As far as the short-term wave statistics considered by the model by Malliouri et al. [33] is concerned, this consists of two parts. The first part refers to the decomposition of every sea state in deep waters to individual random waves using the probabilistic information of the sea state, and the second one concerns the linear wave propagation of each individual wave from deep towards shallower waters, thus without considering non-linearities like the non-linear wave-wave interactions. In the next sections, the capability of the model to produce properly the short-term wave statistics in deep and intermediate waters will be investigated via comparisons of its results with measurements in deep waters and the results of a commercial and well-known for its accuracy wave propagation model from deep to intermediate waters, respectively.

3.2.1 Comparisons concerning deep waters

Referring to the probabilistic information of a sea state in deep waters, a joint probability density function (pdf) of wave height H and period T should be used, e.g. a theoretical one by Longuet-Higgins [24] or alternatively by Memos and Tzanis ([29]; [30]), in which a directional spreading function should be incorporated. Both of these approaches refer to nonlinear wind-generated sea waves in deep waters. In both approaches, wave height is considered as a peak-to-trough excursion and wave period as the zero-crossing period. As for the joint pdf of T and H according to Longuet-Higgins [24], which has been described in section 2.4.1.2 and is appropriate for narrow band spectrum, the input data for its formation are the zeroth moment of the wave spectrum, the spectral bandwidth and the spectral mean wave period. Thus, the input data are the spectral wave parameters. However, the joint pdf of H and T by Memos and Tzanis ([29]; [30]) uses the standard deviation of sea surface elevation or the mean wave height from time-domain analysis and produces numerical results for deep water waves of any spectral bandwidth. Therefore, there are some differences between the two approaches concerning their input data and their domain of validity.

Since both methods can produce dimensionalized joint pdfs of H and T of the the same type, the two methods can be compared with each other and with wave measurements in deep waters obtained from an oceanographic buoy located at Station S (see Figure 3.5). The buoy belongs to the POSEIDON Marine Monitoring Network operating under the responsibility of the Hellenic Centre of Marine Research (HCMR) (see [44], [45]), and measures the sea surface elevation for 17 min with a recording interval of 1Hz every 3 hr.

Then, a zero-upcrossing analysis method was applied to the sea surface elevation's measurements in order that the period and height of each individual wave occurred within each 17 min recording period be derived. Besides, a spectral wave analysis was applied to the same signal and the spectral wave energy parameters were estimated.

In the present thesis, three sea states were examined and presented in order of increasing sea severity. Specifically, the comparisons of the scatter plot of wave heights and periods in deep waters at Station S for these sea states, as derived from zero-up crossing analysis applied to the signals, with the numerical results (joint pdf of H and T) produced according to Longuet-Higgins [24] and Memos and Tzani [29] are depicted in Figures 3.16 - 3.18.

Besides, a large number, of random samples of H and T that correspond to each joint pdf estimated by each method, was then produced. The statistical wave parameters that represent the results of the two approaches (actually the mean values of the samples) and those derived from wave measurements are presented in Table 3.9. Also, in Table 3.10, the mean relative difference of the two methods' results from those extracted directly from measurements is presented. It is noted that the spectral bandwidth parameters ν and ε for the three sea states ranges between 0.33 and 0.40, and between 0.53 and 0.72, respectively.

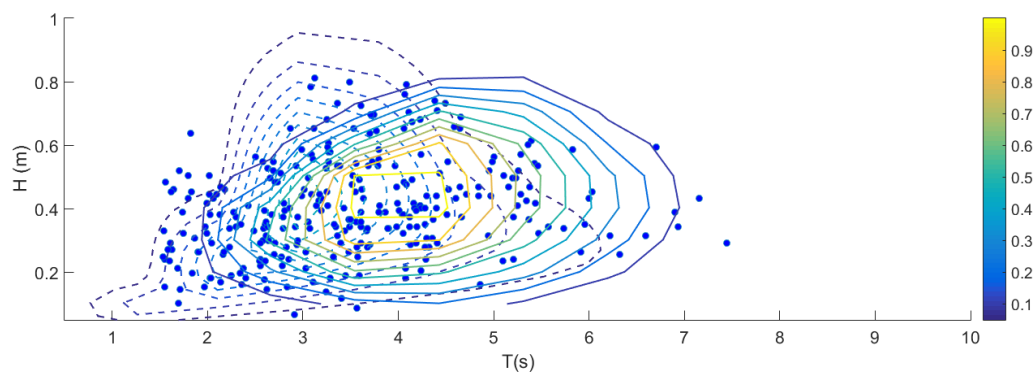


Figure 3.16 Comparisons in deep waters between wave measurements (blue points) and the results derived by Longuet-Higgins [24] (dotted lines) and by Memos and Tzani [29] (solid lines) for a sea state with $H_{1/3}=0.55$ m, $H_m=0.40$ m and $T_m=3.67$ s (contour step 0.05 1/m/s)

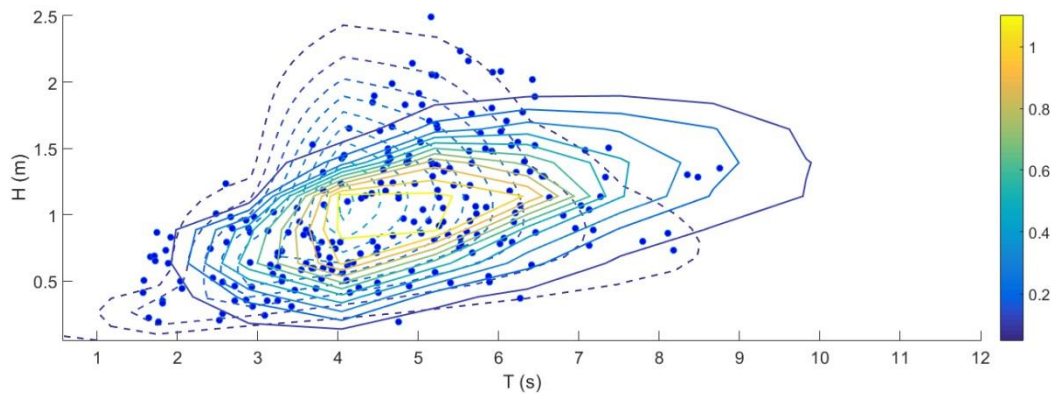


Figure 3.17 Comparisons in deep waters between wave measurements (blue points) and the results derived by Longuet-Higgins [24] (dotted lines) and by Memos and Tzanis [29] (solid lines) for a sea state with $H_{1/3}=1.56$ m, $H_m=1.01$ m and $T_m=4.62$ s (contour step 0.05 1/m/s)

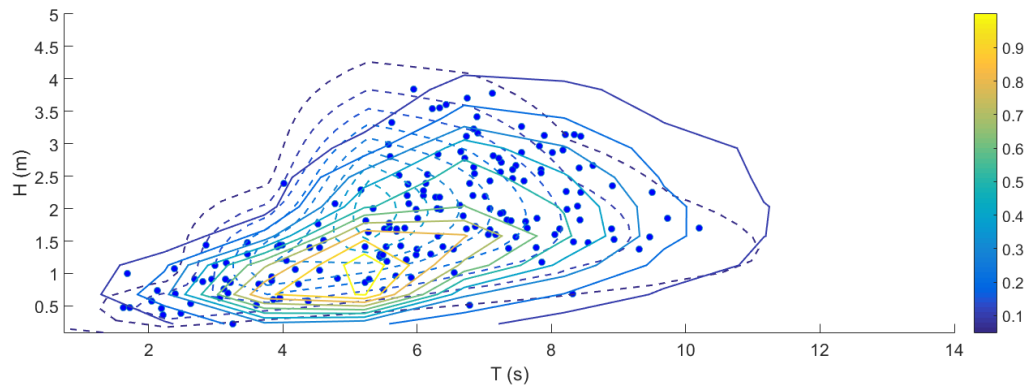


Figure 3.18 Comparisons in deep waters between wave measurements (blue points) and the results derived by Longuet-Higgins [24] (dotted lines) and by Memos and Tzanis [29] (solid lines) for a sea state with $H_{1/3}=2.89$ m, $H_m=1.80$ m and $T_m=5.96$ s (contour step 0.05 1/m/s)

Table 3.9 Spectral bandwidth parameters of the three sea states tested and comparisons of the statistical wave parameters between wave measurements and those estimated by the two approaches

Sea state	Data/Results	Statistical wave parameters			Spectral bandwidth parameters	
		$H_{1/3}$ (m)	H_m (m)	T_m (s)	ν	ε
1	Wave measurements	0.66	0.40	3.54	0.33	0.53
	L-H (1983)	0.76	0.53	3.08		
	M & T (1994)	0.57	0.38	3.90		
2	Wave measurements	1.56	1.01	4.62	0.37	0.65
	L-H (1983)	1.76	1.17	4.19		
	M & T (1994)	1.49	1.04	5.32		
3	Wave measurements	2.89	1.80	5.96	0.40	0.72
	L-H (1983)	2.98	1.96	5.44		
	M & T (1994)	2.86	1.72	6.50		

Table 3.10 Relative difference of the two methods' results from those extracted directly from measurements

Sea state	Data/Results	Statistical wave parameters			Spectral bandwidth parameters	
		$H_{1/3}$ (m)	H_m (m)	T_m (s)	ν	ϵ
1	L-H (1983)	15%	33%	-13%	0.33	0.53
	M & T (1994)	-14%	-5%	10%		
2	L-H (1983)	13%	16%	-9%	0.37	0.65
	M & T (1994)	-4%	3%	15%		
3	L-H (1983)	3%	9%	-9%	0.40	0.72
	M & T (1994)	-1%	-4%	9%		

As noticed from Figures 3.16 to 3.18 and Tables 3.9 and 3.10, the two approaches' results have some differences with each other and with wave measurements for the three sea states considered, which are non-narrow banded. Specifically, the statistical wave parameters corresponding to Memos and Tzani ([29]; [30]) results approximate more accurately the wave measurements for most of the cases considered, compared against to Longuet-Higgins results [24]. A clear difference between the two approaches was noticed to mean wave period referring to the concentration of the joint pdf of H and T by Longuet-Higgins [24] in the vicinity around a characteristic wave period (this could be related to the assumption of narrow band spectra), while in the method of Memos and Tzani ([29]; [30]) waves with large heights tend to a greater degree to have large periods than in the method of Longuet-Higgins.

3.2.2 Comparisons concerning intermediate waters

The range of validity of linear theory is wide, covering all intermediate water depths for most wave steepnesses encountered in engineering practice. In this section, the linear theory will be applied in and outside its range of validity (according to Figure A.2 - Appendix) and compared to a phase-resolving Boussinesq-type module, namely MIKE 21 BW by DHI. The comparisons will be carried out with respect to the estimated time-domain characteristic wave parameters as well as the scatter plot of individual wave height and period within a wave train.

MIKE 21 BW module by DHI is based on the numerical solution of the time-domain formulations of Boussinesq-type equations according to Madsen et al. ([46]; [5]; [47]; [48]) and Sørensen and Sørensen [49] and Sørensen et al. [6]. These enhanced Boussinesq-type

equations make the models suitable for simulation of propagation of non-linear directional waves from deep to shallow waters.

The methodology adopted in order that the results of the linear wave propagation model be compared with those by MIKE 21 BW module (DHI) is described below. Firstly, it is noted that the input data of this module are time series of surface elevation, while the input data of the model by Malliouri et al. [33] are individual waves as produced from the probabilistic image. The order of the individual waves in a wave train does not play any role in the linear model by Malliouri et al. [33]. Since the two models should be compared under the same hydraulic and boundary conditions, the same bathymetry and scatter plot of wave height and period at the same deep or intermediate water depth were used by both models. Also, the same wave transformations are considered by both of them, i.e. wave shoaling, refraction, breaking, and wave reforming after breaking. Then, the surface elevation and individual waves were propagated at the same locations in shallower waters, referring to the case of MIKE 21 BW module and the linear wave propagation model. Finally, by applying zero up-crossing method to sea surface elevation obtained at a certain location, the scatter plot of H and T was extracted and the characteristic time-domain wave parameters were estimated. These results were then compared with those directly extracted by the linear wave propagation model.

3.2.2.1 Normal incidence

A relatively extreme sea state with normal incidence is selected to be presented among 15 other sea conditions examined, since this is considered more useful for the design of coastal structures. The coastal slope in both linear and non-linear models was considered equal to 0.10. The spatial computational grid was uniform with $\Delta x = \Delta y = 1$ m in the two horizontal perpendicular axes.

In Figure 3.19, the scatter plot of T and H used by both models at the depth of 20.95 m is presented, and in Figures 3.20 - 3.23, the results estimated by both models are depicted and compared. In Table 3.10 the time-domain characteristic parameters estimated by MIKE 21 BW module's results are compared with those by the model by Malliouri et al. [33] for this sea state, and the relative difference between these two models' parameters is presented in Table 3.11.

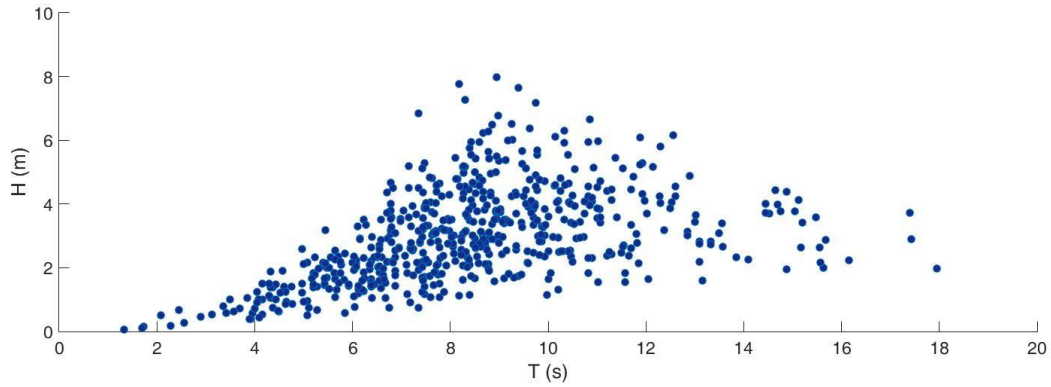


Figure 3.19 Scatter plot of T and H used by both models at the depth of 20.95 m (normal incidence)

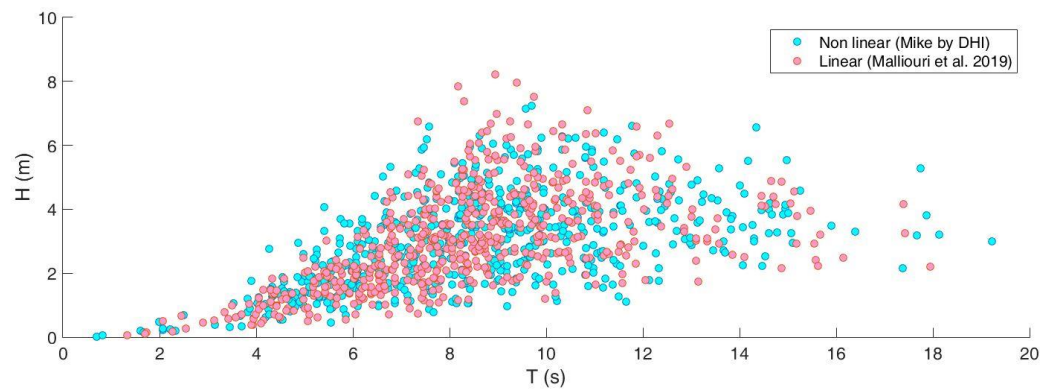


Figure 3.20 Scatter plot of T and H obtained by non-linear module (Mike by DHI) compared to the linear wave propagation model at the intermediate depth of 11.80 m (normal incidence)

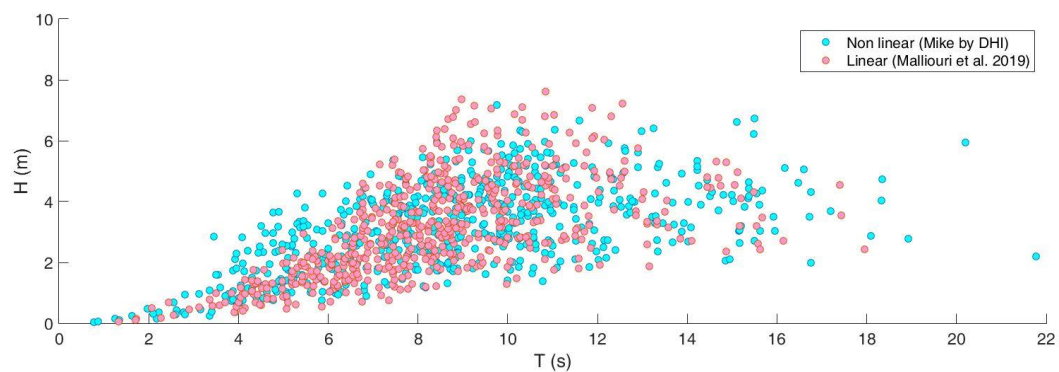


Figure 3.21 Scatter plot of T and H obtained by non-linear module (Mike by DHI) compared to the linear wave propagation model at the intermediate depth of 7.60 m (normal incidence)

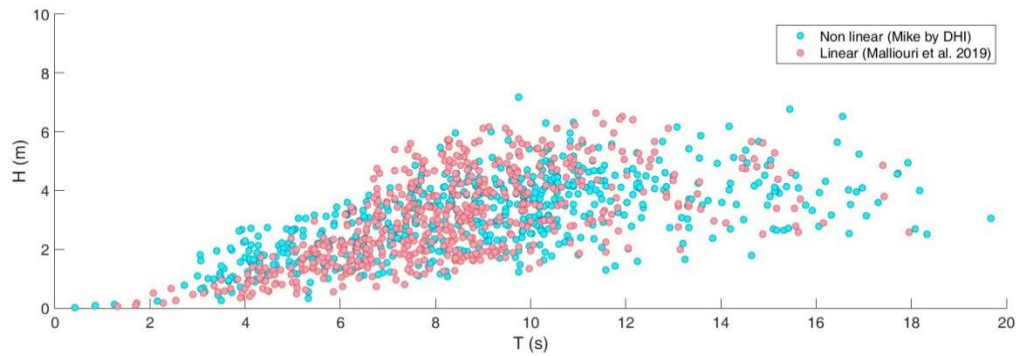


Figure 3.22 Scatter plot of T and H obtained by non-linear module (Mike by DHI) compared to the linear wave propagation model at the intermediate depth of 5.70 m (normal incidence)

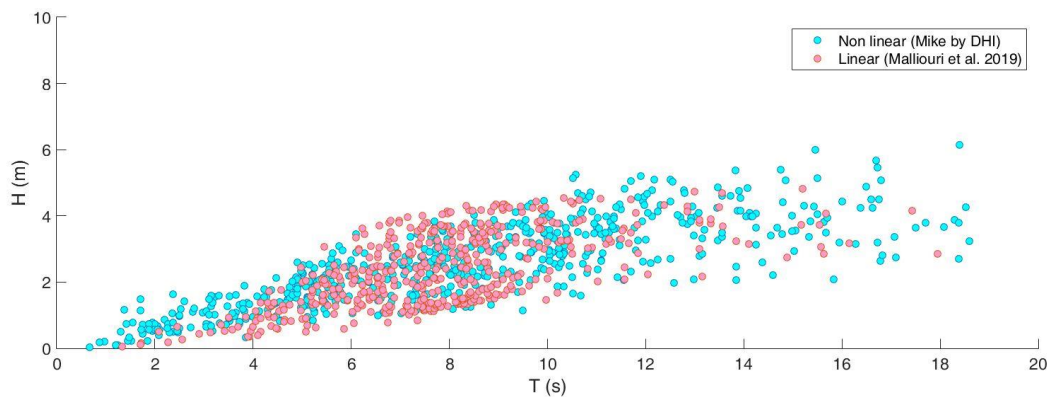


Figure 3.23 Scatter plot of T and H obtained by non-linear module (Mike by DHI) compared to the linear wave propagation model at the intermediate depth of 3.80 m (normal incidence)

Judging by the scatter plots of T and H presented in the above Figures, the comparison between the two models (linear v.s. nonlinear wave propagation) shows good agreement at most intermediate water depths considered. Greater deviations are noticed between the two models as waves propagate in shallower waters (i.e. at the intermediate depth of 3.80 m) due to the nonlinear wave-wave interactions and the wave breaking, which are stronger especially nearshore.

In Tables 3.11 and 3.12, the time-domain characteristic parameters estimated by MIKE 21 BW module's results are compared with those by the model by Malliouri et al. [33]. In those tables, expect for H_m , $H_{1/3}$, and T_m , the mean wave length L_m estimated by the linear dispersion equation (see Eq. A.2 - Appendix) in terms of T_m , the mean wave steepness s_m estimated in terms of $H_{1/3}$ and L_m , and the Ursell number Ur , are also presented.

Table 3.11 Comparison of time-domain characteristic parameters estimated by MIKE 21 BW module's results with those by the model by Malliouri et al. [33] for normal incidence

Model	depth (m)	H_m (m)	$H_{1/3}$ (m)	T_m (s)	L_m (m)	s_m	Ur
MIKE BW	20.95	2.99	4.63	8.40	96.61	$4.79 \cdot 10^{-2}$	4.70
Malliouri et al. 2019	20.95	2.99	4.63	8.40	96.61	$4.79 \cdot 10^{-2}$	4.70
MIKE BW	11.80	3.05	4.69	8.62	82.83	$5.66 \cdot 10^{-2}$	18.36
Malliouri et al. 2019	11.80	3.07	4.81	8.40	80.20	$6.01 \cdot 10^{-2}$	18.83
MIKE BW	7.60	3.17	4.73	8.84	71.33	$6.63 \cdot 10^{-2}$	54.82
Malliouri et al. 2019	7.60	3.15	4.82	8.40	67.27	$7.17 \cdot 10^{-2}$	49.68
MIKE BW	5.70	3.10	4.51	8.97	63.88	$7.06 \cdot 10^{-2}$	99.37
Malliouri et al. 2019	5.70	3.07	4.60	8.39	59.35	$7.75 \cdot 10^{-2}$	89.85
MIKE BW	3.80	2.59	3.96	8.36	49.18	$8.05 \cdot 10^{-2}$	174.52
Malliouri et al. 2019	3.80	2.39	3.68	7.81	45.69	$8.06 \cdot 10^{-2}$	139.97

Table 3.12 Relative difference of Malliouri et al. [33] model's results from those by MIKE 21 BW module for normal incidence

d (m)	d/ L_m	H_m	$H_{1/3}$	T_m	L_m	s_m	Ur
11.80	0.22	0.01	0.03	-0.03	-0.03	0.06	0.03
7.60	0.14	-0.01	0.02	-0.05	-0.06	0.08	-0.09
5.70	0.11	-0.01	0.06	-0.07	-0.07	0.10	-0.10
3.80	0.09	-0.08	-0.07	-0.07	-0.07	0.00	-0.20

As noticed from Tables 3.11 and 3.12, at the deeper intermediate water depths (i.e. 11.40 m, 7.60 m, 5.70 m) the mean wave height H_m estimated by the linear wave propagation model is very close to the corresponding one extracted by the nonlinear wave propagation model. The comparisons concerning the rest parameters are satisfactory, but larger deviations are observed for T_m , and L_m , and even larger differences are noticed for s_m and Ursell number. As it was expected, deviations between the two models' parameters become greater as waves propagate inshore, and especially when waves enter the shallower intermediate water depth examined (i.e. at the depth of 3.80 m).

It is noted that the comparisons between the two models (linear v.s. nonlinear) are made outside the approximate validity region of linear wave theory (see Figure A.2 - Appendix), in order to investigate the capability of the linear statistical model in a wide range of sea states that are probable to occur during a coastal structure's lifetime.

3.2.2.2 Oblique incidence

In this section, two sea states with oblique incidence are examined, the first one with mean wave direction θ_m equal to 19.11° and the other one with θ_m equal to 42.33° from the normal direction (i.e. perpendicular to depth-contours and shoreline), at the depth of 20.95 m. To estimate θ_m at a certain depth by using timeseries extracted from MIKE 21 BW module, the approximate technique, described in section 2.4.1.1, was applied. Specifically, the timeseries of three spatial points that formed a right angle on the horizontal plane were used for this purpose. It is noted that one of these three points was the point of interest and the distance between this point and each one of the other two points were set equal to 1 m. Therefore, the free surface timeseries at the point of interest and its slopes in orthogonal directions could be estimated and then the Maximum Entropy Method could be applied.

By applying this methodology, the results by linear [33] and nonlinear (MIKE 21 BW by DHI) wave propagation model were obtained and compared. Both models' results are presented in Tables 3.13 and 3.15, and the relative difference of linear wave propagation model's results from those by nonlinear model are presented in Tables 3.14 and 3.16, for θ_m equal to 19.11° and 42.33° , respectively at the depth of 20.95 m.

Table 3.13 Comparison of MIKE BW module by DHI results with the corresponding ones by the model by Malliouri et al. [33] for oblique incidence ($\theta_m=19.11^\circ$ from normal)

Model	depth (m)	H_m (m)	$H_{1/3}$ (m)	T_m (s)	θ_m ($^\circ$)	L_m (m)	s_m	Ur
MIKE BW	20.95	2.07	3.25	8.39	19.11	96.44	$3.37 \cdot 10^{-2}$	3.29
Mall. et al.	20.95	2.07	3.25	8.39	19.11	96.44	$3.37 \cdot 10^{-2}$	3.29
MIKE BW	11.40	2.25	3.43	8.99	15.08	86.04	$3.99 \cdot 10^{-2}$	17.14
Mall. et al.	11.40	2.11	3.37	8.39	15.95	79.05	$4.26 \cdot 10^{-2}$	14.21
MIKE BW	7.60	2.37	3.62	9.16	13.31	74.27	$4.87 \cdot 10^{-2}$	45.49
Mall. et al.	7.60	2.20	3.56	8.39	13.78	67.18	$5.30 \cdot 10^{-2}$	36.60
MIKE BW	5.70	2.46	3.68	9.33	11.74	66.69	$5.52 \cdot 10^{-2}$	88.39
Mall. et al.	5.70	2.24	3.63	8.31	12.50	58.67	$6.19 \cdot 10^{-2}$	67.51
MIKE BW	3.80	2.26	3.35	8.75	9.59	51.64	$6.49 \cdot 10^{-2}$	162.81
Mall. et al.	3.80	1.89	2.99	7.46	9.89	43.45	$6.88 \cdot 10^{-2}$	102.89

Table 3.14 Relative difference of Malliouri et al. [33] model's results from those by MIKE 21 BW module for oblique incidence ($\theta_m=19.11^\circ$ from normal)

d (m)	d/L_m	H_m	H_{1/3}	T_m	θ_m	L_m	s_m	Ur
11.40	0.13	-0.06	-0.02	-0.07	0.06	-0.08	0.07	-0.17
7.60	0.10	-0.07	-0.02	-0.08	0.04	-0.10	0.09	-0.20
5.70	0.09	-0.09	-0.01	-0.11	0.06	-0.12	0.12	-0.24
3.80	0.07	-0.16	-0.11	-0.15	0.03	-0.16	0.06	-0.37

Table 3.15 Comparison of MIKE BW module by DHI results with the corresponding ones by the model by Malliouri et al. [33] for oblique incidence ($\theta_m=42.33^\circ$ from normal)

Model	depth (m)	H_m (m)	H_{1/3} (m)	T_m (s)	θ_m (°)	L_m (m)	s_m	Ur
MIKE BW	20.95	1.87	2.94	8.81	42.33	103.52	$2.84 \cdot 10^{-2}$	3.43
Mall. et al.	20.95	1.87	2.94	8.81	42.33	103.52	$2.84 \cdot 10^{-2}$	3.43
MIKE BW	11.40	1.79	2.85	8.87	31.08	84.65	$3.37 \cdot 10^{-2}$	13.78
Mall. et al.	11.40	1.82	2.89	8.81	34.19	83.95	$3.44 \cdot 10^{-2}$	13.75
MIKE BW	7.60	1.82	2.88	9.09	23.62	73.63	$3.91 \cdot 10^{-2}$	35.56
Mall. et al.	7.60	1.86	3.00	8.81	28.97	71.05	$4.22 \cdot 10^{-2}$	34.50
MIKE BW	5.70	1.86	2.99	9.06	20.48	64.58	$4.63 \cdot 10^{-2}$	67.34
Mall. et al.	5.70	1.88	3.05	8.66	25.64	61.44	$4.96 \cdot 10^{-2}$	62.18
MIKE BW	3.80	1.85	2.86	8.93	16.32	52.78	$5.42 \cdot 10^{-2}$	145.17
Mall. et al.	3.80	1.65	2.59	8.04	21.63	47.15	$5.49 \cdot 10^{-2}$	104.92

Table 3.16 Relative difference of Malliouri et al. [33] model's results from those by MIKE 21 BW module for oblique incidence ($\theta_m=42.33^\circ$ from normal)

d (m)	d/L_m	H_m	H_{1/3}	T_m	θ_m	L_m	s_m	Ur
11.40	0.13	0.02	0.01	-0.01	0.10	-0.01	0.02	0.00
7.60	0.10	0.02	0.04	-0.03	0.23	-0.03	0.08	-0.03
5.70	0.09	0.01	0.02	-0.04	0.25	-0.05	0.07	-0.08
3.80	0.07	-0.11	-0.09	-0.10	0.33	-0.11	0.01	-0.28

Judging from Tables 3.11 – 3.16, similar observations to normal incidence could be made for both cases of oblique incidence concerning H_m , $H_{1/3}$, T_m , L_m , s_m , Ur . As for θ_m in oblique incidence, it was noticed that as the angle from the normal direction increases, mean wave direction estimated by linear wave propagation model differ to a greater degree from that estimated by MIKE 21 BW module, whilst the other characteristic wave parameters show better agreement. Some differences of θ_m between the two models could be attributed to the fact that this refers to a statistical parameter in case of the model by Malliouri et al. [33],

while in case of the MIKE 21 BW this parameter is a spectral wave parameter defined as the mean direction of the directional spectrum.

3.2.3 Determination of the validity domain of the model

As for the deep water short-term wave statistics considered by Malliouri et al. [33], it was shown that the joint pdf of T and H of a real sea state could be well represented by using the dimensionless probabilistic images by Memos and Tzanis ([29]; [30]). The latter refer to nonlinear deep water waves. Referring to intermediate water short-term wave statistics considered by Malliouri et al. [33], comparisons between the linear wave propagation model and the nonlinear Boussinesq-type model showed good agreement in most of the intermediate water depths examined for both normal and oblique incidence. At the shallower intermediate water depth tested, the results of the two models differed more significantly than in deeper intermediate water depths. Therefore, as it was expected and has been already mentioned, the linear model adopted could cover the deeper and medium zone of intermediate waters and thus could be used for engineering design purposes.

Furthermore, a general conclusion could be extracted from the above analysis (see sections 3.2.2.1 and 3.2.2.2). This is that inside the approximate region of the linear theory (i.e. $Ur < 40$ and $s_m < 0.04$) the linear model by Malliouri et al. [33] can satisfactorily approximate the results of a nonlinear Boussinesq wave module such as MIKE 21 BW. However, this linear model can be used for engineering purposes in a wider region, in the deeper and medium intermediate water zone. It is recommended that the extension of the application area of the model beyond the limits of the linear wave theory should simultaneously meet these two conditions: $Ur < 80$ and $s_m < 0.07$. Further extension could lead to unsatisfactory estimation of characteristic wave parameters with relative deviations beyond 10%, compared with nonlinear wave propagation models.

3.2.4 Comparisons with respect to simulation time

In this section, the linear wave model by Malliouri et al. [33] is compared with the nonlinear Boussinesq wave model (MIKE 21 by DHI) with respect to the simulation time. Comparisons presented refer to the same wave scenaria, simulated by the same computer via a Matlab code generated by the author for the linear model and the Mike 21 (2d) Boussinseq wave module.

The computer had a processor of Intel(R) Core (TM) i7-2700 K CPU @ 3.50 GHz-3.80 GHz, 8.00 GB installed memory (RAM), and a 64-bit Operating System. As for the simulation time by the nonlinear wave model, it was a little more than 9 hr, while the linear wave model runs in about 1 s. It is noted, that the 2d area of the bathymetry, tested by the nonlinear wave model, was 800 m by 600 m, and the grid step was set equal to 1m for the two horizontal axes. As shown, the computational cost is significantly reduced in the case of the linear wave propagation model enabling this to propagate the long-term wave climate information from deep to intermediate waters in a faster manner compared with the nonlinear wave propagation model.

3.3 Reliability analysis of a rubble mound breakwater

In the present section, a thorough probabilistic methodology is presented, aiming at estimating the reliability of coastal structures, such as rubble mound breakwaters during their lifetime, based on the probabilistic representation of load environmental and resistance parameters. One of the innovative points and main objectives of this study is the estimation of failure probability of the structure based on the long-term wave climate at a coastal structure's location, usually met in intermediate waters, using wave observations or measurements in deeper waters. This is accomplished by applying a wave propagation statistical model in order that the joint probability density function of all stochastic load parameters be estimated at the structure's location. Moreover, a comparative evaluation of an event-based extreme value analysis and an analysis on sea-state conditions within storm events is attempted with respect to their outputs and their pros and cons. Besides, another specific issue of scientific originality could be considered the investigation on the proper time step denoting the sea state in the sea state analysis applied. In this manner, the actual history and shape of each storm event is taken into consideration. Furthermore, it is shown that these two approaches could be incorporated in the design of a coastal structure.

Besides, two different fully probabilistic methods, Direct Integration Method (DIM) and Monte Carlo Method (MCM), were applied (and compared) by using a combination of variables with zero and non-zero hazard rate, referred here as a combined time-invariant and time-variant analysis. Another scientific contribution of this PhD thesis, related to the reliability analysis, is the description of the assessment of the failure probability of a coastal structure by DIM and MCM via clarifying mathematical equations developed within the framework of this dissertation. These equations developed are different for the extreme event-based method and all sea conditions-based method.

It is noted that mainly hydraulic uncertainties are considered in this PhD thesis. Nevertheless, the methodology adopted could be expanded to consider also the effect of more and different types of parameters as random variables on the assessed failure probability of the structure, except for loading variables. Finally, it is shown that the methodology derived from this study could be incorporated into a coastal structure's design process to meet specific safety requirements.

3.3.1 A short review of structural reliability assessment

Structural reliability assessment, aiming at estimating the probability of a structure to meet predefined safety and performance levels, with due consideration of all uncertainties related to actions, resistance, and design tools, has been a topic of extensive research in many different engineering application areas. The most versatile solution technique, available for this purpose, is the Direct Integration Method (DIM) or the alternative Monte Carlo Method (MCM). Although DIM approach is the most theoretically direct solution for structural reliability problems, in practice reliabilities of many offshore structures are more likely to be evaluated using simulation-based methods (e.g. direct MCM). Therefore, several advanced approximate methods have been also developed so far for estimating the structural failure, such as the first and second order reliability methods, environmental contour methods, response surface methods and emulator-based analysis.

Referring to these approximate methods, a brief literature description will be provided below. In the first-order reliability method (FORM) the failure surface is approximated by a tangent hyperplane at the design point [199], while a more accurate and similar method is the second-order reliability method (SORM) which uses a quadratic approximation to the failure surface (see e.g. [200]). Moreover, the concept of environmental contours is a method developed for estimating extreme conditions as basis for design, e.g. [201];[202], and is widely used in marine structural design (see e.g. [203];[204];[205];[206];[207];[208]). This approach is close to the first-order reliability method approximation. Moreover, whereas the response surface method motivated by Box and Wilson in 1951 [209] was traditionally utilized for chemical or industrial engineering, its application area has been expanded in structural engineering (see e.g. [210]). Also, one way to address the computational cost incurred in the simulation of the structural reliability assessment could be to apply a less demanding approximation, e.g. a metamodel or emulator (see e.g. [211]).

Two main criteria for selecting one of the aforementioned methods for structural reliability assessment could be the high degree of accuracy required in a very narrow region, i.e. the small failure probability, and the computational cost incurred. The latter could become significantly demanding, depending on the application case.

Focusing now on coastal structures, the reliability based design methods are divided into four categories, related to the accuracy in determining the reliability of their elements and the consideration of the involved uncertainties, cited below [1]:

- Deterministic method (Level 0)
- Semi-Probabilistic Method (Level I)
- Probabilistic Methods with Approximations (Level II)

- Fully Probabilistic Methods (Level III)

Conventional design practice for coastal structures is often deterministic in nature (Level 0), and its reliability is based on the exceedance probability of the design wave load. Specifically, the notion of design wave parameters and especially that of wave height associated with a certain return period is adopted [2]. In addition to the deterministic method, partial factors can be implemented for resistance and load, based on standards [3]. This calculation is classified as a semi-probabilistic (Level I) method. However, this approach does not allow accurate determination of the reliability of the design. In order to overcome this problem, more advanced probabilistic methods should be applied that consider the uncertainties of all stochastic variables of load and strength of the structure.

Fully probabilistic methods (Level III) belong in the category of advanced probabilistic methods, which consider the joint probability density function of all stochastic variables involved. There are two main methods classified as Level III methods, i.e. the Direct Integration Method (DIM) and Monte Carlo Method (MCM). Another possibility, though less accurate regarding the estimation of the reliability of the design, are methods with approximations (Level II).

Referring, at this point, to the general gap in current practice of reliability assessment of coastal structures, despite that the probabilistic representation of environmental parameters at the location of coastal structures is vital for the reliability based design of these structures, there is a lack of long-term environmental data at the location of coastal structures under design making thus difficult to estimate their joint probabilistic distribution at this location. Therefore, one of the main objectives of this thesis is to deal with the issue of how to properly describe the long-term wave climate at the coastal structures' location, and then to use this core information for the reliability assessment and design of coastal structures.

3.3.2 Significant issues in the reliability analysis

Currently, there are some significant issues that need to be solved during the reliability assessment, and consequently the design process of coastal structures. Some of them, which should be duly considered, are listed below, focusing on the case of a rubble mound breakwater. However, the discussion and the methodology that will be presented below can easily be adjusted to account for every coastal structure.

(1) Input data of the coastal structure's load parameters that affect the limit state function of its elements should be collected before performing the reliability analysis. Input data on the long-term wave climate and sea level should be collected at the project site. Such data should include variables like significant wave height H_s , mean wave period T_m , mean wave direction θ_m , sea level or similar. This can be implemented by:

(i) Measurements at the structure's location for a period of time, ideally of the order of the structure's design operating life. Obviously such requirement can be rarely met.

(ii) Measurements of the same type but in deep water if the location of the structure was in shallower water, during a time span ideally of the order of the structure's design operating life. Then, either linear or non-linear models (e.g. [5]; [6];[7]) may be applied to transfer each sea state from deep towards shallower waters.

(iii) Hindcasting methods for a period of several years ([8]; [1]). Particularly, regarding the long-term wave climate at the structure's location, wind data in the wave generation area (e.g. [9]) can be used to provide this information under a probabilistic framework.

Furthermore, the target of the aforementioned input data collection is to gain a thorough probabilistic representation of the long-term wave climate, sea level conditions, and other environmental parameters, at the coastal structure's location, usually met in intermediate waters. In case (ii) of issue (1), it is worth mentioning that non-linear models might be more accurate than linear models, as they account for wave-wave interactions that may play a considerable role in the final outcome depending on water depth; however, non-linear models are quite demanding in terms of computing resources, especially when they have to account for reliability analysis based on fully probabilistic methods. In this case, a fast and adequately accurate model could be applied that enables the integration of short- with long-term wave statistics [33] and transfers the probabilistic information to the structure's location.

(2) A functional dependency may exist between certain environmental parameters involved in the reliability analysis. Specifically, the total mean sea level (including tide, storm surge etc.) often plays a role in modifying the wave climate at the structure's location, since it forms the water depth conditions affecting as a result the wave conditions at this location.

(3) Referring to wave parameters that affect the stability of a rubble mound breakwater, oblique wave attack does play a significant role in the stability of a breakwater's armor layer (see e.g. [12]). In particular, it is accepted that the stability of armor layers can be significantly higher for oblique waves compared against perpendicular wave attack ([212]),

thus neglecting the effect of oblique waves on the structure's stability leads to a conservative assumption. According to [12], the consideration of this effect can be accomplished by using the notion of the equivalent normal wave height. Therefore, the principal or mean wave direction that characterizes each sea state at the breakwater's location has been included in the analysis and this type of functional dependence, i.e. between wave direction and resistance of an element is considered via the limit state equation.

(4) Another issue is related to the hazard rate of some of parameters considered in the reliability analysis, referred here as time dependence. Then the random variables of a design formula should be examined with relevance to their dependence on time, and a combination of time-dependent and time-invariant reliability analysis may be applied when extrapolating the failure probability from the reference period of one year to the lifetime of the structure.

(5) The exceedance probability of a design value of a time-dependent core load variable is commonly regarded as the failure probability of the structure in the conventional design, estimated in the sample of extreme values of the variable (e.g. values above a predefined high threshold (Peak over Threshold- POT)). In a conventional POT analysis [50], the exceedance probability of a storm event is considered as the ratio of the expected number of events exceeding this specific storm event to the number of extreme events expected to occur in a reference time period, i.e. annually. It is noted that all these (event-based) probabilities do not provide direct information on the time period that the structure will fail during a reference time period. The latter information can be provided by the methodology developed in the present thesis (see section 3.3.5).

3.3.3 Preliminary design based on an event-based extreme value analysis applied to wave data

A univariate extreme value analysis concerning POT modelling for peaks over threshold will be used here for the predominant variable $H_{s,p}$, i.e. the maximum H_s within a storm event, following the relevant event-based framework for over-threshold modelling introduced by Bernardara et al. [50], which will be then associated with the concurrent values T_m and θ_m of that particular storm [51].

Firstly, homogenization is applied to the sequential wave data at a given time step enabling the separation of data/sea states into independent wave systems or else events. This is attempted by selecting an initial threshold u_1 for H_s distinguishing weak and intense storms from the dataset. Besides, a minimum calm period, e.g. of 6 hr [51], (i.e., a time separation interval) between two consecutive storms was selected to ensure that the two events are

independent. Therefore, the dataset of the maximum significant wave heights $H_{s,p}$ is derived from this procedure. Referring to the selection of u_1 , it should be high enough to distinguish and separates two consecutive storms, but also low enough to be below the extreme area [52].

The second step is the selection of another threshold u_2 higher than u_1 . The selection of u_2 needs to be more precise than that of u_1 , since the storm peaks above u_2 should follow the same extreme probability distribution. Referring to modeling from the perspective of peaks over threshold, Pickands [53] showed that this extreme probability distribution can be approximated by a Generalized Pareto distribution (see also [54]). That is, for $H_{s,p} > x_o$ given that $H_{s,p} > u_2$,

$$\Pr(H_{s,p} > x_o | H_{s,p} > u_2) = \left(1 + \xi \frac{x_o - u_2}{\sigma}\right)^{-1/\xi} \quad (3.20)$$

where: x_o is a value higher than u_2 , $\xi \in (-\infty, +\infty)$ and $\sigma > 0$ are the shape and scale parameter, respectively, of GP distribution.

Using the properties of the GP distribution (if storm peaks follow a GP distribution) to determine u_2 , two different methodologies are commonly used. Precisely, an appropriate threshold u_2 value could be selected by examining the domain of stability of the shape parameter ξ and the modified scale parameter $\sigma^* = \sigma - \xi u_2$, or the linearity of the scale parameter σ of the GP distribution with respect to u_2 (see e.g. [61]). The second procedure for threshold selection is to search for the domain of threshold u_2 where the mean residual life plot is approximately linear in u_2 [213].

The return value of $H_{s,p}$ from GP model is extracted as below:

$$\begin{aligned} H_{s,p-T_r} &= u_2 + \frac{\sigma}{\xi} \left[(T_r \lambda_e)^\xi - 1 \right], \quad \text{for } \xi \neq 0 \\ H_{s,p-T_r} &= u_2 + \sigma \log(T_r \lambda_e), \quad \text{for } \xi = 0 \end{aligned} \quad (3.21)$$

Therefore, the design storm event corresponds to a return value of $H_{s,p}$ associated with the most probable values of mean wave period T_m , and mean wave direction θ_m estimated from their scatter diagram.

To assess the exceedance of the design $H_{s,p}$ during the reference period of L years in the sample of extreme events, i.e. of $H_{s,p}$, considered here as an equivalent failure probability, Eq. 2.7 should be applied substituting $P_{f,e,1y}^*$ by $P_{ex,H_{s,p},e,1y}$.

However, there are some subjective steps and uncertainties involved in the design approach based on the above extreme value analysis: specifically, as for the domain of stability of the generalized Pareto parameters with respect to its threshold, although objective methods ([62]; [61]) have been developed for this purpose, the accurate selection of the generalized Pareto threshold may still be difficult in some cases [52]. However, this threshold selection is critical, since it determines the expected number of extreme events per year λ_e , and consequently the exceedance probability of the design storm, leading thus to uncertainties of the analysis results. Also, another issue in this approach is the difficulty in estimating the exceedance probability of the design $H_{s,p}$ defined as the percentage of the structure's lifetime that the structure will fail. This is a drawback of the event-based extreme value analysis. Nevertheless, this method enables assessment of the exceedance probability of the design $H_{s,p}$ in the sample of extreme events during the structure's lifetime.

Also, as far as the multivariate extreme value analysis is concerned, according to the classification proposed by Mazas and Hamm [63], whereby wave spectral parameters are different physical quantities that belong to the same phenomenon, i.e. the wave storm, firstly the choice of the event-defining variable should be made, i.e. of $H_{s,p}$, which should then be associated to the concurrent values of the other covariate (spectral) parameters. Referring now to different components of a single phenomenon, like waves and sea levels conditions, the predominant component should be chosen firstly [165] that leads to the choice of the event-describing variable (e.g. the event-describing variable is sea level in case of a macro-tidal environment) with the concomitant H_s value. Furthermore, in case of equivalent components, two event-based describing variables should be considered [63] in combination with a bivariate threshold by using multivariate generalized Pareto (GP) distributions (e.g. [214]).

3.3.4 Fully probabilistic event-based reliability analysis

The fully probabilistic analysis, to be presented in this section, could be applied to maximum H_s within storm events in a POT analysis, or maximum H_s per years. Here, we proceed with a

POT analysis, applied thus to $H_{s,p}$ associated to its concurrent values of the other covariate variables. The joint pdf of those variables of extreme events could be estimated by a copula multivariate analysis represented by their kernel joint pdf. The result of this approach is the failure probability of the structure, estimated in the sample of extreme events. Therefore, this output cannot be transformed to the percentage of a reference period that the structure will be exposed to risk. However, this approach has a main advantage, which is that enables extrapolation of the failure probability during 1 year to that during the structure's lifetime, since this method uses independent values of the variables involved. In the following section, this issue will be tackled considering, also, the case when variables with zero and non zero hazard rate are all considered.

3.3.4.1 *Time extrapolation of an element's failure probability using time-invariant and time-variant random variables by Direct Integration Method (DIM)*

In a reliability analysis, there may be time-variant but also time-invariant parameters, i.e. parameters with nonzero and zero hazard rate, that all play a role in the reliability or the average failure probability of the structure during its lifetime, estimated in the sample of extreme events, denoted by $P_{f,e,L}$. Time-invariant parameters, however, are independent of the reference period L . In practice, such time-invariant parameters can usually be considered those related to the resistance of the structure's element. Thus, $P_{f,e,L}$ is estimated via the following equation developed here to account for a combined time-variant and -invariant analysis:

$$P_{f,e,L} = \iint_{\Omega(\vec{r}, \vec{x})} f_{\vec{R}}(\vec{r}) f_{\vec{X},e,L}(\vec{x}) d\vec{x} d\vec{r} = \int f_{\vec{R}}(\vec{r}) \left(\int_{\Omega(\vec{r}, \vec{x})} f_{\vec{X},e,L}(\vec{x}) d\vec{x} \right) d\vec{r} \quad (3.22)$$

where hereinafter $f_{\vec{R}}(\vec{r})$ is the joint pdf of the time-invariant resistance parameters \vec{r} , $f_{\vec{X},e,L}(\vec{x})$ is the joint pdf of time-variant random load variables \vec{x} of extreme events during design lifetime L , and $\Omega(\vec{r}, \vec{x})$ is the failure domain, which is equal to the union of the definition domains of all random variables involved under the condition that the limit state function is less than zero, i.e. $g(\vec{r}, \vec{x}) < 0$. Therefore, it is evident that:

$$\Omega(\vec{r}, \vec{x}) = \{g(\vec{r}, \vec{x}) < 0\} \quad (3.23)$$

Application of Eq. 2.7 to Eq. 3.22 results in:

$$P_{f,e,L} = \int f_{\vec{R}}(\vec{r}) \left[1 - \left(1 - \int_{\Omega(\vec{r}, \vec{x})} f_{\vec{X},e,1y}(\vec{x}) d\vec{x} \right)^{\lambda_e L} \right] d\vec{r} \quad (3.24)$$

where $f_{\vec{X},e,1y}(\vec{x})$ is the average joint pdf of \vec{x} referring to the reference period of one year, extracted from Y years of observations. As it was aforementioned, the time-variant load parameters \vec{x} consist of sea-state parameters, such as $H_{s,p}$, T_m , or similar, sea level variation due to storm surge, denoted by SL, current velocity, etc.

3.3.4.2 Inclusion of sea level variation due to astronomical tide

The most common environmental parameter, unrelated to the wave field, present around coasts is the sea-level variation due to the astronomical tide (TL). This variable is deterministic, and depends on the tidal cycle of the site. Nevertheless, it can combine randomly with waves, and thus can be considered as a stochastic variable. However, it is not statistically correlated with wave parameters, but the depth-limited wave parameters depend on the sea level value which can be strongly affected by tide, storm surge etc.

The timing of tide is mainly associated with the relative position of the Moon to the Earth and advances at about 50 minutes a day; tides also vary seasonally, while only minor variations occur outside a period of about 19 years [55]. Therefore, given that the lifetime of most coastal structures ranges between 20-50 years, the astronomical tide can be considered as a time invariant parameter, and its pdf stable over the years. Thus, the incorporation of tide in Eq. 3.24 is accomplished as follows:

$$P_{f,e,L} = \iint f_{\vec{R}}(\vec{r}) f_{TL}(tl) \left[1 - \left(1 - \int_{\Omega(\vec{r}, \vec{x}, tl)} f_{\vec{X},e,1y}(\vec{x}) d\vec{x} \right)^{\lambda_e L} \right] d\vec{r} dtl \quad (3.25)$$

where: $f_{TL}(tl)$ is the pdf of sea level due to tide and $\Omega(\vec{r}, \vec{x}, tl)$ is the expanded failure domain.

Eq. 3.25 could be estimated by defining each definite integral as the limit of a Riemann sum:

$$P_{f,e,L} = \lim_{\delta \vec{r} \rightarrow 0} \sum_{\vec{r}} f_{\vec{R}}(\vec{r}) \left\{ \lim_{\delta tl \rightarrow 0} \sum_{tl} f_{TL}(tl) \left[1 - \left(1 - \lim_{\delta \vec{x} \rightarrow 0} \sum_{\vec{x}} \Omega(\vec{r}, \vec{x}, tl) f_{\vec{X},e,1y}(\vec{x}) \delta \vec{x} \right)^{\lambda_e L} \right] \delta tl \right\} \delta \vec{r} \quad (3.26)$$

Eq. 3.26 implies that the increments of all random variables must be small enough in order that $P_{f,e,L}$ be estimated properly.

3.3.4.3 Resistance parameters

Resistance parameters are considered those related to the strength/ resistance of the structure and usually have some variability from their characteristic value. The density of stone or artificial armor units, the density of water, geometric parameters or even empirical formulas' parameters derived from calibration based on experimental studies belong in this category. In the preliminary design of coastal structures, resistance parameters are replaced by their characteristic or mean values in the design formula for every element. However, in probabilistic design (see Figure 2.15), resistance parameters can follow probability distributions. A straightforward way to model their variability is to consider them as normal random variables.

3.3.4.4 Monte Carlo Method (MCM)

In MCM the frequency density of TL, and the joint pdfs of SL, θ_m , T_m , and $H_{s,p}$ are also used, aiming at generating a random sample for each variable that should follow its pdf, but also at maintaining the statistical correlation between correlated variables. Therefore, Eqs 3.25 and 3.26 still apply in this method. The generation of the artificial sample of θ_m , T_m , and H_s that corresponds to a total sea level value at the structure's location can be produced in the simple way, by randomly generating an integer number of groups of T_m , $H_{s,p}$, and θ_m between the limits of each joint class, equal to the new frequency of each joint class.

It is worth mentioning that if the total number of the random sample of sea level data components SL, TL and resistance parameters R produced by MCM are denoted by N_s , N_{tl} , N_r

respectively, then the final result of $P_{f,e,L}$ by combining Eq. 2.36 and Eq. 3.25 is given below:

$$P_{f,e,L} = \sum_{N_r} \left(\sum_{N_{it}} \left[1 - \left(1 - \sum_{N_s} \frac{N_{f,i}}{N} / N_s \right)^{\lambda_e L} \right] / N_{it} \right) / N_r \quad (3.27)$$

where: $N_{f,i}$ is the number of occurrence of the i -th element's failure and N is the total number of simulations/ extreme events.

3.3.4.5 Assessing failure probability of the system

A simple way to capture the union probability of the elements' failure events is to check whether all elements of the structure fail under the same loading and resistance conditions. An illustrative example of this procedure concerning a series system of three elements of a rubble mound breakwater is presented in Table 3.17 referring to the case of MCM.

Table 3.17 Estimation of a series system's failure frequency via consideration of the frequency of union of the elements' failure events ([34]; [56]) for MCM

Sea state Simulation number	Sea side armor failure	Toe failure	Rear side armor failure	System failure
1	1	0	1	1
2	0	0	0	0
3	0	1	1	1
⋮	⋮	⋮	⋮	⋮
N	1	0	0	1
Total	$N_{f,s}$	$N_{f,t}$	$N_{f,r}$	N_f

In case of Direct Integration Method (DIM), Table 3.17 can be rewritten in the following form (see Table 3.18):

Table 3.18 Estimation of a series system's failure probability via consideration of the probability of union of the elements' failure events for DIM

Load parameters' joint probability	Sea side armor failure	Toe failure	Rear side armor failure	System failure
p_1	p_1	0	p_1	p_1
p_2	0	0	0	0
p_3	0	p_3	p_3	p_3
\vdots	\vdots	\vdots	\vdots	\vdots
p_n	p_n	0	0	p_n
Total=1	pf_s	pf_t	pf_r	pf

Therefore, according to DIM, the failure probability of a series system $P_{f,e,L,s}$, which consists of three elements, is estimated as follows:

$$P_{f,e,L,s} = \iint f_{\vec{R}}(\vec{r}) f_{TL}(tl) \left[1 - \left(1 - \int_{g_1(\vec{r}, tl, \vec{x}) < 0 \cup g_2(\vec{r}, tl, \vec{x}) < 0 \cup g_3(\vec{r}, tl, \vec{x}) < 0} f_{\vec{X},e,1y}(\vec{x}) d\vec{x} \right)^{\lambda_e L} \right] d\vec{r} dtl \quad (3.28)$$

where, the term $\int_{g_1(\vec{r}, tl, \vec{x}) < 0 \cup g_2(\vec{r}, tl, \vec{x}) < 0 \cup g_3(\vec{r}, tl, \vec{x}) < 0} f_{\vec{X},e,1y}(\vec{x}) d\vec{x}$ is equal to pf estimated in Table 3.18.

In similarity with DIM, in MCM, the failure probability of a series system $P_{f,e,L,s}$, which consists of three elements, is estimated as follows:

$$P_{f,e,L,s} = \sum_{N_r} \left(\sum_{N_{tl}} \left[1 - \left(1 - \sum_{N_s} \frac{N_f}{N} \right)^{\lambda_e L} \right] / N_{tl} \right) / N_r \quad (3.29)$$

where N_f is estimated according to Table 3.17.

3.3.5 Fully probabilistic reliability analysis using all sea conditions

The fully probabilistic analysis, to be presented in this section, is applied to sequential wave data within “weak” and “intense” storms by adopting a time step, enabling equally-discrete representations of the temporal variation of sea-state conditions within storm events, denoted from now on simply as sea states. The result of this approach is the failure probability of the structure, estimated in the total sample of data, extracted directly from initial data in contrast to the approach based on the extreme value analysis of section 3.3.3.

3.3.5.1 *Sea state multivariate analysis*

In this fully probabilistic analysis, the individual data used describing sea-state conditions, are not required to be mutually independent. Besides, depending on the intended use of the analysis, the time step applied on the initial sequence of sea states could be equal or higher from that of the time interval between successive measurements, in which sea conditions are considered stationary. It is noted that a short time interval between successive measurements, e.g. of 1 hr, is preferable since such an interval enables avoidance of record loss of a fast change or peak in sea conditions. Furthermore, the time step used for representation of sea-state conditions for the design and operation of coastal structures, is desirable to range between 1 hr and 3 hr depending on the type of the structure element to be assessed. Specifically, regarding the reliability analysis of the main armor of coastal structures, the minimum three hours interval is recommended to be used in order that the data correspond to more than 1000 waves per loading event, as suggested by limit state function [57] associated to the said design element. Obviously other limit state functions in the realm of coastal engineering may require other time lengths for optimum data assimilation. It is underlined that the issue of loading duration is directly linked with the notion of structural resilience, i.e. the ability of a structure to withstand a storm containing several sea states, as defined above. This ability is not warranted by the successful result over sea states contained in the storm, when such result is based on a limit state assuming a small amount of damage as in the armoring of mound breakwaters. The reason for this is that in reality small damages in such structures cannot be repaired during storms, a fact commonly not accounted for in relevant design formulae.

By adopting a proper time step denoting representations of sea-state conditions of equal duration to be considering as loadings events upon the structure, e.g. of 3 hr, the maximum H_s within this duration associated with its concurrent covariate parameters, i.e. T_m and θ_m , should be selected, in order to represent the corresponding loading of the structure. In this manner, the actual history and shape of each storm event is taken into consideration. Therefore, in the

fully probabilistic analysis examined, this vital information is not missed in contrast to the event-based extreme value analysis mentioned in section 3.3.3. Besides, it is recommended that first this fully probabilistic reliability analysis should be applied to the sample of sea states of medium and extreme events and then the estimated conditional failure probability should be multiplied by the probability of the threshold exceedance in order that the unconditional one be derived. Thus, working on the basis of sea states of equal duration, defined as above, enables the direct derivation of the percentage of time during which the structure will be in a failure state, a useful metric in risk analysis.

In the analysis of sea conditions within storm events applied to the initial time series of wave spectral parameters (wave data), the conditional model is used to fit bivariate distributions of H_s and T_m to the available data set for each directional sector, written as below:

$$f_{T_m, H_s, \theta_{m_i}}(T_m, H_s, \theta_{m_i}) = f_{\theta_m}(\theta_{m_i}) f_{H_s | \theta_m}(H_s | \theta_{m_i}) f_{T_m | (H_s, \theta_{m_i})}(T_m | (H_s, \theta_{m_i})) \quad (3.30)$$

where: $f_{\theta_m}(\theta_{m_i})$ is the probability density of the i -th directional sector with the central value of θ_{m_i} and bin size of $d\theta_m$, i.e. $\theta_m \in \left(\theta_{m_i} - \frac{d\theta_m}{2}, \theta_{m_i} + \frac{d\theta_m}{2} \right)$ measured from North, $f_{H_s | \theta_m}(H_s | \theta_{m_i})$ is the conditional pdf of H_s given that θ_m belongs to the i -th directional sector, and $f_{T_m | (H_s, \theta_{m_i})}(T_m | (H_s, \theta_{m_i}))$ is the conditional pdf of T_m given that H_s has a certain value and θ_m belongs to the i -th directional sector.

The conditional bivariate pdf of T_m and H_s , given θ_m belongs to the i -th directional sector, $f_{H_s, T_m | \theta_m}(T_m, H_s | \theta_{m_i})$ was modeled according to Mathisen and Bitner-Gregersen [58]. The pdf $f_{H_s | \theta_m}(H_s | \theta_{m_i})$ can well be represented by a Weibull pdf in many cases [16], while the pdf $f_{T_m | (H_s, \theta_{m_i})}(T_m | (H_s, \theta_{m_i}))$ can be modeled by a lognormal probability distribution, and the location and scale parameters of the conditional lognormal pdf can be written as functions of $H_s | \theta_{m_i}$ as below [58], adjusted here to consider also θ_m :

$$\begin{aligned} \mu(H_s | \theta_{m_i}) &= a_1 + a_2 H_s^{a_3} \\ \sigma(H_s | \theta_{m_i}) &= b_1 + b_2 \exp(b_3 H_s) \end{aligned}, \quad \theta_m \in \left(\theta_{m_i} - \frac{d\theta_m}{2}, \theta_{m_i} + \frac{d\theta_m}{2} \right) \quad (3.31)$$

where, a_1, a_2, a_3, b_1, b_2 , and b_3 are constants determined from fitting of the curves described by Eq. 3.31 to the data.

3.3.5.2 *Data reduction technique for reliability analysis using all sea conditions*

If the location of the structure is in shallower waters than that of wave measurements collected for the design of the structure, which is a common case, an easy-to-use method is recommended in order that the procedure, of transformation of the probabilistic information of the long-term sea conditions from deep waters to the structure's location, be adjusted to the available computer capacities.

The proposed easy-for-application method [34] can be incorporated into the advanced fully probabilistic methods DIM and MCM and generates an artificial sample of environmental data, e.g. data of significant wave height H_s , mean wave period T_m , mean wave direction θ_m , sea level SL, etc. at the structure's location. These can be so selected to validly represent the full dataset covering a certain time period. The method can be easily applied when wave data in deep waters are available. In this case a wave propagation model has to be applied, e.g. a fast and adequately accurate model via integration of short- and long-term wave statistics [33], to transfer the probabilistic information to the structure's location.

The steps of the methodology applied at correlated environmental parameters in deeper waters than the structure's location are listed below:

- a) Application of a relatively high threshold (e.g. corresponding to 80 or 90% quantile of H_s) to H_s data, which are available in deep waters, to filter the most significant sea states that should be transferred to the structure's location. In this way, not only the most critical sea states are distinguished from the total sample, but also the amount of data to be transferred to the structure location has been significantly reduced.
- b) Grouping of the filtered (over threshold) data into joint classes of adequately small bin size containing all correlated parameters and estimation of the frequency of each joint class. The joint classes can be extracted from the scatter diagram of correlated parameters.
- c) Selection of the reduced sum of the filtered data of the new dataset to optimise computational demands, and attain further data reduction. The size of the new dataset can range at about 8-2% of the initial dataset but not less than 2% to avoid elimination of rare and extreme events in the reduced sample.

- d) Calculation of the new frequencies of the joint classes of the new dataset using proportionate stratification to the size of the new dataset.
- e) To obtain the new dataset, the reduced sample can be produced by randomly generating an integer number of groups of parameters between the limits of each joint class, matching the new frequency of each class, calculated previously.
- f) Estimation of the sample's parameters at the structure's location by propagating the new dataset (step (e)) from deep waters to the structure's location.
- g) Application of the conditional model of the above correlated parameters to the sample of the previous step in order to estimate their joint pdf at the structure's location.
- h) Calculation of the new frequencies of each joint class, by rounding to the nearest integer the product of the joint probability of each class (step (g)) by an adequately large number N .
- i) To obtain the artificial data set of parameters at the structure's location, a sample of N size can be provided by randomly generating an integer number of groups of parameters within the range of each joint class, equal to the new frequency of each joint class (step (h)).

Specifically, if the available data in deep waters covers a period of about 1 decade, only step (a) should be applied and all filtered data should be transferred to the structure's location. Otherwise, the whole method could be applied. Also, the selection of the size of the reduced sample depends on the size of the filtered data, which is related to the time period that the initial data covers, and the time step between the sequential initial data.

It is noted that a part of the aforementioned data reduction technique has been already presented in section 3.1.1. However, in the present section, the main interest is focused on extreme sea conditions, which are critical for the reliability analysis of coastal structures, to a greater degree than in section 3.1.1; the latter described the issue of data reduction in a more general manner.

Returning again to the application example presented in 3.1.6.2, the new sample that could be derived from application of steps (a) to (e) is depicted in the scatter diagram of Figure 3.24. Referring to step (a), an initial threshold corresponding to 80 quantile of H_s has been applied here and then the new dataset generated by this process is 3.8% of the initial dataset presented in Figure 3.6. To check the quality of the new dataset compared with the initial sample of data, the probability distributions selected to represent the two samples could be compared (e.g. see this issue tackled in section 3.1.6.2).

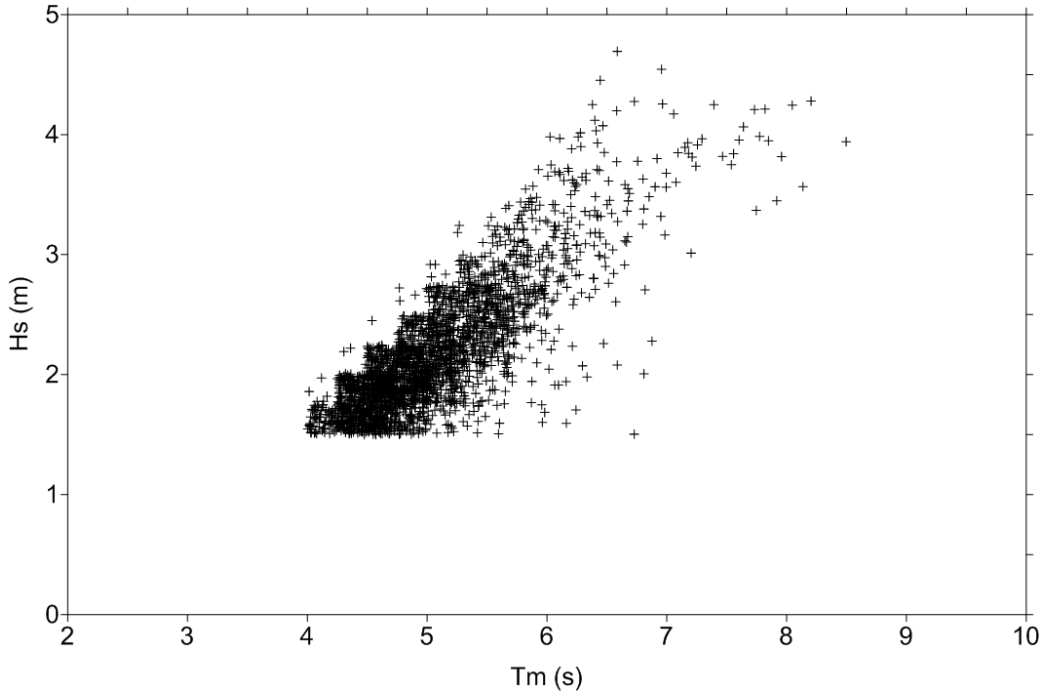


Figure 3.24 The new sample in deep waters derived from the data reduction technique recommended for reliability analysis of coastal structures

3.3.5.3 Assessing an element's failure probability using all sea conditions within storm events by Direct Integration Method (DIM)

In the present reliability analysis, if we have Y years of wave measurements, the time-variant variables, like the sequential spectral data of H_s , T_m at a given time step, correspond to the time period of Y years considering stationary conditions among years. Thus, in this analysis, the unconditional and conditional failure probabilities of the element's failure during Y years can be estimated. The conditional one refers to the sample that exceeds a fixed threshold. Further extrapolation cannot be permitted since the time-variant variables are not independent, or else adequately time-distanced. The unconditional failure probability of the element's failure during Y years is then estimated as follows:

$$P_{f,Y} = \iint_{\Omega(\vec{r}, \vec{x})} f_{\vec{R}}(\vec{r}) f_{\vec{X},Y}(\vec{x}) d\vec{x} d\vec{r} = \int f_{\vec{R}}(\vec{r}) \left(\int_{\Omega(\vec{r}, \vec{x})} f_{\vec{X},Y}(\vec{x}) d\vec{x} \right) d\vec{r} \quad (3.32)$$

where hereinafter $f_{\vec{R}}(\vec{r})$ is the joint pdf of the time-invariant resistance parameters \vec{r} , $f_{\vec{X},Y}(\vec{x})$ is the joint pdf of time-variant random load variables \vec{x} during the reference period

Y , and $\Omega(\vec{r}, \vec{x})$ is the failure domain, which is equal to the union of the definition domains of all random variables involved under the condition that the limit state function is less than zero, i.e. $g(\vec{r}, \vec{x}) < 0$. Therefore, it is evident that:

$$\Omega(\vec{r}, \vec{x}) = \{g(\vec{r}, \vec{x}) < 0\} \quad (3.33)$$

The incorporation of tide in Eq. 3.32 is accomplished as follows:

$$P_{f,Y} = \iint f_{\vec{R}}(\vec{r}) f_{TL}(tl) \int_{\Omega(\vec{r}, \vec{x}, tl)} f_{\vec{X},Y}(\vec{x}) d\vec{x} d\vec{r} dtl \quad (3.34)$$

3.3.5.4 Monte Carlo Method (MCM)

In MCM, the frequency density of TL, and the joint pdfs of SL, θ_m , T_m , and H_s are used, aiming at generating a random sample for each variable that should follow its pdf, but also at maintaining the statistical correlation between correlated variables. Eq. 2.36 could be used to produce a MCM sample, firstly by generating θ_m values that follow their pdf. Then, for every θ_m value depending on its class, i.e. its directional sector, a conditional inverse cumulative distribution function (icdf) of $H_s|\theta_{mi}$ can be used to produce H_s values whose sum is an integer linearly related to the frequency of θ_m class. Therefore, for every θ_m value, there is an H_s value that subsequently determines the conditional icdf's parameters of $T_m|H_s|\theta_{mi}$, which are functions of H_s . Thus, by using again Eq. 2.37, N groups of θ_m , H_s , T_m are produced, where N is a large enough integer to attain convergence of the solution of MCM.

It is worth mentioning that if the total number of the random sample of sea level data components SL, TL and resistance parameters R produced by MCM are denoted by N_s , N_{tl} , N_r respectively, then the final result of $P_{f,L}$ by combining Eq. 2.37 and Eq. 3.34 is given below:

$$P_{f,Y} = \sum_{N_r} \left[\sum_{N_{tl}} \left(\sum_{N_s} \frac{N_{f,i}}{N} / N_s \right) / N_{tl} \right] / N_r \quad (3.35)$$

where: $N_{f,i}$ is the number of occurrence of the i -th element's failure and N is the total number of simulations/ sea state events.

3.3.5.5 Assessing failure probability of the system

According to DIM, the failure probability of a series system $P_{f,Y,s}$, which consists of three elements, is estimated as follows:

$$P_{f,Y,s} = \iint f_{\vec{R}}(\vec{r}) f_{TL}(tl) \int_{g_1(\vec{r},tl,\vec{x}) < 0 \cup g_2(\vec{r},tl,\vec{x}) < 0 \cup g_3(\vec{r},tl,\vec{x}) < 0} f_{\vec{X},Y}(\vec{x}) d\vec{x} d\vec{r} dtl \quad (3.36)$$

where, the term $\int_{g_1(\vec{r},tl,\vec{x}) < 0 \cup g_2(\vec{r},tl,\vec{x}) < 0 \cup g_3(\vec{r},tl,\vec{x}) < 0} f_{\vec{X},Y}(\vec{x}) d\vec{x}$ is equal to pf estimated in Table 3.18.

In similarity with DIM, in MCM, the failure probability of a series system $P_{f,Y,s}$, which consists of three elements, is estimated as follows:

$$P_{f,Y,s} = \sum_{N_r} \left[\sum_{N_{tl}} \left(\sum_{N_s} \frac{N_f}{N} / N_s \right) / N_{tl} \right] / N_r \quad (3.37)$$

where, N_f is estimated according to Table 3.17.

3.3.6 Comparative evaluation of the two fully probabilistic approaches

In this section, the pros and cons of the two probabilistic approaches for the reliability assessment of coastal structures are presented and discussed. The main differences between the two reliability methods with respect to five significant criteria relevant to coastal structures are presented in Table 3.19.

Table 3.19 The pros and cons of the event-based and all sea conditions-based reliability methods

Criterion	Extreme event-based method	All sea conditions-method
1. Can accept as input a short period of measurements or observations Y	x	x x
2. Independent values - Ability to extrapolate from ly to L	✓	x
3. Use of the information of all critical sea conditions in the reliability assessment	x	✓
4. Assessment of the percentage of a reference period that the structure will be in a given state, easily incorporated into a risk analysis	x	✓
5. Incorporation of time, a significant parameter in the design and operation of coastal structures.	x	✓
6. Arrive at probability values independent of any limitations associated to sampling methodology.	x	✓

Referring to the first criterion, it is noted that both methods need a large period of measurements, ideally higher than the lifetime of the structure. Specifically, the extreme event-based method can estimate in a reliable manner return values whose return periods do not exceed 2 - 2.5 times the years of measurements Y. Besides, this method wastes a large amount of the available data that could be critical for the design or operation of a coastal structure. Therefore, in POT method and to a greater degree in Block Maxima Method a large amount of extreme data, and therefore a large period of data, is needed so as to be represented

by an appropriate extremal probability distribution. The second method that uses all sea conditions needs to a greater degree a large period of data/measurements, due to its inability for extrapolation –see 2nd criterion.

In the second criterion, it is evident that in the second method the estimated failure probability corresponds to the period of measurements Y and no extrapolation can be made from one reference period to another. This is because the sequential data used in this method are not independent in general. Contrariwise, in the first method, the peaks of storm events per year or maximum values per year could be considered as independent, enabling thus a time extrapolation of the failure probability, estimated in the sample of extreme events, from the average one year to the lifetime of the structure.

As for the third criterion, since the event-based method wastes a large amount of data, some of which are sea conditions within storm events that probably could be higher than peaks of other storms, a part of critical information is lost. This is because storm events are represented by storm peaks and therefore the storm's profile and history is not taken into consideration. Besides, each storm peak cannot be associated with the total storm duration, and thus the information on storm duration might be also not used properly. On the contrary, the method that uses all sea conditions, e.g. sequential wave spectral data at a given time step, can consider all critical loadings upon a coastal structure with the same duration, equal to the adopted time step.

In the fourth criterion the property mentioned above enables the assessment of the percentage of a reference period, e.g. the lifetime that the structure will be in a failure state (ULS) by the second method, which can be easily incorporated into a risk analysis. However, the first method can estimate the failure probability of a coastal structure in the sample of storm peaks that cannot easily be transformed to the percentage of the lifetime that the structure will be exposed to risk. The same reasoning is applied even more in SLS conditions when risk-informed approaches are used for design, e.g. in wave overtopping, coastal flooding, etc. There, one should be able to assess the behaviour or serviceability of a coastal structure in terms of running time under a predefined range of limit states.

The 5th criterion relates to the fact that time plays a considerable role in the design of coastal structures, especially of rubble mounds. Methods are currently available that require the number of design waves impinging on the structure in one row. Advancements of this notion lead to the concept of structural resilience, where a slightly damaged structure is examined through a storm period and more. This concept is being applied in physical model studies so

far, but it is a matter that credible numerical models will be able to tackle design under such conditions.

The 6th criterion is added to reveal the qualitative difference between the two methods compared. Indeed, results from the extremes method should be accompanied by a statement on the sampling method, denoting in this way what exactly the result means, e.g. “20% probability that a given extreme value will be surpassed during the lifetime of the structure by values in a sample of extremes obtained through the following method: ...”, whereas results from the all sea conditions method could be simply expressed as “1% probability that a given value will be surpassed during the lifetime of the structure”.

It is noted that a combination of the two methods could be applied as a third method so as to gather the pros of both methods. This third method can be used in case of sufficiently independent values above a satisfactorily high threshold. The timeseries independence is possible to apply for a very high threshold but should be checked a priori to ensure validity of the method. Since this is a POT method (independent values), even if this is not an event-based one, could extrapolate its conditional failure probability given the threshold exceedance from one reference period to another. Besides, the corresponding failure probability referred to the total sample could be also estimated, but only under the condition that the whole sample below the threshold belongs to the safe domain and thus has no contribution to the outcome of failure probability. However, the latter becomes more difficult in case of a very high threshold. An illustrative example is the case when lower significant wave heights than a very high threshold can become critical, e.g. for overtopping of the structure or armor layer’s erosion, when combined with specific wave periods.

In short, it could be stated that if the period of measurements Y is much lower than the lifetime of the structure L , the extreme event-based method could be used for the design of a coastal structure (e.g. ULS), considering however its cons, and the second method for the operation of the structure (e.g. SLS). However, if Y is close to or higher than L , then the second method is preferable than the first one.

3.3.7 Incorporation of the reliability analysis into a design process

The steps of the methodology adopted in this study are described below and can formulate a reliability analysis of a coastal structure under wave action, e.g. a rubble mound breakwater considered as a system, with a known fault tree. This reliability analysis is indicatively incorporated in a design process example below:

Step (a) Define design requirements for Limit State adopted (e.g. Serviceability Limit State (SLS), Ultimate Limit State denoted by ULS), such as Design lifetime, and allowable failure probability during the lifetime

Step (b) Split the fault tree into parallel and series subsystems that consist of individual modes of failure

Step (c) For every subsystem, choose a robust design formula for every element of the subsystem to examine the element's reliability and formulate the limit state function g of each element, e.g. the sea-side armor stability.

Step (d) For every element of a subsystem, apply a preliminary design, e.g. deterministic design, which will provide an initial result (i.e. some structure's characteristics, like mass of armor units), for the fully probabilistic design.

Step (e) For every element of a subsystem, apply a fully probabilistic method to estimate the failure probability of the element.

Step (f) Evaluate the subsystem's reliability by estimating the subsystem's probability of failure. The latter can be calculated via consideration of the probability of union or of intersection of the elements' failure events referring to the case of series or parallel subsystem, respectively.

Step (g) The total system's probability of failure can then be estimated by considering the failure probability of all subsystems and their linking to the total system.

Step (h) Optimize the structure's characteristics according to the design requirements and economic costs.

A flowchart of the aforementioned methodology has already been presented in Figure 2.15 of section 2.3.2.

3.3.8 Individual failure modes

The type of structure studied in the present thesis is a conventional rubble mound with rock armored slopes and with no crest element. However, the methodology can well be expanded to cater for other types of coastal structures too.

Three modes of failure are selected to be described here by the stability formulas of their corresponding elements. These modes are the seaside armor instability, the rear-side armor instability due to overtopping, and the toe instability. In the following subsections a well-known, suitable stability formula that corresponds to each failure mode will be described and rewritten to reliability formula for a rock armored rubble mound breakwater. For brevity, only the formulas applied in section 3.4, and not all existing formulas, will be presented here.

3.3.8.1 Seaside armor stability

The seaside armor element is the core element of a rubble mound breakwater since this is severely exposed to wave action. Therefore, a reliable design formula must be selected to ensure the element's stability. Besides, the water depth at the structure's location should be a criterion for the selection of the type of the formula applied.

To examine the deep water conditions, the formula by Van der Meer [57] is used. The rock armor stability formulas by Van der Meer [57] were based on earlier work by Thompson and Shuttler [215] and on a series of physical model tests performed in relatively deep-water wave conditions at the structure's toe. Besides, the formulas were dependent on the wave breaking type upon the structure slope, thus a distinction was made between "plunging" and "surging" waves, based on the value of the surf-similarity parameter. In the following stability formulas the wave heights were assumed to be Rayleigh distributed:

For plunging waves ($\xi_m < \xi_{mc}$):

$$\frac{S}{\sqrt{N}} = \left(\frac{1}{6.2} P^{-0.18} \xi_m^{0.5} \frac{H_s}{\Delta D_{n50}} \right)^5 \quad (3.38)$$

For surging waves ($\xi_m \geq \xi_{mc}$):

$$\frac{S}{\sqrt{N}} = \left(P^{0.13} \xi_m^{-P} \tan a^{0.5} \frac{H_s}{\Delta D_{n50}} \right)^5 \quad (3.39)$$

where: H_s is the incident significant wave height at the toe of the structure, $\Delta = (\rho_s / \rho_w) - 1$ is the relative buoyant density, ρ_s is the rock density, ρ_w is the water density, ξ_m is the surf-similarity parameter using the mean wave period T_m from time domain analysis, a is the angle of the structure slope, D_{n50} is the nominal diameter of the rock armor unit, P is a permeability parameter of the structure, N is the number of incoming waves, and S is the damage level as defined by Broderick [216]: $S = \frac{A_e}{D_{n50}^2}$, in which A_e is the erosion area in the cross-section profile of the structure around the still-water level (SWL). The transition from "plunging" to "surging" waves occurs at the critical value of the surf-similarity parameter:

$$\xi_{mc} = \left(6.2P^{0.31} \sqrt{\tan a}\right)^{\frac{1}{P+0.5}} \quad (3.40)$$

The above formulas can be rewritten in the following form of limit state functions:

For plunging waves ($\xi_m < \xi_{mc}$):

$$g = 6.2S^{0.2} P^{0.18} N^{-0.1} \xi_m^{-0.5} - \frac{H_s}{\Delta D_{n50}} \quad (3.41)$$

For surging waves ($\xi_m \geq \xi_{mc}$):

$$g = 1.0S^{0.2} P^{-0.13} N^{-0.1} (\cot a)^{0.5} \xi_m^P - \frac{H_s}{\Delta D_{n50}} \quad (3.42)$$

Therefore, if $g < 0$, the element's state belongs to the failure domain.

As far as the damage level S is concerned, the Rock Manual [55] provides some guidance for 3 stages of damage depending on the seaside slope of the structure (see Table 3.20). Furthermore, as for the number of the incoming waves N , equations are accurate for $1000 \leq N \leq 7500$. After this value, equilibrium damage is more or less reached [1]. Moreover, equations are valid for a certain range for each parameter involved. The latter will not be

displayed here due to lack of space. However, these constraints are considered in the application examples presented in section 3.4.

Table 3.20 Guidelines for selection of damage parameter for armor stone in a double layer [55]

Slope (cot(a))	Stage of damage		
	Initial damage	Intermediate damage	Failure
1.5	2	3-5	8
2	2	4-6	8
3	2	6-9	12
4	3	8-12	17

By modifying the above Van der Meer formulas, Van Gent *et al.* [217] extended their applicability to include also shallow water conditions. Smith *et al.* [218] proposed to waive the assumption on the Rayleigh distributed wave heights. Hence, in their modified form of Van der Meer's formulas, valid for both deep- and shallow-water wave conditions, include the ratio $\frac{H_{2\%}}{H_s}$ where $H_{2\%}$ is the wave height exceeded by 2% of the waves in the sea state.

Moreover, in this approach, Van Gent *et al.* [217] proved that another wave period, which considers the shape of the wave energy spectra, gives more reliable results for the stability formulas, than the mean wave period T_m from time-domain analysis does. This optimal period is the spectral wave period $T_{m-1,0}$ which is obtained from the measured wave energy spectrum as follows:

$$T_{m-1,0} = \frac{m_{-1}}{m_0} \quad (3.43)$$

where:

$$m_n = \int_0^{\infty} f^n S(f) df, \text{ for } n = -1 \text{ or } 0, \quad (3.44)$$

in which, f is the frequency and $S(f)$ the density of the wave energy spectrum. For a standard Jonswap spectrum $T_{m-1,0}$ can be approximately estimated based on the spectral peak wave period via the following relation:

$$T_p = 1.1T_{m-1,0} \quad (3.45)$$

Besides, the coefficients of Van der Meer [57] formulas were recalibrated and the confidence bounds were adapted. The modified formulas are as follows:

For plunging waves, ($\xi_{s,-1} < \xi_c$):

$$\frac{S}{\sqrt{N}} = \left(\frac{1}{c_{plunging}} P^{-0.18} \xi_{s,-1}^{0.5} \frac{H_s}{\Delta D_{n50}} \left(\frac{H_{2\%}}{H_s} \right) \right)^5 \quad (3.46)$$

For surging waves, ($\xi_{s,-1} \geq \xi_c$):

$$\frac{S}{\sqrt{N}} = \left(\frac{1}{c_{surging}} P^{0.13} \xi_{s,-1}^{-P} \tan a^{0.5} \frac{H_s}{\Delta D_{n50}} \left(\frac{H_{2\%}}{H_s} \right) \right)^5 \quad (3.47)$$

The transition from "plunging" to "surging" waves is denoted by a critical value of ξ_c according to:

$$\xi_c = \left(\frac{c_{plunging}}{c_{surging}} P^{0.31} \sqrt{\tan a} \right)^{\frac{1}{P+0.5}} \quad (3.48)$$

where $\xi_{s,-1}$ is the surf similarity parameter using the $T_{m-1,0}$, $c_{plunging} = 8.4$, and $c_{surging} = 1.3$.

The above formulas can be rewritten in the following form of limit state functions:

For plunging waves, ($\xi_{s,-1} < \xi_c$):

$$g = c_{plunging} S^{0.2} P^{0.18} N^{-0.1} \xi_{s,-1}^{-0.5} \left(\frac{H_{2\%}}{H_s} \right) - \frac{H_s}{\Delta D_{n50}} \tag{3.49}$$

For surging waves, ($\xi_{s,-1} \geq \xi_c$):

$$g = c_{surging} S^{0.2} P^{-0.13} N^{-0.1} (\cot a)^{0.5} \xi_{s,-1}^P \left(\frac{H_{2\%}}{H_s} \right) - \frac{H_s}{\Delta D_{n50}} \tag{3.50}$$

According to the Rock Manual [55] it is recommended that the original Van der Meer formulas should be used for deep water, and the Van Gent et al [217] version in shallow water, while caution should be taken in the transition zone between both formula-sets (see Figure 3.25). However many structures have to be designed in the transition zone, or else in intermediate waters, and it is not clear which is the contribution of the shallowness and slope of the foreshore to the stability of the structure [219].

Item	Water depth characterisation		
	Very shallow water	Shallow water	Deep water
Parameter: Relative water depth at the toe: h/H_{s-toe}	$\approx 1.5 - \approx 2$	< 3	> 3
Wave height ratio, $R_H = H_{s-toe}/H_{s0}$	$< 70\%$	$70\% < R_H < 90\%$	$> 90\%$
Stability formulae: Van der Meer – deep water, Equation nos 5.136 and 5.137			
Van der Meer – shallow water Equation nos 5.139 and 5.140			

Figure 3.25 Recommendation on the use of the formulas by Van der Meer [57] and Van Gent et al [217] version [55]

As noticed in Figure 3.24, there are a number of parameters that affect results of armor stone size related to definition of shallow water. According to Guler et al. [220], these parameters could be regarded as “design constraints” also including the parameter $(h/H_{s,toe})$ recommended by The Rock Manual [55]. Definitions of design constraints are given as follows:

Constraint 1: Depth at the toe of the structure over significant wave height at the toe of the structure should be less than 3, i.e. $h/H_{s,toe} < 3$.

Constraint 2: Wave height exceeded by 2% of the waves at the toe over significant wave height at the toe of the structure should be less than 1.4, i.e. $H_{2\%}/H_{s,toe} < 1.4$.

Constraint 3: Significant wave height at the toe of the structure over deep water significant wave height should be less than 0.9, i.e. $R_H = H_{s,toe}/H_{s,0} < 0.9$.

According to The Rock Manual [55], Van Gent et al. [217] formula is recommended to be used when Constraint 1 is smaller than 3. However, in many cases these three constraints are not satisfied simultaneously, making thus not clear which formula is more appropriate between the two formula-sets.

Guler et al. [220] declared that since Van der Meer [57] approach is tested in practice widely in deep and intermediate or moderate shallow water, it seems more appropriate to use this formulation in this range. Thus, Guler et al. derived the following design flowchart based on this discussion (see Figure 3.26), according to which, when all the design constraints are satisfied, Van Gent et al. [217] approach is recommended; otherwise, Van der Meer [57] approach is recommended.

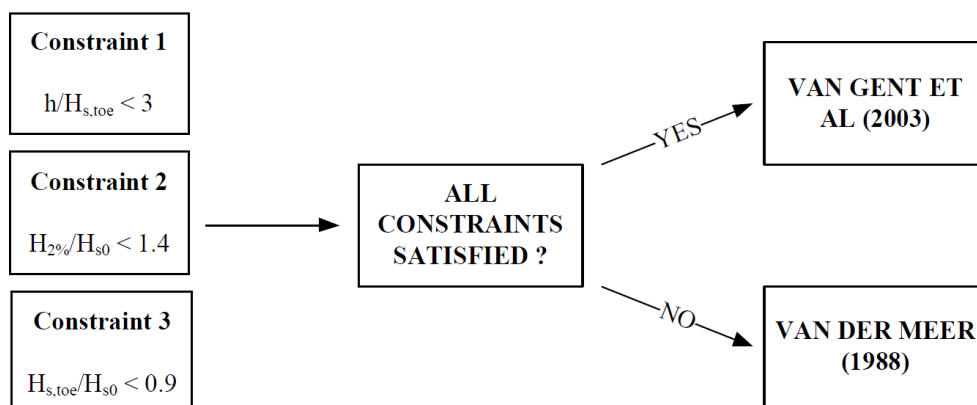


Figure 3.26 Design flowchart providing recommendation on the use of the two formulas-sets [220]

The validity of the design flowchart presented in Figure 3.26 has been approved by Guler et al. [220] within a number of physical model experiments, and therefore has been adopted in this thesis.

3.3.8.2 *Rear-side armor stability*

For rubble mound structures, the rear-side armor instability and damage is related to wave runup and overtopping that causes erosion at the rear side. The rear-side stability formula used in the present thesis is the one by Van Gent and Pozueta [60] which refers to rubble mound breakwaters without crest elements.

Van Gent and Pozueta [60] adopted a three step approach to predict erosion at the rear side (see Figure 3.27). The three steps are described below:

Step 1: Estimation of fictitious wave run-up level based on wave conditions at the structure's toe.

Step 2: Estimate wave overtopping parameters from wave runup.

Step 3: Estimate the amount of erosion at the rear side from wave overtopping parameters.

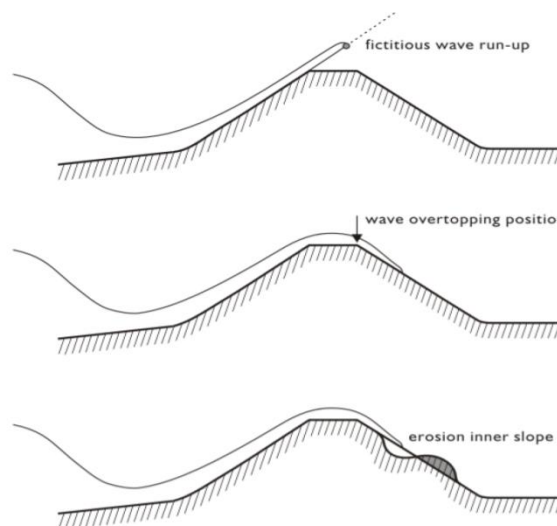


Figure 3.27 The three-step approach for prediction of erosion at the rear side [60]

To estimate wave run-up levels the formula by Van Gent ([221], [222]) is used for situations where the seaward slope is extended such as the breakwater is not overtopped, as given below:

$$\begin{aligned} z_{1\%} / (\gamma H_s) &= c_0 \xi_{s,-1} && \text{for } \xi_{s,-1} \leq p \\ z_{1\%} / (\gamma H_s) &= c_1 - c_2 / \xi_{s,-1} && \text{for } \xi_{s,-1} \geq p \end{aligned} \quad (3.51)$$

where H_s is the significant wave height (i.e. $H_{1/3}$) at the toe of the structure, and $\gamma = \gamma_f \gamma_\beta$ is the reduction factor that considers the effects of angular wave attack (γ_β) and roughness (γ_f). The parameters c_2, p are determined as $c_2 = 0.25 c_1^2 / c_0$ and $p = 0.5 c_1 / c_0$ and the surf

similarity parameter is defined as $\xi_{s,-1} = \frac{\tan a}{\sqrt{\frac{2\pi H_s}{gT_{m-1,0}^2}}}$. Table 3.21 provides the values for

coefficients c_0 and c_1 for 3 exceedances levels (1%, 2%, and 10%).

Table 3.21 Coefficients for wave run-up predictions [221], [222]

Parameter	c_0	c_1
$Z_{1\%}$	1.45	5.1
$Z_{2\%}$	1.35	4.7
$Z_{10\%}$	1.10	4.0

In the situation where the fictitious wave run-up is higher than the crest level, the following formula by Van Gent [223] can be used to estimate wave overtopping characterized by the maximum velocity exceeded by 1% of the incident waves $u_{1\%}$

$$\frac{u_{1\%}}{\sqrt{gH_s}} = 1.7 (\gamma_{f-c})^{0.5} \left(\frac{z_{1\%} - R_c}{\gamma_f H_s} \right)^{0.5} / \left(1 + 0.1 \frac{B_c}{H_s} \right) \quad (3.52)$$

where: B_c is the crest width, γ_{f-c} is a factor for the friction at the crest and γ_f is a parameter for the friction at the seaward slope.

The formula by Van Gent and Pozueta [60], aiming at predicting erosion at the rear side of the structure, follows these two equations for run-up and overtopping and is written here in the form of a reliability function:

$$g = 0.008 \left(\frac{S}{\sqrt{N}} \right)^{-1/6} \left(\frac{u_{1\%} T_{m-1.0}}{\sqrt{\Delta}} \right) (\cot a_{rear})^{-2.5/6} \left(1 + 10 \exp \left(-\frac{R_{c,rear}}{H_s} \right) \right)^{1/6} - D_{n50} \quad (3.53)$$

where a_{rear} is the angle of rear side slope, $R_{c,rear}$ is the crest free board relative to still water level (SWL) at rear side, while the rest parameters are defined, as previously, in section 3.3.8.1.

3.3.8.3 Toe stability

The stability of a toe berm formed by 2 layers of stone can be calculated by the formula by Van der Meer et al. [59] written in the form of a limit state function as follows:

$$g = D_{n50} - \frac{H_s}{\left(2 + 6.2 \left(\frac{h_t}{h} \right)^{2.7} \right) N_{od}^{0.15} \Delta} \quad (3.54)$$

where h_t is the water depth above the toe, h is the water depth just in front of the toe.

Based on Gerding [224] and the Rock Manual [55] damage to rock toe structures with a width of three stone diameters or more can be classified as follows:

NOD= 0.5: start of damage

NOD= 2: intermediate damage and

NOD= 4: severe damage/failure.

For wider toe structures higher NOD values can be used [225].

3.3.9 Considering the effect of oblique wave attack in the reliability analysis

Stability formulae for rubble mound breakwaters are usually being applied assuming perpendicular wave attack. However, neglecting of the effect of oblique waves on the structure's stability leads to a conservative assumption. According to Galland [12], the consideration of this effect can be accomplished by using the notion of the equivalent normal wave height which is defined as follows:

$$H_{s,e} = H_s \cos \beta^X \quad (3.55)$$

where X is equal to 0.25, 0.60, and 1/3 for quarry stone corresponding to seaside armor, toe, and rear-side armor stability, respectively, and β is the angle between the mean wave direction and the perpendicular axis of the structure.

3.4 Examples of reliability analysis of a rubble mound breakwater

In this section, two examples of reliability analysis of a rubble mound breakwater will be examined and described. The presentation of these two examples has the following main and significant objectives, which are listed below:

- The estimation of the long-term wave climate at a coastal structure's location in intermediate waters using wave observations or measurements in deeper waters
- The application of a preliminary event-based extreme value analysis and an analysis on sea-state conditions within storm events in order that both of these two approaches could be incorporated in the reliability assessment and design of a coastal structure
- The investigation of the effect, of considering more and different types of parameters as random variables, on the assessed failure probability of the structure.

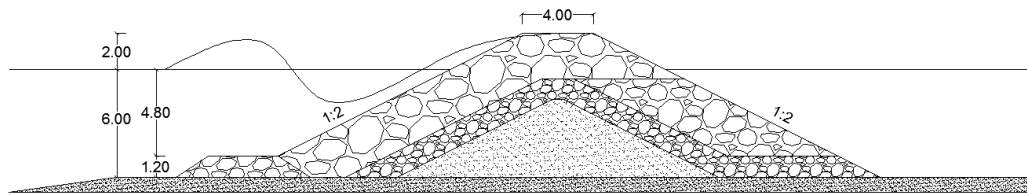
3.4.1 Define design requirements and structural characteristics

The coastal structure of interest is a rubble mound breakwater, whose characteristics, presented in Table 3.22, are the same in both examples. Besides, a typical cross section of the structure is depicted in Figure 3.28. The lifetime of the structure is considered equal to 10 years, a little higher than the period of measurements, in order that both reliability approaches be appropriate for the design of the structure. Furthermore, the marginal return periods for $H_{s,p}$ examined concerning the extreme value analysis are 10 years and 100 years in both examples. The two examples refer to two different points in the Mediterranean Sea; the first point is located off Malaga (Spain), and the second one in the central Aegean off Mykonos (Greece). The wave data used in the first example were derived from a buoy located at the intermediate water depth of 15 m and covered 8 years of measurements, while in the second example from a buoy located at the depth of 140 m, i.e. in deep waters, and covered 12 years of measurements. Therefore, the lifetime of the structure is considered equal to 15 years, a little higher than the period of measurements, in order that both reliability approaches be appropriate for the design of the structure. Moreover, long-term wave statistics are estimated concerning these two locations, and then the long-term wave statistics are estimated at the structure's location via a wave propagation model, i.e. from the depth of 15 m to 6 m and from 140 m to the depth of 6 m, in the first and the second example, respectively.

The permeability parameter used in limit state functions was 0.40 according to Van der Meer [57], while the damage parameters S and N_{OD} correspond to initial damage for both seaside and rear-side armor, and toe stability, respectively [1].

Table 3.22 Structural characteristics of a specific rubble mound breakwater

Parameter	Value
Seaward slope	1:2
Freeboard at the seaward side (m)	2.0
Water depth above the structure's toe / water depth just in front of the toe	0.8
Crest width (m)	4.0
Rear side slope	1:2
Freeboard at the rear side (m)	2.0
Permeability parameter P	0.4
Damage level S	2
Damage level N_{OD}	0.5

**Figure 3.28 A typical cross section of the rubble mound breakwater [35]**

In this step, the design requirements should be defined, as well as the fault tree that should include all the fundamental individual failure modes. Since a rubble mound breakwater with armor slopes commonly does not fail immediately after a storm, but the damage progresses gradually during its lifetime, the design Limit State here is selected to be the Serviceability Limit State considering limited damage (SLS-Id). Thus, the design rubble mound breakwater in the present thesis will be checked for initial damage to its elements and to the total system.

As far as the fault tree is concerned, a series fault tree is used, as is usually the case for coastal structures [1], that consists of three individual main failure modes, i.e. the sea side armor failure, the toe instability, and the rear side armor failure due to overtopping. The formulas used for the aforementioned structural elements have been developed by [57], [59], and [60], respectively. Regarding the sea side rock armor stability, after conducting a comparative

analysis on three stability formulas, i.e. [57]; [226]; [226], the former was selected based on the design constraints recommended in the Rock Manual [55].

Besides, it is worth mentioning that the effect of oblique wave attack on these three elements' stability has been also taken into consideration via the use of the equivalent normal H_s proposed by Galland [12].

3.4.2 Case study off Malaga (Spain)

3.4.2.1 Case study description

The methodology presented in this study is applied to measured long-term historical wave data of H_s , T_m , and θ_m that cover the time period from 2010 to 2017 obtained from an oceanographic buoy. The latter is located in intermediate water depth of about 15m (i.e. 36.69° N, 4.42° W) near the port of Malaga (Spain) in the Mediterranean Sea. The recording interval is basically 1 h, while they are some missing values which have been excluded from the analysis. Furthermore, long-term sea level measurements have also been used covering the period from 1992 till 2019 obtained from a tide gauge located in the port of Malaga (specifically: 36.71° N, 4.42° W). The recording interval is 1 h too and the sea level data is divided by the gauge in two components, i.e. the astronomical (tide) TL and the meteorological component SL (e.g. storm surge). The locations of these two stations (buoy and tide gauge) are depicted in Figure 3.29.

Regarding the statistical correlation between wave parameters obtained from the buoy, the Pearson correlation coefficient between T_m and H_s is estimated at 0.68, given as an initial presentation of their correlation, while directional effects on the joint pdf of T_m and H_s were also noticed. The scatter diagram of T_m and H_s measurements is depicted in Fig. 3.30.



Figure 3.29 Locations of the buoy (red point) and tide gauge (yellow point) near the port of Malaga (Spain)

<http://www.puertos.es/en-us/oceanografia/Pages/portus.aspx>

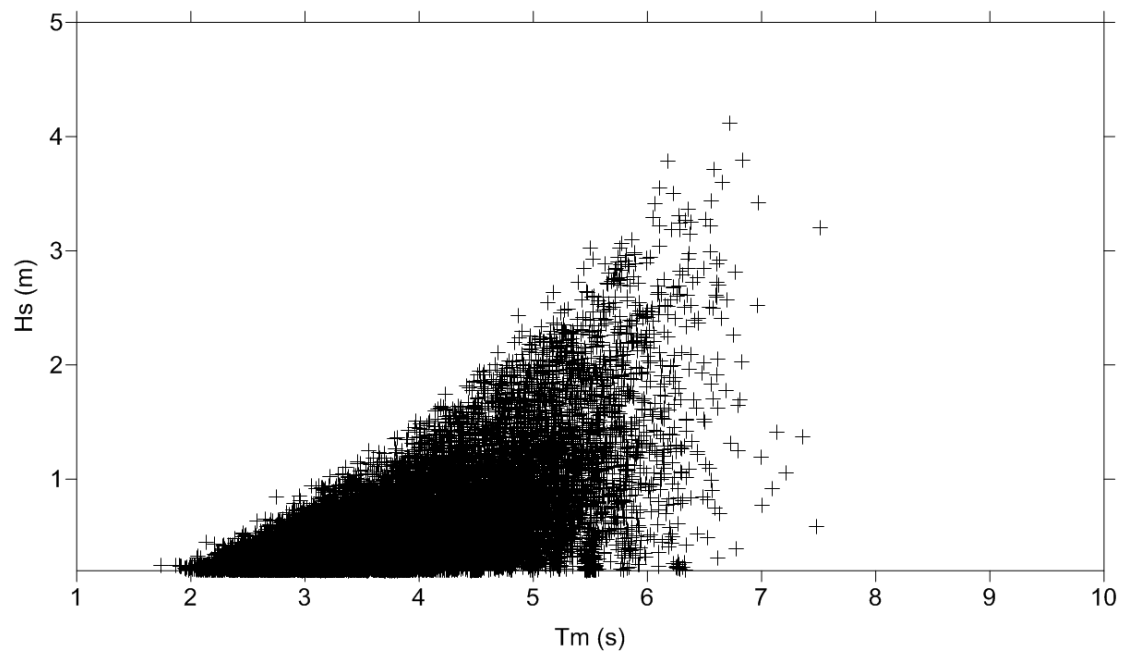


Figure 3.30 Scatter diagram of T_m and H_s measurements obtained from the buoy [35]

The Pearson correlation coefficient between TL and SL in the case of Malaga is estimated at 0.001; thus they can be considered uncorrelated. Furthermore, the Pearson correlation coefficient between TL and H_s and between SL and H_s are about 0.01 and 0.1, respectively. Despite that SL and H_s seem to be more correlated compared against the other two variables

with H_s , this correlation is not considered significant and thus will not be considered in this study. The frequency density polygons of TL and SL as measured by the tide gauge are presented in Figure 3.31. As seen in Figure 3.31, the case of Malaga refers to a micro-tidal and -storm surge sea, thus wave parameters are more critical than the sea level variations, for the design of a coastal structure off Malaga.

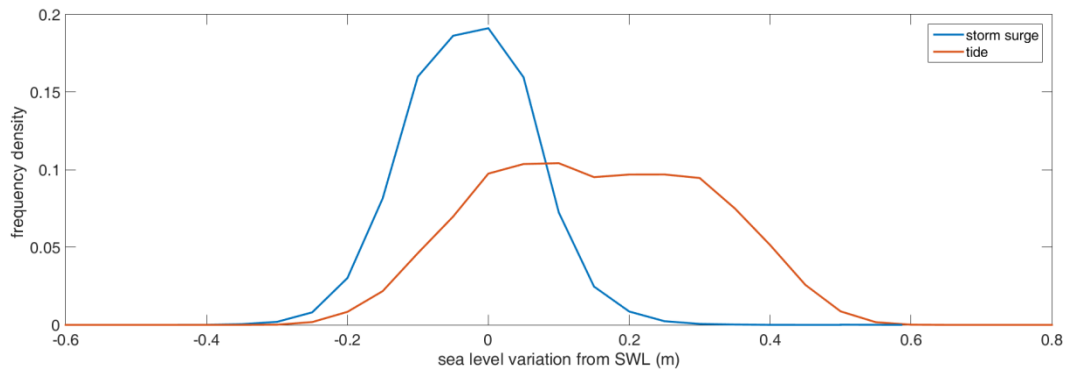


Figure 3.31 Frequency density polygons of TL and SL as measured by the tide gauge [35]

3.4.2.2 Identification of storm events at the buoy location (Malaga)

An initial threshold u_1 was selected for H_s distinguishing weak and intense storms from the dataset. Besides, a minimum calm period of 6 hr [51] between two consecutive storms was selected to ensure that the two events are independent resulting in reducing storm events from 101 dependent to 82 independent events in this dataset. Then, the dataset of the maximum significant wave heights $H_{s,p}$ throughout the storms is derived from this procedure. In this study, the initial threshold u_1 is selected equal to 1.65 m, which corresponds to the 98.5-quantile of H_s data. The histograms and the scatter diagram of duration and $H_{s,p}$ of independent events exceeding this initial threshold 1.65 m are shown in Figure 3.32. Furthermore, the histograms and the scatter diagram of mean wave period of storms and $H_{s,p}$ and that of storm mean wave direction and $H_{s,p}$ are presented in Figures 3.33 and 3.34, respectively. As shown from Figure 3.34, all storms mean wave direction fall within the interval of 100 to 125 ° from North. The most severe storm has a mean wave direction of 113 ° from North.

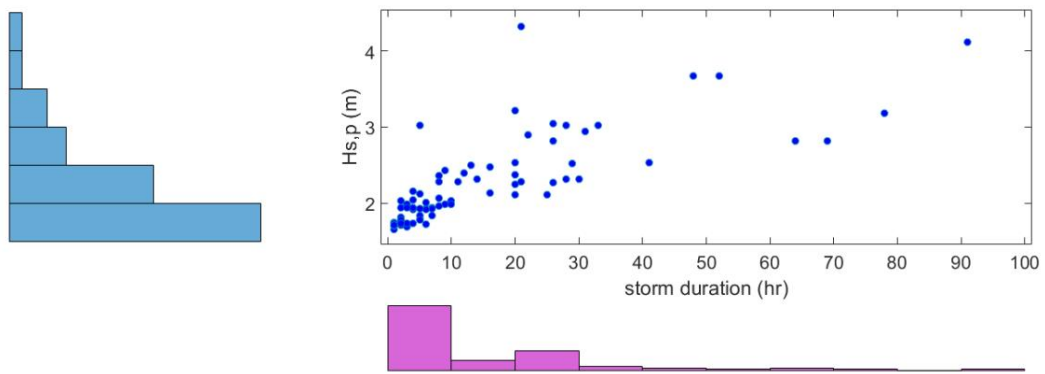


Figure 3.32 Histograms and scatter diagram of $H_{s,p}$ and storm duration at the buoy location (Malaga)

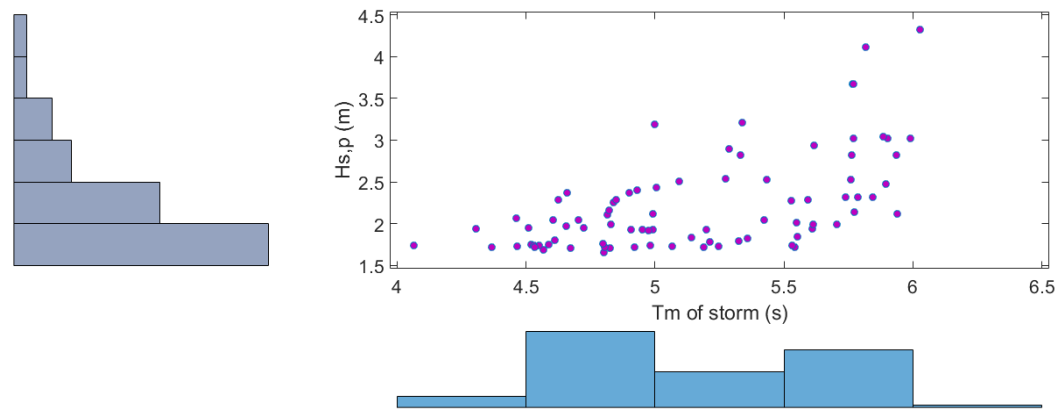


Figure 3.33 Histograms and scatter diagram of $H_{s,p}$ and storm T_m at the buoy location (Malaga)

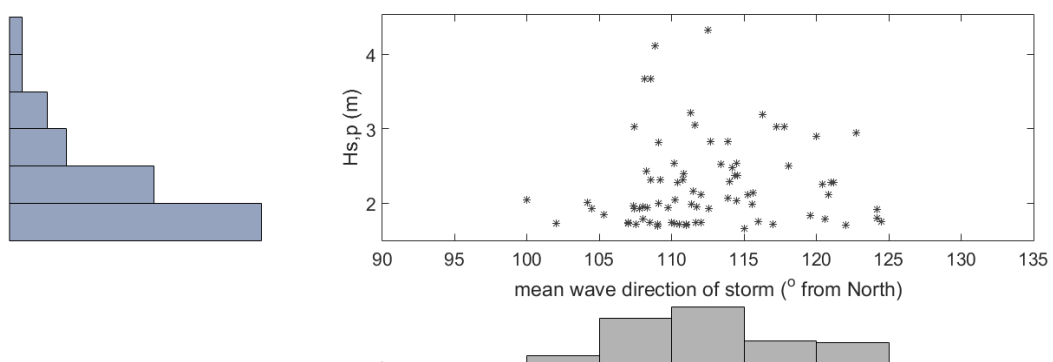


Figure 3.34 Histograms and scatter diagram of $H_{s,p}$ and storm θ_m at the buoy location (Malaga)

3.4.2.3 Transferring storm events from the buoy to the structure's location (Malaga)

The sea bottom is considered uniform with a mean slope of 5% in deep and intermediate waters. Thus, sea level and wave data need to be transferred to the structure's water depth. In contrast to deep waters, where wave parameters are not affected by water depth and sea level variations, in intermediate water depths the latter two do affect wave parameters. In Figure 3.35, a comparison is made between the scatter diagrams of storm duration and $H_{s,p}$ at the buoy (depth of 15 m) and structure (depth of 6 m) location, and in Figure 3.36 the histograms and the scatter diagrams of storm mean wave direction and $H_{s,p}$ are presented. As shown in Figure 3.36, the most severe storm has a mean wave direction of 113° from North, which is normal to the shoreline, as in the buoy location.

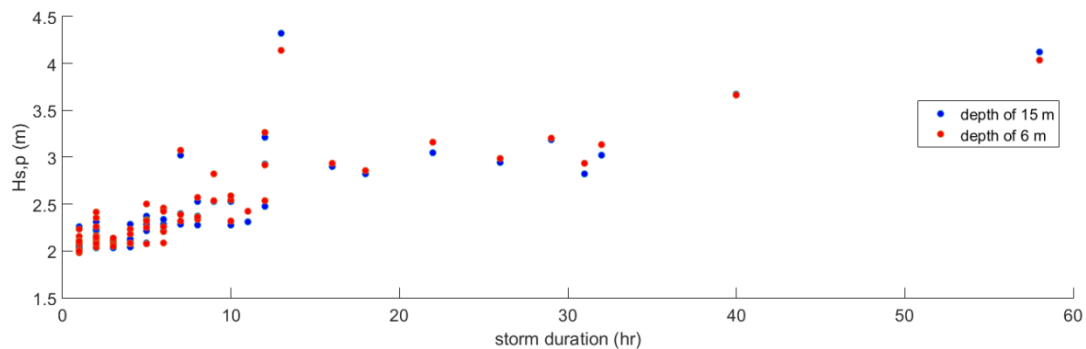


Figure 3.35 Scatter diagram of storm duration and $H_{s,p}$ at the buoy (depth of 15 m) and structure (depth of 6 m) location (Malaga)

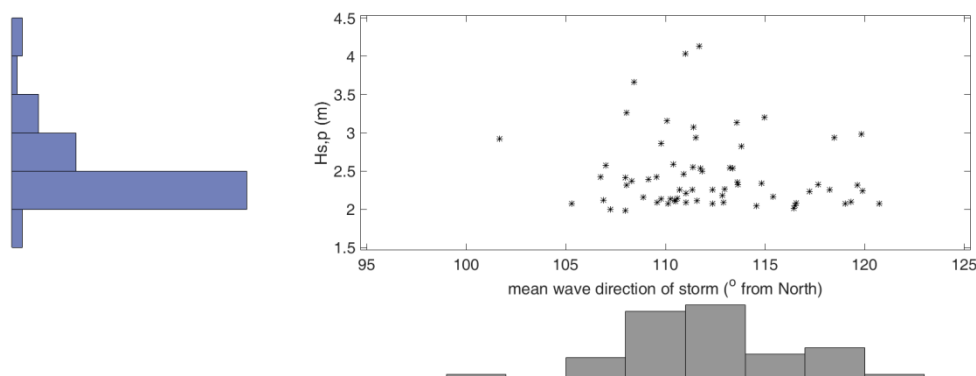


Figure 3.36 Histograms and scatter diagram of $H_{s,p}$ and storm θ_m at the structure location (Malaga)

The next step is the selection of another threshold u_2 higher than u_1 . Judging from the two methods (i.e. [61], [62]) results for the selection of the most appropriate GP parameters and

threshold value, the value of 2.409 m is selected for threshold u_2 . The parameter λ_e that corresponds to this value of u_2 is 3.125, i.e. approximately 3 extreme events per year.

The return periods and values for $H_{s,p}$ associated with the most probable values of their covariate parameters at the structure's location selected for the preliminary design are presented in Table 3.23. The duration of $H_{s,p}$ is considered here equal to 3 hr in order that more than 1000 waves correspond per loading event. The use of this duration will be explained further in section 3.4.2.5.

Table 3.23 Return periods and values for $H_{s,p}$ associated with the most probable values of the covariate parameters at the structure's location (depth of 6 m) selected for the preliminary design

Return Period T_r for $H_{s,p}$ (years)	Return value - $H_{s,p}$ (m)	T_m (s)	duration (hr)	θ_m (deg)
10	4.03	6.25	3	113
100	4.54	6.58	3	113

It is noted that in this thesis, only a univariate event-based extreme value analysis has been conducted, and the most probable values of the covariate variables have been selected approximately from the scatter diagrams. Therefore, a multivariate event extreme value analysis (e.g. [63]) is recommended for a more accurate estimation of those parameters. This is not dealt with in the present thesis, since the statistical analysis of sea state conditions within storm events is used for the probabilistic design of coastal structures.

3.4.2.4 Preliminary design based on the design storm events (Malaga)

Since the input data for the preliminary design have been estimated, the median mass of the rock units of the structure's elements (i.e. seaside armor, rear side armor and toe) will be computed at this step. Median mass M_{50} is defined [55] as the mass of the theoretical block for which half of the mass of the sample is lighter. Some other deterministic parameters that have not been specified yet are the rock density ρ_s , and the water density ρ_w , which are considered equal to 2.650 t/m³ and 1.025 t/m³, respectively.

As for the structure's orientation, judging from Figure 3.35, the structure's perpendicular axis has been selected to have a direction of 113 ° from North so as to protect the shoreline from the most severe storms.

The results of the preliminary design after using the design formulas, i.e. by Van der Meer [57]; Van der Meer [59]; Van Gent and Pozueta [60], for seaside armor, toe, and rear side armor, for initial damage are shown in the following Table 3.24. The equivalent failure probabilities per annum (estimated in the sample of $H_{s,p}$) and during structure's Lifetime (estimated by Eq. 2.7), associated to the return periods of $H_{s,p}$ at the depth of 6 m, are displayed in Table 3.25.

Table 3.24 Median mass of the elements' units estimated by the preliminary design (Malaga)

T_r for $H_{s,p}$ (years)	Seaside armor units (kg)	Rear-side armor units (kg)	Toe units (kg)
10	5018	1241	379
100	6980	1915	542

Table 3.25 Equivalent failure probabilities per annum and over structure's Lifetime (15 years), associated to return period of $H_{s,p}$ at the depth of 6 m (Malaga)

T_r for $H_{s,p}$ (years)	$P_{ex,H_{s,p},e,1y}$	$P_{f,e,L}$
10	$3.20 \cdot 10^{-2}$	$7.82 \cdot 10^{-1}$
100	$3.20 \cdot 10^{-3}$	$1.40 \cdot 10^{-1}$

However, in the above analysis, the variability of resistance parameters and of sea level variation, and the statistical correlation of the individual failure modes have not been taken into account, in contrast to fully probabilistic design methodologies that will follow next.

3.4.2.5 Statistical analysis of sea states at the buoy location (Malaga)

In this section, the statistical analysis of the sea state conditions within storm events was carried out to be considered as wave loadings upon the structure. First, the same threshold as in the event-based extreme value analysis was applied to H_s data at the buoy's location to filter the most significant sea states that will be transferred to the structure's location. It is noteworthy that the relative frequency of the threshold exceedance ($H_s > 1.65$ m in this case) was equal to 1.5%.

It is noted that a lower threshold than the 98.5 quantile of H_s could be also applied considering a larger part of sea conditions' contribution to the final outcome of failure probability of the structure. However, the same threshold is applied here to both the extreme event-based method and all sea conditions-based method to attain compatibility between the two methods in order that a comparative analysis be made.

Furthermore, as noticed in Figure 3.37, the threshold applied to H_s data at the buoy location to filter the most significant sea states that will be transferred to the structure location, was in accordance with step (a) of data reduction technique described in section 3.3.5.2. Besides, since the wave data collected in deeper waters than the structure's location covers a period of about one decade, only this step will be applied to attain data reduction. In this way, not only the most critical sea states are distinguished from the total sample, but also the amount of data to be transferred to the structure location has been significantly reduced.

In Figure 3.37, the histograms and scatter diagram of H_s and mean wave direction of sea states at the buoy location are depicted. Furthermore, by comparing Figures 3.34 and 3.37, the directions of the most extreme storms and severe sea states both range between 100 and 125 ° from North at the buoy location.

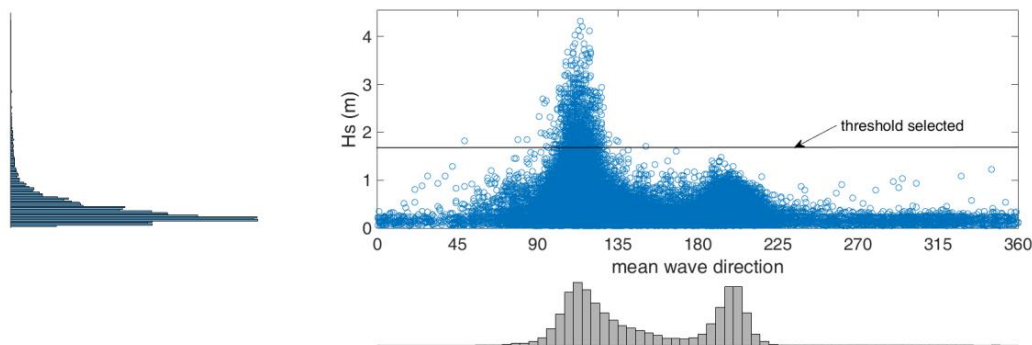


Figure 3.37 Histograms and scatter diagram of H_s and θ_m of sea states at the buoy location (Malaga) [35]

In this application, the three hour time step has been used concerning the representation of sea state conditions in the reliability analysis of the rubble mound breakwater, in order that the data correspond to more than 1000 waves per loading event. The maximum H_s in a sequence of three hourly measurements of H_s within a storm is selected to represent the sea state.

3.4.2.6 *Transferring the reduced sample of sea states from the buoy to the structure location (Malaga)*

By applying the same wave propagation model [33] as with storm events, the subset of sea states of a 3 hr time step is transferred to the structure location (at the depth of 6m) and long-term wave statistics are extracted concerning this location. The histograms and scatter diagram of H_s and mean wave direction of the propagated subset of sea states at the depth of 6 m are depicted in Figure 3.38.

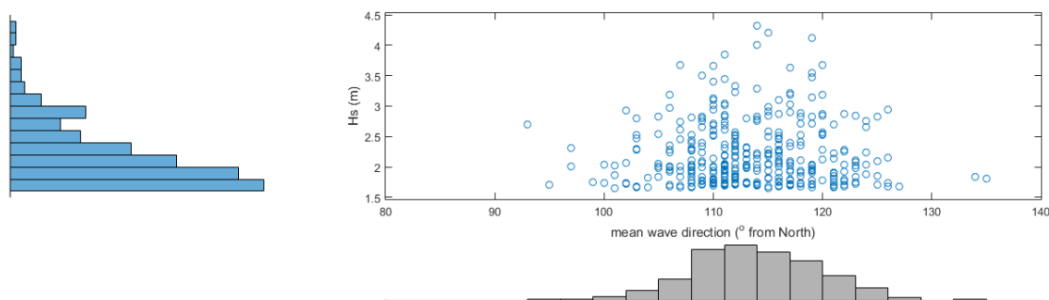


Figure 3.38 Histograms and scatter diagram of H_s and θ_m of the subset sea states at the structure location (Malaga)

Judging from Figure 3.38, the mean wave direction of subset of sea states selected for the design is concentrated in a narrow range of directions, and actually the same with that of storms, as it was expected. Therefore, in this case, a simplification could be made by considering that all sea states of this subset have a mean wave direction that is perpendicular to the structure, i.e. wave attack is considered normal for all them. It is noted that this simplification should be avoided in cases of wide range of mean wave direction of sea states and storms.

By applying, thus, the conditional model for only two variables, i.e. H_s and T_m , the conditional joint pdf of H_s and T_m given that sea states belong to the subset selected previously are presented in Figure 3.39 concerning the buoy and the structure location. As seen in Figure 3.39, the conditional joint pdf of H_s and T_m at the structure location differs from that at the buoy location and is more depth-limited, despite that both locations belong in intermediate water depths.

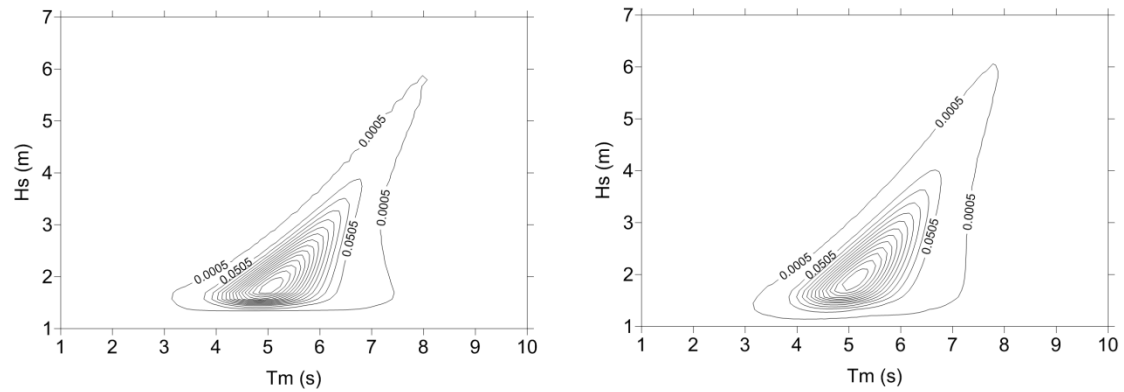


Figure 3.39 Conditional joint pdf of H_s and T_m , given that sea states belong to the subset selected, concerning the buoy (1) and the structure location (2) (iso-probability density contours step equal to 0.05 1/s/m) (Malaga)

3.4.2.7 Sea level parameters at the structure location (Malaga)

As for the sea level data, they have been transferred to the buoy's location by considering sea level variations due to tide and storm surge as long waves, undergone only to shoaling effects. The frequency density polygons of sea level variation from still water level (SWL) due to storm surge and tide estimated at the structure location are displayed in Figure 3.40.

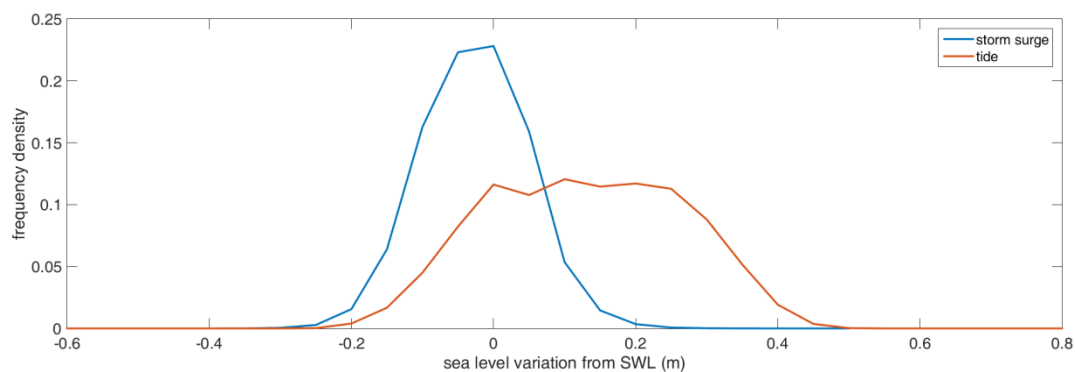


Figure 3.40 Frequency density polygons of sea level variation from SWL due to storm surge and tide estimated at the structure location

As seen from Figure 3.40, storm surge total sample can well be represented by a normal pdf, with a mean value of -0.0015 m and standard deviation of 0.0712 m.

3.4.2.8 Assessing failure probability via DIM and MCM (Malaga)

Since one of the objectives was to investigate the effect of considering more and different types of parameters as random variables on the assessed failure probability of the structure, three cases were examined here; firstly only wave parameters, secondly wave and sea level parameters, and finally wave, sea level parameters and one resistance parameter were considered as random variables. It is noted that, in the first case, SL and TL were considered equal to zero.

In the third case, the rock mass density was treated as stochastic parameter. Because its distribution is not known, a normal distribution was used in order to predict its variability. The mean value of this normal distribution is equal to the one used when this variable was regarded as a deterministic one, i.e. 2650 kg/m³, while the standard deviation is considered here equal to 10 kg/m³, which could be a reasonable variability of quarry stones density.

It is noted that in order to simplify the computations, and because the case of Malaga refers to a micro tidal and storm surge sea, the functional dependence between wave parameters and the two components of sea level TL, SL at the structure's location has not been taken into consideration in this study. To clarify this statement, this could be described by the following equation:

$$f_{TL,SL,H_s,T_m}(tl, sl, H_s, T_m) = f_{TL}(tl) f_{SL}(sl) f_{H_s, T_m | TL, SL}(H_s, T_m | (tl, sl)) \quad (3.56)$$

where:

$$f_{T_m, H_s | (TL, SL)}(T_m, H_s | (tl, sl)) = f_{T_m, H_s}(T_m, H_s) \quad (3.57)$$

The right hand of Eq. 3.57 has been estimated for $tl = \bar{tl}, sl = \bar{sl}$. The accurate estimation of $f_{T_m, H_s | (TL, SL)}(T_m, H_s | (tl, sl))$, for every tl and sl value, is preferable than its approximation via Eq. 3.57, especially in seas with significant tide and storm surge variability.

As for the evaluation of Eq. 3.34 in this study via DIM, δtl and δsl were kept equal to 0.05 m, and δH_s and δT_m equal to 0.10 m and 0.10 s, respectively, which were considered satisfactorily small.

In MCM, a random sample was generated for each variable that followed its pdf, but also at maintaining the statistical correlation between correlated variables, e.g. T_m and H_s . In Figure 3.41, the scatter diagram of T_m and H_s transferred at the structure location, their joint pdf, estimated via the conditional model, and the MC sample, are depicted, showing good comparison.

The selection of the total number of simulation for each variable depends on its variability and its contribution to the structure's failure. For example, in this study the total number of simulations for waves was 1500, while for SL and TL 50, and 20 for resistance parameters, which results in $7.5 \cdot 10^7$ iterations. From the above, it is seen that the computational demands of MCM simulation can become very high.

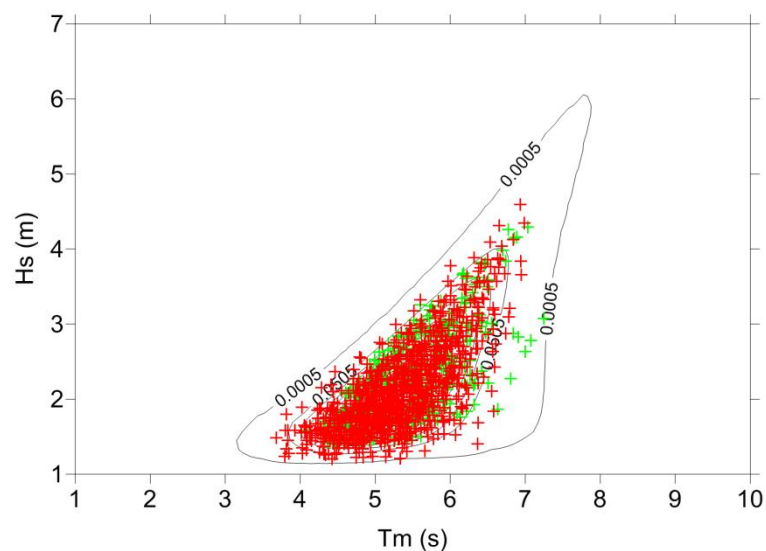


Figure 3.41 Comparison of the random sample generated by Monte Carlo simulation (red) with the transferred reduced data sample (green) to the structure's location (iso-probability density contours step equal to 0.05 1/m/s)

3.4.2.9 Results and discussion (Malaga)

The estimated solution derived from the preliminary design based on the design storm events at the structure's location became the preliminary solution for DIM for the first case. In the first case, DIM considers only wave parameters as random variables (see Table 3.26). As seen in Table 3.26, the results produced by DIM for case 1 are the conditional (given exceedance of 98.5 quantile of H_s) and the unconditional system's failure probability in the period of measurements. The results by DIM applied on all sea conditions differ to a significant degree

from those by the preliminary event-based design. This could be attributed to the different type of failure probabilities that are estimated by the two methods.

Moreover, it is noted that the event-based extreme value analysis was applied only to wave data. To account for several phenomena that are possible not of the same kind, i.e. waves and storm surge, a multivariate event-based extreme value analysis could be applied, and, then, could be incorporated in the design of a coastal structure (see e.g.[63]).

Table 3.26 Conditional and Unconditional probability of failure of the system during Y=8 yr derived from the fully probabilistic reliability method (Direct Integration) applied on all sea conditions for the first case (Malaga)

Return Period (years) for $H_{s,p}$ (years)	Conditional (case 1)	Unconditional (case 1)
10	$2.42 \cdot 10^{-2}$	$3.97 \cdot 10^{-4}$
100	$6.99 \cdot 10^{-3}$	$1.15 \cdot 10^{-4}$

Also, DIM results for the three cases examined are presented in Table 3.27. Judging from Table 3.27, the probability of failure of the structure is higher in the second case, when the sea level parameters have been considered as random variables, than in the first case. Obviously, this could be avoided, if the structure had been designed for a higher tide and storm surge value. This optimization is recommended for the design of the structure.

Furthermore, the failure probabilities estimated in case 3 are almost the same with those in case 2. This could be explained by the fact that in the case 2 computations have been made considering the mean value of the resistance parameter, and in case 3 considering a symmetrical distribution, i.e. a normal pdf, with the same mean value.

Table 3.27 System's unconditional probability of failure during Y=8 yr derived from fully probabilistic reliability method (Direct Integration) applied on all sea conditions for the three cases considered (Malaga)

Return Period (years) for $H_{s,p}$ (years)	Fully probabilistic (Case 1)	Fully probabilistic (Case 2)	Fully probabilistic (Case 3)
10	$3.97 \cdot 10^{-4}$	$4.03 \cdot 10^{-4}$	$4.05 \cdot 10^{-4}$
100	$1.15 \cdot 10^{-4}$	$1.22 \cdot 10^{-4}$	$1.20 \cdot 10^{-4}$

In Table 3.28, a comparison between DIM and MCM results for case 3 is presented. Particularly, both methods' results are close to each other. However, a small difficulty in MCM solution convergence arose by altering the total number of simulations. The latter might lead to the conclusion that DIM is more appropriate for structural reliability assessment than MCM. However, the problem examined here might be quite simple and simulation-based methods could give more efficient solutions in more complex cases.

Table 3.28 System unconditional failure probability within during Y=8 yr estimated by DIM and MCM (for case 3) (Malaga)

Return Period (years) for $H_{s,p}$ (years)	DIM (Case 3)	MCM (Case 3)
10	$4.05 \cdot 10^{-4}$	$4.79 \cdot 10^{-4}$
100	$1.20 \cdot 10^{-4}$	$1.45 \cdot 10^{-4}$

Finally, the step of optimization (see Figures 2.14 and 2.15) based on target reliability and economic criteria can then be made by applying the fully probabilistic approach for different solutions (i.e. by altering the nominal mass of the elements' units, geometric parameters etc.). This step is not included in the present thesis, but is necessary for the design of a coastal structure in order to meet predefined safety and cost requirements.

3.4.2.10 Design of the structure (Malaga)

Regarding the design of the rubble mound breakwater (see Figure 2.15), the first step is to define a target failure probability, considered in this case study equal to 10^{-5} . As we can see, this is closer to the second solution that correspond to the return period of 100 years for $H_{s,p}$, compared against the first solution that corresponds to 10 years for $H_{s,p}$. The values of SL and TL examined for the design are the return value corresponding to 10 years for SL (SL-10yr) and the maximum TL (max TL) at the structure's location. It is noted that the return period selected for SL was lower than than of the dominant component of $H_{s,p}$. This is mainly because sea level variation due to storm surge is an accompanying component which is not of such a high uncertainty as that of $H_{s,p}$, due to the fact that this case study is a micro-tidal and micro-storm surge sea. Therefore SL-10 yr is estimated at 0.28 m, via POT method, and max TL is equal to 0.48 m, both above the Still Water Level (SWL) of 6 m.

Therefore, by using SL-10 yr, max TL and $H_{s,p}$ -100 yr associated to the most probable values of T_m and θ_m , presented in Table 3.23, the nominal mass of rock armor units of the elements of the structure and the corresponding failure probability are presented in the first row of Table 3.29, as extracted from DIM. In this case, wave, sea level parameters and the resistance parameter r_s were considered as stochastic variables.

In the second row of Table 3.29 the optimized solution selected for the design of the structure's elements is presented resulting in a failure probability $P_{f,Y}$ a little lower than the target $P_{f,Y}$. The final solution has been derived from a simple iterative procedure regarding the target reliability $P_{f,Y}$, i.e. excluding any economic and social costs.

Table 3.29 Median mass of the elements units and system failure probability within Y=8 yr estimated by DIM for the design of the structure (Malaga)

Solution	Seaside armor units (kg)	Rear-side armor units (kg)	Toe units (kg)	$P_{f,Y}$
Initial solution	6980	1915	542	$7.01 \cdot 10^{-5}$
Final solution	10120	3064	812	$9.89 \cdot 10^{-6}$

3.4.3 Case study off Mykonos (Greece)

The input wave data for the reliability analysis in the case off Mykonos were measurements of T_m , H_s , and θ_m , obtained from Station M (see Figure 3.5). As it is aforementioned, the recording interval is 3 hr and the wave measurements cover the period from 1.1.2000 to 12.31.2011, i.e. 12 years.

3.4.3.1 Identification of storm events at the buoy location (Mykonos)

A univariate extreme value analysis concerning POT modelling for peaks over threshold will be used here for the predominant variable H_s , which will then be associated with the most frequent value of T_m and θ_m .

Firstly, homogenization will be applied to the sequential wave data at the given time step of 3 hr, i.e. the separation of data/sea states into independent wave systems or else events. This is attempted by selecting an initial threshold u_1 equal to 95% quantile of H_s (i.e. 2.42 m) distinguishing weak and strong storms from the dataset. Besides, a minimum calm period of 6 hr [51] between two consecutive storms was selected to ensure that the two events are independent resulting in reducing storm events from 300 dependent to 262 independent events (see Figure 3.42) in this dataset. Furthermore, the histograms and the scatter diagram of mean wave period of storms and $H_{s,p}$ and that of storm mean wave direction and $H_{s,p}$ are presented in Figures 3.43 and 3.44, respectively. As shown from Figure 3.44, storms mean wave direction has a wide range of spreading at the depth of 140 m. This range of spreading is expected to be narrower at the structure's location than in deep waters.

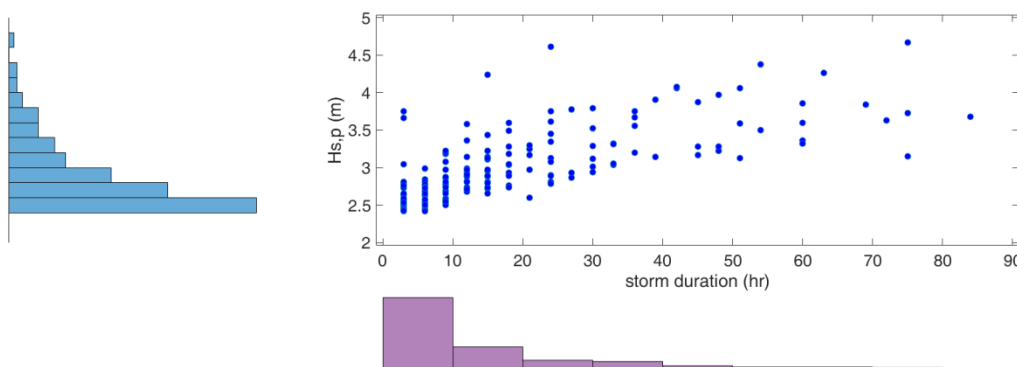


Figure 3.42 Histograms and scatter diagram of $H_{s,p}$ and storm duration at the buoy's location (Mykonos)

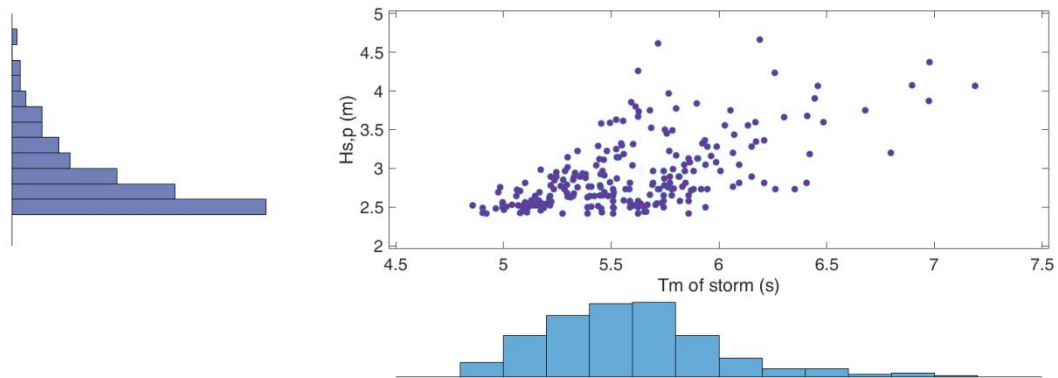


Figure 3.43 Histograms and scatter diagram of $H_{s,p}$ and storm T_m at the buoy's location (Mykonos)

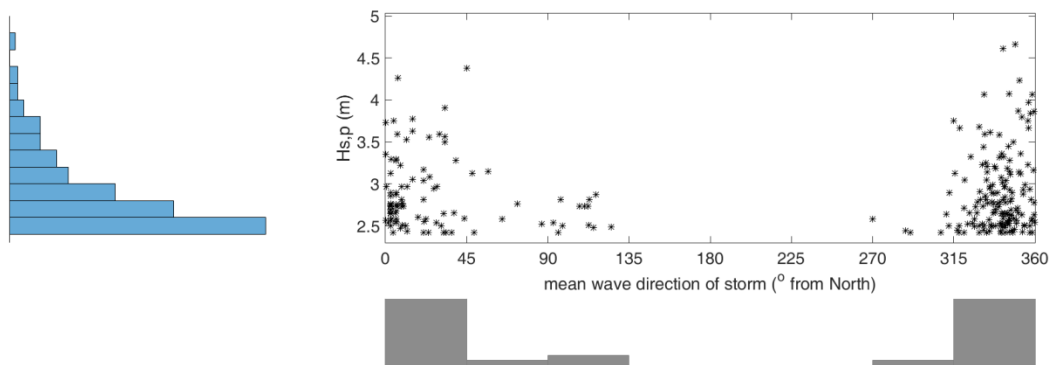


Figure 3.44 Histograms and scatter diagram of $H_{s,p}$ and storm θ_m at the buoy's location (Mykonos)

3.4.3.2 Transferring storm events from the buoy to the structure's location (Mykonos)

The sea bottom is considered uniform with a mean slope of 7% in deep and intermediate waters. The perpendicular axis to the coastline has a direction of 45° from North. Thus, storm events need to be transferred to the structure's water depth. In contrast to deep waters, where wave parameters are not affected by water depth, in intermediate water depths the latter does affect wave parameters. In Figure 3.45, a comparison is made between the scatter diagrams of storm duration and $H_{s,p}$ at the buoy (depth of 140 m) and structure (depth of 6 m) location, and in Figure 3.46 the histograms and the scatter diagrams of storm mean wave direction and $H_{s,p}$ are presented. As shown in Figure 3.46, the mean wave direction of the most severe

storms ranges between 5° and 45° from North, with mean value of 25° from North, i.e. normal to the shoreline. By comparing, Figures 3.44 and 3.46, one can notice that storms mean wave direction has a wider range of spreading at the depth of 140 m than at the structure location, as it was expected. However, the mean wave direction spreading of storms at the depth of 6 m is not as narrow as in the case off Malaga, necessitating thus a directional analysis. Also, in Figure 3.47, the histograms and the scatter diagrams of storm mean wave period and $H_{s,p}$ are presented.

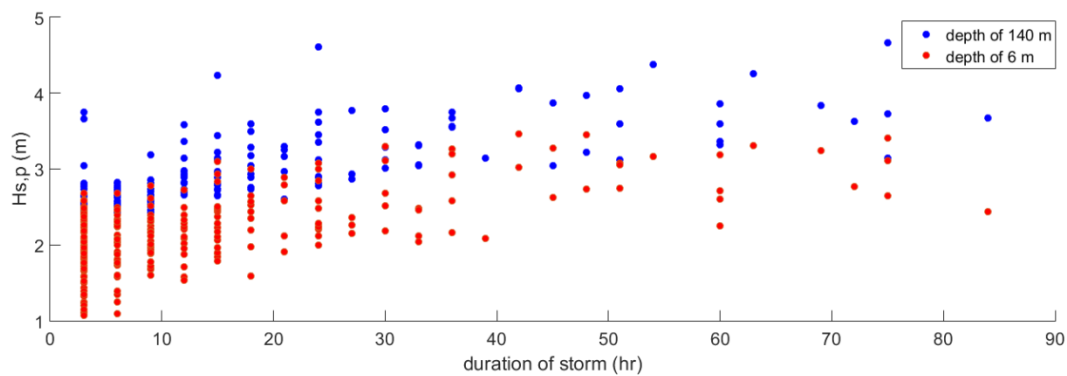


Figure 3.45 Scatter diagram of storm duration and $H_{s,p}$ at the buoy's (depth of 140 m) and structure's (depth of 6 m) location (Mykonos)

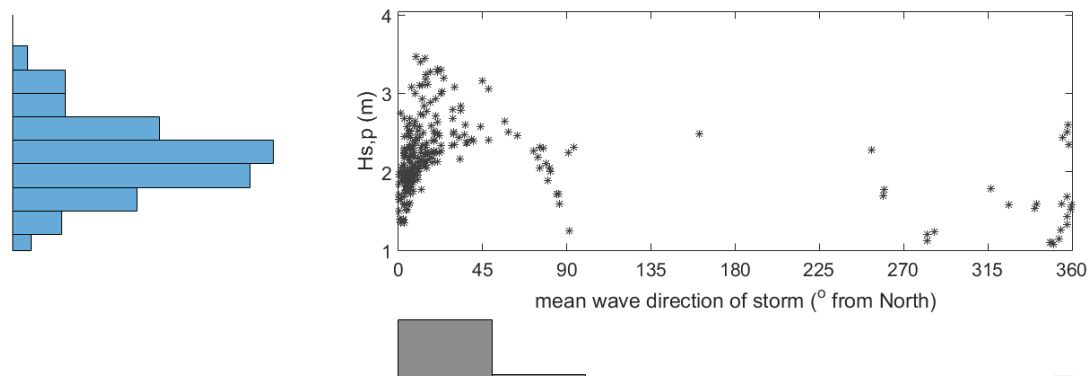


Figure 3.46 Histograms and scatter diagram of $H_{s,p}$ and storm θ_m at the structure's location (Mykonos)

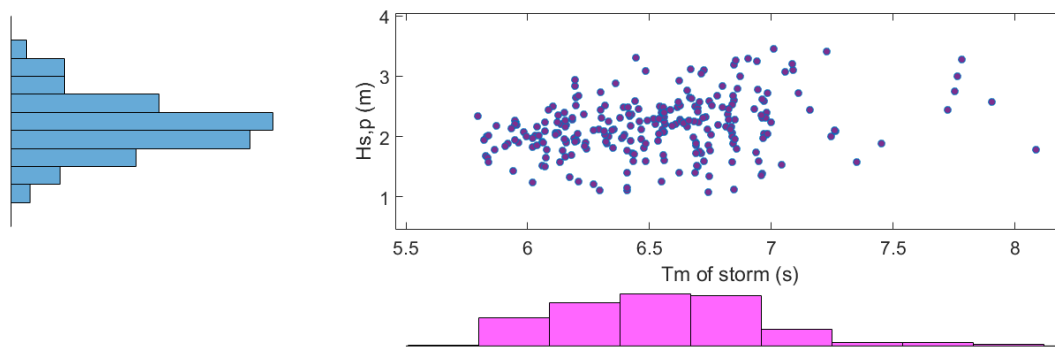


Figure 3.47 Histograms and scatter diagram of $H_{s,p}$ and storm T_m at the structure location (Mykonos)

The next step is the selection of another threshold u_2 higher than u_1 . Judging from the two methods ([61]; [62]) results for the selection of the most appropriate GP parameters and threshold value, the value of 2.205 m is selected for threshold u_2 . The parameter λ_e that corresponds to this value of u_2 is 9.83, i.e. approximately 9-10 extreme events per year.

The return periods and values for $H_{s,p}$ associated with the most probable values of their covariate variables at the structure's location selected for the preliminary design are presented in Table 3.30.

Table 3.30 Return periods and values for $H_{s,p}$ associated with the most probable values of the covariate parameters at the structure's location (depth of 6 m) selected for the preliminary design

Return Period T_r for $H_{s,p}$ (years)	Return value - $H_{s,p}$ (m)	storm T_m (s)	storm duration (hr)	storm θ_m ($^\circ$ from North)
10	3.51	6.65	3	25
100	3.75	6.90	3	25

3.4.3.3 Preliminary design based on the design storm events (Mykonos)

Since the input data for the preliminary design have been estimated, the median mass of the rock units of the structure's elements (i.e. seaside armor, rear side armor and toe) will be computed at this step. Some other deterministic parameters are the rock density ρ_s , and the water density ρ_w , which are considered equal to 2.650 t/m^3 and 1.025 t/m^3 , respectively.

As for the structure's orientation, the structure's perpendicular axis has been selected to have a direction of 25 ° from North so as to protect the shoreline from the most intense storm.

The results of the preliminary design after using the design formulas, i.e. by Van der Meer [57]; Van der Meer [59]; Van Gent and Pozueta [60], for seaside armor, toe, and rear side armor, for initial damage are shown in the following Table 3.31. The equivalent failure probabilities per annum (estimated in the sample of $H_{s,p}$) and during structure's Lifetime (estimated by Eq. 2.7), associated to the return periods of $H_{s,p}$ at the depth of 6 m, are displayed in Table 3.32.

Table 3.31 Median mass of the elements' units estimated by the preliminary design (Mykonos)

T_r for $H_{s,p}$ (years)	Seaside armor units	Rear-side armor units	Toe units
	(kg)	(kg)	(kg)
10	3962	1216	250
100	4806	1617	305

Table 3.32 Equivalent failure probabilities per annum and over structure's Lifetime (15 years), associated to return period of $H_{s,p}$ at the depth of 6 m (Mykonos)

T_r for $H_{s,p}$ (years)	$P_{ex,H_{s,p},e,1y}$	$P_{f,e,L}$
10	$1.02 \cdot 10^{-2}$	$7.79 \cdot 10^{-1}$
100	$1.00 \cdot 10^{-3}$	$1.39 \cdot 10^{-1}$

However, in the above analysis, the variability of resistance parameters the statistical correlation of the individual failure modes have not been taken into account, in contrast to the fully probabilistic design methodologies that will follow next.

3.4.3.4 Statistical analysis of sea states at the buoy's location (Mykonos)

In this section, the statistical analysis of the sequential data of sea states within storm events at the time step of 3 hr was carried out. Since the time interval between successive wave measurements is 3 hr, the same interval is used as the time step adopted for representation of sea state conditions within storm events as recommended in section 3.3.5.1. It is noted that in

the case of Malaga the time interval between successive wave measurements was shorter than in the case of Mykonos.

As noticed in Figure 3.48, the threshold that corresponds to 95% quantile of H_s (i.e. 2.42 m) was applied to H_s data at the buoy location to filter the most significant sea states that will be transferred to the structure location, in accordance with step (a) of data reduction technique presented in section 3.3.4.1. Besides, since the wave data collected in deeper waters than the structure's location covers a period of about one decade, only this step will be applied to attain data reduction. In this case, the threshold used is the same as the threshold u_1 applied to the dataset for the identification of storms. In this way, not only the most critical sea states are distinguished from the total sample, but also the amount of data to be transferred to the structure location has been significantly reduced. It is noteworthy that the relative frequency of the threshold exceedance ($H_s > 2.42$ m in this case) was equal to 5.04%.

In Figure 3.48, the histograms and scatter diagram of H_s and mean wave direction of sea states at the buoy location are depicted. Furthermore, by comparing Figures 3.44 and 3.48, the directions of the most extreme storms and severe sea states both range between -50° and $+50^\circ$ from North at the buoy location.

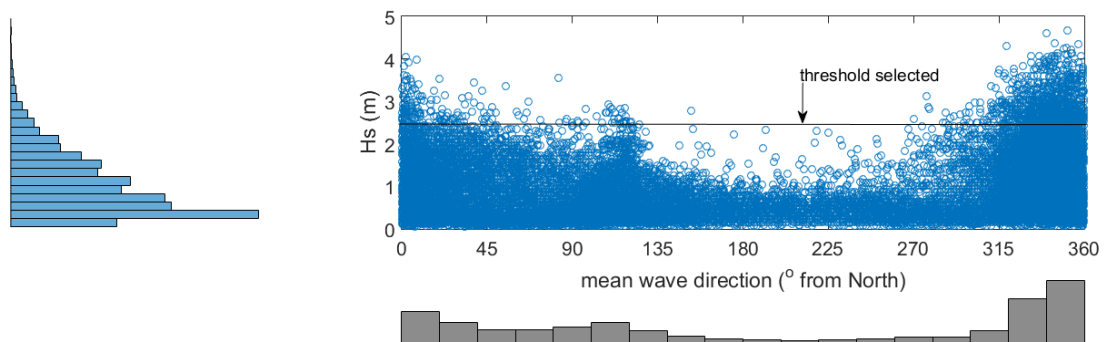


Figure 3.48 Histograms and scatter diagram of H_s and θ_m of sea states at the buoy's location (Mykonos)

3.4.3.5 Transferring the reduced sample of sea states from the buoy to the structure location (Mykonos)

By applying the same wave propagation model [33] as with storm events, the subset of sea states is transferred to the structure location (at the depth of 6m) and long-term wave statistics are extracted concerning this location. The histograms and scatter diagram of H_s and mean

wave direction of the propagated subset of sea states at the depth of 6 m are depicted in Figure 3.49.

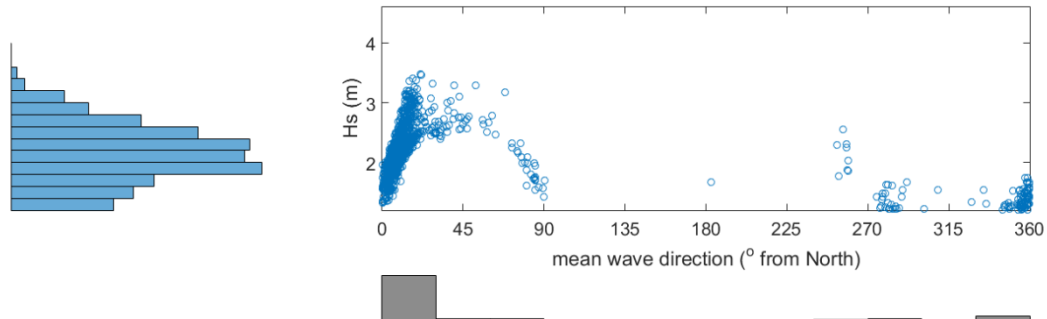


Figure 3.49 Histograms and scatter diagram of H_s and θ_m of the subset sea states at the structure's location (Mykonos)

Judging from Figure 3.49, the spreading of the mean wave direction of the subset of sea states selected for the design is not as narrow as in the case off Malaga, necessitating thus a directional analysis. Therefore, the joint conditional probability distribution of T_m and H_s given the threshold exceedance (i.e. $H_s > 2.42$ m) will be estimated for each directional sector of 22.5° , by applying the conditional probability model for the three variables, i.e. θ_m , H_s and T_m , (see sector 3.3.5.1).

Indicatively, the conditional joint pdf of H_s and T_m for two directional sectors, given that sea states belong to the subset selected previously, are presented in Figure 3.50 concerning the buoy and the structure location. As seen in Figure 3.50, the conditional joint pdfs of H_s and T_m at the structure location differs from those at the buoy location since they are depth-limited.

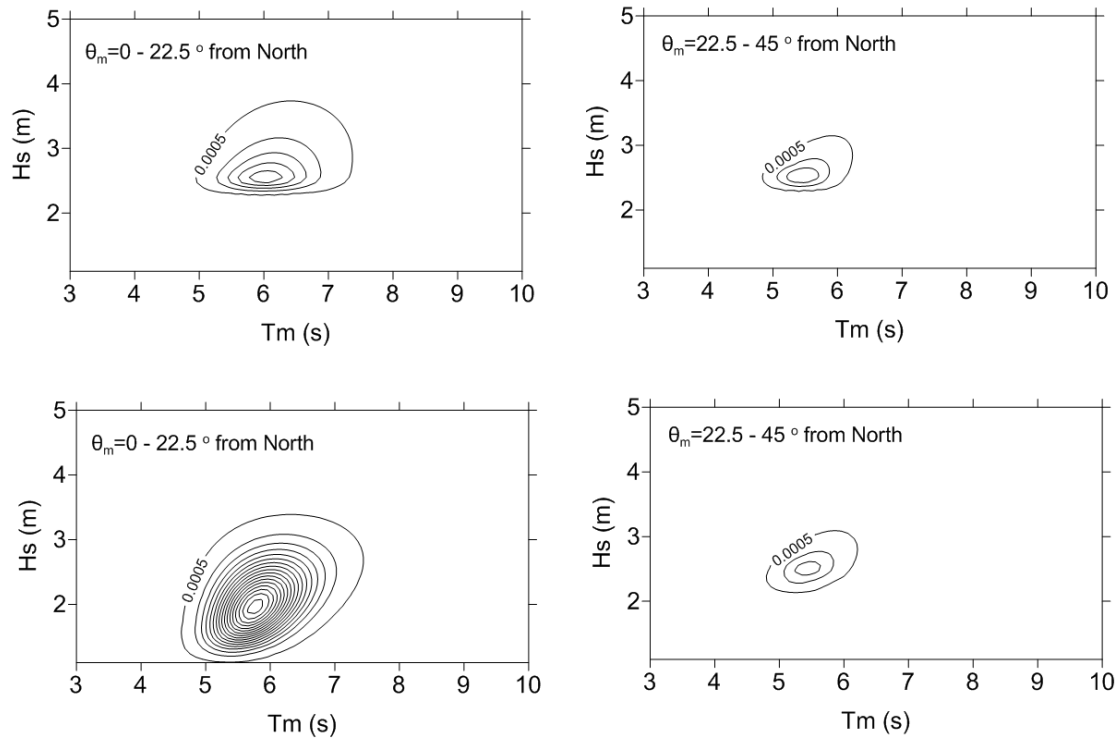


Figure 3.50 Conditional joint pdf of H_s and T_m for two directional sectors, given that sea states belong to the subset selected, concerning the buoy's (up) and the structure's location (iso-probability density contours step equal to 0.002) (Mykonos)

3.4.3.6 Assessing structure's failure probability via DIM (Mykonos)

Since one of the objectives of the present thesis was to investigate the effect of considering more and different types of parameters as random variables on the assessed failure probability of the structure, two cases were examined here; first only wave parameters, and second wave parameters and one resistance parameter were considered as stochastic variables.

In the second case, the rock mass density was treated as stochastic parameter similarly to the case of Malaga. Because its distribution is not known, a normal distribution was used in order to predict its variability. The mean value of this normal distribution is equal to the one used when this variable was regarded as a deterministic one, i.e. 2650 kg/m^3 , while the standard deviation is considered here equal to 10 kg/m^3 , which could be a reasonable variability of quarry stones density.

Since, in the case of Malaga, DIM seemed to be applied more easily than MCM, in this case of Mykonos only DIM will be applied. As for the evaluation of Eq. 3.30, δH_s , and δT_m were equal to 0.10 m and 0.10 s, respectively, which were considered satisfactorily small. As for $\delta \theta_m$, it was kept 22.5° , which is quite large in order that an adequate number of sea states

belong to each directional sector, and, thus, the joint pdf of T_m and H_s associated to every directional sector could be estimated.

The estimated solutions derived from the preliminary design based on the design storm events at the structure's location became the preliminary solution for DIM for the two cases. As seen in Table 3.33, the unconditional failure probabilities during the ($Y=12$ yr) time period of measurements by DIM in case 2 are almost the same with those in case 1. This could be explained by the fact that in the case 1 computations have been made considering the mean value of the resistance parameter, and in case 2 by considering a symmetrical distribution, i.e. a normal pdf, with the same mean value.

Table 3.33 Unconditional probability of failure during $Y=12$ yr derived from the fully probabilistic reliability method (Direct Integration) applied on all sea conditions for the two cases (Mykonos)

Return Period (years) for $H_{s,p}$ (years)	DIM (Case 1)	DIM (Case 2)
10	$3.47 \cdot 10^{-4}$	$3.50 \cdot 10^{-4}$
100	$8.70 \cdot 10^{-5}$	$8.72 \cdot 10^{-5}$

3.4.3.7 Design of the structure (Mykonos)

Regarding the design of the rubble mound breakwater (see Figure 2.15), the first step is to define a target failure probability, considered in the case study equal to 10^{-5} , which is the same with the case study of Malaga. As we can see, this is quite close to the second solution that correspond to the return period of 100 years for $H_{s,p}$.

Therefore, by using the design solution corresponding to $H_{s,p}$ -100 yr extracted from the preliminary design as an initial solution, an iterative process is applied in order that the target (allowable) failure probability be met. In this case, wave and the resistance parameter r_s were considered as stochastic variables.

In the second row of Table 3.34 the final solution selected for the design of the structure's elements is presented resulting in a failure probability $P_{f,Y}$ a little lower than the target $P_{f,Y}$.

Table 3.34 Median mass of the elements units and system failure probability within Y=12 yr estimated by DIM for the design of the structure (Mykonos)

Solution	Seaside armor units (kg)	Rear-side armor units (kg)	Toe units (kg)	$P_{f,y}$
Initial solution	4806	1617	305	$8.72 \cdot 10^{-5}$
Final solution	5766	2394	366	$9.79 \cdot 10^{-6}$

3.4.4 Remarks and recommendations on reliability analysis

Referring to the application examples of the reliability assessment of a rubble mound breakwater, the following remarks and recommendations can be drawn:

- All sea conditions-based method is preferable to be used for the reliability analysis of coastal structures compared with the extreme event-based method. This is due to the fact that in the former analysis the useful information on all critical sea conditions is utilized for the reliability assessment of coastal structures, in contrast to the extreme event-based method whereby a large part of the critical information is wasted.
- In both approaches, an initial threshold should be applied to the initial dataset to filter the most significant information used for the reliability analysis. In this PhD thesis the same threshold was used in both approaches to attain compatibility between them. However, a lower threshold could be also applied for the all sea conditions-based method.
- Information of sea states or storm events' direction is necessary for the accurate assessment of their contribution to the final outcome of the coastal structure's failure probability. As noticed from the two application examples of the reliability analysis presented above, a threshold of 95 quantile could support a directional analysis of extreme sea conditions, while a 98.5 quantile an omnidirectional one. However, it is noted that the reliability analysis should be based on a preliminary analysis of wave data or measurements with consideration of directional effects [227].
- The frequency of occurrence of wave data that exceed the threshold is taken into account also in the analysis of all sea conditions, since this frequency should be multiplied with the conditional failure probability of the structure given the threshold exceedance, in order that the unconditional failure probability be estimated.
- Working with sea states of equal duration facilitates the estimation of the failure probability of the structure, defined here as the percentage of the structure's lifetime that the structure will be in a failure state, a useful metric in risk analysis. The latter is easily estimated in this manner, since this is equal to frequency of failure in this case. Ofcourse, this condition is not valid when working with sea states and events of unequal duration.
- The methodology's differences between the event-based extreme value analysis and the reliability analysis applied on sea states within storm events are mainly attributed to the fact the two methods estimate different types of failure probabilities. The first method estimates the failure probability in the sample of extreme events, and the second one the failure probability in the total sample of data.

- A significant advantage of the event-based reliability method is that, despite that both methods need a large period of measurements; the former analysis can extrapolate its output to the lifetime of structure, whilst the second method cannot.
- Besides, it is recommended that if the event-based extreme value analysis has been chosen to be solely applied for the reliability assessment of a coastal structure, a more accurate multivariate extreme value analysis should be applied than the one applied here in the application examples (e.g. derived from a copula analysis).
- In this thesis, the fully probabilistic reliability analysis applied on sea states within storm events is recommended for reliability and design purposes of coastal structures, especially when applying the risk-informed design format. In such cases, preliminary results can be estimated by the extreme value analysis as applied in the present thesis.
- Nevertheless, it could be stated that if the period of measurements Y is much lower than the lifetime of the structure L , the extreme event-based method could be used for the design of a coastal structure (e.g. ULS), considering however its cons, and the second method for the operation of the structure (e.g. SLS). However, if Y is close to or higher than L , then the second method is more preferable for the design than the first one.

CHAPTER 4

Conclusions and Future Research

4 Conclusions and Future Research

4.1 Summary and concluding remarks

4.1.1 Summary

In this PhD thesis, an overall probabilistic methodology for reliability assessment of coastal structures under wave action is described, which starts from the step of wave data collection referring usually to deep waters, and ends to the estimation of failure probability of coastal structures during their design Lifetime. In an intermediate step, a statistical linear wave propagation model that integrates short- with long-term wave statistics from deep to intermediate waters has been developed and applied. The capability of the statistical linear wave propagation model to produce properly the short-term wave statistics in deep and intermediate waters has been investigated via comparisons of its results with measurements in deep waters and the results of a commercial, and well-known for its accuracy, Boussinesq wave propagation model from deep to intermediate waters, respectively. As for the reliability analysis of coastal structures, a thorough probabilistic methodology is presented, focusing on the case of rubble mound breakwaters during their lifetime, based on the probabilistic representation of load environmental parameters at the structure's location (usually met in intermediate water depths) and resistance parameters. Finally, two examples of reliability analysis of a rubble mound breakwater using data from two stations in the Mediterranean Sea are examined and described, elaborating on some of the significant current issues concerning the reliability assessment of coastal structures.

4.1.2 Integrating short- with long-term wave statistics from deep to intermediate waters

One of the main issues with probabilistic design of coastal structures is how to properly and correctly describe the intermediate water long-term wave climate. Thus, in this Ph.D. thesis, the failure probability of coastal structures is estimated based on the long-term wave climate at the structure's location. This is accomplished by applying a data reduction technique in deep waters and a statistical linear wave propagation model that integrates short- with long-term wave statistics from deep to intermediate waters, developed for this purpose.

As shown from the model's results in deep and in intermediate waters, the long-term joint pdfs of T_m and H_s in deep waters differ to some degree from those in intermediate waters. This is due to the wave transformations that take place as waves move inshore, such as wave

shoaling, refraction, breaking etc. However, it was noticed that the type of the marginal pdf that best represented H_s data and the conditional pdf of T_m given H_s was the same in deep and in intermediate waters for each one of the three Stations examined.

Besides, the model developed [33], aiming at integrating short- with long-term wave statistics from deep to intermediate waters, estimates the mean wave direction θ_m , except for H_s , and T_m , in intermediate waters, using H_s , T_m , θ_m in deep waters as input data. This has been made via incorporation of a theoretical expression for wave directional spreading into a statistical wave by wave analysis. This approach is based on the assumption that, among waves that belong to the same class of T, those with larger H tend to have directions closer to θ_m ; that is, they show less directional spread than waves with lower H, suggesting that H and θ are not independent. This assumption is in agreement with Tucker [37].

Moreover, the model [33] provides information on the long-term joint pdf of H, T, θ , as well as the long-term joint probability density function of H_s , T_m , θ_m , estimated in intermediate waters via modification of Battjes approach [36] extended to consider also T and θ , except for H. In other words, information is provided not only on the time-integrated parameters that describe a sea state or a storm event attacking a coastal structure, but also on the direct loadings of the structure, i.e. the individual waves that are probable to occur during the structure's lifetime. This information is vital for many engineering applications, e.g. fatigue analysis, and reliability assessment of coastal structures.

4.1.3 Investigating the capability of the model

As for the deep water short-term wave statistics and the validity domain of the statistical wave propagation model by Malliouri et al. [33], it was shown that the joint pdf of individual wave period T and wave height H of a real sea state could be well represented by using the dimensionless probabilistic images by Memos and Tzani ([29]; [30]). The latter refer to nonlinear deep water sea waves. Referring to intermediate waters' short-term wave statistics considered by Malliouri et al. [33], comparisons between the linear wave propagation model and the nonlinear Boussinesq-type model showed good agreement in most of the intermediate water depths examined for both normal and oblique incidence. At the shallower intermediate water depth tested, the results of the two models differed more significantly than in deeper intermediate water depths. Therefore, as it was expected and has been already mentioned, the linear model adopted could cover the deeper and medium zone of intermediate waters and thus could be used for many engineering design purposes.

Furthermore, a general conclusion could be extracted; this is that inside the approximate region of the linear theory (i.e. $U_r < 40$ and $s_m < 0.04$) the linear model by Malliouri et al. [33] can satisfactorily approximate the results of a nonlinear Boussinesq wave module such as MIKE 21 BW. However, this linear model can be used for engineering purposes in a wider region, in the deeper and medium intermediate water zone. It is recommended that the extension of the application area of the model beyond the limits of the linear wave theory should reach up the surf zone. Further extension could lead to unsatisfactory estimation of characteristic wave parameters with relative deviations beyond 10% compared with nonlinear wave propagation models.

4.1.4 Using an event-based extreme value analysis and an analysis on all sea conditions

Two thorough probabilistic methodologies are presented, aiming at estimating the reliability of coastal structures, such as rubble mound breakwaters during their lifetime, based on the probabilistic representation of load environmental and resistance parameters. Moreover, their pros and cons with respect to their outputs and constraints are discussed. The main differences between the event-based extreme value analysis and the reliability analysis applied on all sea conditions are focused on the fact the two methods estimate different types of failure probabilities. The first method estimates the failure probability in the sample of extreme events, and the second one the failure probability in the total sample of data. The latter can be translated as the percentage of the structure's lifetime that the structure will be in a failure situation, which can be efficiently incorporated into a risk analysis with consideration of social and economic costs.

The fully probabilistic reliability analysis, applied on all sea conditions, is recommended for reliability and design purposes of coastal structures, when the period of measurements or of data used is close to the lifetime of the structure. In other cases, the extreme event-based method could be used for the design of a coastal structure (e.g. ULS), considering however its cons, and the second method for the operation of the structure (e.g. SLS).

4.1.5 Reliability assessment of coastal structures

It is noteworthy that in the fully probabilistic methodologies adopted in this thesis, the failure probability of the structure, referred here as a system, can be estimated via consideration of

the statistical correlation of the elements' failure, i.e. the probability of the union of the elements' failure events in case of a series fault tree.

Besides, two different fully probabilistic methods, Direct Integration Method (DIM) and Monte Carlo Method (MCM), were applied (and compared) by using a combination of variables with zero and non-zero hazard rate, referred here as a combined time-invariant and time-variant analysis. Finally, the effect of considering more and different types of parameters as stochastic variables on the assessed failure probability of the structure was investigated.

Regarding the case of the rubble mound breakwater examined here, DIM was a more straightforward method than MCM, since it was applied directly to the joint pdf of the random variables. As for MCM simulations, some difficulty in MCM solution convergence was met. Nevertheless DIM seemed to be more appropriate in the problem examined here, this case might be considered quite simple, and simulation-based methods could give more efficient solutions in more complex cases.

As far as the time step denoting the sea state within storm events, for reliability analysis of rubble mound breakwaters, is concerned, numerical tests showed that the time step of 3hr results are well balanced between statistical accuracy (low values) and resilience-type requirements (high values).

In short, some of the significant current issues concerning the reliability assessment of coastal structures were clarified, by giving application examples, flowchart and mathematical equations that describe the procedure. However, there are more issues that need to be tackled in order that engineers could be able to design those structures to meet certain predefined reliability requirements.

4.2 Future research

Referring to the wave propagation model, it is noted that wave transformations from deep to shallower waters could also be performed in a more advanced way by taking into consideration non-linearities, like non-linear wave shoaling, and nonlinear wave-wave interactions. Such models have been developed till now but are not enabled to handle a large amount of long-term data in such a fast and easy manner. Besides, regarding the bed bathymetry, in all cases examined here the bed slope was considered uniform, but the same methodology can also be applied to more complex bathymetries. These topics are suggested for further research.

Another step along the line of research, adopted in this PhD thesis, would be the incorporation of the equations, derived from the analysis of extreme events, aiming to combine variables that present and do not present extremal probabilistic behavior, into a more thorough multivariate event-based extreme value analysis.

References

- [1] U.S. Army Corps of Engineers, *Coastal Engineering Manual*. Washington, D.C., 2006.
- [2] Z. Liu and H. F. Burcharth, “Design Wave Height Related to Structure Lifetime,” in *Coastal Engineering 1996, 1997*, pp. 2560–2572.
- [3] PIANC, “Analysis of rubble mound breakwaters. Report of working group 12 (PTC II). Supplement to Bulletin no. 78/79.,” Brussels, 1992.
- [4] Yoshimi Gōda, *Random Seas and Design of Maritime Structures(2nd Edition)*. World Scientific Publishing Company, 2000.
- [5] P. A. Madsen and O. R. Sørensen, “A new form of the Boussinesq equations with improved linear dispersion characteristics. Part 2. A slowly-varying bathymetry,” *Coast. Eng.*, vol. 18, no. 3–4, pp. 183–204, Dec. 1992.
- [6] O. R. Sørensen, H. A. Schäffer, and L. S. Sørensen, “Boussinesq-type modelling using an unstructured finite element technique,” *Coast. Eng.*, vol. 50, no. 4, pp. 181–198, Feb. 2004.
- [7] M. K. Chondros and C. D. Memos, “A 2DH nonlinear Boussinesq-type wave model of improved dispersion, shoaling, and wave generation characteristics,” *Coast. Eng.*, vol. 91, pp. 99–122, Sep. 2014.
- [8] C. L. Bretschneider, “Forecasting relations for wave generation,” *Look Lab*, vol. 1, no. 3, 1970.
- [9] D. Malliouri, V. Afentoulis, V. Bonaros, C. Memos, and V. Tsoukala, “Integrated Design of Coastal Structures and Adaptation to Climate Change Hazards,” in *CEST*, 2017.
- [10] M. K. Ochi, *Ocean Waves – The Stochastic Approach*. Cambridge University Press, 1998.
- [11] M. A. Losada and L. A. Gimenez-Curto, “The joint effect of the wave height and period on the stability of rubble mound breakwaters using Iribarren’s number,” *Coast. Eng.*, vol. 3, pp. 77–96, Jan. 1979.
- [12] J. C. Galland, “Rubble mound breakwater stability under oblique waves: and experimental study,” in *Coastal Engineering Proceedings*, 1994.

-
- [13] V. Laface, F. Arena, and C. G. Soares, "Directional analysis of sea storms," *Ocean Eng.*, vol. 107, pp. 45–53, Oct. 2015.
- [14] M. K. Ochi, "On long-term statistics for ocean and coastal waves," in *Proceedings of the 16th Conference on Coastal Engineering*, 1978, pp. 59–75.
- [15] N. Fang, Z.S., Hogben, "Analysis and Prediction of Long-term Probability Distributions of Wave Height and Periods," London, 1982.
- [16] S. Haver, "Wave climate off northern Norway," *Appl. Ocean Res.*, vol. 7, no. 2, pp. 85–92, Apr. 1985.
- [17] E. M. Bitner-Gregersen and S. Haver, "Joint long term description of environmental parameters for structural response calculations," in *Proceedings of the Second International Workshop on Wave Hindcasting and Forecasting*, 1989, pp. 25–28.
- [18] C. Guedes Soares, L. C. Lopes, and M. D. S. Costa, "Wave climate modelling for engineering purposes," in *Computer Modelling in Ocean Engineering*, B. A. Schrefler and O. C. Zienkiewicz, Eds. A.A. Balkema Pub., 1988, pp. 169–175.
- [19] C. Lucas and C. Guedes Soares, "Bivariate distributions of significant wave height and mean wave period of combined sea states," *Ocean Eng.*, vol. 106, pp. 341–353, Sep. 2015.
- [20] M. G. Papanikolaou, D. I. Malliouri, and C. D. Memos, "Wave climate description via longterm joint distributions of wave height and wave period," in *Proceedings of the 7th National Conference on Harbour Works*, 2016.
- [21] G. A. Athanassoulis, E. K. Skarsoulis, and K. A. Belibassakis, "Bivariate distributions with given marginals with an application to wave climate description," *Appl. Ocean Res.*, vol. 16, no. 1, pp. 1–17, Jan. 1994.
- [22] M. S. Longuet-Higgins, "On the joint distribution of the periods and amplitudes of sea waves," *J. Geophys. Res.*, vol. 80, no. 18, pp. 2688–2694, Jun. 1975.
- [23] S. O. Rice, "Mathematical Analysis of Random Noise," *Bell Syst. Tech. J.*, vol. 23, no. 3, pp. 282–332, Jul. 1944.
- [24] M. S. Longuet-Higgins, "On the joint distribution of wave periods and amplitudes in a random wave field," in *Proceedings of the Royal Society A*, 1983.
- [25] R. Cavanie, A., Arhan, M., Ezraty, "A Statistical Relationship Between Individual

- Heights and Periods of Storm Waves,” in *1st Int. Conf. on Behavior of Offshore Structures, BOSS '76*, 1975, pp. 354–360.
- [26] G. Lindgren and I. Rychlik, “Wave characteristic distributions for Gaussian waves—Wave-length, amplitude and steepness,” *Ocean Eng.*, vol. 9, no. 5, pp. 411–432, Jan. 1982.
- [27] K. T. Shum and W. K. Melville, “Estimates of the joint statistics of amplitudes and periods of ocean waves using an integral transform technique,” *J. Geophys. Res.*, vol. 89, no. C4, p. 6467, 1984.
- [28] C. D. Memos, “On the theory of the joint probability of heights and periods of sea waves,” *J. Coast. Eng.*, pp. 201–215, 1994.
- [29] C. D. Memos and K. Tzani, “Numerical results of the joint probability of heights and periods of sea waves,” *Coast. Eng.*, vol. 22, no. 3–4, pp. 217–235, Feb. 1994.
- [30] C. D. Memos and K. Tzani, “Joint Distribution of Wave Heights and Periods in Waters of Any Depth,” *J. Waterw. Port, Coastal, Ocean Eng.*, vol. 126, no. 3, pp. 162–172, May 2000.
- [31] K. Tzani, “Stochastic description of random sea states,” National Technical University of Athens, 2003.
- [32] M. K. Chondros and C. D. Memos, “On the joint probability of wave-heights and periods in intermediate and shallow waters,” *Coast. Eng. J.*, vol. 58, no. 3, 2016.
- [33] D. I. Malliouri, C. D. Memos, N. D. Tampalis, T. H. Soukissian, and V. K. Tsoukala, “Integrating short- and long-term statistics for short-crested waves in deep and intermediate waters,” *Appl. Ocean Res.*, vol. 82, no. 3, pp. 346–361, 2019.
- [34] D. I. Malliouri, C. D. Memos, T. H. Soukissian, and V. K. Tsoukala, “Reliability analysis of rubble mound breakwaters - An easy-to-use methodology,” in *DMPCO 2019*, 2019.
- [35] D. I. Malliouri, C. D. Memos, T. H. Soukissian, and V. K. Tsoukala, “Assessing failure probability of coastal structures based on probabilistic representation of sea conditions at the structures’ location,” *Appl. Math. Model.*, vol. 89, pp. 710–730, Jan. 2021.
- [36] J. A. Battjes, “Long-term wave height distribution at seven stations around the British Isles,” *Hydrogr. Zeitschrift*, vol. 24, no. 4, pp. 180–189, 1972.

- [37] M. . Tucker, "The statistics of particle velocities and accelerations under waves with directional spread," *Ocean Eng.*, vol. 25, no. 6, pp. 481–496, Jun. 1998.
- [38] P. D. Komar and M. K. Gaughan, "Airy Wave Theory and Breaker Height Prediction," in *Coastal Engineering 1972*, 1972, pp. 405–418.
- [39] R. G. Weggel, "Maximum breaker height," *J. Waterw. Harb. Coast Eng Div, ASCE* 98, pp. 529–548, 1972.
- [40] J. A. Battjes, "Surf similarity," in *14th International Conference on Coastal Engineering*, 1974, pp. 466–480.
- [41] B. Le Mebaute, "On non-saturated breakers and the wave run-up," in *8th Int. Conf. Coast. Eng.*, 1962, pp. 77–92.
- [42] K. Horikawa and C.-T. Kuo, "A Study on Wave Transformation Inside Surf Zone," in *Coastal Engineering 1966*, 1967, pp. 217–233.
- [43] W. R. Dally, R. G. Dean, and R. A. Dalrymple, "Wave height variation across beaches of arbitrary profile," *J. Geophys. Res.*, vol. 90, no. C6, p. 11917, 1985.
- [44] T. H. Soukissian and G. Chronis, "Poseidon: A marine environmental monitoring, forecasting and information system for the Greek seas," *Mediterr. Mar. Sci.*, vol. 1, no. 1, pp. 71–78, Jun. 2000.
- [45] T. H. Soukissian, D. E. Sifnioti, A. Prospathopoulos, and D. Kastriti, "Short - Term Wave Statistics in the Greek Seas," in *Twenty-Second Int. Offshore Polar Eng. Conf. 4*, 2012, pp. 784–791.
- [46] P. A. Madsen, R. Murray, and O. R. Sørensen, "A new form of the Boussinesq equations with improved linear dispersion characteristics," *Coast. Eng.*, vol. 15, no. 4, pp. 371–388, Jul. 1991.
- [47] P. A. Madsen, O. R. Sørensen, and H. A. Schäffer, "Surf zone dynamics simulated by a Boussinesq type model. Part I. Model description and cross-shore motion of regular waves," *Coast. Eng.*, vol. 32, no. 4, pp. 255–287, 1997.
- [48] P. A. Madsen, O. R. Sørensen, and H. A. Schäffer, "Surf zone dynamics simulated by a Boussinesq type model. Part II: surf beat and swash oscillations for wave groups and irregular waves," *Coast. Eng.*, vol. 32, no. 4, pp. 289–319, 1997.
- [49] O. R. Sørensen and L. S. Sørensen, "Boussinesq-type modelling using an unstructured

- finite element technique,” in *Proc 27th Coastal Eng. Conf.*, 2001, pp. 190–202.
- [50] P. Bernardara, F. Mazas, X. Kergadallan, and L. Hamm, “A two-step framework for over-threshold modelling of environmental extremes,” *Nat. Hazards Earth Syst. Sci.*, vol. 14, no. 3, pp. 635–647, Mar. 2014.
- [51] F. Li, P. H. A. J. . van Gelder, D. P. Callaghan, R. B. Jongejan, C. de. Heijer, and R. Ranasinghe, “Probabilistic modeling of wave climate and predicting dune erosion,” *J. Coast. Res.*, vol. 65, pp. 760–765, Jan. 2013.
- [52] F. Mazas and L. Hamm, “A multi-distribution approach to POT methods for determining extreme wave heights,” *Coast. Eng.*, vol. 58, no. 5, pp. 385–394, May 2011.
- [53] J. Pickands, “Statistical Inference Using Extreme Order Statistics,” *Ann. Stat.*, vol. 3, no. 1, pp. 119–131, 1975.
- [54] P. Embrechts, C. Klüppelberg, and T. Mikosch, *Modelling Extremal Events*. Berlin, Heidelberg: Springer Berlin Heidelberg, 1997.
- [55] CIRIA; CUR; CETMEF, *The Rock Manual. The use of rock in hydraulic engineering (2nd edition)*. C683, CIRIA, London, 2007.
- [56] P. S. Everts, “Probabilistic Design of a rubble mound breakwater,” Delft University of Technology, 2016.
- [57] J. W. Van der Meer, “Rock Slopes and Gravel Beaches under Wave Attack,” Delft University, the Netherlands, 1988.
- [58] J. Mathisen and E. Bitner-Gregersen, “Joint distributions for significant wave height and wave zero-up-crossing period,” *Appl. Ocean Res.*, vol. 12, no. 2, pp. 93–103, Apr. 1990.
- [59] E. Van der Meer, J.W., d’ Angremond, K., Gerding, “Toe Structure Stability of Rubble Mound Breakwaters.,” in *Proc. Coastlines, Marine Structures and Breakwater.*, 1995, pp. 308–321.
- [60] M. R. A. Van Gent and B. Pozueta, “Rear-side Stability of rubble mound structures,” in *Coastal Engineering 2004*, 2004, pp. 3481–3493.
- [61] T. Embrechts, P., Klüppelberg, C., Mikosh, *Modelling Extremal Events for Insurance and Finance*. Springer, Berlin, 2003.

- [62] S. G. Coles, *An Introduction to Statistical Modeling of Extreme Values*. Springer London, 2001.
- [63] F. Mazas and L. Hamm, “Extreme Meteo-Oceanic Events,” *Coast. Eng.*, 2018.
- [64] T. S. Hedges, “Regions of validity of analytical wave theories,” in *Inst. Civ. Eng., Wat., Marit., & Energy*, 1995.
- [65] H. F. Burcharth and Z. Liu, “Rubble Mound Breakwater Failure Modes,” in *Final (MAS2- CT92-0042) Workshop: Rubble mound failure modes*, 1995.
- [66] S. Jonkman, R. Steenbergen, O. Morales-Nápoles, A. C. W. M. Vrouwenvelder, and J. K. Vrijling, *Probabilistic Design : Risk and Reliability Analysis in Civil Engineering*. Delft University of Technology, 2015.
- [67] N. Dai Viet, H. J. Verhagen, P. H. J. M. V. Gelder, and J. K. Vrijling, “Optimisation of Structural Systems by Appropriately Assigning Probabilities of Failure . Application to RubbleMound Breakwaters.,” 2008.
- [68] H. F. Burcharth, “Introduction of Partial Coefficient in the Design of Rubble Mound Breakwaters,” in *Conference on Coastal Structures and Breakwaters*, 1991, pp. 543–565.
- [69] H. F. Burcharth and J. D. Sørensen, “The PIANC Safety Factor System for Breakwaters,” in *Proceedings of Coastal Structures*, 1999, pp. 1125–1144.
- [70] R. Y. Hudson, “Laboratory investigation of rubble mound breakwaters,” *J. Waterw. Harb. Div., ASCE* 85, pp. 93–121, 1959.
- [71] H. J. Verhagen, “Computation of a coastal protection, using classical method, the PIANC-method or a full probabilistic approach ?,” in *3rd International Conference Port Development and Coastal Environment: PDCE 2003*, 2003.
- [72] C. A. Cornell, “A Reliability-Based Structural Code,” *ACI-Journal*, vol. 66, pp. 974–985, 1969.
- [73] G. J. Schiereck, *Introduction to bed, bank, shore protection*. TU Delft, Department Hydraulic Engineering, 1993.
- [74] P. Rudnick, “Correlograms for Pacific Ocean waves,” in *2nd Berkeley Symp. on Math. Stat. & Probability*, 1951, pp. 627–38.
- [75] W. Pierson, G. Neumann, and R. W. James, “Practical methods for observing and

- forecasting ocean waves by means of wave spectra and statistics.,” 1958.
- [76] C. L. Bretshneider, *Wave variability and wave spectra for wind-generated gravity waves*. U.S. Army Corps of Eng., Beach Erosion Board, Tech. Memo. 118, 1959.
- [77] ISSC, “Proceedings of the Second International Ship Structures Congress,” 1964.
- [78] J. R. Scott, “A sea spectrum for model test and long-term ship prediction,” *J. Sh. Res.*, vol. 9, pp. 145–152, 1965.
- [79] ITTC, “Recommendations of the 11th International Towing Tank Conference,” in *11th ITTC*, 1966.
- [80] P. C. Liu, “Normalized and Equilibrium Spectra of Wind-Wave in Lake Michigan,” *J. Phys. Ocean.*, vol. 1, no. 4, pp. 249–257, 1971.
- [81] H. Mitsuyasu, “The one-dimensional wave spectra at Limited Fetch,” in *Proceedings of 13th Conference on Coastal Engineering*, 1972.
- [82] W. J. Pierson and L. Moskowitz, “A proposed spectral form for fully developed wind seas based on the similarity theory of S. A. Kitaigorodskii,” *J. Geophys. Res.*, vol. 69, no. 24, pp. 5181–5190, Dec. 1964.
- [83] K. Hasselmann *et al.*, “Measurements of wind-wave growth and swell decay during the Joint North Sea Wave Project (JONSWAP),” 1973.
- [84] E. Bouws, H. Günther, W. Rosenthal, and C. L. Vincent, “Similarity of the wind wave spectrum in finite depth water: 1. Spectral form,” *J. Geophys. Res.*, vol. 90, no. C1, pp. 975–986, 1985.
- [85] S. A. Kitaigorodskii, V. P. Krasitskii, and M. M. Zaslavskii, “On Phillips’ Theory of Equilibrium Range in the Spectra of Wind-Generated Gravity Waves,” *J. Phys. Oceanogr.*, vol. 5, no. 3, pp. 410–420, Jul. 1975.
- [86] D. I. Malliouri, C. D. Memos, and M. K. Chondros, “A simple method for obtaining wave directional spreading,” *J. Appl. Water Eng. Res.*, vol. 5, no. 2, 2017.
- [87] M. S. Longuet-Higgins, D. E. Cartwright, and N. D. Smith, “Observations of directional spectrum of sea waves using the motions of a floating buoy,” in *Proceedings of the Conference on Ocean Wave Spectra*, 1963.
- [88] H. Mitsuyasu *et al.*, “Observations of the directional spectrum of ocean waves using a cloverleaf buoy,” *J Phys Ocean.*, vol. 5, no. 4, pp. 750–760, 1975.

- [89] R. Pinkel and J. A. Smith, "Open ocean surface wave measurement using Doppler sonar," *J. Geophys. Res.*, vol. 92, no. C12, pp. 12967–12973, 1987.
- [90] H. E. Krogstad, R. L. Gordon, and M. C. Miller, "High resolution directional wave spectra from horizontally mounted acoustic Doppler current meters," *J. Atmos. Ocean Tech.*, vol. 5, pp. 340–352, 1988.
- [91] F. C. Jackson, W. T. Walton, and P. L. Baker, "Aircraft and satellite measurement of ocean wave directional spectra using scanning-beam microwave radars," *J. Geophys. Res.*, vol. 90, no. C1, pp. 987–1004, 1985.
- [92] O. H. Shemdin, H. M. Tran, and S. C. Wu, "Directional measurements of short ocean waves with stereography," *J. Geophys. Res.*, vol. 93, pp. 13891–13901, 1988.
- [93] L. H. Holthuijsen, "Observations of the directional distribution of ocean-wave energy in fetch-limited conditions.," *J. Phys. Ocean.*, vol. 13, pp. 191–207., 1983.
- [94] S. Lehner, "Radar wave measurements," in *Measuring and analysing the directional spectra of ocean waves*, D. Hauser, K. Kahma, H. E. Krogstad, S. Lehner, J. Monbaliu, and L. R. Wyatt, Eds. EU cost action 714. Luxembourg: COST Office, 2005, pp. 117–185.
- [95] J. Capon, R. J. Greenfield, and R. J. Kolker, "Multidimensional maximum-likelihood processing of a large aperture seismic array," in *Proceedings of Institute of Electrical and Electronics Engineers*, 1967.
- [96] M. Isobe, K. Kondo, and K. Horikawa, "Extension of MLM for estimating directional wave spectrum," in *Proceedings of Symposium on Description and Modelling of Directional Seas*, 1984.
- [97] H. E. Krogstad, "Maximum likelihood estimation of ocean wave spectra from general arrays of wave gauges," *Model Ident. Control*, vol. 9, pp. 81–97, 1988.
- [98] C. E. Shannon, "A mathematical theory of communication," *Bell Syst Tech J.*, vol. 27, pp. 379–423, 1948.
- [99] K. Kobune and N. Hashimoto, "Estimation of directional spectra from the maximum entropy principle," in *Proceedings of 5th Symposium of Offshore Mechanics and Arctic Engineering*, 1986.
- [100] O. U. Nwogu, E. P. . Mansard, M. D. Miles, and M. Isaacson, "Estimation of directional wave spectra by the maximum entropy method," in *17th International*

- Association for Hydro-Environment Engineering and Research-IAHR*, 1987.
- [101] O. U. Nwogu, "Maximum entropy estimation of directional wave spectra form an array of wave probes," *Appl Ocean Res.*, vol. 11, pp. 176–182, 1989.
- [102] A. Lygre and H. E. Krogstad, "Maximum entropy estimation of the directional distribution in ocean wave spectra," *J Phys Ocean.*, vol. 16, pp. 2052–2060, 1986.
- [103] L. E. Borgman, "Directional spectra model for design use for surface waves," 1969.
- [104] A. J. Kuik, G. Van Vledder, and L. H. Holthuijsen, "A method for the routine analysis of pitch-and-roll buoy wave data," *J Phys Ocean.*, vol. 18, pp. 1020–1034, 1988.
- [105] M. Benoit and C. Teisson, "Laboratory comparison of directional wave measurement systems and analysis techniques," in *24th International Conference on Coastal Engineering*, 1994, pp. 42–56.
- [106] W. Pierson, G. Neumann, and R. W. James, "Practical methods for observing and forecasting ocean waves by means of wave spectra and statistics," *H. O. Publ.*, vol. 603, 1955.
- [107] D. E. Longuet-Higgins, M.S. Cartwright and N. D. Smith, "Observations of the directional spectrum of sea waves using the motions of a floating buoy," in *Conf. Ocean Wave Spe*, 1961, pp. 111–132.
- [108] Y. Goda and Y. Suzuki, "Computation of refraction and diffraction of sea waves with Mitsuyasu's directional spectrum," 1975.
- [109] D. E. Hasselmann, M. Dunckel, and J. A. Ewing, "Directional wave spectra observed during JONSWAP 1973," *J.Phys. Ocean.*, vol. 10, pp. 1264–1280, 1980.
- [110] M. S. Longuet-Higgins, "On the statistical distribution of the wave heights of sea waves," *J. Mar. Res.*, vol. 11, pp. 245–266, 1952.
- [111] M. S. Longuet-Higgins, "The statistical analysis of a random, moving surface," *Phil. Trans. Roy. Soc. London A*, vol. 966, no. 249, pp. 321–387, 1957.
- [112] IAHR, "List of sea states parameters," Brussels, Belgium, 1986.
- [113] M. Abramowitz and I. A. Stegun, *Handbook of Mathematical Functions with Formulas, Graphs, and Mathematical Tables*. New York: Dover Publications Inc., 1965.

- [114] A. M. Tayfun, "Effects of spectrum band width on the distribution of wave heights and periods," *Ocean Eng.*, vol. 10, no. 2, pp. 107–118, Jan. 1983.
- [115] A. M. Tayfun, "Nonlinear effects on the distribution of crest-to-trough wave heights," *Ocean Eng.*, vol. 10, no. 2, pp. 97–106, Jan. 1983.
- [116] G. Z. Forristall, "The distribution of measured and simulated wave heights as a function of spectral shape," *J. Geophys. Res.*, vol. 89, no. C6, pp. 10547–10552, 1984.
- [117] D. Myrhaug and S. P. Kjeldsen, "Steepness and asymmetry of extreme waves and the highest waves in deep water," *Ocean Eng.*, vol. 13, no. 6, pp. 549–568, Jan. 1986.
- [118] Shore Protection Manual, *Shore Protection Manual*, 4th editio. Washington, D.C.: U.S. Government Printing Office, 1984.
- [119] V. Katsardi, L. de Lutio, and C. Swan, "An experimental study of large waves in intermediate and shallow water depths. Part I: Wave height and crest height statistics," *Coast. Eng.*, vol. 73, pp. 43–57, Mar. 2013.
- [120] I. Karpadakis, C. Swan, and M. Christou, "Laboratory investigation of crest height statistics in intermediate water depths," *Proc. R. Soc. A Math. Phys. Eng. Sci.*, vol. 475, no. 2229, p. 20190183, Sep. 2019.
- [121] M. S. Longuet-Higgins, "The distribution of intervals between zeros of a stationary random function," *Philos. Trans. R. Soc. London. Ser. A, Math. Phys. Sci.*, vol. 254, no. 1047, pp. 557–599, May 1962.
- [122] C. L. Bretschneider, "Wave Forecasting," in *Handbook of Ocean and Underwater Engineering*, J. J. Myers, Ed. New York: McGraw-Hill Book Co., 1969.
- [123] S. K. Chakrabarti and R. P. Cooley, "Statistical distribution of periods and heights of ocean waves," *J. Geophys. Res.*, vol. 82, no. 9, pp. 1363–1368, Mar. 1977.
- [124] C. Guedes Soares, "Probabilistic models of waves in the coastal zone," in *Advances in Coastal Modelling*, V. C. Lakan, Ed. Elsevier, 2003, pp. 159–187.
- [125] P. Stansell, J. Wolfram, and B. Linfoot, "Improved joint probability distribution for ocean wave heights and periods," *J. Fluid Mech.*, vol. 503, pp. 273–297, Mar. 2004.
- [126] H. D. Zhang, Z. Cherneva, and C. Guedes Soares, "Joint distributions of wave height and period in laboratory generated nonlinear sea states," *Ocean Eng.*, vol. 74, pp. 72–80, Dec. 2013.

- [127] J. I. Collins, "Probabilities of breaking wave characteristics," in *12th Coastal Engineering Conference*, 1994, pp. 399–414.
- [128] H. Mase and Y. Iwagaki, "Wave height distributions and wave grouping in surf zone," in *18th Conf. on Coast. Engin. ASCE*, 1982, pp. 58–76.
- [129] W. R. Dally and R. G. Dean, "Discussion on: Mass flux and underflow in a surf zone," *J. Coast. Eng.*, vol. 10, no. 3, pp. 289–299, 1986.
- [130] W. R. Dally, "Random breaking waves: A closed-form solution for planar beaches," *Coast. Eng.*, vol. 14, no. 3, pp. 233–263, Jun. 1990.
- [131] W. R. Dally, "Random breaking waves: Field verification of a wave-by-wave algorithm for engineering application," *Coast. Eng.*, vol. 16, no. 4, pp. 369–397, Mar. 1992.
- [132] Y. Kuriyama, "Models of wave height and fraction of breaking waves on a barred beach," in *25th Coastal Eng. Conf. ASCE*, 1996, pp. 247–260.
- [133] B. H. Glukhovskiy, "Investigation of wind waves," *Gidrometeoizdat Publ.*, vol. 284, 1966.
- [134] G. Klopman, "Extreme wave heights in shallow water," 1996.
- [135] J. A. Battjes and H. W. Groenendijk, "Wave height distributions on shallow foreshores," *Coast. Eng.*, vol. 40, pp. 161–182, 2000.
- [136] D. Myrhaug and S. Fouques, "Joint distributions of wave height with surf parameter and breaker index for individual waves," *Coast. Eng.*, vol. 60, pp. 235–247, Feb. 2012.
- [137] D. Myrhaug and S. P. Kjeldsen, "Parametric modelling of joint probability density distributions for steepness and asymmetry in deep water waves," *Appl. Ocean Res.*, vol. 6, no. 4, pp. 207–220, Oct. 1984.
- [138] M. K. Chondros and C. D. Memos, "Directionality in stochastic simulation of sea waves," in *3rd IAHR Europe Congress*, 2014.
- [139] R. B. Crowder, *The wonders of the weather*. Canberra, Australia: Australian Government Publishing Service, 1995.
- [140] J. C. Freeman, L. Baer, and G. H. Jung, "The Bathystrophic Storm Tide," *J. Mar. Res.*, vol. 16, no. 1, 1957.

- [141] J. Wu, "Wind Stress and Surface Roughness at Sea Interface," *J. Geophys. Res.*, vol. 74, pp. 444–453, 1969.
- [142] W. C. Van Dorn, "Wind Stress on an Artificial Pond," *J. Mar. Res.*, vol. 12, 1953.
- [143] R. G. Dean and R. A. Dalrymple, *Water Wave Mechanics for Engineers and Scientists*, vol. 2. World Scientific, 1991.
- [144] J. A. Battjes, "Computation of set-up, longshore currents, run-up and overtopping due to wind generated waves," 1974.
- [145] A. J. Bowen, D. L. Inman, and V. P. Simmons, "Wave 'set-down' and 'set-Up,'" *J. Geophys. Res.*, vol. 73, no. 8, pp. 2569–2577, Apr. 1968.
- [146] O. M. Phillips, "The equilibrium range in the spectrum of wind-generated waves," *J. Fluid Mech.*, vol. 4, pp. 426–434, 1958.
- [147] J. W. Miles, "On the generation of surface waves by shear flows," *J. Fluid Mech.*, vol. 3, pp. 185–204, 1957.
- [148] M. W. Szabados, "Intercomparison of the offshore wave measurements during ASLOE," in *OCEANS 82 Conference*, 1982, pp. 876–881.
- [149] R. T. Cox, "Probability, Frequency and Reasonable Expectation," *Am. J. Phys.*, vol. 14, no. 1, pp. 1–13, Jan. 1946.
- [150] E. T. Jaynes, "Bayesian Methods: General Background," in *Maximum-Entropy and Bayesian Methods in Applied Statistics*, J. H. Justice, Ed. Cambridge: Cambridge University Press, 1986.
- [151] B. de Finetti, *Theory of Probability : A Critical Introductory Treatment*. Chichester: John Wiley & Sons Ltd, 2017.
- [152] R. Burrows and B. A. Salih, "Statistical Modelling of Long-Term Wave Climates," in *Coastal Engineering 1986, 1987*, pp. 42–56.
- [153] J. A. Ferreira and C. Guedes Soares, "Modelling the long-term distribution of significant wave height with the Beta and Gamma models," *Ocean Eng.*, vol. 26, pp. 713–725, 2000.
- [154] M. K. Ochi, "New approach for estimating the severest sea state from statistical data," in *23rd Int. Conf. on Coastal Engng, 1*, 1992, pp. 512–25.

- [155] C. Memos, D. Malliouri, E. Kazakidou, and V. Tsoukala, "Impact of wavelength on the stability of rubble mound breakwaters," in *Coastlab*, 2018.
- [156] A. Repko, P. H. A. J. M. Van Gelder, H. G. Voortman, and J. K. Vrijling, "Bivariate description of offshore wave conditions with physics-based extreme value statistics," *Appl. Ocean Res.*, vol. 26, no. 3–4, pp. 162–170, May 2004.
- [157] P. Jonathan and K. Ewans, "Statistical modelling of extreme ocean environments for marine design: A review," *Ocean Eng.*, vol. 62, pp. 91–109, Apr. 2013.
- [158] S. Kotz and S. Nadarajah, *Extreme Value Distributions: Theory and Applications*. London: Imperial College Press, 2000.
- [159] J. R. M. Hosking, "L-moments: analysis and estimation of distributions using linear combinations of order statistics," *J. R. Stat. Soc. (Series B)*, vol. 52, pp. 105–124, 1990.
- [160] J. Pickands, "Statistical inference using extreme order statistics," *Ann. Stat.*, vol. 3, pp. 119–131, 1975.
- [161] F. A. Haight, *Handbook of the Poisson Distribution*. New York: John Wiley & Sons, 1967.
- [162] R. D. Yates and D. J. Goodman, *Probability and Stochastic Processes: A Friendly Introduction for Electrical and Computer Engineers*, 2nd ed. Hoboken, USA: Wiley, 2014.
- [163] M. Mathiesen *et al.*, "Recommended practice for extreme wave analysis," *J. Hydraul. Res.*, vol. 32, no. 6, pp. 803–814, 1994.
- [164] F. Li, P. H. A. J. M. van Gelder, D. P. Callaghan, R. B. Jongejan, C. den Hijer, and R. Ranasinghe, "Probabilistic modelling of wave climate and predicting dune erosion considering sea level rise," in *12th International Coastal Symposium (Plymouth, England)*, 2013, pp. 760–765.
- [165] T. Wahl, N. G. Plant, and J. W. Long, "Probabilistic assessment of erosion and flooding risk in the northern Gulf of Mexico," *J. Geophys. Res. Ocean.*, vol. 121, no. 5, pp. 3029–3043, May 2016.
- [166] F. Li, C. Bicknell, R. Lowry, and Y. Li, "A comparison of extreme wave analysis methods with 1994–2010 offshore Perth dataset," *Coast. Eng.*, vol. 69, pp. 1–11, Nov. 2012.

- [167] G. Schwarz, “Estimating the dimension of a model,” *Ann. Stat.*, vol. 6, pp. 461–464, 1978.
- [168] H. Akaike, “Information theory and an extension of the maximum likelihood principle,” in *Second International Symposium on Information Theory*, 1973, pp. 267–281.
- [169] P. Jonathan, D. Randell, Y. Wu, and K. Ewans, “Return level estimation from non-stationary spatial data exhibiting multidimensional covariate effects,” *Ocean Eng.*, vol. 88, pp. 520–532, Sep. 2014.
- [170] P. Jonathan and K. Ewans, “Statistical modelling of extreme ocean environments for marine design: A review,” *Ocean Eng.*, vol. 62, pp. 91–109, Apr. 2013.
- [171] A. C. Davison and R. L. Smith, “Models for Exceedances Over High Thresholds,” *J. R. Stat. Soc. Ser. B*, vol. 52, no. 3, pp. 393–425, Jul. 1990.
- [172] M. E. Robinson and J. A. Tawn, “Statistics for Extreme Sea Currents,” *J. R. Stat. Soc. Ser. C (Applied Stat.)*, vol. 46, no. 2, pp. 183–205, Jan. 1997.
- [173] J. A. Tawn, “Bivariate extreme value theory: models and estimation,” *Biometrika*, vol. 75, pp. 397–415, 1988.
- [174] J. A. Tawn, “Modelling multivariate extreme value distributions,” *Biometrika*, vol. 77, pp. 245–253, 1988.
- [175] S. G. Coles and J. A. Tawn, “Modelling multivariate extreme events,” *J. R. Stat. Soc. Ser. B*, vol. 53, pp. 377–392, 1991.
- [176] J. A. Ferreira and C. Guedes Soares, “Modelling bivariate distributions of significant wave height and mean wave period,” *Appl. Ocean Res.*, vol. 24, no. 1, pp. 31–45, Feb. 2002.
- [177] S. Dong, N. Wang, W. Liu, and C. Guedes Soares, “Bivariate maximum entropy distribution of significant wave height and peak period,” *Ocean Eng.*, vol. 59, pp. 86–99, Feb. 2013.
- [178] J. E. Heffernan and J. A. Tawn, “A conditional approach for multivariate extreme values (with discussion),” *J. R. Stat. Soc. Ser. B (Statistical Methodol.)*, vol. 66, no. 3, pp. 497–546, Aug. 2004.
- [179] M. Kereszturi, J. Tawn, and P. Jonathan, “Assessing extremal dependence of North

- Sea storm severity,” *Ocean Eng.*, vol. 118, pp. 242–259, May 2016.
- [180] A. Sklar, “Fonctions de répartition à n dimensions et leurs marges,” *Publ. Inst. Stat. Univ. Paris*, vol. 8, pp. 229–231, 1959.
- [181] J. Bender, T. Wahl, and J. Jensen, “Multivariate design in the presence of non-stationarity,” *J. Hydrol.*, vol. 514, pp. 123–130, Jun. 2014.
- [182] J. De Kort, “Modeling tail dependence using copulas-literature review,” 2007.
- [183] H. Joe and J. J. Xu, “The Estimation Method of Inference Functions for Margins for Multivariate Models,” 1996.
- [184] P. Galiatsatou and P. Prinos, “Joint probability analysis of extreme wave heights and storm surges in the Aegean Sea in a changing climate,” in *E3S Web of Conferences 7*, 2016.
- [185] C. Genest, K. Ghoudi, and L.-P. RIVEST, “A semiparametric estimation procedure of dependence parameters in multivariate families of distributions,” *Biometrika*, vol. 82, no. 3, pp. 543–552, 1995.
- [186] G. Salvadori, C. De Michele, and F. Durante, “Multivariate design via Copulas,” *Hydrol. Earth Syst. Sci. Discuss.*, vol. 8, no. 3, pp. 5523–5558, Jun. 2011.
- [187] B. Gräler *et al.*, “Multivariate return periods in hydrology: a critical and practical review focusing on synthetic design hydrograph estimation,” *Hydrol. Earth Syst. Sci.*, vol. 17, no. 4, pp. 1281–1296, Apr. 2013.
- [188] M. Schubert *et al.*, “On the distribution of maximum crest and wave height at intermediate water depths,” *Ocean Eng.*, vol. 217, p. 107485, Dec. 2020.
- [189] G. Z. Forristall, “On the statistical distribution of wave heights in a storm,” *J. Geophys. Res.*, vol. 83, no. C5, p. 2353, 1978.
- [190] P. Boccotti, “On mechanics of irregular gravity waves,” *Atti Accad. Naz. Lincei, Mem. VIII 19*, pp. 111–170, 1989.
- [191] Y. Wu, D. Randell, M. Christou, K. Ewans, and P. Jonathan, “On the distribution of wave height in shallow water,” *Coast. Eng.*, vol. 111, pp. 39–49, May 2016.
- [192] D. E. Cartwright and N. D. Smith, “Buoy techniques for obtaining directional wave spectra,” in *Proc. Buoy Technol. Sym.*, 1964, pp. 173–182.

- [193] M. K. Chondros, "Stochastic simulation of sea waves," National University of Athens, 2014.
- [194] T. Sakai and J. A. Battjes, "Wave shoaling calculated from Cokelet's theory," *Coast. Eng.*, vol. 4, pp. 65–84, Jan. 1980.
- [195] J. D. Fenton and W. D. McKee, "On calculating the lengths of water waves," *Coast. Eng.*, vol. 14, no. 6, pp. 499–513, Dec. 1990.
- [196] P. D. Komar, *Beach Processes and Sedimentation*, 2nd ed. Englewood-Cliffs: Prentice-Hall, 1998.
- [197] J. P. Le Roux, "A simple method to determine breaker height and depth for different deepwater wave height/length ratios and sea floor slopes," *Coast. Eng.*, vol. 54, no. 3, pp. 271–277, Mar. 2007.
- [198] G. D. Faulkenberry, C.-E. Sarndal, B. Swensson, and J. Wretman, "Model-Assisted Survey Sampling," *J. Am. Stat. Assoc.*, vol. 89, no. 428, p. 1563, Dec. 1994.
- [199] R. E. Melchers, "Structural Reliability Analysis and Prediction," *Ellis Horwood Limited, UK.*, 1987.
- [200] S. R. K. Koyluoglu, H. U. Nielsen, "New Approximations for SORM Integrals," *Struct. Saf.*, vol. 13, no. 4, pp. 235–246, 1994.
- [201] S. Winterstein, S., Ude, T., Cornell, C., Bjerager, P., Haver, "Environmental parameters for extreme response: Inverse FORM with omission factors.," in *6th International Conference on Structural Safety and Reliability*, 1993.
- [202] S. Haver, S., Winterstein, "Environmental contour lines: A method for estimating long term extremes by a short term analysis.," *Trans. Soc. Nav. Archit. Mar. Eng.*, vol. 116, pp. 116–127, 2009.
- [203] O. Ditlevsen, "Stochastic model for joint wave and wind loads on offshore structures," *Struct. Saf.*, vol. 24, pp. 139–163, 2002.
- [204] T. Moan, "Development of accidental collapse limit state criteria for offshore structures," *Struct. Saf.*, vol. 31, pp. 124–135, 2009.
- [205] O. D. Baarholm, G.S., Haver, S., Økland, "Combining contours of significant wave height and peak period with platform response distributions for predicting design response.," *Mar. Struct.*, vol. 23, pp. 147–163, 2010.

- [206] V. Fontaine, E., Orsero, P., Ledoux, A., Nerzic, R., Prevesto, M., Quiniou, “Reliability analysis and response based design of a moored FPSO in West Africa,” *Struct. Saf.*, vol. 41, pp. 82–96, 2013.
- [207] J. Jonathan, P., Ewans, K., Flynn, “On the estimation of ocean engineering design contours,” in *30th International Conference on Offshore Mechanics and Arctic Engineering (OMAE2011)*. American Society of Mechanical Engineers (ASME), 2011.
- [208] A. Bang Huseby, E. Vanem, and B. Natvig, “A new approach to environmental contours for ocean engineering applications based on direct Monte Carlo simulations,” *Ocean Eng.*, vol. 60, pp. 124–135, Mar. 2013.
- [209] K. Box, GEP, Wilson, “On the experimental attainment of optimum conditions,” *J. R. Stat. Soc. Ser. B*, vol. 13, pp. 1–45, 1951.
- [210] U. Bucher, C, Bourgund, “A fast and efficient response surface approach for structural reliability problems,” *Struct. Saf.*, vol. 7, pp. 57–66, 1990.
- [211] P. O. Hristov, F. A. DiazDelaO, K. J. Kubiak, and U. Farooq, “Adaptive emulation-based reliability analysis,” in *Proceedings of the 2nd International Conference on Uncertainty Quantification in Computational Sciences and Engineering (UNCECOMP 2017)*, 2017, pp. 198–211.
- [212] M. R. A. van Gent, “Oblique wave attack on rubble mound breakwaters,” *Coast. Eng.*, vol. 88, pp. 43–54, Jun. 2014.
- [213] S. Coles, *An Introduction to Statistical Modeling of Extreme Values*. London: Springer London, 2001.
- [214] A. Kiriliouk, H. Rootzén, J. Segers, and J. L. Wadsworth, “Peaks Over Thresholds Modeling With Multivariate Generalized Pareto Distributions,” *Technometrics*, vol. 61, no. 1, pp. 123–135, Jan. 2019.
- [215] D. M. Thompson and R. M. Shuttler, “Riprap design for wind-wave attack, a laboratory study in random waves,” 1975.
- [216] L. L. Broderick, “Riprap stability, a progress report,” in *Coastal Structures '83*, 1983, pp. 320–330.
- [217] M. R. A. Van Gent, A. J. Smale, and C. Kuiper, “Stability of Rock Slopes with Shallow Foreshores,” in *Coastal Structures 2003*, 2003, pp. 100–112.

- [218] G. M. Smith, I. Wallast, and M. R. A. Van Gent, "Rock slope stability with shallow foreshores," in *ICCE 2002*, 2002, pp. 1524–1536.
- [219] H. J. Verhagen and M. Mertens, "Riprap stability for deep water, shallow water and steep foreshores," in *Coasts, marine structures and breakwaters: Adapting to change*, London: Thomas Telford Ltd, 2010, pp. 2: 486-495.
- [220] H. G. Guler, A. Ergin, and G. Ozyurt, "A comparative study on the stability formulas of rubble mound breakwaters," *Coast. Eng. Proc.*, vol. 1, no. 34, p. 27, Oct. 2014.
- [221] M. R. A. van Gent, "Physical model investigations on coastal structures with shallow foreshores - Single and double-peaked wave energy spectra - Report H3608," 1999.
- [222] M. R. A. van Gent, "Wave Runup on Dikes with Shallow Foreshores," *J. Waterw. Port, Coastal, Ocean Eng.*, vol. 127, no. 5, pp. 254–262, Oct. 2001.
- [223] M. R. A. van Gent, "Low-exceedance wave overtopping events: Estimates of wave overtopping parameters at the crest and landward side of dikes," 2002.
- [224] E. Gerding, "Toe structure stability of rubble mound breakwaters," TU Delft, 2003.
- [225] M. R. A. van Gent and I. M. van der Werf, "Rock toe stability of rubble mound breakwaters," *Coast. Eng.*, vol. 83, pp. 166–176, Jan. 2014.
- [226] M. R. A. Van Gent, A. J. Smale, and C. Kuiper, "Stability of Rock Slopes with Shallow Foreshores," in *Proceedings of 4th International Coastal Structures Conference*, 2004.
- [227] P. Jonathan, K. Ewans, and G. Forristall, "Statistical estimation of extreme ocean environments: The requirement for modelling directionality and other covariate effects," *Ocean Eng.*, vol. 35, no. 11–12, pp. 1211–1225, Aug. 2008.
- [228] D. Reeve, A. J. Chadwick, and C. Fleming, *Coastal Engineering: Processes, Theory and Design Practice*, 2nd editio. E & FN Spon, 2012.

Appendix A. Water wave theories

This section explains briefly some theories of periodic progressive waves and their interaction with sea bed, shorelines and coastal structures. Also, it focuses on wind waves providing a descriptive overview of their characteristics, the processes which control their movement, and transformation.

Wave generation

Ocean waves are mainly generated by the action of wind on water. Specifically, waves are formed initially by a complex process of resonance and shearing action, in which waves of differing wave height, length, and period are produced and travel in various directions. Once formed, ocean waves can travel for vast distances, often out of the storm wave generation area, thus spreading in area and reducing in height, but maintaining wavelength and period (see Figure A.1).

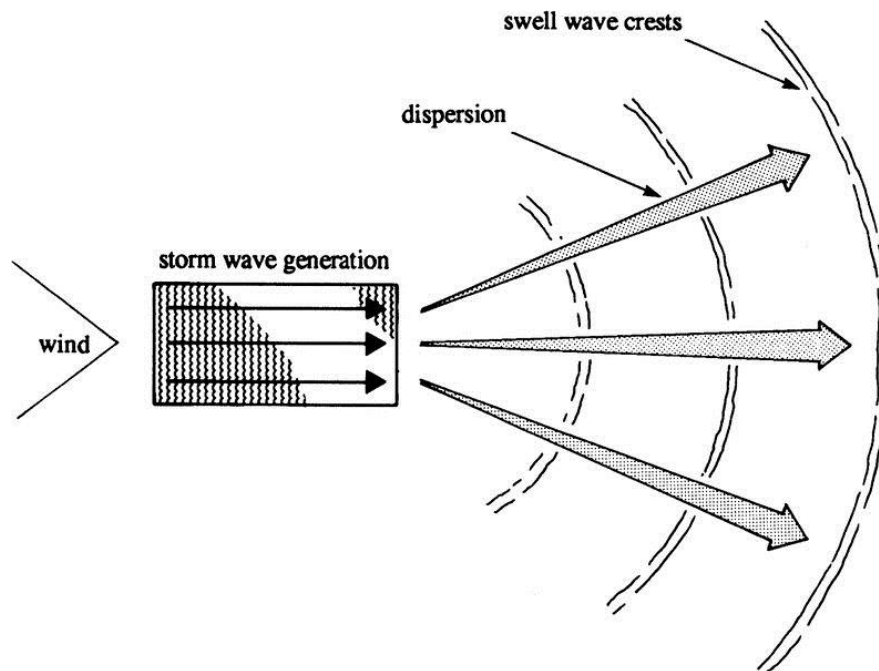


Figure A.1 Wave generation and dispersion [228]

In the storm zone generation area, waves with larger periods propagate at a higher speed than waves of smaller periods, thus the wave energy of the latter is both dissipated and transferred

to long-period wave components, which lead the wave train. When the above process results in a swell sea condition, it is called as dispersion opposed to storms sea condition. Therefore, wind waves contain a large range of frequencies and directions consist and may be characterized as irregular, short crested, and steep. On the other hand, swell waves consist of a small range of low frequencies and directions, and may be characterized as regular, long crested, and not very steep.

Small amplitude wave theory

The earliest mathematical description of periodic progressive waves is that attributed to Airy in 1845, and is strictly applicable to conditions in which the wave height is small compared to the wavelength and the water depth, i.e. $H \ll L$ and $H \ll d$. This theory is commonly referred to as linear or first order wave theory, because of the simplifying assumptions made in its derivation.

The Airy wave theory was derived using the concepts of two-dimensional ideal fluid flow, which is a reasonable starting point for ocean waves that are not greatly influenced by viscosity, surface tension or turbulence [228]. The derivation of the Airy wave equations derives from the Laplace equation for irrotational flow of an ideal fluid. According to the assumptions of this theory, the wave celerity c is given by:

$$c = (gT / 2\pi) \tanh(2\pi d / L) = (g / \omega) \tanh(kh) \quad (\text{A.1})$$

where the wave number is $k = 2\pi / L$ and the angular frequency is $\omega = 2\pi / T$.

By substituting that $c = L / T$ into the above equation, the wave dispersion equation is derived, given by:

$$\omega^2 = gk \tanh(kh) \quad (\text{A.2})$$

Referring to the influence of water depth on wave characteristics, three categories of water depths are distinguished, i.e. deep waters, transitional or intermediate, and shallow waters. In deep waters, waves are unaffected by depth, and the ratio of water depth towards wave length is higher than 0.5, thus it applies:

$$d / L \geq 0.5, \tanh(kd) \approx 1, c_0 = gT / 2\pi = (gL_0 / 2\pi)^{1/2} \quad (\text{A.3})$$

where the subscript 0 corresponds to deep water.

In intermediate waters:

$$0.5 > d / L > 0.04, \tanh(kd) < 1, c = gT / 2\pi \tanh(kd) = c_0 \tanh(kd) < c_0 \quad (\text{A.4})$$

and in shallow water:

$$d / L < 0.04, \tanh(kd) \approx 2\pi d / L, c = \sqrt{gd} \quad (\text{A.5})$$

Thus, wave celerity is determined by water depth in shallow water, whilst by wave period in deep water.

Wave transformations

As wind-generated waves propagate from deep waters towards shallower waters, and sea bed starts affecting them, various mechanisms take place simultaneously with temporal and spatial variations, e.g. wave shoaling, refraction, diffraction, reflection, depth-induced wave breaking, reflection, bottom friction, wave-current interactions and wave-wave interactions.

As a first step, the theory of wave transformations, e.g. shoaling and refraction, were restricted to considering only monochromatic waves. However, a real sea state is more realistically represented as a system that consists of a large number of components of differing periods, heights and directions (known as the directional spectrum). Therefore, one way to determine an inshore sea state is to take into account the offshore directional spectrum.

This can be achieved in a relatively straightforward way, via application of the aforementioned linear superposition, which however implies that non-linear processes such as seabed friction and higher-order wave theories are excluded. The principle of the method is to implement a refraction and shoaling analysis for each individual component of a certain wave frequency and direction, and then to sum the resultant inshore energies at the new inshore directions at each frequency, and hence assemble an inshore directional spectrum [4]. Numerical models simulating wave propagation in intermediate and shallow waters based on spectral energy-balance equation are the well-known phase-averaged models.

Finite amplitude waves

As it has already been noted, the Airy wave equations strictly apply to waves of relatively small height in comparison to their wavelength and water depth. For steep waves and shallow water waves their celerity and wavelength are affected by wave height and are better described by other wave theories. To categorize finite amplitude waves, three parameters are required, i.e. the wave height (H), the water depth (d) and wavelength (L). Using these parameters various non-dimensional parameters can be defined, namely relative depth (d/L), wave steepness (H/L), wave height to water depth ratio (H/d) and another useful non-dimensional parameter the Ursell number ($Ur=HL^2/d^3$), first introduced in 1953 [228].

The first finite amplitude wave theory was developed by Stokes in 1847, and is applicable to steep waves in deep and intermediate waters. Following Stokes, Korteweg and de Vries developed a shallow-water finite amplitude wave theory in 1895, termed Cnoidal theory, analogous to the sinusoidal Airy wave theory. Both of these theories relax the assumptions made in Airy theory which linearize the kinematic and dynamic surface boundary conditions. In Stokes' wave theory, H/L is assumed small, and d/L is allowed to assume a wide range of values. Stokes also derived the second order solution. In Cnoidal theory, H/d is assumed small, and Ur of the order of unity. More recently (1960's to 1980's), these two theories have been extended to higher orders (third and fifth). The mathematics is complex and as a result other researchers developed new methods, whereby solutions could be obtained to any

arbitrary order, by numerical solution [228]. In Figure A.2, the approximate validity region of various wave theories is depicted as a function of wave steepness and Ursell number.

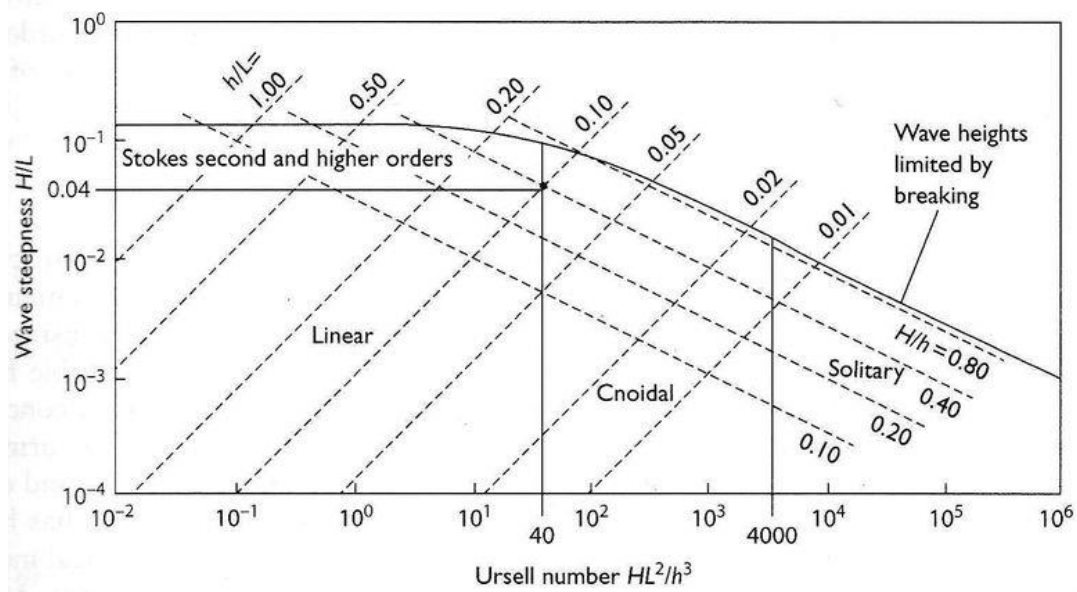


Figure A.2 Approximate validity region of various wave theories (h is the water depth) [64]

It is noted that the range of validity of linear theory is reassuringly wide, covering all of the intermediate water depths for most wave steepnesses encountered in practice. However, for engineering design purposes, the application of linear theory outside its range of validity could lead to wave celerity and wavelength not being strictly correct, leading to (some) inaccuracies in refraction and shoaling analysis (see e.g. [228]).

